Design and Characterization of Vaccine Candidates for Therapeutic Vaccination Against Papillomaviruses

DISSERTATION ZUR ERLANGUNG DES DOKTORGRADES DER NATURWISSENSCHAFTEN (DR. RER. NAT.) DER FAKULTÄT FÜR BIOLOGIE UND VORKLINISCHE MEDIZIN DER UNIVERSITÄT REGENSBURG

vorgelegt von

Patrick Lukas Neckermann

aus

Füssen

im Jahr

2023

Das Promotionsgesuch wurde eingereicht am:

04.12.2023

Diese Arbeit wurde angeleitet von:

Prof. Dr. Ralf Wagner

Unterschrift:

Patrick Lukas Neckermann

Content Declaration

This thesis comprises three manuscripts, the first and the second are published in peer-reviewed journals and the third manuscript is submitted for peer-reviewed publication.

Manuscript 1: "Design and Immunological Validation of *Macaca fascicularis* Papillomavirus Type 3 Based Vaccine Candidates in Outbred Mice: Basis for Future Testing of a Therapeutic Papillomavirus Vaccine in NHPs"

This manuscript is published online under the above-named title in the peer-reviewed journal Frontiers in Immunology on 28th of October 2021. DOI: 10.3389/fimmu.2021.761214

Authors: **Patrick Neckermann***, Ditte Rahbaek Boilesen*, Torsten Willert, Cordula Pertl, Silke Schrödel, Christian Thirion, Benedikt Asbach, Peter Johannes Holst, Ralf Wagner

*Authors contributed equally and share first authorship

Author contribution: PH, CT and RW designed the study and acquired funding, **PN**, DB, BA, TW, CP, SS planned and performed the experiments, **PN**, DB, BA, PH, CT and RW interpreted the data, **PN** and DB wrote the draft, **PN**, DB, BA, PH, RW wrote, reviewed and edited the manuscript.

Detailed personal contribution within the experiments: Patrick Neckermann (PN) designed the antigens (Figure 7), cloned the antigens into DNA vaccine vectors and shuttle vectors for the generation of adenoviral vectors and characterized the antigens shuttled by DNA vaccine vectors and adenoviral vectors regarding their expression in vitro using western blot and flow cytometry analysis (Figure 8A and B, Figure 10, Supplementary Figure 1, Supplementary Figure 4). PN investigated the influence of the molecular adjuvant on ubiquitination and degradation of the antigens *in vitro* (Figure 13). PN also contributed to the design of the mouse studies, the immunological experiments/validation and data interpretation.

Manuscript 2: "Efficacy and Synergy with Cisplatin of an Adenovirus Vectored Therapeutic E1E2E6E7 Vaccine against HPV Genome-Positive C3 Cancers in Mice"

This manuscript is published online under the above-named title in the peer-reviewed journal Cancer Immunology Research on 3rd of February 2023. DOI: 10.1158/2326-6066.CIR-22-0174, ©2022 American Association for Cancer Research.

Authors: Ditte Rahbaek Boilesen*, **Patrick Neckermann***, Torsten Willert, Mikkel Dons Müller, Silke Schrödel, Cordula Pertl, Christian Thirion, Benedikt Asbach, Ralf Wagner, Peter Johannes Holst

*Authors contributed equally and share first authorship

Author contribution: DB**:** Data curation, formal analysis, validation, investigation, visualization, methodology, writing–original draft, project administration. **PN:** Data curation, software, formal analysis, validation, investigation, visualization, methodology, writing–original draft. TW**:** Investigation, methodology, writing–review and editing. MM**:** Validation, investigation, methodology, writing–review and editing. SS**:** Investigation, methodology, writing–original draft, project administration. CP**:** Investigation, methodology, writing–review and editing. CT**:** Conceptualization, resources, data curation, supervision, funding acquisition. BA**:** Conceptualization, data curation, supervision, methodology, writing–review and editing. RW**:** Conceptualization, resources, data

curation, supervision, funding acquisition, writing–review and editing. PH**:** Conceptualization, resources, data curation, supervision, funding acquisition, writing–review and editing.

Detailed personal contribution within the experiments: Patrick Neckermann (PN) designed the antigens (Figure 14A, Supplementary Figure 7), predicted the MHC-I epitopes of the antigens *in silico* (Figure 14B, Supplementary Table 1) and characterized the expression of the antigen constructs *in vitro* using western blot and flow cytometry analysis (Figure 14C and D, Supplementary Figure 9A and Supplementary Figure 10). PN investigated the ability of E6-mediated p53 degradation in a flow cytometry-based assay using DNA-transfected human cells (Figure 14E, Supplementary Figure 9B). PN evaluated the transforming potential of the antigens in a soft-agar-transformation assay, by cloning and producing lentiviral vectors of the antigens, generated mouse embryonic stable cell lines by lentiviral transduction, proved the correct antigen expression with western blot analysis (Supplementary Figure 9C) and conducted the soft-agar transformation assay (Figure 14F, Supplementary Figure 9D). PN also contributed to the design of the mouse studies, the immunological experiments/validation and data interpretation.

Manuscript 3: "Transgene expression knock-down in recombinant Modified Vaccinia virus Ankara vectors improves genetic stability and sustained transgene maintenance across multiple passages"

This manuscript has been submitted on 14th of November 2023 for publication under the above named title in the peer-reviewed journal Frontiers in Immunology.

Authors: **Patrick Neckermann**, Madlen Mohr, Martina Billmeier, Alexander Karlas, Ditte Rahbaek Boilesen, Christian Thirion, Peter Johannes Holst, Ingo Jordan, Volker Sandig, Benedikt Asbach, Ralf Wagner

Author contribution: Writing original draft: **PN**; writing review editing: PN, MM, MB, AK, DB, CT, PH, IJ, VS, BA, RW; Funding acquisition: CT, PH, RW; Resources: RW; Conceptualization: **PN**, IJ, VS, RW; Investigation: **PN**, MM, AK, IJ; Methodology: **PN**, MB, AK, IJ, VS, BA, RW; Supervision: RW; Formal analysis: **PN**, AK, IJ, VS, BA, RW; Visualization: **PN**; Project administration: RW; Data curation: **PN**

Detailed personal contribution within the experiments: Patrick Neckermann (PN) cloned the set of 10 antigens into different MVA transfer vectors suitable for integration into different loci (Supplementary Figure 14) and controlled the expression of these antigens with western blot analysis (not shown). PN investigated the expression of the rMVA (received from AK, IJ and VS) using western blot, flow cytometry and RT-qPCR (Figure 20, Supplementary Figure 2, Supplementary Figure 3). PN analyzed the replication kinetics and plaque morphology (Figure 21). PN passaged the virus CR19 M-DelIII on both cell lines (Supplementary Figure 4), titrated the passages (Figure 22A), and measured the transgene expression of the passaged CR19 M-DelIII virus stocks (Figure 23A, Supplementary Figure 18). PN analyzed the passaged virus stocks of CR19 M-DelIII and CR19 M-TK using next-generation sequencing and PCR (Figure 24, Figure 25, Supplementary Figure 19, Supplementary Figure 20, Supplementary Figure 21).

Furthermore, PN supervised and supported the Master's thesis of student Madlen Mohr, who provided the data for Figure 22B and Figure 23B as well as Supplementary Figure 22.

This PhD thesis has been carried-out within the SARS-CoV-2 pandemic. The research group of Ralf Wagner has received funding from international (EU H2020, Virofight), national (BMBF, German ministry of education and research) and local (Bavarian StmWK, states ministry of science and arts) and obliged to collect data supporting political measures to fight the epidemic. Therefore, the appendix of this thesis mentions five additional publications in peer-reviewed journals where the PhD candidate Patrick Neckermann has contributed as co-author during the duration of my PhD thesis. The abstract, author contributions and personal contribution can be found in the appendix.

Appendix publication 1: "Symptoms, SARS-CoV-2 Antibodies, and Neutralization Capacity in a Cross Sectional-Population of German Children"

Authors: Otto Laub, Georg Leipold, Antoaneta A Toncheva, David Peterhoff, Sebastian Einhauser, **Patrick Neckermann**, Natascha Borchers, Elisangela Santos-Valente, Parastoo Kheiroddin, Heike Buntrock-Döpke, Sarah Laub, Patricia Schöberl, Andrea Schweiger-Kabesch, Dominik Ewald, Michael Horn, Jakob Niggel, Andreas Ambrosch, Klaus Überla, Stephan Gerling, Susanne Brandstetter, Ralf Wagner, Michael Kabesch; Corona Virus Antibodies in Children from Bavaria (CoKiBa) Study Group

Published on 4th of October 2021 in Frontier in Pediatrics

DOI: 10.3389/fped.2021.678937

Author contribution: OL, GL, SG, KÜ, RW, and MK were responsible for the study design. OL, GL, HB-D, SL, AS-K, DE, MH, JN, and MK performed the data collection. AT, DP, SE, **PN**, NB, ES-V, PK, PS, RW, and AA carried out the laboratory analysis and the data interpretation. Data Analysis was performed by DP, SE, **PN**, SB, RW, and MK. OL, GL, DP, SE, SB, RW, and MK wrote this manuscript.

Personal contribution: PN supervised and supported the Master's thesis of student Sebastian Einhauser, who established a pseudovirus-based assay for the quantification of neutralizing antibodies against SARS-CoV-2. PN further evaluated, analyzed and interpreted the data.

Appendix publication 2: "Analysis of Serological Biomarkers of SARS-CoV-2 Infection in Convalescent Samples From Severe, Moderate and Mild COVID-19 Cases"

Javier Castillo-Olivares, David A Wells, Matteo Ferrari, Andrew C Y Chan, Peter Smith, Angalee Nadesalingam, Minna Paloniemi, George W Carnell, Luis Ohlendorf, Diego Cantoni, Martin Mayora-Neto, Phil Palmer, Paul Tonks, Nigel J Temperton, David Peterhoff, **Patrick Neckermann**, Ralf Wagner, Rainer Doffinger, Sarah Kempster, Ashley D Otter, Amanda Semper, Tim Brooks, Anna Albecka, Leo C James, Mark Page, Wilhelm Schwaeble, Helen Baxendale, Jonathan L Heeney

Published on 19th of November 2021 in Frontiers in Immunology

DOI: 10.3389/fimmu.2021.748291

Author contribution: JC-O: Coordinating the laboratory work; analysis of results; conception of the manuscript; writing the manuscript. DW: Statistical analysis. MF: Semiautomated immunology-blotting; analysis of results. AC: ELISA, Lateral flow testing; sample processing; analysis off results; PS: Blood processing, samples archiving, ELISA testing. AN: ELISA set up; pseudo neutralisation assay. MiP: Laboratory set up; ELISA set up. LO: Semi-automated immunoblotting. DC: pseudoneutralization assays. MMN: pseudoneutralization assay. PP: Statistical analysis. NJT: pseudoneutralization. DP:

Design constructs, expression and purification of recombinant RBD. **PN**: Design constructs, expression and purification of recombinant RBD. RW: Design constructs, expression and purification of recombinant RBD. RD: Luminex assay. SK: Sample selection and provision pre-pandemic sera. AO: Electrochemiluminescence assays. AS: Electrochemiluminescence assays. AS: Electrochemiluminescence assays. TB: Electrochemiluminescence assays. AA: EDNA assay. LCJ: EDNA assay. MaP: Consultation on Standardization of serological assays. WS: Grant holder; assessing manuscript; scientific direction. HB: Clinical Lead; clinical assessment; coordination clinical work. JLH: Scientific direction.

Personal contribution: PN contributed to this publication by the supply of critical reagents. He designed expression constructs for the recombinant expression of the receptor-binding domain of SARS-CoV-2 Spike protein (RBD). PN further cloned the constructs, expressed the recombinant proteins in human cell culture, purified and quality-controlled the recombinant proteins by ELISA. These proteins were used to analyze RBD-binding antibodies in reconvalescent COVID-19 patients and SARS-CoV-2-positive and -negative health care workers.

Appendix publication 3: "Liposome-based high-throughput and point-of-care assays toward the quick, simple, and sensitive detection of neutralizing antibodies against SARS-CoV-2 in patient sera"

Authors: Simon Streif, **Patrick Neckermann**, Clemens Spitzenberg, Katharina Weiss, Kilian Hoecherl, Kacper Kulikowski, Sonja Hahner, Christina Noelting, Sebastian Einhauser, David Peterhoff, Claudia Asam, Ralf Wagner, and Antje J. Baeumner

Published on 9th of February 2023 in Analytical and Bioanalytical Chemistry

DOI: 10.1007/s00216-023-04548-3

Author contribution: Conceptualization, AJB, RW, and SS; performed HTS experiments, SS; performed POC experiments, SS and KW; liposome synthesis and optimization, SS, KH, CS, KK; cloning of recombinant protein expression plasmids, **PN** and CA; expression, purification, and quality control of recombinant ACE2 and RBD, **PN**, CA, DP, SH; pseudovirus neutralization assays, SE; RBD binding antibody test, CN; writing — original draft, SS; writing — review and editing, SE, **PN**, RW, AJB.

Personal contribution: PN contributed to this publication by the supply of critical reagents, in particular antigens suitable for the immobilization on liposomes. For this, PN designed expression constructs for the recombinant expression of the SARS-CoV-2 receptor Angiotensin-converting-enzyme-2 (Ace2) and multiple variants of the receptor-binding domain of SARS-CoV-2 Spike protein (RBD) suitable for either side-specific or non-directional immobilization on particles. He further cloned the constructs, expressed the recombinant proteins in human cell culture, purified and quality-controlled the recombinant proteins regarding their antigenicity and accessibility of the domains used for immobilization by ELISA. These proteins were used for the development of a liposome-based assay to detect neutralizing antibodies against SARS-CoV-2.

Appendix publication 4: "Glycan masking of a non-neutralising epitope enhances neutralising antibodies targeting the RBD of SARS-CoV-2 and its variants"

Authors: George W Carnell, Martina Billmeier, Sneha Vishwanath, Maria Suau Sans, Hannah Wein, Charlotte L George, **Patrick Neckermann**, Joanne Marie M Del Rosario, Alexander T Sampson,

Sebastian Einhauser, Ernest T Aguinam, Matteo Ferrari, Paul Tonks, Angalee Nadesalingam, Anja Schütz, Chloe Qingzhou Huang, David A Wells, Minna Paloniemi, Ingo Jordan, Diego Cantoni, David Peterhoff, Benedikt Asbach, Volker Sandig, Nigel Temperton, Rebecca Kinsley, Ralf Wagner, Jonathan L Heeney

Published on 23rd of February 2023 in Frontiers in Immunology

DOI: 10.3389/fimmu.2023.1118523

Author contribution: Conceptualization, JH, RW, RK. Data curation: GC, MB, SV. Investigation: GC, MB, SV, BA, JH, RK, RW. Methodology: GC, MB, SV, HW, AS, MSS, CG, JDR, ATS, AN, CH, DW, MF, MP, PT, DP. Critical reagents: SE, **PN**, DC, NT, IJ, VS. Project administration: JH, RW. Resources: JH, RW. Supervision: JH, RW, RK. Visualization: GC, MB, SV. Writing—original draft: GC, MB, SV. Writing—review and editing: GC, MB, SV, JH, RW, IJ.

Personal contribution: For this publication, PN supplied critical reagents to detect binding antibodies and distinguish between binding and neutralizing antibody titers. In order to develop vaccine candidates targeting not only the wild-type but also different virus variants (e.g. VOCs) and measuring their humoral immune responses, PN designed and cloned expression constructs for the recombinant expression of RBD proteins of different VOCs, e.g. alpha, beta, gamma, delta, omicron BA1. PN further expressed the recombinant VOC-RBD proteins in human cell culture, purified and quality-controlled the antigenicity of recombinant proteins by ELISA. These proteins were used for the evaluation of binding antibody responses in DNA vaccine vector-immunized mice, DNA-MVA-immunized mice, DNA-MVA-immunized mice pre- and post-challenge with SARS-CoV-2 live virus. These binding antibody titers were instrumental for the comparison of binding antibody titers with neutralization titers.

Appendix publication 5: "A computationally designed antigen eliciting broad humoral responses against SARS-CoV-2 and related sarbecoviruses"

Authors: Sneha Vishwanath, George William Carnell, Matteo Ferrari, Benedikt Asbach, Martina Billmeier, Charlotte George, Maria Suau Sans, Angalee Nadesalingam, Chloe Qingzhou Huang, Minna Paloniemi, Hazel Stewart, Andrew Chan, David Arthur Wells, **Patrick Neckermann**, David Peterhoff, Sebastian Einhauser, Diego Cantoni, Martin Mayora Neto, Ingo Jordan, Volker Sandig, Paul Tonks, Nigel Temperton, Simon Frost, Katharina Sohr, Maria Teresa Lluesma Ballesteros, Farzad Arbabi, Johannes Geiger, Christian Dohmen, Christian Plank, Rebecca Kinsley, Ralf Wagner, Jonathan Luke Heeney

Published on 25th September 2023 in Nature Biomedical Engineering

DOI: 10.1038/s41551-023-01094-2

Author contribution: S.V., D.A.W. and S.F. developed the computational pipeline. G.W.C., M.F., C.G., M.S.S., A.N., C.Q.H., M.P., H.S. and A.C. performed the *in vitro* assays. G.W.C. and P.T. performed the animal experiments. B.A., M.B., **P.N.**, D.P. and S.E. performed DNA purification and preparation. M.B., I.J. and V.S. performed MVA production and purification. K.S., M.T.L.B., F.A., J.G., C.D. and C.P. performed mRNA production and purification. D.C., M.M.N. and N.T. provided key reagents. S.V. and G.W.C. analysed and visualized the data. R.K., R.W. and J.L.H. acquired funding, conceptualized the investigation, reviewed data and administered the project. R.W. and J.L.H. supervised the project. S.V. wrote the original draft. S.V., G.W.C. and J.L.H. reviewed and edited the manuscript.

Personal contribution: PN contributed to this publication by the supply of critical reagents for the characterization of novel vaccine candidates against SARS-CoV-2 VOCs. PN purified LPS-free DNA vaccine vector constructs of novel SARS-CoV-2 antigens, computationally-designed to elicit broad antibody responses against multiple SARS-CoV-2 VOCs, for the immunization of BALB/c mice, guinea pigs and K18-hACE2 mice. Further, PN controlled the quality of the vaccine plasmids by restriction digests, sequencing and expression analysis.

Table of Content

1 Abstract

Despite the availability of highly efficacious prophylactic vaccines against human papillomaviruses (HPV), the predominantly sexually transmitted viruses are still highly prevalent worldwide and represent the most significant part of virus-induced tumor diseases. Infection with HPV is the leading cause of cervical dysplasia and cancer, but moreover, it can also cause tumors in the other parts of the anogenital tract and in the head and neck area, especially in the oropharynx. Thus, the global burden of morbidity and mortality is immense. The prophylactic vaccines only protect from virus infection but cannot extirpate virus-infected cells, which renders them ineffective as a treatment for HPV-induced dysplasia and cancer. Hence, a novel therapy against HPV-induced malignancies is of the highest urgency.

Natural regression of HPV-induced dysplasia is connected to rigid T cell responses against the regulatory early proteins of the virus. This renders these proteins a possible candidate for therapeutic vaccination. Therapeutic vaccine candidates are mainly focused on the oncoproteins E6 and E7, thus varying in clinical efficacy. Hence, this thesis aims to expand the restricted antigen usage in order to generate novel type-specific therapeutic vaccine candidates.

First, with the lack of a small animal model for sexually-transmitted HPV, *Macaca fascicularis* papillomavirus type 3 (MfPV3) was chosen as a model virus due to its high homology and phylogenic relationship to HPV16 and its ability to induce HPV-like dysplasia in persistently infected *Macaca fascicularis*. A set of antigens of MfPV3 was designed based on the regulatory early proteins E1, E2, E6, and E7 and the N-terminal fusion of the MHC-II-associated invariant chain (Ii). Biochemical and molecular biological *in vitro* as well as immunological *in vivo* characterization of DNA vaccine vector- and adenoviral vector-delivered antigens proved that the artificially fused polyprotein Ii-E1E2E6E7 is not inferior compared to the combination of single antigens, thus renders this antigen the lead therapeutic vaccine candidate for pre-clinical efficacy trials in persistently-infected macaques.

Second, HPV16 represents the most critical clinical relevant HPV type. Hence, HPV16 antigens were designed based on the blueprints of the MfPV3 antigens. Biochemical, molecular, and cell biological characterization proved the absence of transformation capacity of the antigens. Moreover, in-depth immunological characterization of adenoviral-delivered antigens revealed potent anti-tumor efficacy in a translational HPV genome-positive tumor model in inbred mice, especially in synergy with cisplatin. Therefore, the HPV16 Ii-E1E2E6E7 therapeutic vaccine candidate might be a promising contender in future clinical investigations to combat HPV16-induced malignancies.

Finally, recombinant poxviral vectors based on the Modified Vaccinia virus Ankara (MVA) comprising MfPV3 Ii-E1E2E6E7 were generated in a duck-derived continuous cell line, which was modified to knock down transgene expression. Thorough characterization of the cell line side-by-side with the non-modified parental cell line exhibited better replication, resulting in higher virus titers, and enhanced genetic stability across serial passaging of both recombinant MVA (rMVA) in the absence of transgene expression. Furthermore, it was shown that the genetic stability depends on the integration site within the rMVA. particularly the mode of action how instability is manifested differs between the integration sites. Thus, the knock-down of transgene expression while rMVA generation and production might be a promising strategy for manufacturing recombinant viruses with demanding transgenes.

In summary, the generation of novel therapeutic vaccine constructs against HPV-associated disease with broader antigen capacity due to the inclusion of E1 and E2 and also of vectors suitable for antigen delivery is shown in this work. The data presented here argues for the potential beneficial use of the

Ii-E1E2E6E7 antigen in the therapy against HPV-induced malignancies. A future pre-clinical efficacy trial with an adenovirus-prime and MVA-boost scheme in persistently MfPV3-infected macaques may guide the way for the clinical development of the promising HPV16 Ii-E1E2E6E7 therapeutic vaccine candidate.

2 Zusammenfassung

Trotz der Verfügbarkeit hochwirksamer prophylaktischer Impfstoffe gegen humane Papillomviren (HPV) sind die vorwiegend sexuell übertragbaren Viren weltweit immer noch stark verbreitet und stellen den größten Teil der virusbedingten Tumorerkrankungen dar. Die Infektion mit HPV ist die Hauptursache für Dysplasie und Krebs des Gebärmutterhalses, kann aber auch Tumore in anderen Teilen des Anogenitaltrakts und im Kopf und Nackenbereich, insbesondere im Oropharynx, verursachen. Deshalb ist die globale Belastung durch Morbidität und Mortalität immens. Die prophylaktischen Impfstoffe schützen nur vor einer Virusinfektion, können aber die virusinfizierten Zellen nicht ausrotten, so dass sie zur Behandlung von HPV-induzierten Dysplasien und Krebs unwirksam sind. Daher ist eine neue Therapie gegen HPV-induzierte Entartungen von höchster Dringlichkeit.

Die natürliche Regression von HPV-induzierten Dysplasien ist mit einer rigiden T-Zell-Reaktion gegen die regulatorischen frühen Proteine des Virus verbunden. Dies macht diese Proteine zu einem möglichen Kandidaten für eine therapeutische Impfung. Therapeutische Impfstoffkandidaten konzentrieren sich hauptsächlich auf die Onkoproteine E6 und E7 und variieren daher in ihrer klinischen Wirksamkeit. Ziel dieser Arbeit ist es daher, die eingeschränkte Verwendung von Antigenen zu erweitern, um neuartige typspezifische therapeutische Impfstoffkandidaten zu entwickeln.

In Ermangelung eines Kleintiermodells für sexuell übertragbare HPV wurde *Macaca fascicularis* Papillomavirus Typ 3 (MfPV3) als Modellvirus ausgewählt, da es eine hohe Homologie und phylogenetische Verwandtschaft mit HPV16 aufweist und in der Lage ist, HPV-ähnliche Dysplasien in persistent infizierten *Macaca fascicularis* zu induzieren. Eine Reihe von MfPV3-Antigenen wurde auf der Grundlage der frühen regulatorischen Proteine E1, E2, E6 und E7 sowie der N-terminalen Fusion der MHC-II-assoziierten invarianten Kette (Ii) entwickelt. Die biochemische und molekularbiologische *in vitro*- sowie die immunologische *in vivo*-Charakterisierung der durch DNA-Vakzine-Vektoren und adenovirale Vektoren verabreichten Antigene zeigte, dass das künstlich fusionierte Polyprotein Ii-E1E2E6E7 einer Kombination der einzelnen Antigene nicht unterlegen ist, was dieses Antigen zum führenden therapeutischen Impfstoffkandidaten für präklinische Wirksamkeitsstudien an persistent infizierten Makaken macht.

HPV16 stellt den wichtigsten klinisch relevanten HPV-Typ dar. Daher wurden HPV16-Antigene auf der Grundlage der MfPV3-Antigene entwickelt. Die biochemische, molekulare und zellbiologische Charakterisierung bewies, dass die modifizierten Antigene keine Transformationsfähigkeit mehr besitzen. Darüber hinaus ergab eine detailierte immunologische Charakterisierung der adenoviral-verabreichten Antigene eine starke Anti-Tumor-Wirksamkeit in einem translationalen HPV-Genom-positiven Tumormodell bei Inzuchtmäusen, insbesondere in Synergie mit Cisplatin. Daher könnte der therapeutische HPV16-Ii-E1E2E6E7-Impfstoffkandidat ein vielversprechender Kandidat für künftige klinische Untersuchungen zur Bekämpfung von HPV16-induzierten malignen Tumoren sein.

Schließlich wurden rekombinante pockenvirale Vektoren auf der Grundlage des modifizierten Vaccinia-Virus Ankara (MVA), das MfPV3 Ii-E1E2E6E7 als Transgen enthält, in einer kontinuierlichen Zelllinie von Enten erzeugt. Dazu wurde die Zelllinie und das Virus so modifiziert, dass die Transgenexpression unterdrückt wurde. Eine gründliche Charakterisierung der modifizierten Zelllinie im Vergleich zur nicht modifizierten parentalen Zelllinie ergab eine bessere Replikation, die zu höheren Virustitern führte, und eine verbesserte genetische Stabilität bei serieller Passage beider rekombinanter MVA (rMVA) ohne Transgenexpression. Darüber hinaus konnte gezeigt werden, dass die genetische Stabilität von der Integrationsstelle innerhalb des rMVA abhängt, insbesondere die

Wirkungsweise, d. h. die Art und Weise, wie sich die Instabilität manifestiert, unterscheidet sich zwischen den Integrationsstellen. Der Knockdown der Transgenexpression während der rMVA-Generierung und Produktion könnte daher eine vielversprechende Strategie für die Herstellung rekombinanter Viren mit anspruchsvollen Transgenen sein.

Zusammenfassend lässt sich sagen, dass in dieser Arbeit die Herstellung neuartiger therapeutischer Impfstoffkonstrukte gegen HPV-assoziierte Krankheiten mit einer breiteren Antigenkapazität aufgrund der Einbeziehung von E1 und E2 sowie von passenden Shuttle-Vektoren gezeigt wurde. Die hier vorgestellten Daten sprechen für den potenziell vorteilhaften Einsatz des Ii-E1E2E6E7-Antigens bei der Therapie von HPV-induzierter malignen Erkrankungen. Eine zukünftige präklinische Wirksamkeitsstudie mit einem adenoviralen-Prime- und einem MVA-Boost-Schema in persistent MfPV3-infizierten Makaken könnte den Weg für die klinische Entwicklung des vielversprechenden therapeutischen HPV16 Ii-E1E2E6E7-Impfstoffkandidaten weisen.

3 General Introduction

Human papillomavirus (HPV) are small, non-enveloped viruses comprising about 8 kb of histone-bond dsDNA genome (1) (Figure 1A). These viruses can be further subdivided into multiple genera, further into more than 200 types, with either cutaneous or mucosal tropism (2). Infections with mucosal HPV are most commonly transmitted sexually (3–5) and display the most common sexually transmitted infection worldwide. There are estimations that probably all sexually active individuals will be infected at least once in life (6). HPV is historically well known for its connection to cervical cancer since about 99% of all cervical cancers contain HPV DNA (7). Because of their likelihood of inducing cancer, HPVs are often characterized into high-risk (hrHPV) and low-risk (lrHPV) types (8,9).

The icosahedral virion is approximately 55-60 nm in size and is composed of 72 capsomeres, each assembled out of 5 late-1 (L1) protein molecules, each thereof resembling a beta-jellyroll core folding (10,11) (Figure 1A). Interestingly, the capsomeres are linked by disulfide bonds (12). Approximately 12 molecules of L2 proteins are embedded within the capsid (13). These L2 proteins are not fully surface-exposed (14) but become available for extracellular matrix binding and are cleaved by furin during infection (15).

The papillomavirus (PV) genome comprises several partially overlapping ORFs, which can be further divided into early and late regions (2) (Figure 1B). The virus protein expression is tightly regulated at the level of transcript expression and RNA editing and, therefore, dependent on alternative splicing and mRNA post-transcriptional processing (16,17) since all proteins are derived from three polycistronic pre-mRNAs.

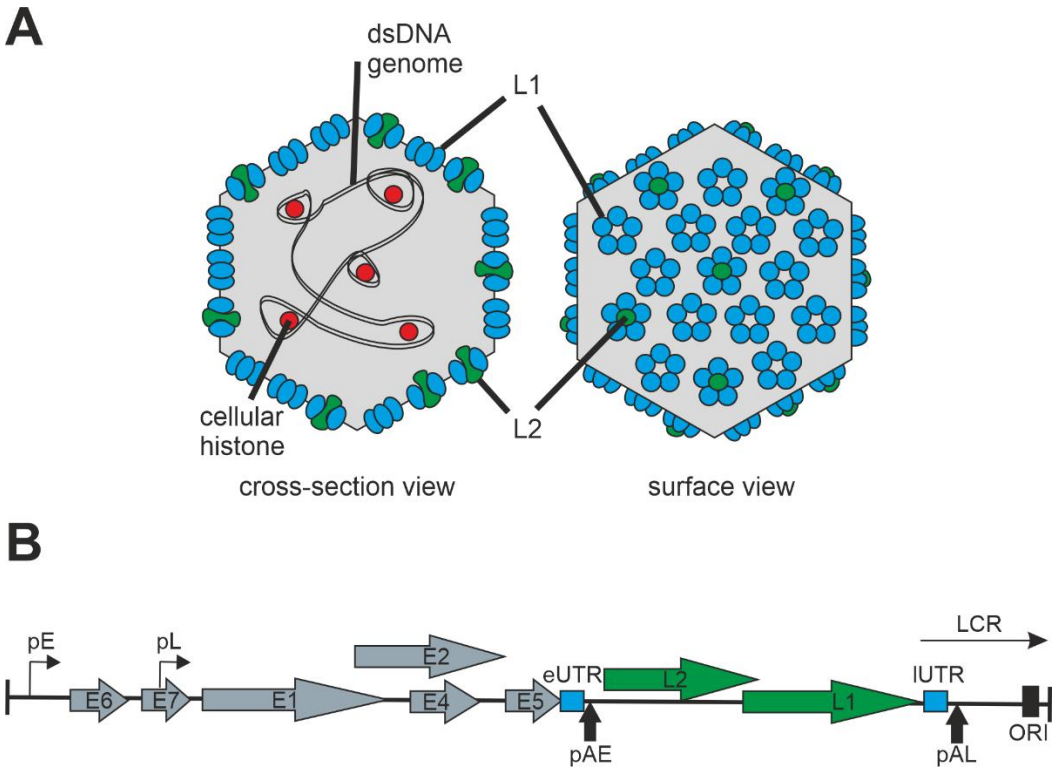

Figure 1: Schematic representation of PV virion and genome.
(A) Schematic representation of PV virion in cross section and surface view. Virus capsid is formed by the late (L) proteins L1 (blue) and L2 (green). Circular dsDNA genome is bound to cellular histones. (B) Linear representation of the genome based on HPV16. Early (E) proteins are colored in grey; late (L) proteins are colored in green; small black arrow indicate early (pE) and late promoter (pL); bold black arrows indicate early (pAE) and late polyadenylation site (pAL); block box indicate the origin of replication (ORI); small black arrow

indicate the long control region (LCR); blue boxes indicate early (eUTR) or late untranslated region (lUTR). Figure based on Johansson *et al.* 2013 (17).

3.1 Evolution of Papillomaviruses

The *Papillomaviridae* is a very old family, infecting possibly all mammals and other amniotes; therefore, ancestral PVs can be dated back to the Paleozoic age (18) (Figure 2A). Meanwhile, PVs are also detected in fishes (19), leading to the subdivision of the *Papillomaviridae* family into *Firstpapillomavirinae* and *Secondpapillomavirinae* (13), thus implying even older origins of the ancient PV. With the emergence of the first reptiles 350 million years ago and the accompanying changes in the epithelium of their ancestral host, these viruses started to coevolve with their respective host (18). About 200 million years ago, with the evolution of hair and sweet glands in mammals, PVs gained mucosal tropism.

Most of the PVs cause chronic asymptomatic infections (20). Even in immunocompetent individuals in the general population, HPV can be frequently isolated from skin swaps and plucked hair, leading to the assumption that HPV persists in the population as commensals (21,22).

Double-stranded DNA viruses show the slowest evolutionary rates among viruses (23,24), especially PVs (25). For the taxonomic categorization, the identity at the nucleotide level of the L1 gene was selected. One PV type is defined by more than 90% nucleotide identity within this gene (26). This threshold is restricted because of the multimodal distribution of the evolutionary distances among PVs (26–28). Despite the slow evolution, the PV diversity yielded in more than 200 types (18) (Figure 2B).

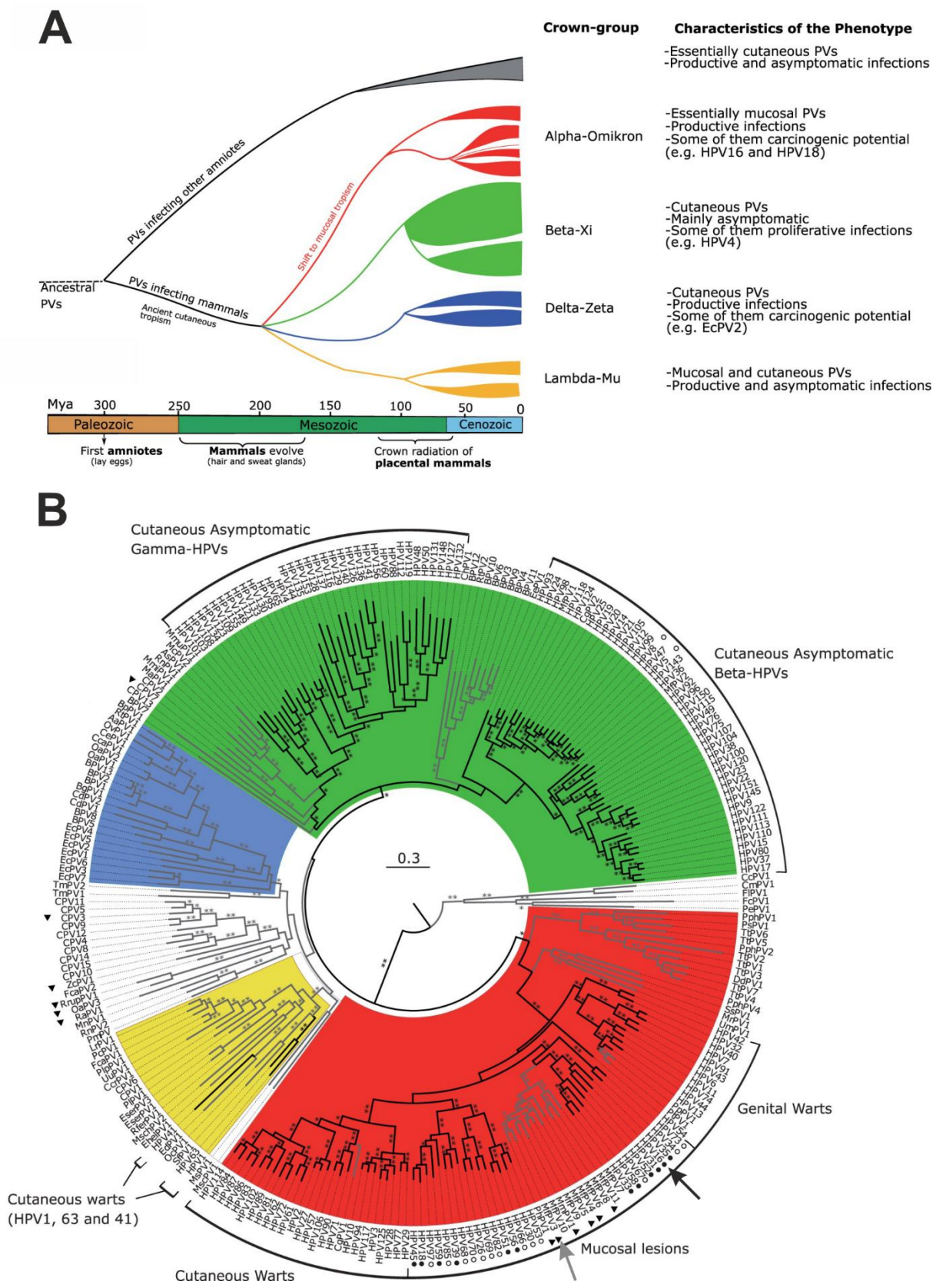

Figure 2: Evolution and diversity of PVs.
(A) Evolution of PVs with cutaneous and mucosal tropism. The evolution of hair and sweat glants triggered the separation of PVs into the crown groups based on their phenotypes. These crown groups further diversified with the evolution of mammalian radiation. The group of Alpha-Omikron PVs developed the ability to infect the mucosal epithelium. (B) Phylogenic tree of PVs. Black arrow indicate HPV16, grey arrow indicate MfPV3. Figure adapted from Bravo *et al*. 2015 (18) and further modified.

3.2 Epidemiology of HPV and HPV-Induced Disease

The *Alphapapillomaviruses* are the most characterized HPV genus since this genus is the most clinically relevant because of their infection of the oral and anogenital mucosa, therefore their induction of the HPV-related disease in non-immunocompromised individuals, and harboring most of the high-risk type, like HPV16 and HPV18 (8,13). In the following, if not mentioned elsewhere, HPV describes the matters related to human *Alphapapillomaviruses*.

HPV infection is one of the most frequent viral infections in the world and probably the most prevalent sexually transmitted infection, with an estimated nearly 300 million HPV-positive women worldwide in 2007 (29). In asymptomatic women, an HPV prevalence of 11.7% could be observed in 2010 (30). The prevalence was even higher in developing regions compared to developed regions (29,30). The highest infection rate could be observed in adolescent girls and young women (31). Similar global prevalence rates and transmission rates could be observed for genital HPV infection in men but without age differences (31). Asymptomatic infections are often featured by several HPV types, including HPV16 with just 3.2%, HPV18 with 1.4%, HPV31, and HPV58, each below 1%. With increasing disease severity, also the HPV detection rate increases (30). At cervical intraepithelial neoplasia grade 1 (CIN1, see chapter 3.6) the HPV detection positivity rate is between 50-70% (30), but in invasive cervical cancer the HPV detection positivity rate is between 90-100% (32), which mainly correlated with HPV16 (61%) and HPV18 (10%) (8).

According to the GLOBOCAN analysis, more than 600000 new cases of cervical cancer and 340000 deaths occurred in 2020, rendering cervical cancer the fourth most common type of female cancer. Most of these occurred in low- and middle-income countries (LMIC) (33,34).

HPV is not only responsible for cervical cancer, but it also causes other cancers in the anogenital tract, such as anal cancer (88%), vulvar cancer (43%), vaginal cancer (70%), and penile cancer (50%) (31), but also attributable for oropharyngeal squamous cell cancer (OPSCC). The latter displays an emerging threat.

Although the prevalence of head and neck cancer (HNC) has been decreasing within the last few decades, the incidence of HPV-positive OPSCC, a subgroup of HNC, has increased (35). OPSCC comprises cancers in the soft palate, uvula, tonsils, and base of the tongue. Depending on the study, the incidence of HPV-positive OPSCC is indicated between 38% and 70% (36–38), of which HPV16 is responsible for at least 85% (39). In fact, HPV-positive OPSCC displays one of the fastest-rising incidence rates in high-income countries (HIC) (40,41), and the incidence of OPSCC in men has even surpassed the incidence of cervical cancer in women in the UK and the US (40). On a global scale, the incidence of HPV-positive OPSCC is utterly higher in HICs compared to LMICs, despite the high incidence of HPV-associated cervical cancer in these countries (38).

3.3 HPV Replication and Function of Virus Proteins

HPVs can only infect cells in the basal layer of the epidermis and can only fully replicate in terminally differentiated keratinocytes. The HPV replication can be subdivided into three phases: (i) infection and establishment phase, (ii) genome maintenance, and (iii) differentiation-induced amplification (42) (Figure 3A).

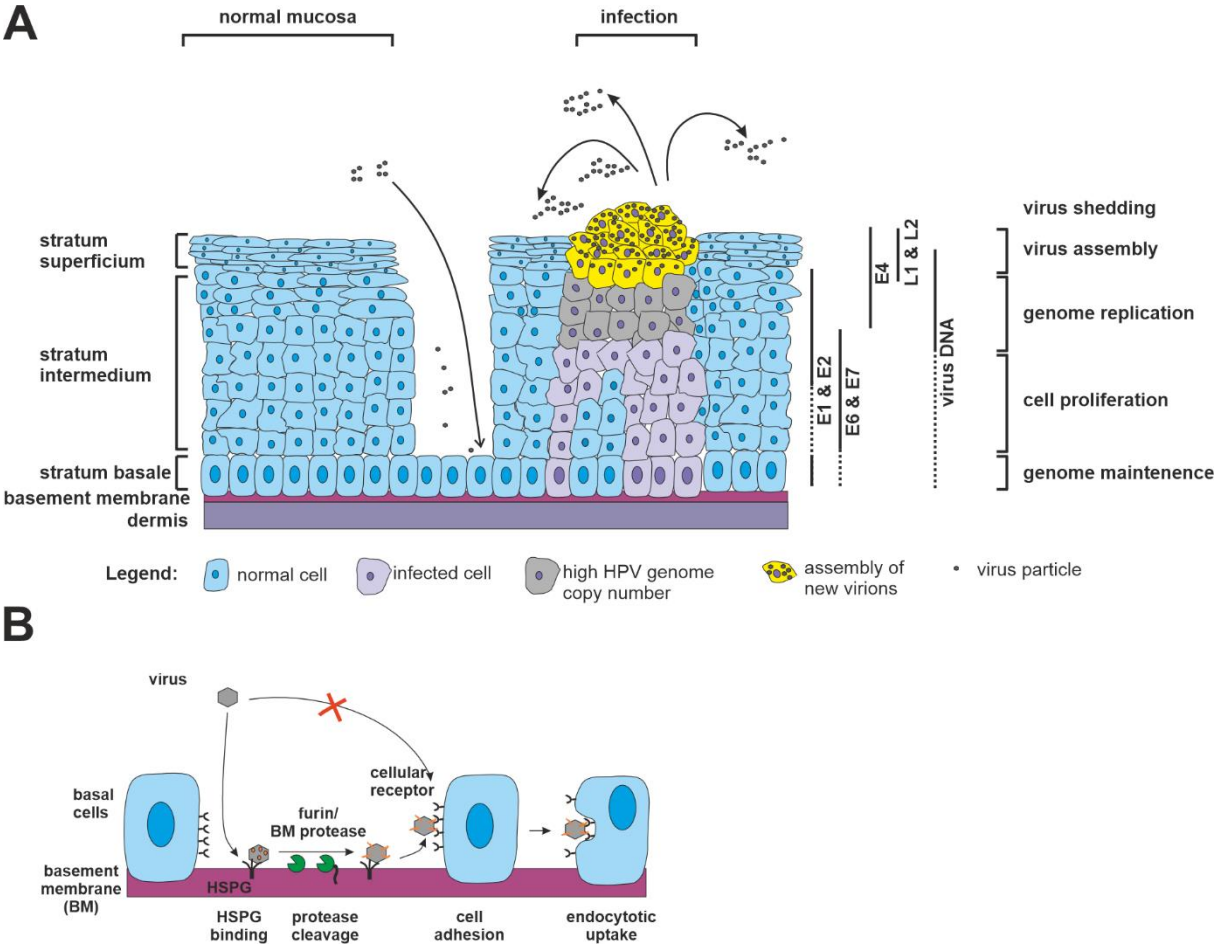

Figure 3: HPV replication in the mucosa.
(A) Schematic replication of HPV in the mucosa. Righthand panel indicate the expression of the different viral proteins and multiplicity of the viral genomic DNA, which is dependent on the differentiation state of the cell. Lines indicate high-level expression; dotted lines indicate low-level expression. Color code is explained in the legend. Figure based on Middleton *et al*. 2003 and Doorbar 2006 (43,44) (B) Infection of a basal cell by HPV. The virus cannot infect the basal cell directly but needs to bind to HSPG of the basement membrane (BM) via L1, thus leads to cleavage of L2 by furin or BM-protease. After cleavage, HPV can infect the basal cell. Figure based on Schiller *et al*. 2012 (11).

The virions get in proximity to the basal layer cells in the stratum basale through microabrasions or trauma within the epithelium. These allow the virions to bind via their L1 capsid protein at the heparan sulfate proteoglycan (HSPG) on the surface of the basement membrane (45) (Figure 3B). Subsequently, upon binding of L1 to HSPG, a conformational change in L2 is induced by cyclophilin B (46), which leads to exposure of the N-terminus of L2. This enables the proteolytic cleavage of L2 by furin or proprotein convertase 5/6, a prerequisite for virus uptake and internalization (15). Upon the cleavage of L2, a previously masked surface of L1 gets exposed that facilitates binding to the unknown receptor on the basal layer cells (15,45,47). Receptor engagement induces endocytosis of the virions. Acidification of the endosomes leads to degradation of L1. Via an unknown mechanism, L2 in a complex with the viral genome mediates its escape from the endosome and translocates into the trans-Golgi-network (48). Active cell division is necessary for the entry of the L2-genome complex into the nucleus. A prerequisite for nuclear localization of the L2-genome complex is the transient breakdown of the nuclear membrane in mitotic cells (49). Within the nucleus, the L2-genome complex associates with the promyelocytic leukemia nuclear bodies (PML bodies/ND-10), the site of PV DNA replication (50–52). Initial virus protein expression from the early promoter (pE, p97 in HPV16) leads to the expression of

viral replication proteins E1 and E2 (17) for an initial phase of genome amplification, prior to the maintenance of the viral DNA as an episome (49,53). For this, E2 binds to conserved sequence elements in the origin of replication (ORI) within the long control region (LCR) of the HPV genome, which further recruits E1, an ATP-dependent helicase (54). E1 thereby recruits the host DNA replication machinery (50,55), which leads to bidirectional replication, yielding about 50-100 episomal copies per cell (56). This initial amplification phase of the genome highly depends on E1 and E2 (42). The ability of E2 to bind to the cellular bromodomain-containing protein 4 (Brd4) and the minichromosome maintenance element (MME) can tether the viral genome to the host chromosomes and facilitate correct genome partitioning and segregation into progeny cells (57–59).

After cell division and migration of progeny cells into the suprabasal cell layer (stratum intermedium), a process of differentiation forces the progeny cells into cell cycle arrest. The oncoproteins E6 and E7, as well as E5, are transcribed from the early promoter pE, additionally to E1 and E2 (p97 in HPV16) (16,17). Expression of E6 and E7 in this cell layer circumvents cell cycle arrest by inactivating members of the retinoblastoma proteins (pRb) and the tumor-suppressor protein p53 (60). In uninfected cells, monophosphorylated pRb binds and inactivates the transcription factor E2F. As a consequence, the cell cycle cannot progress from the G1- to the S-phase. In mitotically active cells, pRb is hyperphosphorylated by cyclin D (CycD)-activated cyclin-dependent kinase 4 or 6 (Cdk4 or 6), which leads to the release of E2F. HPV E7 interacts with pRb, thus releasing E2F, which induces Cdk-independent cell cycle progression (60). The tumor-suppressor protein p53, also referenced as the “guardian of the genome” (61), is tightly regulated in normal cells by its negative regulator Mdm2 via binding to its activator domain and inducing ubiquitin-dependent degradation of p53 (62). P53, on the other way, works as a transcription factor of Mdm2. Therefore, low amounts of p53 are present in the cytoplasm under normal conditions. Upon activation of stress signal pathways (e.g., DNA damage, UV-irradiation), p53 is phosphorylated by several stress-induced kinases (e.g., ATM kinases), which prevents regulation by Mdm2. The protein accumulates, translocates into the nucleus, and activates cell cycle arrest-associated or apoptosis-associated gene transcription (62). HPV oncoprotein E6 inactivates p53 function and thus prevents cell growth inhibition and apoptosis of infected cells (60). This is further enhanced by E5, which is involved in koilocyte formation, a characteristic of HPV-infected cells (63), and enhances epidermal growth factor receptor (EGFR) signaling (60,64), optimizes genome amplification (65) and therefore contributing to the hyperproliferation of the cells. Consequently, the partially-differentiated keratinocytes of the stratum intermedium further undergo cell cycle progression, resulting in cell division. Therefore, HPV genome-containing cells expand within the epidermis towards the superficial layer.

The level of E2 is essential for the switch from early to late gene expression. Migration of the HPV16-infected cells towards the superficial layer results in differentiation-induced altered cellular gene expression, activating the late promoter (pL, p670 in HPV16) and enhancing the expression of E1, E2, and E4 (17). E4 prepares the cells for virus assembly, interacts with the cytokeratin, and plays a role in virus release (66–68). The increased levels of E1 and E2 promote genome amplification (69) and increase episomal genome copy number by approximately a factor of 100 (56). Transcription of E1 and E2 from both, early and late, promoters of the initial genomes and additional the newly synthesized genomes generate a positive feedback loop resulting in higher concentrations of E2. E2 works as a transcription repressor for pE and thus represses E5, E6, and E7 expression (17,70), and the infected cells fully commit to viral genome replication. The peaking levels of E2 additionally induce E2-binding to the early polyadenylation signal, resulting in transrepression of the pL-derived early proteins and inducing late protein expression, which pave the way for genome packaging (17,70). Cellular factors in

terminally-differentiated keratinocytes regulate the splice site in the bicistronic mRNA of the late gene product (17). The minor capsid protein L2 is expressed shortly before the expression of L1, which is necessary for the correct order of virus assembly. E2 recruits L2 to the viral genomes within the PML body-associated replication regions in the nucleus, thus resulting in an L2-genome complex. After the expression of L1, the infectious particles are assembled in the nucleus (52,64,69). PVs are non-lytic but simply shedding from the superficial cells, which is enhanced by the destabilization of cytokeratin by E4 (64,66,69).

3.4 Molecular Functions of hrHPV to Facilitate Dysplasia and Cancer Formation

The hrHPVs, compared to lrHPVs, evolved multiple mechanisms that facilitate the development of dysplastic lesions and cancer rather than self-limiting infections. These viruses have no lytic cell death and restrict high-level gene expression as well as virus replication to the upper layers of the epithelium, which contains only few immune cells. Still, only hrHPVs are involved in the manipulation of many pathways of, for example, immune regulation, cell growth, apoptosis, and angiogenesis, summarized as "hallmarks of cancer" (60,71–74) (Figure 4). Only the heterologous expression of hrHPV oncoproteins E6 and E7 ultimately immortalizes primary keratinocytes but not the oncoproteins of lrHPVs (1).

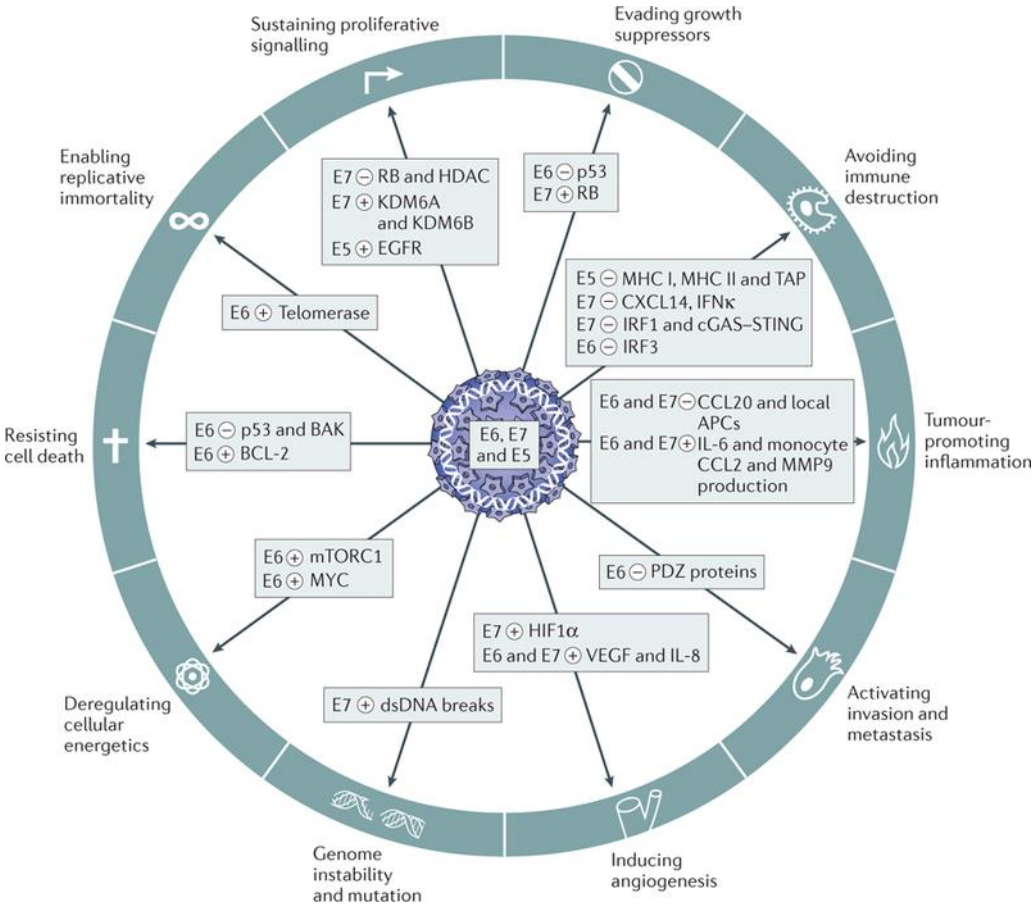

Figure 4: Molecular function of oncoproteins to facilitate malign transformation.
The viral proteins E5, E6 and E7 of hrHPV interact with several cellular pathways, which contribute to the development of malign transformation. The characteristics of these proteins are sorted by the "hallmarks of cancer" (74). The figure shows with which cellular components these viral proteins interact and how the cellular components are manipulated. Figure adapted from Roden *et al.* 2018 (71) under license (license number 5630110191784), *'Reproduced with permission from Springer Nature*' ©2018 Macmillan Publishers Limited, part of Springer Nature. All rights reserved. https://www.nature.com/articles/nrc.2018.13.

First of all, the mode of inactivation of p53 and pRb in hrHPVs is different compared to lrHPVs (60). Rather than inactivation by binding, hrHPV E6 protein leads to proteasomal degradation of p53 via the cellular ubiquitin ligase E6-associated protein (E6AP) (75–78). A similar mechanism is observed for E7, which can degrade pRb in a ubiquitin-dependent manner using the cullin-2 ubiquitin ligase complex (76,79,80). This prevents apoptosis, contributes to sustained proliferative signaling, and evades growth suppression (71).

Moreover, E6 of hrHPV can activate and upregulate the cellular telomerase (81–83), amongst others, by interaction with c-myc (84), which supports cell longevity during repeated cell division and enables replicative immortality (71). PDZ (PSD95/Dlg/ZO-1) proteins are involved in the signaling and regulation of differentiation, cell polarity and adhesion (85,86). E6 has a PDZ binding motif (PBM) at its C-terminus, which facilitates the binding and degradation of a panel of PDZ domain-containing proteins, especially in an E6AP-dependent manner (87,88). This is further involved in invasion and metastasis (71).

Besides pRb degradation, E7 of hrHPV is known to reprogram the epigenetics of the infected cell, which is presumed to be necessary for cell-cycle reentry and progression. The C-terminal zink-finger domain of E7 interacts with Mi2β, a component of the nucleosome remodeling and deacetylase complex (NuRD complex), which blocks histone deacetylase (HDAC) (72,89,90). Furthermore, E7 stimulates lysine-specific demethylase KDM6A and KDM6B (71,91) but also stimulate DNA methyltransferase 1 (DNMT1) (60,72), which induces methylation of many promoters of gene necessary for immune surveillance. Overall, these changes lead to extensive proliferation of the infected cells and dysregulation of immune signaling (72).

Dysregulation of the proto-oncogene EGFR, a receptor tyrosine kinase of the family of ErbB/HER, is often associated with the formation of cancer (92). Viral E5 of hrHPV can upregulate vascular endothelial growth factor (VEGF), cyclooxygenase 2 (COX-2), mitogen-associated protein kinase (MAPKs), and activating protein-1 (AP-1) by manipulating the correct EGFR signaling (60). This is achieved by stabilizing the EGF-activated EGFR, which displays increased phosphorylation, and through lower EGFR degradation by enhanced EGFR recycling from endosomal degradation (60). As a consequence, VEGF and hypoxia-inducible factor 1 α (HIF1α) are expressed, leading to angiogenesis. Furthermore, the Golgi-resident E5 leads to the retention of MHC-I and, therefore, compromises the processing and display of HPV-derived viral peptides on the surface of infected cells (93), preventing the recognition of $CD8^+$ T cells (94).

An important step towards malign transformation is the E7-induced mitigation of cellular DNA repair (60,71) and the introduction of extra centrosomes (95), which lead to genome instability and the acquisition of secondary mutations within HPV-infected cells (96).

E6 and E7 are also involved in the dysregulation of cellular energetics, especially by direct or indirect stimulation of the PI3K/Akt/mTOR (phosphoinositide 3-kinase/PI3K-/protein kinase B/mammalian target of rapamycin) cascade. Both proteins lead to active mTORC1, either E7, by binding the molecular inhibitor protein phosphatase 2a (PP2A) of Akt, thus keeping Akt active, or E6, by direct activation of Akt or indirect by degradation of tuberous sclerosis complex 2 (TSC2), an inhibitor of mTORC1 (60). The activation of mTORC1 activates protein translation, lipid and nucleotide synthesis, and especially inhibition of autophagy (60,71). Therefore, the simultaneous expression of E6 and E7 prevents autophagy of infected and transformed cells, which is even enhanced by E5 (60).

Lastly, the oncoproteins of hrHPV heavily influence the immune receptors and signaling to avoid recognition, especially by interference with cGAS-STING, TLR9, IRF1/3, STAT1/2, Tyk2 (60,71,72,97–99). The blocking of IFNκ, CXCL14, and CCL20 production inhibits the recruitment of antigen-presenting cells (APCs) to the infection site, prolonging the activation of adaptive immune response. E6 and E7 additionally lead to interleukin-6 (IL-6) secretion, which attracts monocytes to the infected tissue (71). Upon the production and secretion of CCL2 and matrix metalloprotease 9 (MMP9) by these monocytes, the building of a tumor-promoting inflammation starts, which also induces polarization and differentiation of monocytes to tumor-associated macrophages (TAM) and myeloid-derived suppressor cells (MDSC) (60,71,72).

3.5 Prophylactic Vaccines Against HPV Infection

Currently, three prophylactic vaccines are licensed (Gardasil® 4, Cervarix™, Gardasil® 9), which protect against persistent infection and neoplasia in the anogenital tract by the vaccine-types (100,101). Even if these vaccines are licensed for protection against anogenital HPV-derived malignancies, there are reports that the vaccines may have additional efficacy in preventing OPSCC. It could be found that non-vaccinated individuals have a substantially higher risk of developing OPSCCs compared to vaccinated individuals (102). The vaccines are based on the recombinant L1 protein and their ability to self-assemble into virus-like particles (VLPs) when expressed in different heterologous expression systems (71,101). Cervarix™ is produced in a baculovirus-based insect cell expression system, is adjuvanted with aluminum hydroxide and monophosphoryl lipid A, and comprises L1 of HPV16 and HPV18. Gardasil® 4 and Gardasil® 9 are produced in *S. cerevisiae*, are adjuvanted with aluminum hydroxyphosphate sulfate, and include L1 of HPV16, HPV18, HPV6 and HPV11 in the case of Gardasil® 4 and HPV16, HPV18, HPV6, HPV11, HPV31, HPV33, HPV45, HPV52, and HPV58 in Gardasil® 9 (71). Due to protection against HPV6 and HPV11, both Gardasil® vaccines protect against genital warts. It is widely accepted that neutralizing antibodies are the primary effector of protection (71). Many countries have included the prophylactic HPV vaccine in their vaccination program for young girls and also boys (103).

Although these vaccines provide strong protection from HPV-induced diseases and exhibit an excellent safety profile (71,100,101), vaccine uptake, even in HIC, remains incomplete and insufficient to stop vaccine-type HPV transmission ultimately (103,104). Persisting vaccination barriers, such as questioning vaccine safety by parents, socioeconomic factors, and lack of awareness, might keep vaccination rates insufficient (40,105–107).

Since the vaccines comprise only L1, a nuclear protein expressed in the uppermost surficial layers of the epidermis, the possibly vaccine-induced T cell responses are insufficient to eradicate infected keratinocytes in the basal and intermedium layer. Clinical trials have shown that L1-based vaccines have no direct therapeutic effect in already-infected individuals (108) but may protect against recurring infections (109). Thus, together with the approximation that prevention of primary infection by prophylactic vaccination may be impacting OPSCC incidence not until 2060 (110), leads to the urge for an effective therapeutic vaccine.

3.6 Development of HPV-Induced Dysplasia and Invasive Cancer

As mentioned before, most hrHPV from the *Alphapapillomaviruses* are associated with the development of cancers, especially cervical cancers (7). Given the high prevalence of hrHPV infections compared to cancer cases (see chapter 3.2), it is obvious that most infections are subclinical due to spontaneous clearance within a given time frame. Most infections are resolved within two years

without symptoms. Nonetheless, some hrHPV infections become persistent, which can further acquire and accumulate more mutations over time, leading to the development of dysplasia in the squamous cells of the cervical epithelium and further progress to cancer (111,112). These persistent hrHPV infections are the primary factor for the development of such malignancies (112). Without successful clearance of cervical hrHPV infection, such lesions are able to progress to a cervical intraepithelial neoplasia grade 1 (CIN1), which can progress further to CIN2, CIN3, and invasive cervical cancer (113,114). The CIN grade reflects the severity of the dysplasia. Histologically, this can be detected by the extent of basal cell-like cells growing and penetrating into the suprabasal cell layers towards the surface of the epithelium and by the number of suprabasal cells undergoing proliferation (115). Additional to categorization into the CIN system, cervical dysplasia is also characterized by the Bethesda classification system, in which CIN1 is equivalent to low-grade squamous cell intraepithelial lesion (LSIL) and CIN2 and CIN3 are equal to high-grade squamous cell intraepithelial lesion (HSIL) (115,116).

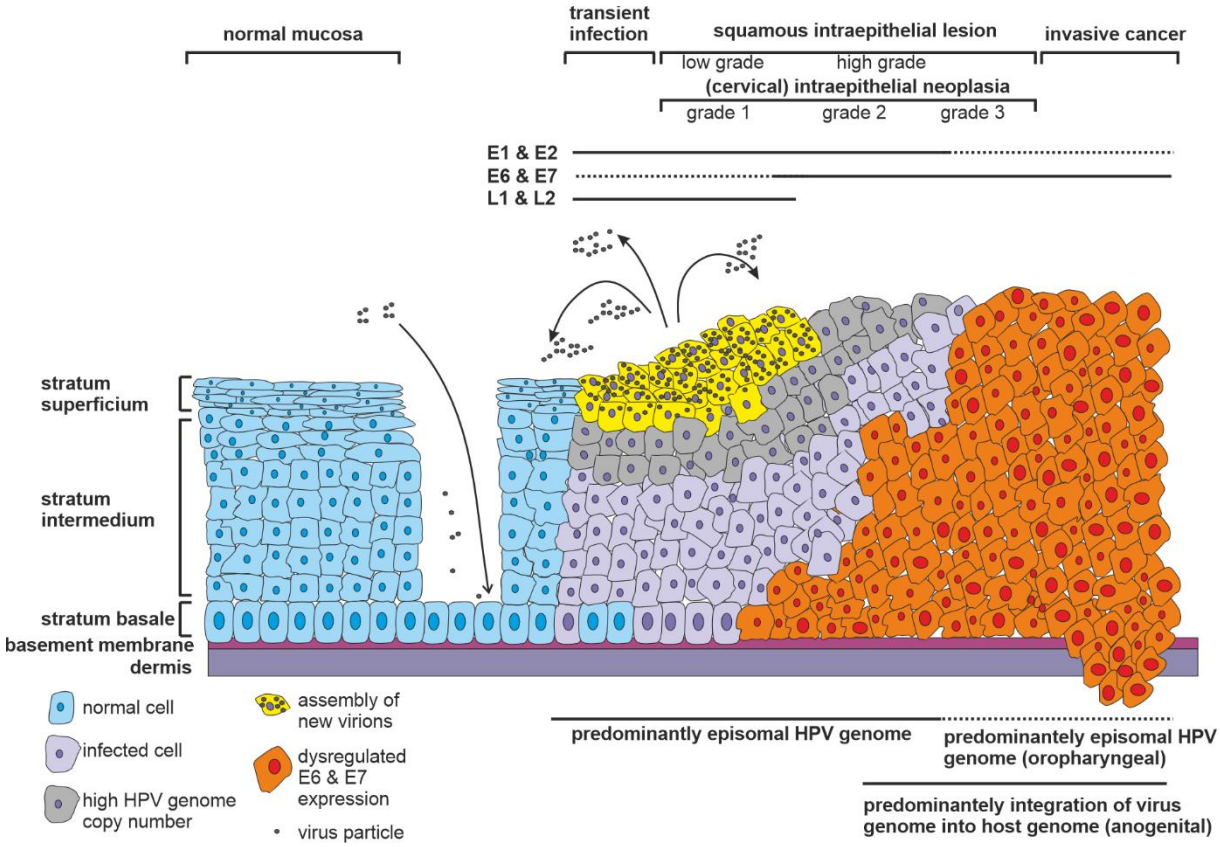

Figure 5: Development of HPV-induced dysplasia and invasive cancer.
Schematic representation of the cellular and molecular events during development of HPV-induced dysplasia and invasive cancer. Upper panel indicate the expression of the different viral proteins within the different stages of dysplasial. Lines indicate high-level expression, dotted lines indicate low-level expression. Color code is explained in the legend. Figure based on Crosbie *et al.* 2013, Doorbar 2006, Doorbar *et al.* 2015 (44,64,117).

Within the progression of the dysplasia, the virus protein expression shifts (43) (Figure 5). Low-grade lesions (CIN1/LSIL) characteristically exhibit still productive infections featured by koilocytes in the suprabasal cell layers and the expression of virus capsid proteins in the superficial cells (43,115). In contrast, high-grade dysplasia (CIN2/3, HSIL) features more extensive proliferation of the basal cell-like cells in the suprabasal cell layer in combination with the loss of productive replication (43). An essential step in the formation of high-grade lesions is the dysregulated overexpression of the

oncoproteins E6 and E7, thus leading to enhanced proliferation. Based on the molecular features of the oncoproteins (see section 3.4), the enhanced cell division and long-lasting uncontrolled cellular replication, in combination with dysregulated cellular pathways and genome maintenance, lead to the accumulation of secondary mutations in the host genome and can promote cancer progression (96,118,119).

The dysregulated oncoprotein expression is mainly derived by one of two factors: epigenetic modification of several genes or integration of the viral genome into the host cell genome (1). Different methylation of the LCR suggested de-regulated promoter usage through epigenetic changes, which hinders full virus replication (120). Since E7 has an influence on several important factors involved in DNA methylation, this might even be aggravated by the dysregulated oncoprotein expression (91). On the other hand, the above-mentioned genomic instability can lead to the viral genome integration into the host genome (121,122). Integration within the E1 or E2 ORF can disturb the productive replication of hrHPV, and the virus replication is trapped in the uncontrolled proliferation phase because of the de-repressed expression of E6 and E7. There are type-specific differences in the integration frequency (123). Cervical carcinomas result from integrated HPV16 sequences in approximately 70%, wherein HPV18 is integrated in almost all cases of cervical cancer (124–128). There are other HPV types, which are inducing cancer without integration (123,129).

HPV-induced malignancies are not restricted to cervical cancer but can also be found in other areas of the anogenital tract, like the vulva, vagina, penis, and anus, and additionally in the oropharynx (64). Similar to dysplasia in the cervix, it can be detected that intraepithelial neoplasia and pre-cancerous lesions are developed at all sites of anogenital infection regions, which are equally referred to as penile, vulvar, anal, or vaginal intraepithelial neoplasia (PIN, VIN, AIN, or VaIN) and exhibit similar histologic abnormalities (64,130,131). Contrary to anogenital cancer development, it is highly discussed whether HPV infections in the oropharynx induce such neoplasia due to the absence of detectable pre-cancerous lesions and a different histological composition in the tonsillar crypt (38,132,133).

Interestingly, there are different details regarding the integration frequency of HPV16-specific DNA sequences in HPV16-positive OPSCC. Data from whole-genome sequencing found viral integration in 74% of patients (134), similar to the data for cervical cancer (123). In contrast, in other studies, more than 70% of the HPV16-positive OPSCCs contained the virus in episomal form (135–137).

The direction of developing invasive cancer from persistent HPV infection via ascending grade of dysplasia is not a one-way drive (Figure 6). In fact, most CIN1 (57%) regress within short time frame (138). About one-third of cases persist in CIN1 without regression or progression. According to longitudinal studies, the development of CIN3 induced by hrHPV proceeds relatively fast within a time frame of 3-5 years (139). Progression from CIN3 to invasive cancer, on the other hand, takes up to several decades (10-20 years), with a rising chance for progression the longer the persistence lasts (130). Depending on the study, progression of CIN3 occurs in more than 12% (138) or up to 30-40% (140).

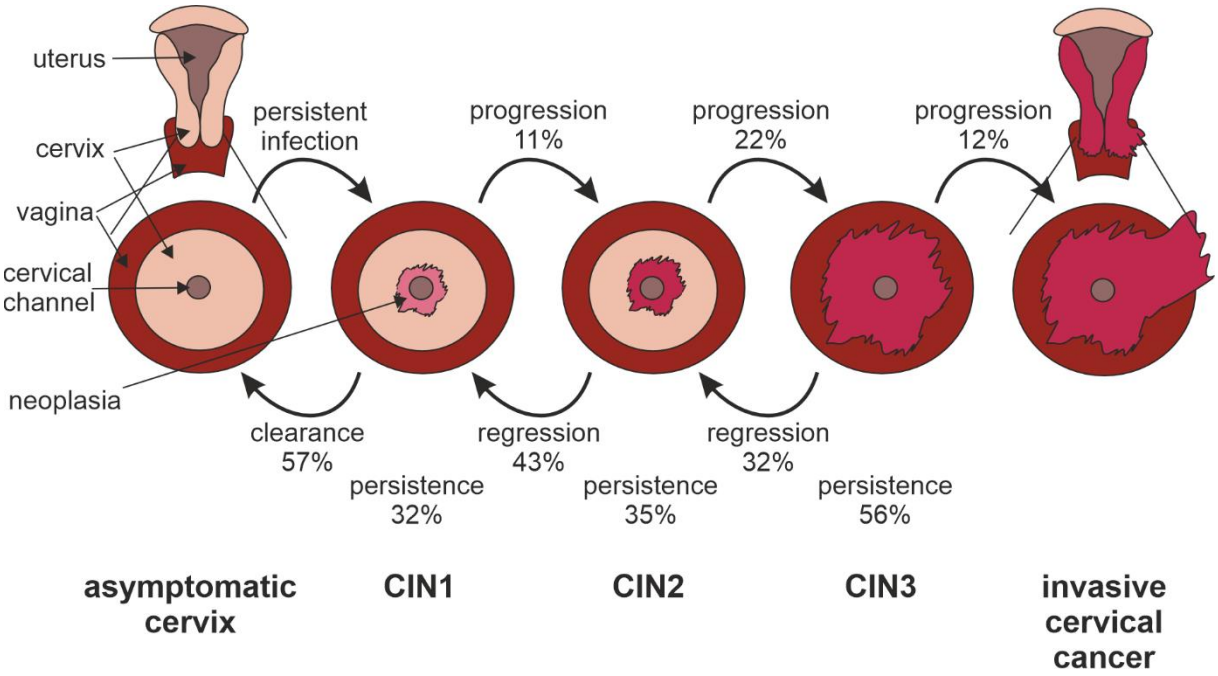

Figure 6: Natural regression and progression rates of CIN.
Schematic and simplified representation of the dynamic development of CIN as seen by colposcopy. Percent numbers indicate the natural rates of progression, regression and persistence at the indicated CIN stage as published by Östor (138).

Most persistent infections or dysplasias are eliminated or cleared by cell-mediated immune response (141,142). An animal model using the canine oral papillomavirus (COPV) and the rabbit oral papillomavirus (ROPV) showed regression of PV-induced malignancies is connected to $CD4^+$ T cell responses with a dominant T_H1 phenotype (143–145). In the human context, it could be observed that T cell responses against HPV early proteins correlate with regression, or at least with lack of progression to cervical cancer (146–154). Although some studies highlighted the importance of $CD8^+$ (146,147) and $CD4^+$ (148) T cell responses against E6 and E7, newer studies showed that T cell responses, especially $CD4^+$, against E2 are frequently detected in the clearance of CIN or VIN (149–152,154) whereas $CD8^+$ T cells against E6 render non-functional and resulting in CIN progression (148,150). In the case of terminally progressed carcinomas, tumor-infiltrating lymphocytes (TIL) seem to be a correlate of improved outcomes in cervical cancer patients (155–157). An important aspect is whether these findings in anogenital HPV-positive malignancies are directly transferable to OPSCCs. Due to the anatomical site, the tumor microenvironment of cervical cancer and OPSCC is slightly different (158). OPSCCs have a higher $CD4^+$:$CD8^+$ ratio, which reflects higher amounts of $CD4^+$ in the tonsils than in the anogenital epithelium (158). The circulation of E7-specific $CD8^+$ T cells in the blood is associated with more prolonged disease-free survival (159). Additionally, E6- and E7-specific $CD4^+$ TILs with T_H1/T_H17 polarization, resulting in the secretion of IFNγ, TNF, IL-2, and IL-17, are demonstrated to improve disease-specific survival in HPV-positive OPSCCs (160).

Several non-HPV factors contribute to the risk of cancer development: Early onset of sexual intercourse, several sexual partners, exposure to mutagens, e.g., cigarette smoking and alcohol, mutagenic infections, long-term use of oral hormonal contraceptives, immunosuppression, especially HIV infection, and genetic predisposition (1,130).

3.7 Therapeutic Vaccination

In contrast to prophylactic vaccination, therapeutic vaccination does not intend to prevent infection but instead delivers tumor antigens to establish or enhance the immune response against these antigens to eradicate tumor cells (161). It is, therefore, in the context of cancer, a type of immunotherapy that is distinct from other immunotherapeutics, which solely rely on, for example, oncolytic viruses, monoclonal antibodies, cytokine therapy, or adoptive cell transfer (161). Instead of neutralizing antibodies, cell-mediated responses are intended to be mounted by a therapeutic vaccine, aiming to induce a strong tumor-specific T_H1 response (162,163). This includes cytotoxic $CD8^+$ T cells (CTLs) that are able to eradicate (tumor-) antigen-expressing cells but also $CD4^+$ helper T cells for enhanced CTL activation and maintenance without the excessive induction of regulatory T cells (163–165). Vaccinating against tumors requires either a tumor-associated antigen (TAA) or a tumor-specific antigen (TSA). TAA and TSA differ regarding the origin of the antigen. TAA are self-antigens associated with high expression in certain tumors but are regulated by self-tolerance, whereas TSA is entirely specific to tumors (161).

3.7.1 Therapeutic Vaccination Against HPV-Induced Malignancies

Standard of care (SOC) therapy of HPV-induced cervical cancer and OPSCCs, including surgery, chemotherapy, or radiation, often with combinations of these to form a multimodal therapy, have high success rates (38,161,166). The burden of such therapy is high, with severe side effects ranging from xerostomia and dysphagia to rarely occurring long-term gastrostomy-tube dependence, osteoradionecrosis, and treatment-related death (161,167). Treatment of cervical lesions by conization (e.g., cryoablation and loop electrosurgical procedure (168)) is also related to side effects, resulting in bleeding (169), an increased risk of adverse pregnancy outcomes (170,171) and has a high chance of lesion recurrence (166,172).

The unique feature of HPV-induced dysplasia and cancer compared to other frequently occurring human cancer entities is the presence of the two viral-derived oncoproteins, E6 and E7. In fact, HPV-transformed cells are rendered dependent on continuous oncogene expression to avoid cell-cycle arrest and apoptosis (173). Both proteins are defined TSAs that can be used to develop a therapeutic vaccine (161,163) since these are only expressed in HPV-infected or HPV-transformed cells. Furthermore, reduced or non-existing T cell responses against HPV are found in cervical cancer patients (152,153). Many attempts were made to generate a therapeutic vaccine targeting E6 and E7 with multiple approaches of delivery (174), either nucleic acid-based, viral vector-based, or peptide-based (38,161,163,166). Some approaches, especially a peptide-based approach using the synthetic long peptide (SLP) vaccine candidate, showed early clinical success against pre-malignant dysplasia (166,175), but these approaches weren't sufficient to durably combat cervical cancer or OPSCCs (38,161,163,166,176). Most of these approaches induced strong cellular immunity but were stuck in clinical testing due to low or mediocre primary overall response rates (38,161).

Besides E6 and E7, most early proteins haven't been used frequently in attempts to generate a therapeutic vaccine, despite the essential roles of E1 and E2 in virus replication (see chapter 3.3) and contribution to cancer development (177,178). Based on older data, it was assumed that HPV-induced cancer mainly integrates via the E2 ORF, which leads to the abrogation or at least downregulation of E1 and E2 expression in advanced lesions and cancers (121,122,179). However, newer studies confirmed that HPV-induced tumors may also arise from non-integrated (135–137) or partially integrated virus genomes (180), indicating the relevance of E1 and E2 as TSA (180). In fact, high mRNA

levels of, and antibody titers against, E1, E2, E4, and E5, on top of E6 and E7, could be measured in OPSCC patients (181–183). With this pioneering data implying the persistence of these proteins, more studies were undertaken to study the relevance of additional early proteins in advanced cancers. It was found that episomal HPV-induced OPSCCs can highly express E2 in OPSCCs (184), but in the case of integration that led to disruption of E2 expression, an unfavorable prognosis is connected (185,186). Furthermore, patients with cervical cancer have present T cell responses against E1, which correlated with improved prognosis (187). Moreover, in HPV-positive OPSCC patients with $CD8^+$ and $CD4^+$ T cell responses against E1, E2, E4, and E5 could be identified (188,189), with responses against E1 where most frequently detected (188). Most recent studies indeed provided evidence for robust T cell responses against HPV16 E1 and E2 in HPV-positive OPSCC patients (190) and against E1 of HPV16, 18, 31, and 45 in HPV-positive cervical cancer patients (191). Deep-proteome analysis revealed that E1 was consistently expressed in the analyzed cohort, emphasizing a central role in the potential therapy of HPV infection-derived cancers (191). Furthermore, the fact that the T cell responses were highly expanded in patients and shared across the OPSCC patients led to the conclusion that E1 and E2 may be good candidates for inclusion into novel therapeutic vaccine candidates (166,190). One of these novel candidates is 5GHPV3, a computationally calculated antigen comprising conserved sequences of E1, E2, E4, E5, E6 and E7 of 5 HPV types (16, 18, 31, 52, 58) (192), which recently started clinical development under the name VTP-200 (NCT04607850).

3.7.2 Non-Human Primate Model for Therapeutic Vaccination Efficacy Trials Against Genital PV Infection and Lesions

Replication of PVs is highly host-restricted (193), which hampers the development of a therapeutic vaccine against HPV. Mouse model systems based on C57BL/6 mice can be exploited for cancer treatment when inoculated with TC-1 or C3 cancer cells. TC-1 cells are C57BL/6 primary lung cells, which are transformed with HPV16 E6 and E7 together with activated human Ras (194). Contrarily, the lesser used C3 model are embryonic C57BL/6 cells, transformed with the whole HPV16 genome and an activated human Ras (195). Unfortunately, these models are limited only to direct cancer treatment and cannot resemble the development of sexually transmitted PV-induced persistent infection and pre-malignant dysplasia. Historically used animal PVs such as bovine papillomavirus (BPV), cottontail rabbit papillomavirus (CRPV), COPV, and ROPV are also no attractive models, mainly due to costs, tissue tropism, or resemble less relevant lrHPV infections (193).

The *Macaca fascicularis* papillomavirus type 3 (MfPV3) offers an exception. These viruses are naturally circulating in the *Macaca fascicularis* (cynomolgus macaques) population as a sexually transmitted disease (196). MfPV3 has a very close genetic, phylogenic, and phenotypic relationship to HPV16, particularly sharing a most recent common ancestor and featuring a similar origin of carcinogenesis (196–199). In fact, naturally occurring infections with MfPV3 can induce persistent infections, which can lead to CIN1-like lesions in the cervix (199,200). Therefore, persistently MfPV3-infected *Macaca fascicularis* is an ideal and valid model to evaluate the efficacy of a therapeutic vaccine against PV-induced genital lesions. A previous study demonstrated MfPV3 clearance in therapeutically vaccinated MfPV3-infected animals, however, without statistical significance due to high virus clearance rates also in the control group, which underlines the relevance of this model but also indicates substantial spontaneous clearance rates (201).

3.7.3 Considerations for the Generation of an Improved Therapeutic Vaccine Approach

The effectiveness of a therapeutic vaccine can be influenced by multiple circumstances, especially by the selection and composition of antigens included in the therapeutic vaccine candidate and the choice of HPV types included, predominantly if whole proteins or just conserved epitopes are comprised. Moreover, the therapeutic vaccine might be highly influenced by adjuvants included in the possible candidate, the vector that delivers the antigens, and last but not least, the potential combination with SOC therapeutics.

3.7.3.1 Inclusion of E1 and E2

The proteins E1 and E2 are expressed throughout most of the replication cycle of PV (see chapter 3.3). As described in the previous chapter, novel investigations have found rigid T cell responses against E1 and also against E2 in cervical cancer and OPSCC, which renders these antigens relevant for future vaccine designs (166,190,191). Additionally, there are reports regarding the BPV1 E1 protein, which show that E1 is an unstable protein that is quickly degraded (202,203). This might influence the early onset of T cell responses (166). Furthermore, E1 and E2 (649 and 365 residues, respectively) are notably bigger proteins than E6 and E7 (158 and 98 residues, respectively) (190). This possibly increases the chance of getting peptides processed and loaded on the diverse HLA molecules displayed by the broad human population, which could reduce the number of non-responders.

3.7.3.2 Multivalent or Type-Specific Approach

All three prophylactic vaccines against HPV are multivalent vaccines that target up to nine different types of HPV (71). Generating such multivalent vaccines is advantageous in terms of production costs and coverage against potential infections by multiple HPV types. However, there are also numerous downsides of multivalent vaccines, mostly in regards to weakening the immune response to the single type-specific antigens in favor of broad immune responses towards all antigens in such multivalent vaccines. This is in particular due to immune competition, basically through epitope competition, immune interference, immunodominance of specific epitopes, antagonistic effects between epitopes, and maybe also overburdening of the immune system (204–208). Nevertheless, the principle of a multivalent vaccine was also addressed by a therapeutic vaccine candidate comprising conserved elements of five HPV types to broaden the immune response by gaining cross-reactive T cells (192). However, a study using ancestral sequences of E1 and E2 derived from MfPV3 and multiple HPV types showed that high sequence similarity (>90%) is needed for rigid cross-reactivity of T cells (197). With this in mind, the generation of a type-specific therapeutic vaccine might be more efficient without compromising the immune response against the broad coverage of possible peptides of a particular HPV type in favor of the reduction to conserved epitopes shared between different HPV types. This is also bolstered because many national screening programs are changing towards detecting hrHPV infection rather than detecting cervical dysplasia (209,210). This is advantageous in terms of risk assessment towards CIN progression (211,212), enables treatment against infection rather than dysplasia, and strikingly generates an opportunity for type-specific treatment.

3.7.3.3 Molecular Adjuvant

To enhance the immune responses against the immunogenic components of a vaccine, adjuvants are included regularly (213). Especially co-administration of immune-stimulatory components of the innate immune system is often used to bolster cellular immune responses (214–216). An improved version of such genetic adjuvants is the direct fusion of the antigen of interest to one or multiple such elements in order to work as a cis-acting molecular T cell adjuvant (217). One of these molecular T cell adjuvants is the MHC class II-associated invariant chain (Ii). Intended initially to enhance $CD4^+$ T cell

responses upon vaccination with adenoviral vectors, it could be observed that $CD8^+$ are enhanced (218). Moreover, it could be demonstrated that cellular immune responses are enhanced in mice, non-human primates, and humans upon vaccination of viral vector-shuttled, Ii-fused antigens (218–223). Despite the proven efficacy of N-terminal Ii-fusion in order to enhance T cell responses, the mechanism of this molecular adjuvant is only investigated rarely. Enhancement of $CD4^+$ T cell responses seems to be induced due to trafficking to the endolysosomal compartments (221). However, the mode of action on how $CD8^+$ T cell responses are enhanced is an open question. This effect is not dependent on the enhanced $CD4^+$ T cell responses (222) but presumably rather due to improved MHC-I loading (221) upon faster degradation (220).

3.7.3.4 Viral Vectors as Vehicle

There are different methods for administering antigens for the purpose of a therapeutic vaccine. DNA vaccine vectors are working quite well to induce cellular immune responses and are a good and fast vehicle to evaluate the immunogenicity of antigens initially (216,224). However, immunogenicity with regard to the induction of cellular immune responses of DNA vaccine vectors is generally inferior compared to viral vectors (217,225–228). In general, the most important viral vectors in therapeutic vaccination are adenoviral and poxviral vectors.

3.7.3.4.1 Adenoviral Vectors

Human adenoviruses (Ad) are a large family of non-enveloped, dsDNA viruses (73). Original, Ad are pathogenic viruses that naturally can induce often-mild respiratory, gastrointestinal, urinary tract, or eye infections (229). For the use of Ad as viral vectors for vaccination, gene therapy, and immunotherapy, the viruses are genetically modified, particularly by inserting the antigen and deleting essential virus protein that renders these vectors replication-deficient (225,230). Ads have high packaging capacity, an excellent immunogenicity profile, and a merely good safety profile and can infect dividing and non-dividing cells (230–234). Regarding the safety profile of Ads, the Ad-based vaccines against SARS-CoV-2 showed ultra-rare cases (1 of 100.000) of vector-induced thrombotic thrombocytopenia (VITT). This severe adverse event had a fatality rate of 23-40% (230). However, an important aspect of adenoviral vectors is their simple and easy construction on HEK293 cells, easy purification as well as high production yields (235).

The most studied adenoviral vector is Ad type 5 (Ad5) (225). Ad5 performs excellently in animal experiments, but unfortunately, pre-existing immunity renders Ad5 inefficient in humans. Such vector immunity, caused by the presence of neutralizing antibodies, can be found in up to 90% of individuals in some regions (236,237). Such vector immunity also hampers repeated administration of the same serotype of adenoviral vectors (238). An additional disadvantage of Ad5 is this viral vector can only transduce cells efficiently if these cells express the coxsackie virus and adenovirus receptor (CAR) (239).

In the last years, more and more Ads were established as viral vectors, such as Ad26, Ad35, and Ad19a/64, as well as animal-derived chimpanzee Ads (ChAd3, ChAd63, and ChAdOx1), all demonstrating good immunogenicity and reduced natural vector immunity (225,230,237,240–246). Multiple adenoviral vectors were used to develop a prophylactic vaccine against SARS-CoV-2, either in a homologous or heterologous prime-boost regimen. These are homologous Ad26 prime and boost (JCOVDEN) (247), homologous ChAdOx1 prime and boost (Vaxzevria) (248), and heterologous Ad26 prime with Ad5 boost (GAM-COVID-Vac) (249). Particular attention should be given to Ad19a/64. Named initially with 19a and later classified as serotype 64 (250), this virus is associated with keratoconjunctivitis and display a seropositivity rate below 20% (251–254). This virus has a comparable potent transgene expression as Ad5 and induces a similar magnitude of T cell responses as Ad5 (255).

Moreover, Ad19a/64 is not dependent on CAR but infects cells via sialic acid, giving the viral vector a broad tropism and allowing transduction of, e.g., dendritic cells (DC) (256–258). Due to its exceptional characteristics, Ad19a/64-based viral vectors can be a promising alternative to Ad5-based viral vectors, mainly because of the induction of mucosal immunity (259,260).

3.7.3.4.2 Poxviral Vectors

Poxviral vectors have a long history in vaccination. Originally used to eradicate smallpox (261), descendants of the Vaccinia strain are now used mainly as recombinant poxviral vectors (262). It was long time presumed that the Vaccinia strain derived from cows (Latin: *vacca*), but newer analysis provided similarities towards other poxvirus strains and traced back to rodent or equine origin (263). Advantages of poxviral vectors include exceptional high packaging capacity, exclusive replication in the cytoplasm, high immunogenicity, and lack of persistence (225–227,262,264). Albeit strong attenuation of Vaccinia-derived poxviral vectors, multiple attempts were taken to reduce the virulence of the virus (265,266), which led to the attenuated New York Vaccinia Virus (NYVAC) (267) and Modified Vaccinia Virus (MVA) (268). MVA was generated by passaging the Chorioallantois Vaccinia Virus Ankara (CVA) by over 500 passages on primary chicken embryo fibroblasts (CEF) (268–270). Because of this extensive passaging, multiple deletions and several mutations occurred in the virus (271,272), which rendered MVA replication-incompetent in most mammalian cells (273–276). Due to its use against smallpox at the end of the smallpox vaccination campaign (277) and its current license as a prophylactic vaccine against the monkeypox virus (278,279), MVA has a proven clinical track record with an exceptionally high safety profile (277). Moreover, since MVA is fully attenuated and cannot replicate in human cells, this viral vector can also be administered in immunocompromised humans (280). The generation of recombinant MVA (rMVA) is a rather complex procedure, which is facilitated by the homologous recombination of a transgene of interest within a suitable shuttle vector into the poxvirus genome (281). Such rMVA are able to elicit high B and T cell responses and are therefore a versatile vector platform (282,283). An example of an approved rMVA-based vaccine is MVA-BN-Filo (284), which is approved in combination with an adenoviral vector (Zabdeno) as a prophylactic vaccine against Zaire ebolavirus (285). Moreover, rMVA with a SARS-CoV-2 spike protein as transgene is currently in preclinical and clinical development (286). In addition to prophylactic vaccines, rMVA is also investigated as a potential vector platform for immunotherapeutics and therapeutic vaccines (192,225–227,287–289).

Classically, clinical grades of rMVAs are generated and produced on primary CEF cells, which is quite demanding in terms of high production scale. Recently, a novel cell line, AGE1.CR pIX was established, which facilitates high replication of MVA and, therefore, high yields of the poxviral vector (290). Moreover, this cell line allows the production of rMVA with pharmaceutical quality (GMP-compatible). Interestingly, serial passaging of MVA on this cell line led to a novel MVA virus strain, MVA-CR19, which has an even enhanced replication rate on AGE1.CR pIX suspension cell line, and therefore streamlines the production of MVA-based poxviral vectors (291,292). CR19 has shown high immunogenicity in multiple small animal models (293,294). Hencefore, CR19 is a potent poxviral vector for generating and large-scale production of future poxviral vector-based vaccines.

3.7.3.5 Immune-Suppressive Microenvironment and Combination Therapy

Therapeutic vaccination against solid tumors might be weakened significantly because of the infiltration of suppressive immune cells, e.g., TAM, MDSC, regulatory T cells (T_{reg}), into the tumor. This may antagonize the HPV-specific T cell responses (163,295). A possible way to tackle this obstacle might be the co-administration of specific immune checkpoint inhibitors (CPI) and therapeutics to

regulate T cell regulation and the tumor microenvironment (161,163). Certain CPIs are approved against recurrent and metastatic OPSCCs (296–298). This eased the combination of clinical trials to test the co-administration of CPIs and therapeutic vaccines to deescalate SOC therapies. Currently, multiple attempts using therapeutic vaccine candidates combined with anti-PD-1 (programmed cell death 1) show initial results in preclinical and clinical settings (166,299–301). Moreover, a combination of therapeutic vaccination and administration of chemotherapeutics, like cisplatin, might be beneficial, as cisplatin possibly induces infiltration of beneficial DCs into the tumor (302). A lack of DCs, which serve as APCs, is associated with $CD8^+$ responses that cannot effectively treat the cancer (303). Such combination therapy is shown to increase anti-tumor response with expanded antigen-specific $CD8^+$ TIL and APCs but with reduced numbers of MDSCs (304).

4 Objective of this Thesis

As outlined in the previous chapters, T cell responses against the early proteins of HPV are beneficial in all stages, from infection to invasive cancer (146–154,187). Therefore, a therapeutic vaccine would be urgently needed, not only to treat cancer and deescalate current OPSCC and cervical cancer SOC therapy but also to regress anogenital dysplasia or at least prevent the progression of these.

Hence, the overall main objective of this thesis is to generate antigens for novel therapeutic vaccine candidates against PVs, which include the oncoproteins E6 and E7, but also E1 and E2 in order to expand the possible breadth of T cell responses (166,190,191) and the subsequent characterization of these antigens.

Such therapeutic vaccine candidates should be generated based on (i) the model virus MfPV3, which enables future efficacy testing of the best-in-class vaccine candidate in the pre-clinical persistently infected *Macaca fascicularis* animal model, and (ii) the most clinically relevant HPV type, HPV16, to streamline the clinical development of a therapeutic vaccine candidate. Additionally, the antigen design of potential therapeutic PV vaccines should include the molecular T cell adjuvant Ii. Moreover, including the oncoproteins E6 and E7 might induce the risk of transformation due to the integration of the therapeutic vaccine nucleic acid into the vaccinee's genome (305). In order to generate a safe vaccine comprising E6 and E7, these oncoproteins must be engineered by several amino acid substitutions in a balanced way that inactivates the oncogenic properties but preserves the immunogenicity.

Next, the designed antigens should be cloned into a DNA vaccine vector and suitable shuttle vectors for the generation of adenoviral vectors of serotype Ad19a/64 and the poxviral vector CR19.

Moreover, the generated antigens within the different vectors should be extensively characterized *in vitro* regarding their biochemical and molecular biological properties. This also should include investigating the mechanism behind the Ii-induced improvement of $CD8^+$ T cell responses. Finally, the proper inactivation of the oncogenic properties of the antigens should be analyzed.

An often-discussed topic is the instability of rMVA regarding the loss of transgene expression upon genomic recombination and expression-abolishing mutations within the generated rMVA (306–308). Hence, as the last topic of this thesis, the transgene stability of the generated rMVA should be extensively characterized. Furthermore, the impact of transgene expression knock-down generation and amplification of rMVA should be analyzed regarding improved stability and yield in order to provide a possible contingency for rMVA with demanding transgenes.

5 Manuscripts

5.1 Overview

This dissertation contains three manuscripts. Two manuscripts of these manuscripts were already published in peer-reviewed journals, the third manuscript is submitted to the journal Frontiers in Immunology. The first two manuscripts were authored by the PhD candidate Patrick Neckermann as shared first author, the third manuscript is authored as sole first author. This work contains the manuscripts printed with the figures and tables as they were already published or as submitted, respectively. For convenience reasons, the style of the references was changed to provide a uniform picture within the thesis itself and are identical with the references in the published manuscripts. Furthermore, the indexing of the figures, supplementary figures and tables was adjusted in order to have a uniform indexing within the thesis.

5.2 Manuscript 1

"Design and Immunological Validation *of Macaca fascicularis* Papillomavirus Type 3 Based Vaccine Candidates in Outbred Mice: Basis for Future Testing of a Therapeutic Papillomavirus Vaccine in NHPs"

Patrick Neckermann [1#], Ditte Rahbaek Boilesen [2 3#], Torsten Willert [4], Cordula Pertl [4], Silke Schrödel [4], Christian Thirion [4], Benedikt Asbach [1], Peter Johannes Holst [2 3*], Ralf Wagner [1 5*]

[1] Institute of Medical Microbiology & Hygiene, Molecular Microbiology (Virology), University of Regensburg, Regensburg, Germany.

[2] Centre for Medical Parasitology, the Panum Institute, Department of Immunology and Microbiology, University of Copenhagen, Copenhagen, Denmark.

[3] InProTher APS, Copenhagen, Denmark.

[4] SIRION Biotech GmbH, Munich, Germany.

[5] Institute of Clinical Microbiology and Hygiene, University Hospital Regensburg, Regensburg, Germany.

[#]These authors have contributed equally to this work and share first authorship

*Correspondence: Ralf Wagner, ralf.wagner@ur.de; Peter Johannes Holst, pholst@sund.ku.dk

Published in Frontiers in Immunology

DOI: 10.3389/fimmu.2021.761214

Received: 19th of August 2021

Accepted: 05th of October 2021

Published: 28th of October 2021

5.2.1 Abstract

Persistent human papillomavirus (HPV) infections are causative for cervical neoplasia and carcinomas. Despite the availability of prophylactic vaccines, morbidity and mortality induced by HPV are still too high. Thus, an efficient therapy, such as a therapeutic vaccine, is urgently required. Herein, we describe the development and validation of *Macaca fascicularis* papillomavirus type 3 (MfPV3) antigens delivered *via* nucleic-acid and adenoviral vectors in outbred mouse models. Ten artificially fused polypeptides comprising early viral regulatory proteins were designed and optionally linked to the T cell adjuvant MHC-II-associated invariant chain. Transfected HEK293 cells and A549 cells transduced with recombinant adenoviruses expressing the same panel of artificial antigens proved proper and comparable expression, respectively. Immunization of outbred CD1 and OF1 mice led to $CD8^+$ and $CD4^+$ T cell responses against MfPV3 antigens after DNA- and adenoviral vector delivery. Moreover, *in vivo* cytotoxicity of vaccine-induced $CD8^+$ T cells was demonstrated in BALB/c mice by quantifying specific killing of transferred peptide-pulsed syngeneic target cells. The use of the invariant chain as T cell adjuvant enhanced the T cell responses regarding cytotoxicity and *in vitro* analysis suggested an accelerated turnover of the antigens as causative. Notably, the fusion-polypeptide elicited the same level of T-cell responses as administration of the antigens individually, suggesting no loss of immunogenicity by fusing multiple proteins in one vaccine construct. These data support further development of the vaccine candidates in a follow up efficacy study in persistently infected *Macaca fascicularis* monkeys to assess their potential to eliminate pre-malignant papillomavirus infections, eventually instructing the design of an analogous therapeutic HPV vaccine.

5.2.2 Introduction

Despite efficient prophylactic vaccines and the possibility to screen for cervical lesions, infection with human papillomavirus (HPV) was still responsible for more than 340.000 cervical cancer-related deaths worldwide in 2020 (33). More than 85% of these cases occurred in middle- and low-income countries (309). Currently, there are three approved prophylactic vaccines providing near complete protection against vaccine-targeted HPV types, yet vaccine uptake is incomplete (310). However, these vaccines do not lead to the eradication of pre-infected cells, since they target the major capsid protein L1, which is not expressed in infected basal layer- and cervical cancer cells (100,311–313). Thus, novel interventions such as therapeutic vaccines are desirable.

Whereas most HPV infections are spontaneously cleared within months, some persist for years (314). These can progress towards low-grade squamous intraepithelial lesions (LSIL), which can further progress to high-grade squamous intraepithelial lesions (HSIL) and cervical cancer. The expression pattern of viral proteins changes during progression of SILs: in LSIL, mainly the early proteins E1/E2 are expressed, whereas in HSIL and transformed cells, E6/E7 are highly expressed and E2 expression is low or absent (315,316).

In many cases of SIL, however, natural regression occurs as a result of $CD4^+$ and $CD8^+$ T cell infiltration (317). It has been shown that $CD4^+$ T cells play a major role in lesion regression with increased CD4:CD8 ratios being found in the stroma of LSIL (318). Genetic studies have shown that resistance and susceptibility loci for chronic infections and cancer cluster in the MHC II region. Cellular immune responses against E1 have been detected in some patients with HPV^+ cervical squamous cell carcinoma, mostly at low magnitude, but strikingly correlating with improved clinical outcomes (319). Conversely, $HPV16^+$ cervical cancer patients have impaired memory $CD4^+$ T-helper responses against E2 and E6, which emphasizes the important role of T cell responses in preventing progression and clearing lesions

(149,150,152,197). It was also reported that HPV-exposed children have E2-specific T cell responses after clearing the infection (320). Current research on therapeutic HPV vaccines is primarily focused on the HSIL and cancer-stage of the disease, and directed toward the oncogenic viral proteins E6 and E7 (313). However, targeting the infection prior to carcinogenesis could be advantageous in terms of reducing morbidity and suffering related to cancer treatment, and might be easier to achieve. Thus, to target pre-malignant infection, other early proteins should be included as antigens.

There is no suitable small animal model to study persistent HPV infections in a preclinical setting, but *Macaca fascicularis* papillomavirus type 3 (MfPV3) has a close phylogenetic and phenotypic relationship to HPV16 (197,198). Naturally occurring infections with this virus are associated with long-term persistence and at least LSIL-like lesions in the cervix of breeding female cynomolgus macaques (*Macaca fascicularis*), making them an ideal non-human primate (NHP) animal model (196,199).

In a previous study using recombinant adenovirus-(rAd)-vectored vaccines encoding ancestral E1 and E2 antigens targeting the most conserved N- and C-terminal domains, we observed strong immune responses in mice and in cynomolgus macaques against these proteins, but cross-reactivity against prevalent MfPV types was only observed in a subset of animals. Nevertheless, 3 out of 3 animals with T-cell responses towards MfPV3-E1/E2 ended up clearing the specific MfPV3 infection (201). Furthermore, therapeutic efficacy of both early E1-E2 or E6-E7 antigen DNA vaccines, and synergy from co-administration of both vaccines, was demonstrated in the cottontail rabbit papillomavirus model (321). Combining both approaches by including E1, E2, E6 and E7 in an immunogen to a specific HPV type could potentially target infected cells in all stages of HPV infection and cancer development could be sufficient as therapeutic vaccine. Here, successful stimulation of E1/E2-specific cellular immunity would primarily clear infections in the LSIL-stage (322), whereas E6/E7-specific responses would mainly target the HSIL and cancer stages. As we decided not to attempt a broad ancestral antigen design, we also had the opportunity to include the less conserved parts of full length antigens thereby providing more epitopes for the immune system to act on.

To develop such a therapeutic vaccine, vectors expressing antigen candidates comprising E1, E2, E6 and E7 of MfPV3 were generated and characterized. The antigens are genetically linked to the intrinsic T cell adjuvant MHC-II-associated invariant chain (Ii) that has been shown to increase viral-vector-induced T cell responses in mice, cynomolgus macaques and humans (218,219,323). The antigens were designed in different configurations as artificial fusion proteins and initially characterized *via* DNA vaccination of outbred CD1 mice. Based on this initial characterization, adenoviral vectors from serotype 19a/64 were generated and characterized *in vitro* as well as *in vivo*.

5.2.3 Methods

5.2.3.1 Antigen Sequences

Parts of the sequences encoding E1, E2, E6, and E7 of MfPV3 (EF558839.2) were designed and synthesized at Geneart/Thermo Fisher (Regensburg, Germany) (324). Mutations were introduced into E6 and E7 to inactivate the oncogenic potential: L110Q and deletion of C-terminal ETEV in E6; E7 was modified by D24G, L71R, C95A; C297A was introduced into E2 to inactivate DNA-binding. Further sequence elements that were optionally used to build the prototype vaccine inserts (Figure 7) comprised (i) the human MHC-II-associated Ii invariant chain (218,219,323) (molecular adjuvant; NM_004355.3), (ii) a 2 amino acid GS-linker connecting E1 and E2 as well as E6 and E7 in the respective fusion proteins as well as (iii) the porcine teschovirus-1 p2A sequence (325) to support co-expression of two fusion proteins, respectively. Vaccine inserts were assembled either with fusion PCR, or using

type IIs exocutter sites (“Golden gate” cloning; BsaI-HF v2, New England Biolabs, Ipswich, USA) or the NEBuilder HIFI DNA Assembly Kit (New England Biolabs, Ipswich, USA) according to manufacturer’s instructions, and cloned into pURVac, a derivative of a DNA vaccine vector with a proven track record in various NHP and clinical trials (326–329). Vaccine inserts were then subcloned into pO6-19a-HCMV-MCS for subsequent generation of recombinant adenoviruses (235).

5.2.3.2 Cell Lines, Transfection, and Viral Infection

HEK293T cells and A549 cells were maintained and grown in Dulbecco’s MEM (DMEM) supplemented with 10% Fetal Calf Serum (FCS) and 1% Penicillin/Streptomycin (Pen/Strep). 9E10 mycI hybridoma cells were cultivated in RPMI supplemented with 10% FCS, 1% Pen/Strep and 2 mM glutamine (Pan). All cell lines were maintained at 37°C and 5% CO_2 in a non-humidified incubator. HEK293T cells were transfected using the polyethylenimide (PEI) method (330). For PEI transfection, 4×10^5 cells were seeded in 6-well plates one day before transfection. The cells were transfected with 2.5 µg plasmid (equimolar amounts, filled with empty vector) and 7.5 µg PEI in DMEM without any supplements. After 6 h incubation, medium was exchanged to DMEM with 10% FCS and 1% Pen/Strep.

Subconfluent A549 cells were infected with Ad19a/64 vectors at an MOI of 30 in DMEM without any supplements. 2 h post infection, medium was exchanged to DMEM with 10% FCS and 1% Pen/Strep.

5.2.3.3 Generation and Titration of Adenoviral Vectors

E1/E3 deficient adenoviral vectors of serotype Ad19a/64 (rAd) were generated as previously described (235). Briefly, the vaccine inserts (Figure 7) were cloned into the shuttle vector pO6-19a- HCMV-MCS under control of a CMV promoter. The resulting plasmids were then inserted *via* Flp-recombination in *E. coli* into a BAC vector containing the genome of a replication deficient Ad-based vector deleted in E1/E3 genes. Recombinant viral DNA was released from the purified BAC-DNA by restriction digest with PacI. The obtained linear DNA was transfected into HEK293T cells for virus reconstitution and propagation. Recombinant viruses were released from cells *via* sodium deoxycholate treatment. Residual free DNA was digested by DNase I. Afterwards, vectors were purified by CsCl gradient ultracentrifugation followed by a buffer exchange to 10 mM Hepes pH 8.0, 2 mM $MgCl_2$ and 4% Sucrose *via* PD10 columns (GE Healthcare, Chicago, USA). Titration was performed using the RapidTiter method by detection of infected HEK293T cells *via* immunohistochemical staining with anti-hexon antibody (Novus, Adenovirus Antibody (8C4)). Insert integrity was confirmed by PCR amplification from the purified vector DNA followed by DNA sequencing.

5.2.3.4 Antibodies and Antibody Purification

The antibody against myc (9E10) was obtained from hybridoma cell supernatants. 9E10 mycI hybridoma cells were seeded at 5×10^5 cell per ml in RPMI supplemented with 1% FCS, 1% Pen/Strep and 2 mM glutamine. The supernatant was harvested 5 days after seeding and the antibody was purified *via* a HiTrap Protein G column (GE Healthcare, Chicago, USA). After washing the column with PBS, the antibody was eluted with 0.1 M glycine/HCl (pH 3.2), neutralized with 0.025 volumes of 1 M Tris/HCl (pH 9) and dialyzed against PBS.

Other antibodies used were: mouse anti-p2a peptide (3H4, 1:2000, Merck, Darmstadt, Germany), mouse anti-tubulin (DM1a, 1:1000, Santa Cruz, Heidelberg, Germany), mouse anti-ubiquitin-Biotin (eBioP4D1, 1:1000, Invitrogen, Carlsbad, USA), goat anti-mouse-HRP (115-036-003, 1:5000, Jackson, West Grove, USA), goat anti-rabbit-HRP (P0448, 1:2000, Dako, Santa Clara, USA), Streptavidin-HRP (11089153001, 1:5000, Roche, Basel, Swiss), rat anti-mouse-PE (A85-1, 1:100, BD, Franklin Lakes, USA).

5.2.3.5 Western Blot Analysis

Western blot analysis was performed as previously described (258). Briefly, cells of interest were lysed in TDLB buffer (50 mM Tris, pH 8.0, 150 mM NaCl, 0.1% SDS, 1% Nonident P-40, 0.5% sodium deoxycholate) supplemented with protease inhibitors (Complete Mini, Roche, Basel, Swiss). Total protein concentration of the supernatants was measured by the Bradford method (Protein Assay, BioRad, Feldkirchen, Germany). The proteins were separated on SDS-PAGE under reducing conditions and blotted on a nitrocellulose membrane for western blot analysis. Targets were probed with primary and secondary antibodies as listed above. HRP-labeled secondary antibodies and enhanced chemiluminescence substrate or Femto ECL (Thermo Fisher, Waltham, USA) were used for detection in a Chemilux Pro device (Intas, Göttingen, Germany).

5.2.3.6 Analysis of Ubiquitination

To analyze ubiquitinylated proteins, 24 h post transfection, cells were treated with 10 µM MG132 proteasome inhibitor for 6 h. Afterwards, cells were harvested in PBS and washed twice. For inactivation of deubiquitination enzymes, 20 mM N-ethylmaleimide from a freshly prepared stock solution were added to the TDLB lysis buffer. Lysates were generated as described above. Before immunoprecipitation, Protein G dynabeads (Thermo Fisher, Waltham, USA) were loaded with 10 µg of pulldown antibody. Using these beads, target protein was immunoprecipitated out of 500 µg cell lysate over night at 4°C under slow rotation. After washing the beads four times with PBS, SDS-PAGE buffer was added to the beads before heating at 95°C for 10 min. The samples were used for western blot analyses as described above.

5.2.3.7 Flow Cytometry Analysis of Cell Lines

Intracellular staining of antigens was performed using standard methods (258). Cells were fixed and permeabilized with Cytofix/ Cytoperm-Buffer (4% PFA, 1% saponine, in PBS). All washing steps were done with Perm/Wash-Buffer (PBS containing 0.1% saponine). The cells were stained with anti-myc antibody (5 µg/ ml, diluted in Perm/Wash-Buffer) and rat anti-mouse-PE (1:100 diluted in Perm/Wash-Buffer) each for 30 min. Flow cytometry was performed using an Attune NxT device (Thermo Fisher, Waltham, USA) with a 488 nm excitation and a 574/26 nm emission filter. Cells were gated on stained, mock-transfected cells. Evaluation of data was performed using Attune NxT software.

5.2.3.8 Animals and Immunizations

BALB/c and CD1 mice were obtained from Envigo (Horst, The Netherlands) and OF1 mice from Charles River (France). All animals were female, 6-8 weeks old and housed at the Panum Institute, University of Copenhagen. All experiments were initiated after allowing the mice to acclimatize for at least 1 wk. Experiments were approved by the National Animal Experiments Inspectorate (Dyreforsøgstilsynet, license no. 2016-15-0201-01131) and performed according to national guidelines. DNA immunizations were performed intradermal (i.d.) with 0.5 g DNA coated onto 1.6 µm gold microcarriers (BioRad, Feldkirchen, Germany) using the Helios Genegun System (BioRad, Feldkirchen, Germany). The mice received four DNA immunizations at intervals of one week each. One group received a mixture of four plasmids, 0.5 µg each, into one site. Immunizations with adenoviral vectors were performed intramuscular (i.m.) with 2×10^7 IFU rAd diluted in 50 µL PBS. Mice were anesthetized with isofluorane before rAd injections. One group received a mixture of four rAd, 2×10^7 IFU each, into one site.

5.2.3.9 Flow Cytometry of Splenocytes

Single cell suspensions of splenocytes were obtained by organ harvest in HANKs followed by straining through 70 µm cell strainers. Cells were incubated for 5 hours in 3 µM monensin with or without 1

µg/mL of relevant peptides. The cells were stained against surface markers: APC-Cy7 or BV421 CD8 (53- 6.7, 1:200, BioLegend, San Diego, USA), PE-Cy7 CD4 (RM4-5, 1:800, BD), FITC CD44 (IM7, 1:100, BioLegend, San Diego, USA) and PerCP-Cy5.5 B220 (RA3-6B2, 1:200, BioLegend, San Diego, USA). After surface staining, cells were fixed in 1% PFA, permeabilized in 0.5% saponine, and stained intracellularly using APC IFN-γ (XMG1.2, 1:100, BioLegend, San Diego, USA) and PE TNF-α (MP6-XT22, 1:100, BioLegend, San Diego, USA) antibodies. The peptides used were 16-mers overlapping by 11 amino acids covering the entire Ii-E1E2E6E7 antigen. The peptides were pooled in 5 separate pools containing Ii (45 peptides), E1 (123 peptides), E2 (70 peptides, E6 (28 peptides) and E7 (21 peptides) peptides respectively. Peptides were obtained from KareBay, Town, China.

Flow cytometry was performed on the Fortessa 3 (BD Biosciences, Franklin Lakes, USA) flow cytometer and data analysis was performed using FlowJo V10 software. Epitope-specific $CD8^+$ T-cell responses were measured as $B220^-$, $CD8^+$ or $CD4^+$, $CD44^+$, IFN-γ^+ cells and are presented in total number of cells per organ. The quality of the IFN-γ^+ responses were evaluated by MFI of IFN-γ and fraction of double positive cells (expressing both IFN-γ and TNF-α) in the IFN-γ^+ $CD8^+$ or $CD4^+$ populations. The gating strategy is shown in Supplementary Figure 2.

5.2.3.10 *In Vivo* Cytotoxicity

The assay was performed similarly to what was previously described (331). Briefly, splenocytes from naïve BALB/c mice were incubated with MfPV3 E1, E2, E6 or E7 peptide pools (same as used for immune response analyses, see above) or no peptide for 30 minutes at 37°C, 5% CO_2, 2.5 µg of each peptide/mL, and subsequently stained with combinations of 0.4 or 5 µM CellTrace CFSE and 0.2 and 2.5 µM CellTraceViolet (CTV; ThermoFisher, Waltham, USA) for 10 minutes at 37°C, 5% CO_2. Pulsed and stained splenocytes were mixed at a 1:1:1:1:1 ratio, and a total of 2.5 x 10^7 cells were injected intravenously into rAd-vaccinated recipient BALB/c mice. As the assay requires adoptive transfer of syngeneic target cells, it was necessary to use inbred mice in order to have HLA-matching. 5 hours later, spleens were harvested, and target cells were identified on the Fortessa 3 (BD Biosciences, Franklin Lakes, USA) flow cytometer by CFSE/CTV staining. The percentage of killing was calculated using the following equation:

$$\%\ targeted\ killing = 100 - \left(\frac{\%\ peptide\ pulsed\ cells\ in\ vaccinated\ mice}{\%\ non-peptide\ pulsed\ cells\ in\ vaccinated\ mice} \Big/ \frac{\%peptide\ pulsed\ cells\ in\ non-vaccinated\ mice}{\%non-peptide\ pulsed\ cells\ in\ non-vaccinated\ mice} \right) * 100$$

5.2.3.11 Analysis of E1 (SIINFEKL) Presentation on MHC-I

HEK293T cells were transfected with 2.5-3.5 µg of pURVac encoding E1, which was C-terminally extended by the SIINFEKL Ovalbumin derived $CD8^+$ T cell epitope and a myc-tag and optionally fused to the Ii T cell adjuvant (218,219,323) at its N-terminus together with a pUC57 encoding H2Kb and β-2-microglobulin (β2m). A transfection with H2Kb alone was included as a negative control, and transfection with the H2Kb plasmid and a pUC57 plasmid encoding SIINFEKL fused directly to β2m was included as a technical positive control. 48 hours post transfection, cells were stained with PE anti-H2Kb-SIINFEKL (25-D1.16, 1:160, Invitrogen, Carlsbad, USA) and presence of SIINFEKL-H2Kb presentation on cell surfaces was detected on the LSRII or Fortessa 3 (BD Biosciences, Franklin Lakes, USA) flow cytometers, as a proxy for E1 presentation. All samples were run in biological 6-plicates, and the experiment was repeated at least two times.

5.2.3.12 Graphical Representation and Statistical Analysis

Non-stimulated samples were used as background controls, and their response values have been subtracted from the peptide-stimulated samples of the corresponding animal before performing statistical analysis and graphical presentation.

In order to aid visual presentation of the results, we applied a threshold for responses based on the average number of $B220^-$, $CD8^+$, $CD44^+$, IFN-γ^+ counts for unstimulated background samples. All samples with less counts than the average + 2 × SD of the background samples, are regarded as non-responding and therefore they have manually been adjusted to a value of 100 for the graphical presentation. All statistical analyses were done on non-adjusted values. The analysis of fraction of double positive (% TNF-α^+ IFN-γ^+ out of all IFN-γ^+) and MFI of IFN-γ^+ was only performed on responders (IFN-γ^+ count > avg + 2 × SD of unstimulated samples).

Statistical analysis was done using GraphPad Prism 8 software (GraphPad Software, San Diego, USA). Values with background subtracted were used to compare the individual groups using the Mann-Whitney test with Bonferroni correction for multiple comparisons. Positive control groups were not included in the multiple comparison analyses. Each symbol represents one mouse. Bars indicate median. Significance levels are marked by * (p<0.05), ** (p<0.01), *** (p<0.005), **** (p<0.001).

5.2.4 Results

5.2.4.1 Design of the Antigens

Aiming towards the generation of a therapeutic vaccine, which is able to eliminate pre-existing papillomavirus-derived premalignant neoplasias, various antigens comprising E1, E2, E6, and E7 were designed. In order to enable future validation of a therapeutic concept in non-human primates, the above antigens were derived from *Macaca fascicularis* papillomavirus type 3 (MfPV3), which was shown to persist and induce LSIL-like lesions in the cervix of breeding female cynomolgus macaques (*Macaca fascicularis*) (196,199). Herein, we describe the construction and immunological down-selection of eight different antigen designs in and outbred mouse model according to potency and breadth of induced T cell responses as basis for further preclinical validation in non-human primates.

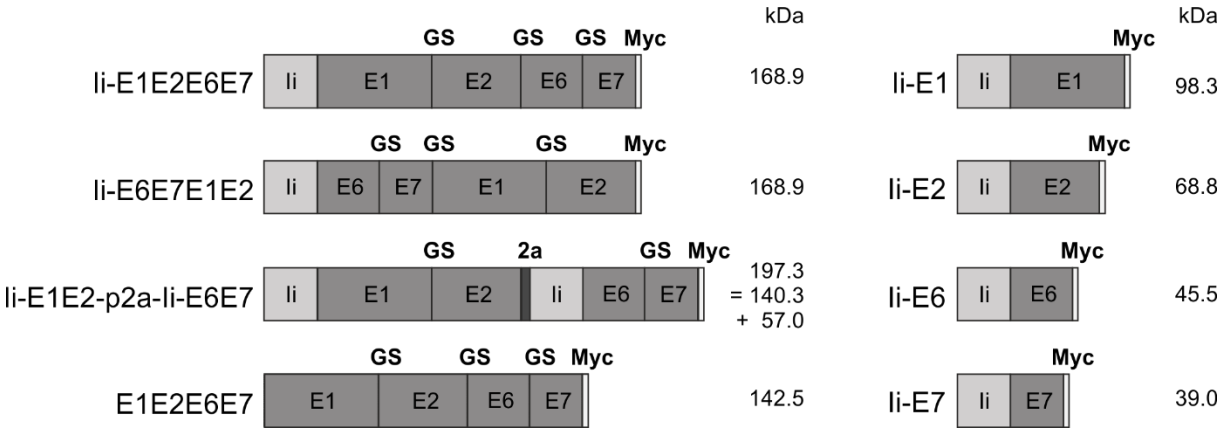

Figure 7: Schematic representation of the conceived MfPV3 antigen variants.
MfPV3 antigens were designed as fusion proteins comprising either E1, E2, E6 and E7 altogether, or E1 plus E2 and E6 plus E7 fusion proteins linked by a p2a peptide, and fused to the MHC-II invariant chain (Ii), respectively. For reference, E1, E2, E6, and E7 were fused as single open reading frames without the Ii coding sequence. Calculated molecular weights are indicated (kDa). Ii, MHC-II associated invariant chain; GS, glycine-serine-linker; 2a, p2a peptide for cotranslational separation; Myc, myc-tag sequence for antibody detection; kDa, kilo Dalton.

Antigens were conceived as (i) read-through polypeptides with all four MfPV3 early antigens encoded in one open reading frame, (ii) alternatively E1-E2 and E6-E7 fusions were linked *via* a p2A site (332) supporting translational coupling and thus co-expression of the two fusion proteins or (iii) as single expression units. Within fusion proteins, the different MfPV3 early proteins were separated by a GS-linker.

With one exception (E1E2E6E7), all polypeptides were NH_2 terminally fused to a the human MHC class II invariant chain (Ii), which has been described earlier to act as a T cell adjuvant (218). Furthermore, all constructs received a C-terminal myc-tag for convenient expression monitoring (Figure 7).

Since E6 and E7 are highly potent oncoproteins, only transformation-defective variants should be used in a therapeutic vaccine setting to ensure safety. Based on the homology to HPV16, the oncoprotein E6 was inactivated by introducing a L110Q substitution to prevent binding of E6 to E6BP and subsequent degradation of tumor suppressor p53 (333). Additionally, the C- terminal PDZ-domain was deleted (DETEV) to abolish binding of telomerase and other LxxLL proteins (334). E7 was inactivated by introducing the substitutions C24G, L71R, and C95A within the central LxCxE motif inhibit dimerization and reduce binding to pRB as well as Mi2β (334,335). Furthermore, we changed E2 (C297A) to reduce DNA binding.

For initial biochemical and immunological characterization, the antigen coding sequences (Figure 7) were inserted into pURVac, a derivative of a DNA vaccine vector with a proven track record in various NHP and clinical trials (326–329). Transcription of the encoded transgenes is controlled by a human cytomegalovirus (CMV) promoter in combination with a human T-cell leukemia virus-1 (HTLV-1) regulatory element (336) and terminated by a bovine growth hormone poly-A site.

5.2.4.2 Biochemical and Cell Biological Characterization of MfPV3 Antigens

Following transient transfection of HEK293T cells with the respective DNA vaccine constructs, all antigens were properly expressed yielding proteins chiefly correlating with the calculated molecular weights (Figure 8A). In some cases, especially for proteins with high signal intensities, bands of higher or lower molecular weight than calculated were observed. These might result from incompletely reduced oligomers (221) or N-terminal degradation products, which is expected as Ii transports some of its linked cargo to endosomal compartments where proteolytic degradation naturally occurs.

Since proteins of different sizes behave differently during blotting and signal intensities may not reflect the real expression levels, MfPV3 antigens were quantified by flow cytometry after intracellular staining with the anti-myc-antibody (Figure 8B and Supplementary Figure 1). Protein levels of the different MfPV3 antigens differed only marginally, except for Ii-E7, which exhibited two- to threefold higher MFI values compared to all other antigens.

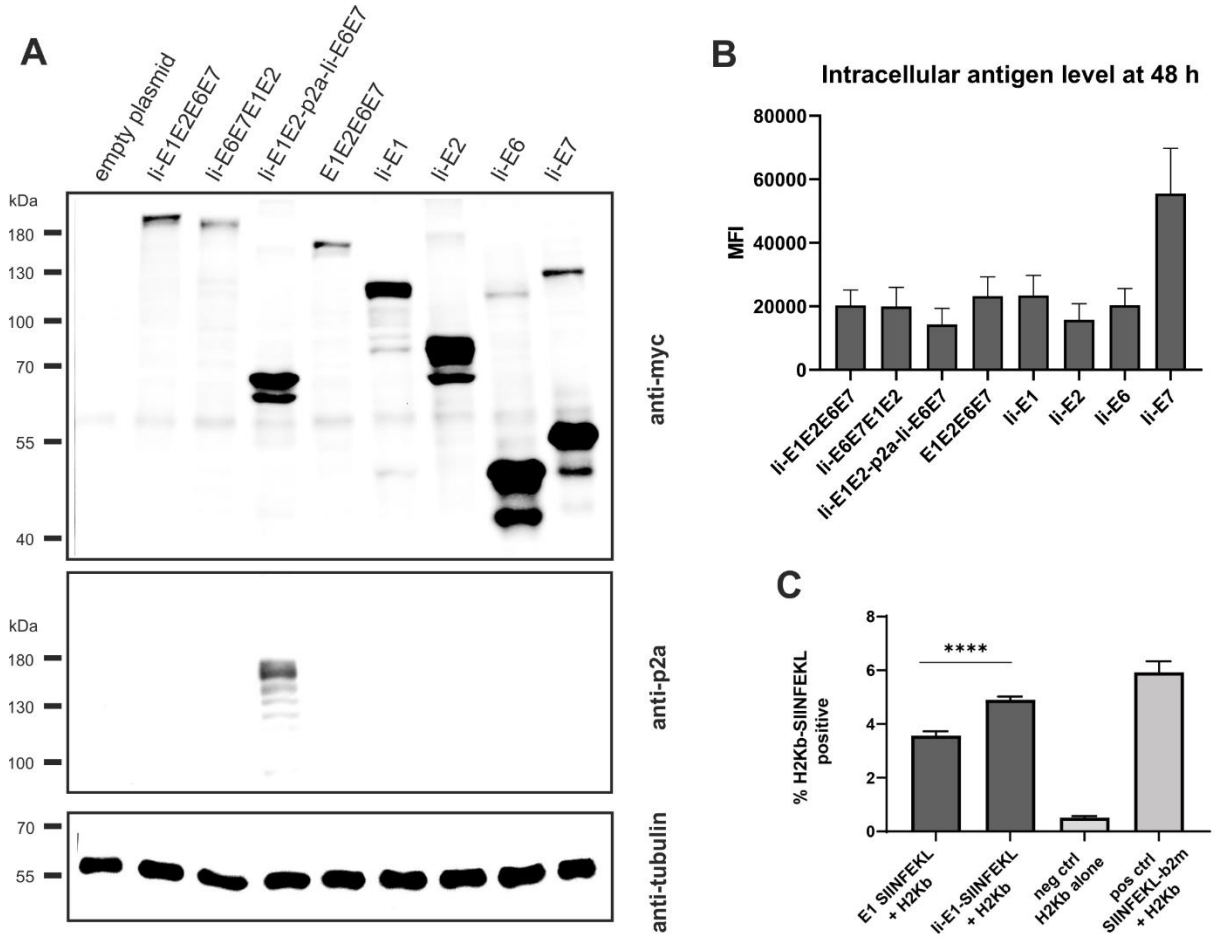

Figure 8: Expression analysis of MfPV3 antigens.
(A) Western blot analysis of HEK293T cell lysates 48 h following transfection with equimolar amounts of pURVac DNA vaccines expressing the various MfPV3 antigens. Antigens were detected with anti-myc (upper panel) and anti-p2a-peptide (middle panel) antibodies. Tubulin levels were monitored using an anti-tubulin antibody as loading control (lower panel). (B) Flow cytometry analysis of HEK293T cells 48 hours following transfection with pURVac DNA vaccines. Intracellular staining was performed with anti-myc antibody. Depicted is the mean fluorescence intensity (MFI) of the average of 3 independent experiments. Error bars indicate standard error of the mean. (C) Co-transfection of HEK293T cells with H2Kb alone or together with pURVac E1-SIINFEKL or Ii-E1-SIINFEKL, respectively. The percentage of SIINFEKL-H2Kb positive cells were determined after 48 hours by flow cytometry using an antibody recognizing the SIINFEKL-H2Kb-complex. Error bars indicate standard error of the mean. Light gray bars are negative (no peptide, H2Kb-plasmid only) and positive controls (SIINFEKL-b2m encoding plasmid + H2Kb), respectively. ****p < 0.001.

5.2.4.3 MHC Class I-Restricted SIINFEKL Epitope Is Processed From E1 Fusion Protein and Abundantly Presented on MHC-I Molecules *In Vitro*

It has been reported that E1 of bovine papillomavirus type 1 is itself an unstable protein which is ubiquitinylated and rapidly degraded in naturally infected cells (202,203). This observation together with the reported low prevalence of E1 specific antibodies in women with cervical disease (337) prompted us to assess whether MHC class I-restricted peptides at all can be processed and presented from E1. Therefore, the minimal H2Kb-restricted OVA epitope SIINFEKL (338) was fused to the C-terminus of E1 or, alternatively, to Ii-E1. The SIINFEKL epitope is a high affinity, highly immunodominant epitope, and therefore it is processing and presentation is easy to detect in *in vitro* studies. Following transfection of the respective pURVac expression constructs, MHC class I-restricted presentation of SIINFEKL could be readily detected using an H2Kb-SIINFEKL specific antibody. This supports the choice of E1 as a relevant antigen

to be included in the therapeutic vaccine. Noteworthy, presentation was enhanced, when this fusion protein was N-terminally linked to the MHC class II invariant chain (Ii) (Figure 8C).

5.2.4.4 DNA Vaccination of Antigen Constructs Induces $CD4^+$ and $CD8^+$ T Cell Responses Against MfPV3 Early Antigens

Intradermal (i.d.) DNA immunization of outbred CD1 mice confirmed that all pURVac DNA vaccines encoding E1 and/or E2 induced E1- and E2-specific IFN-γ^+ $CD8^+$ and $CD4^+$ T cells (Figure 9 and Supplementary Figure 2). More detailed, all DNA vaccine candidates had provided an E1 response on par with the positive control (Ii-E1). None of these vaccines induced responses against E6 or E7 in these outbred mice, including the positive controls for these two antigens (Ii-E6; Ii-E7; Supplementary Figure 3A, B). Importantly, all vaccines encoding all four antigens as a polyprotein generated responses comparable to those induced by a mix of four vaccines encoding the antigens individually (Ii-E1, Ii-E2, Ii-E6, Ii-E7). This suggests that overall no immunogenicity was lost by delivering the MfPV3 early antigens as polyproteins from a single pURVac DNA vaccine. Regardless of the used pURVac vaccine construct, E1 and E2 specific T cell responses showed no statistical differences regarding the frequencies of E1- and E2-specific IFN-γ^+ $CD8^+$ and $CD4^+$ T cells. This is the case regardless (i) of whether Ii is fused to E1E2E6E7, (ii) of the order of the early antigens in the polyprotein, and (iii) of the use of a p2a site to separate Ii-E1E2 from Ii-E6E7. Only pURVac-Ii-E2, when administered alone, trended to induce slightly higher levels of specific $CD4^+$ and $CD8^+$ positive T cells (although statistically not significant). Contrasting previous findings, N-terminal fusion of the Ii molecular adjuvant did not enhance antigen specific T cell responses when delivered as DNA (339,340). However, there are much fewer examples of Ii having an adjuvant effect in a DNA context compared to when it is encoded in viral vector transgenes. Additionally, it might be that the lack of Ii-effect is due to the high number of DNA immunizations (four in total), as the continuous boosting may have saturated the immune activation. It is possible that a difference between the Ii and non-Ii vaccines could have been detected after fewer immunizations. We were satisfied to see that all DNA constructs were immunogenic, and to address the Ii effect properly, we decided to create adenoviral vectors of all vaccine designs (see below). The quality of the T-cell responses was comparable across all vaccines (Supplementary Figure 3C, D), assessed by MFI of IFN-γ and TNF-α production of IFN-γ^+ T-cells. As expected, we found Ii specific $CD8^+$ T cell responses in most mice, and to $CD4^+$ in some mice (Supplementary Figure 3A, B), as the human Ii is allogenic in mice.

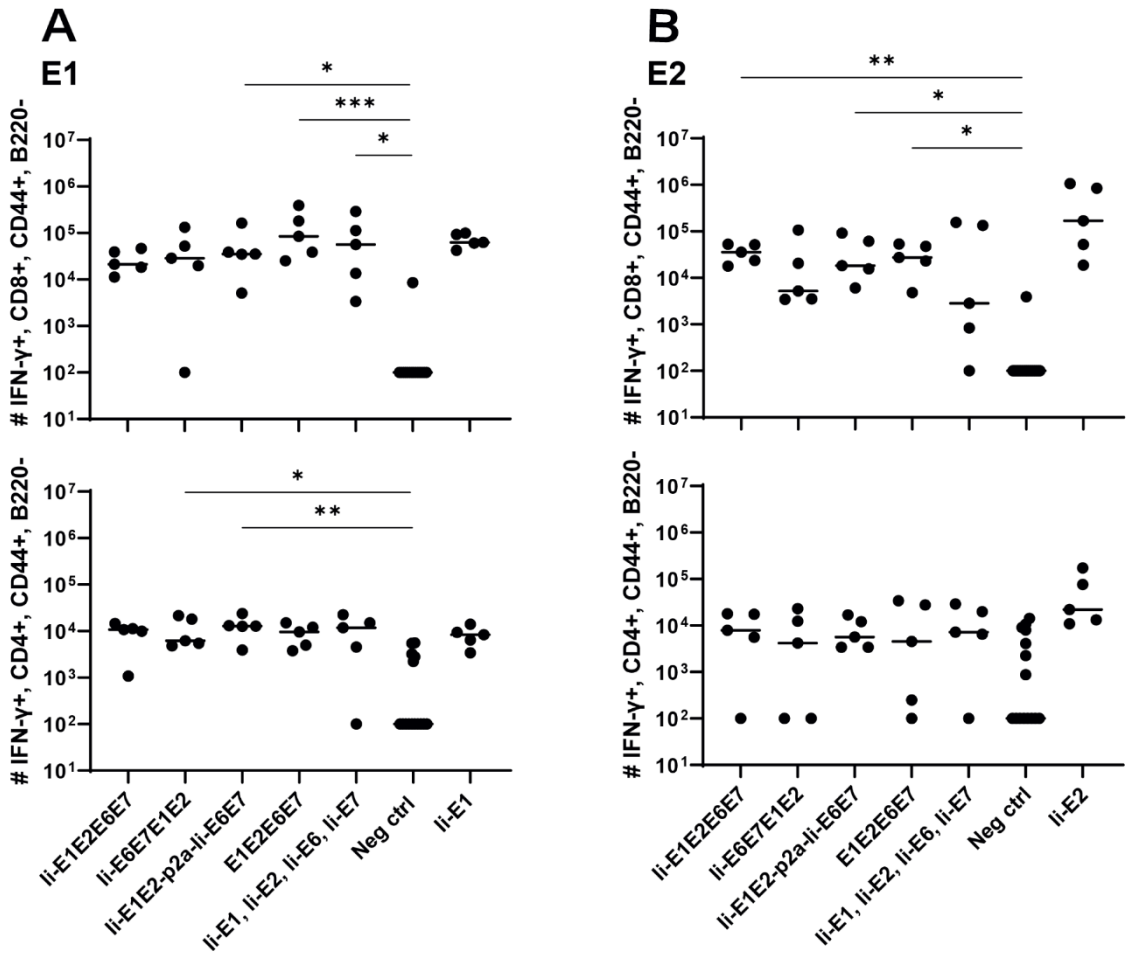

Figure 9: T cell responses induced by the various pURVac DNA vaccines encoding E1, E2, E6 and E7 in outbred CD1 mice.

CD1 mice (5 per group) were immunized 4 times in 1 week intervals with 0.5 µg DNA of pURVac DNA encoding the indicated MfPV3 early antigens. Mice were sacrificed 7 days post last immunization, spleens were harvested and $CD8^+$ (top panels) and $CD4^+$ (bottom panels) T-cell immune responses against E1 (A), and E2 (B) were measured using ICS and flow cytometry. Negative control groups consist of all mice immunized with a pURVac DNA vaccine encoding antigens not covered by the peptide pools used for *in vitro* restimulation. Asterisks between groups indicate significant differences in response-levels after subtraction of background responses. Each symbol represents one mouse; the horizontal bar represents the median. Reference samples (mice vaccinated with pURVac DNA vaccine containing only the individual antigen linked to Ii, respectively) are not included in the statistical analysis (multiple comparison adjustment). *p < 0.05; **p < 0.01, ***p < 0.005.

5.2.4.5 Characterization of Adenoviral Vectors

To further increase antigen specific cellular immune responses, viral vectors were subsequently used for antigen delivery. Adenoviral vectors from serotype 19a/64 (rAd) had been shown earlier to be generally suitable to deliver MfPV3 antigens and to efficiently induce $CD8^+$ T cell response in cynomolgus macaques (255). Based on the above DNA vaccination data, a refined panel of rAd vectors was generated comprising a modified set of recombinant MfPV3 antigens. Ii-E6E7E1E2 was excluded because it was not superior to the other polyproteins. However, the trend toward higher E2 specific T cell when administered alone prompted us to generate two additional adenoviruses, one encoding Ii-E1E6E7 linked to E2 *via* a self-separating p2a peptide (Ii-E1E6E7-p2a-Ii-E2) and for control Ii-E1E6E7 lacking E2. In order to confirm proper expression of the encoded antigens, western blot analysis was performed with A549 cells following transduction with the indicated rAds. All vectors readily expressed the antigens with bands resembling the respective fusion proteins at the expected molecular weights

(Figure 7 and Figure 10A, B). As for Ii-E1E2-p2a-Ii-E6E7, no higher than calculated molecular weight fragment could be detected for Ii-E1E6E7-p2a-Ii-E2, revealing that the complete separation at the p2a site also worked upon delivery *via* rAds. Quantitative analysis of transduced A549 cells by flow cytometry yielded comparable expression levels for the different myc-tagged MfPV3 polypeptides with the exception of higher expression of Ii-E7 (Figure 10C and Supplementary Figure 4). The overall picture was quite similar to the expression efficiencies observed after pURVac mediated antigen delivery in HEK293T cells.

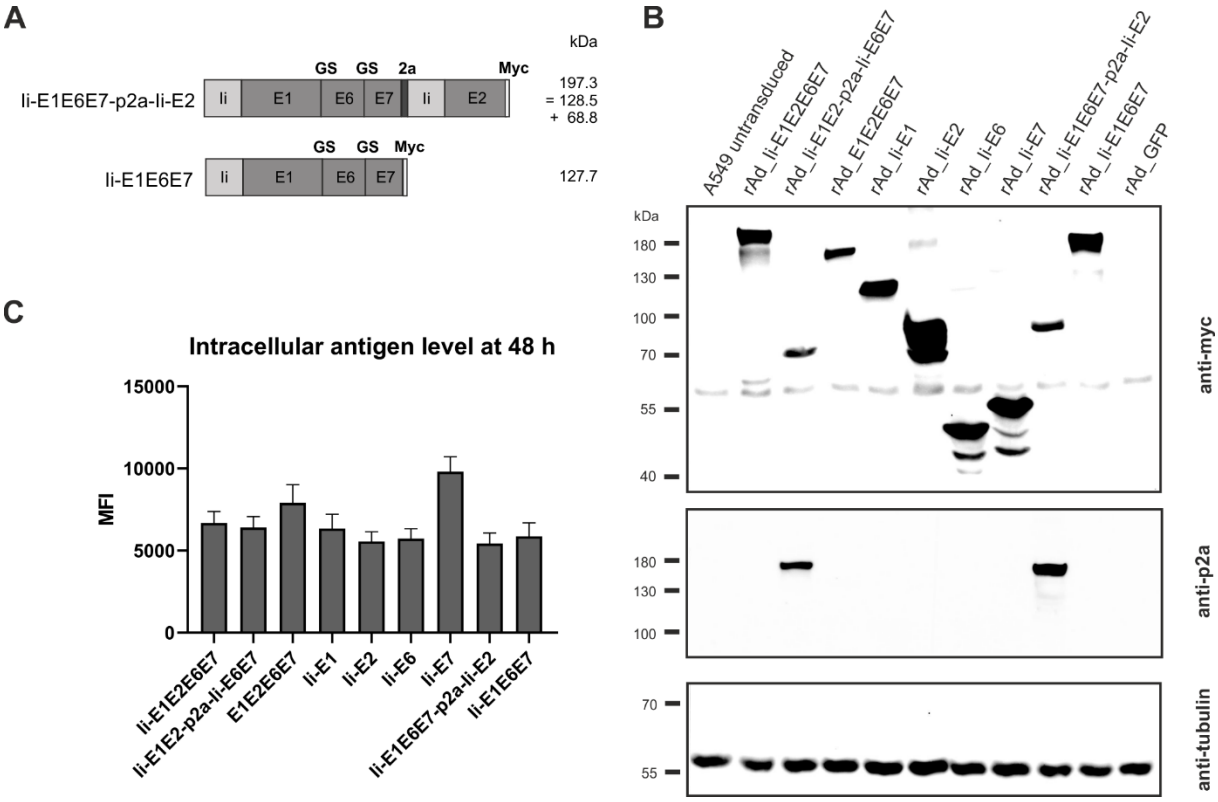

Figure 10: Expression analysis of rAd-shuttled MfPV3 antigen constructs.
(A) Schematic representation of the MfPV3 antigen variants Ii-E1E6E7-p2a-Ii-E2 and Ii-E1E6E7. Expected molecular weights (kDa) of the resulting polypeptides are shown. (B) Western blot analysis of A549 cell lysates 48 h following transduction with rAds encoding the indicated polypeptides at an MOI of 30. Antigens were detected with anti-myc (upper panel) and anti-p2a-peptide (middle panel) antibodies. As loading control, tubulin levels were monitored using an anti-tubulin antibody (lower panel). (C) Flow cytometry analysis of A549 cells 48 hours following transduction with rAds expressing the various MfPV3 antigens, at an MOI of 30. Intracellular staining was performed with anti-myc antibody. Depicted is the mean fluorescence intensity (MFI) of the average of 3 independent experiments. Error bars indicate standard error of the mean.

5.2.4.6 Adenoviral Delivery Induces Potent Cellular Immune Responses Against MfPV3 Early Antigens in Outbred Mice

Intramuscular immunization of outbred CD1 mice confirmed that the rAd-formulation of the vaccines induced both $CD8^+$ and $CD4^+$ T cell responses against E1 and E2 antigens (Figure 11A, B). Notably, vaccines including Ii showed a trend towards higher magnitude responses than the vaccine not encoding Ii (Figure 11A, B: E1E2E6E7 compared to other vaccines). A tendency of Ii-mediated enhancement of responses was observed for both $CD4^+$ and $CD8^+$ T cell responses for some vaccine configurations, but the difference was only significant for E2-specific $CD8^+$ responses induced by Ii-E1E2-p2a-Ii-E6E7 compared to E1E2E6E7 (Figure 11B, upper panel). A direct comparison of the $CD8^+$ T-cell response against E1 from Ii-E1E2E6E7 and E1E2E6E7 (Mann-Whitney rank-sum) revealed a p-value of 0.06, which

is not strictly significant, but strongly indicates a tendency of Ii improving the magnitude of $CD8^+$ T-cells against E1. Further, the vaccine without Ii was the only one for which the $CD4^+$ and $CD8^+$ T-cell responses against E1 was not significantly different from the negative control. This may confirm earlier observations suggesting that Ii can boost T cell responses in the context of adenoviral vaccine delivery. No difference in the quality of the T cell responses was detected, assessed by the MFI values of IFN-γ (Supplementary Figure 5C). When assessing the quality by the fraction of double-positive T cells capable of secreting both IFN-γ and TNF-α it is seen that E1E2E6E7 without Ii seemed to be inferior to other vaccines containing Ii (Supplementary Figure 5D). Based on this, we decided to focus our onwards efforts on antigen-fusion vaccine designs containing the Ii adjuvant.

Even though E6 and E7 represent small proteins as compared to E1 and E2 (11.9%, 8.1%, 50.8% and 29.2%, respectively, of the total antigen size), it was remarkable that no responses against E6 or E7 could be observed in any experiment testing the vaccines in outbred CD1 mice. As the MHC-type of the founders of the CD1 strain is unknown, and has not been controlled for since the establishment of the strain, we wondered whether there were limitations in terms of MHC-restriction in the CD1 mice we had obtained. Limitations of genetic diversity of outbred mouse models has indeed been described previously and almost all outbred mouse strains except OF1 descent from the same 9 founder mice (341). Hence vaccination of OF1 mice was pursued to possibly detect different and broader immune responses than in CD1 mice. Besides vigorous T-cell responses against E1 and E2 (Figure 11C, D), we did indeed see solid $CD4^+$ T-cell responses against E6 (Figure 11D). A few mice also had $CD8^+$ T-cells reacting towards E6, confirming correct *in vivo* processing and immunogenicity of our vaccine constructs. Furthermore, the majority of the IFN-γ^+ cells were producing TNF-α as well, confirming the activation phenotype. Overall, the rAd19 delivery of the vaccines efficiently induced T-cells against at least three of the four MfPV3 polyprotein antigens tested, and the immunogenicity of the antigens was enhanced by inclusion of Ii.

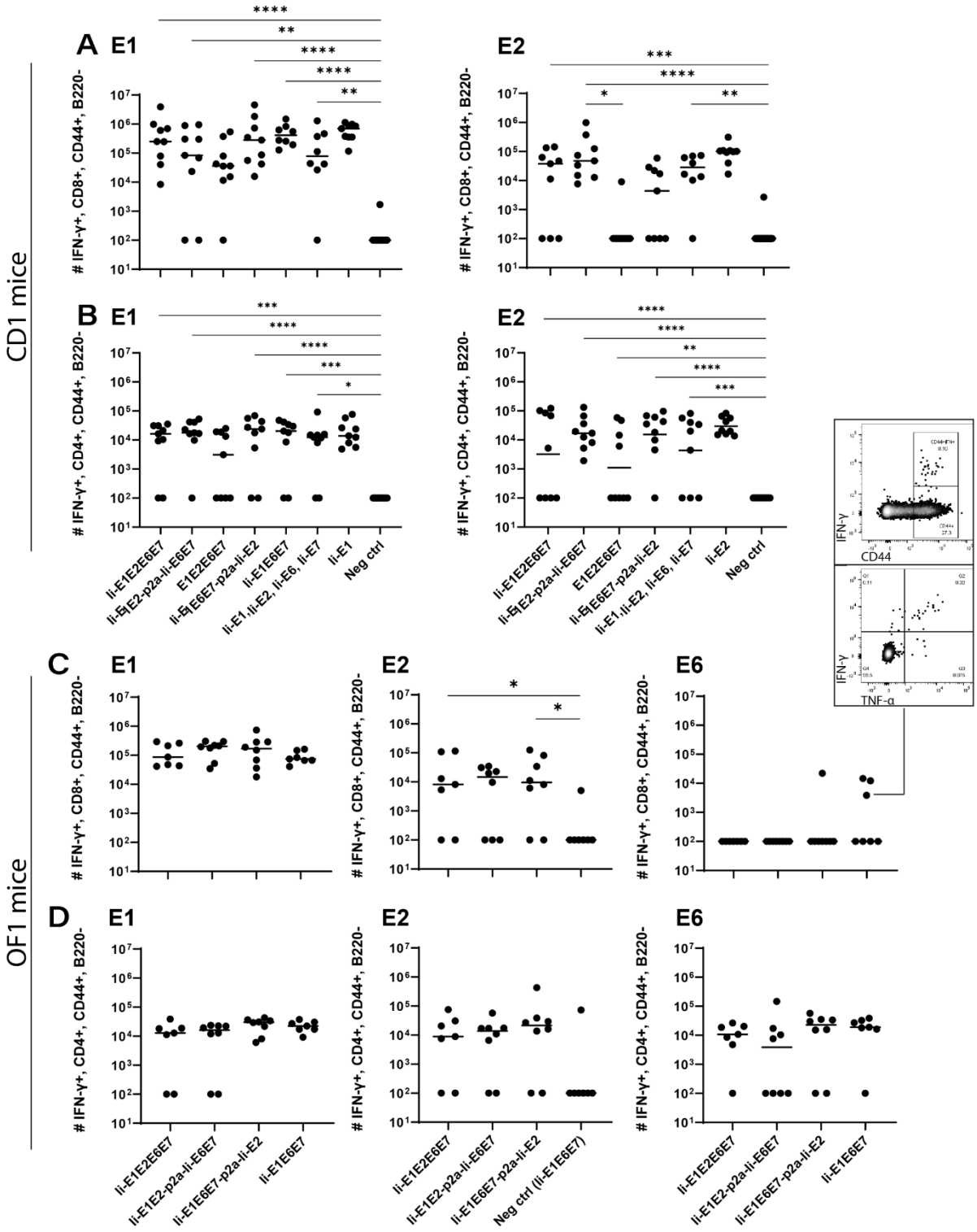

Figure 11: Immunization of mice with adenovirus vectors induces potent cellular immune responses.
CD1 mice (A, B), or OF1 mice (C, D) were immunized with rAd vaccine (2×10^7 IFU) encoding the various MfPV3 early antigens as indicated. Mice were sacrificed on day 14, spleens were harvested and $CD8^+$ and $CD4^+$ T-cell immune responses against E1, E2, E6, and E7 were measured using ICS and flow cytometry. Negative control groups consist of all mice immunized with rAd encoding antigens not matching the peptide pools used for *in vitro* restimulation, respectively. Each symbol represents one mouse; a representative mouse depicted (C), shows a $CD44^+IFN\text{-}\gamma^+$ population. The horizontal bar represents the median. Positive control samples (mice vaccinated with rAd containing only the relevant antigen linked to li) are not included in the statistical analysis (multiple comparison adjustment). *p < 0.05; **p < 0.01, ***p < 0.005, ****p < 0.001.

5.2.4.7 Adenoviral Delivery Induces Specific Killing of Target Cells *In Vivo*

To assure that the cellular responses induced by the rAd-delivered antigens had cytotoxic capacity, we immunized inbred BALB/c mice with rAds expressing Ii-E1E2E6E7, Ii-E1E2-p2a-Ii-E6E7 and E1E2E6E7, and 14 days later challenged these mice with peptide-pulsed pre-stained syngeneic target cells. As the assay required adoptive transfer of syngeneic target cells, it was necessary to use inbred mice. The vaccines induced $CD8^+$ responses against E1 in BALB/c mice (Figure 12A), but not against the other antigens (data not shown), whereas $CD4^+$ responses were raised against E2 and E6 (Supplementary Figure 6). Ii again proved its relevance as molecular adjuvant, as the vaccine without Ii did not give rise to any detectable E1 specific $CD8^+$ responses in this inbred mouse model (Figure 12A). Consistent with the above, the *in vivo* cytotoxicity assay showed specific killing of E1 labelled cells (Figure 12B, C), and the hierarchy of specific killing capability corresponds to the number of IFN-γ^+ $CD8^+$ E1 specific T cells. We can conclude that the designed rAd vaccines induce potent and cytotoxic responses, which supports our hypothesis that this vaccine design will be capable of removing existing MfPV3 infections.

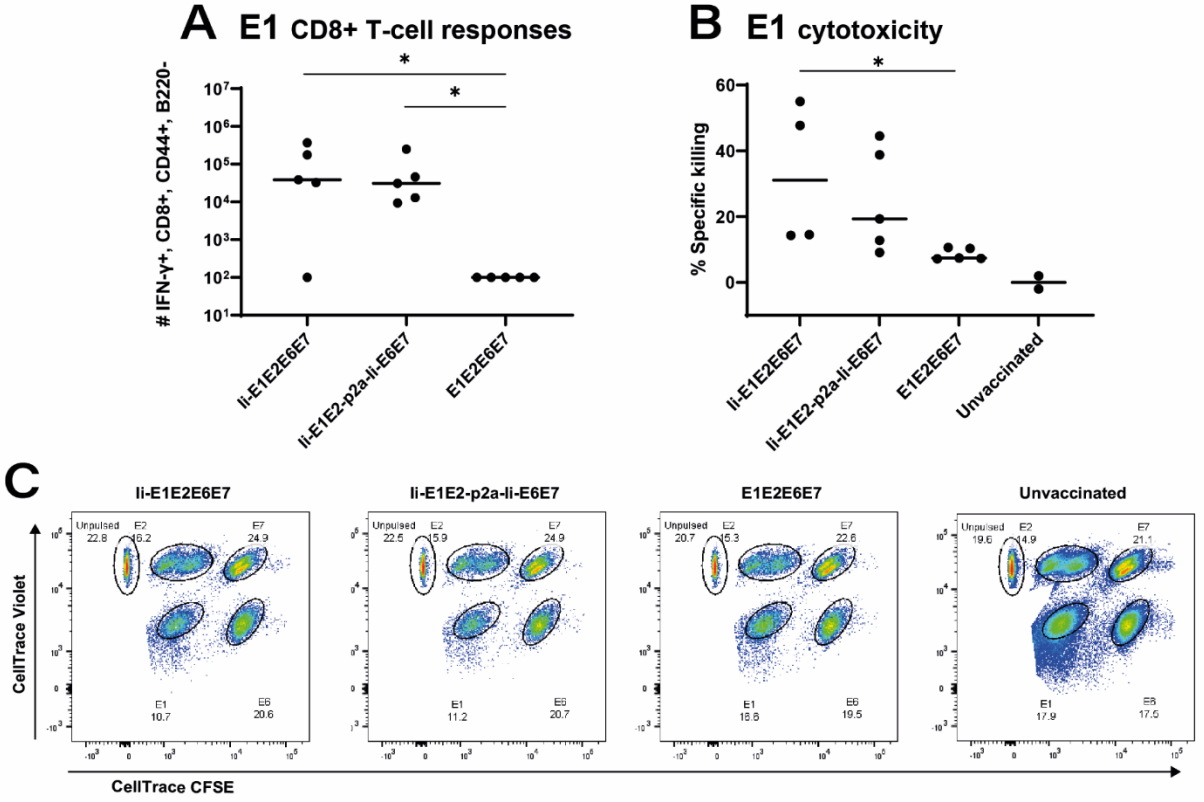

Figure 12: Immune responses in inbred mice and *in vivo* cytotoxicity.
Naïve BALB/c mice were immunized with rAd vectored vaccine encoding the indicated MfPV3 early antigens. 14 days post vaccination, immune responses were analyzed by ICS (A) or *in vivo* cytotoxicity regarding specific killing of E1-peptide pulsed cells (B). Each symbol represents one mouse. Two unvaccinated mice were included as negative controls. (C) Representative plot of *in vivo* cytotoxicity. *p < 0.05.

5.2.4.8 Ii-Fusion Enhanced Ubiquitination and Proteasomal Degradation

The molecular basis of the T cell adjuvant effect of Ii has not been fully clarified yet (221), but one of the suggested mechanisms of action is Ii mediated ubiquitination leading to proteasomal degradation of the linked antigen and thereby enhanced MHC-I presentation (Figure 8C) (323). To investigate if this mechanism could also account for the enhanced $CD8^+$ T-cell responses against the Ii-linked MfPV3 antigens, Ii-E1E2E6E7- and E1E2E6E7-transfected cells were cultivated in absence or presence of the proteasome inhibitor MG132. Anti-ubiquitin western blot analysis of the immunoprecipitated myc-

tagged polypeptides revealed stronger ubiquitin-depending signal intensity for Ii-E1E2E6E7 compared to E1E2E6E7 lacking Ii (Figure 13A). This effect was even more pronounced when MG132 was present. Myc-specific signals confirmed the fidelity of the immunoprecipitation (IP) procedure, and analysis of the IP supernatants by an anti-tubulin western blot confirmed that comparable amounts of cell lysate were used in the IP procedure (Figure 13B, C). A higher level of ubiquitination is commonly associated with faster degradation. This could exemplarily be demonstrated by transiently expressing Ii-E1 and E1, both fused with the C-terminal SIINFEKL peptide, in absence or presence of MG132, respectively (Figure 13D, E). Without MG132, Ii-E1-SIINFEKL was hardly detectable whereas a prominent signal could be visualized when MG132 was added. Lower molecular weight signals are indicative of degradation products. This effect was not observed for E1 without Ii, which suggested that Ii induced an accelerated proteasomal degradation, as also reported by Esposito *et al.* (323).

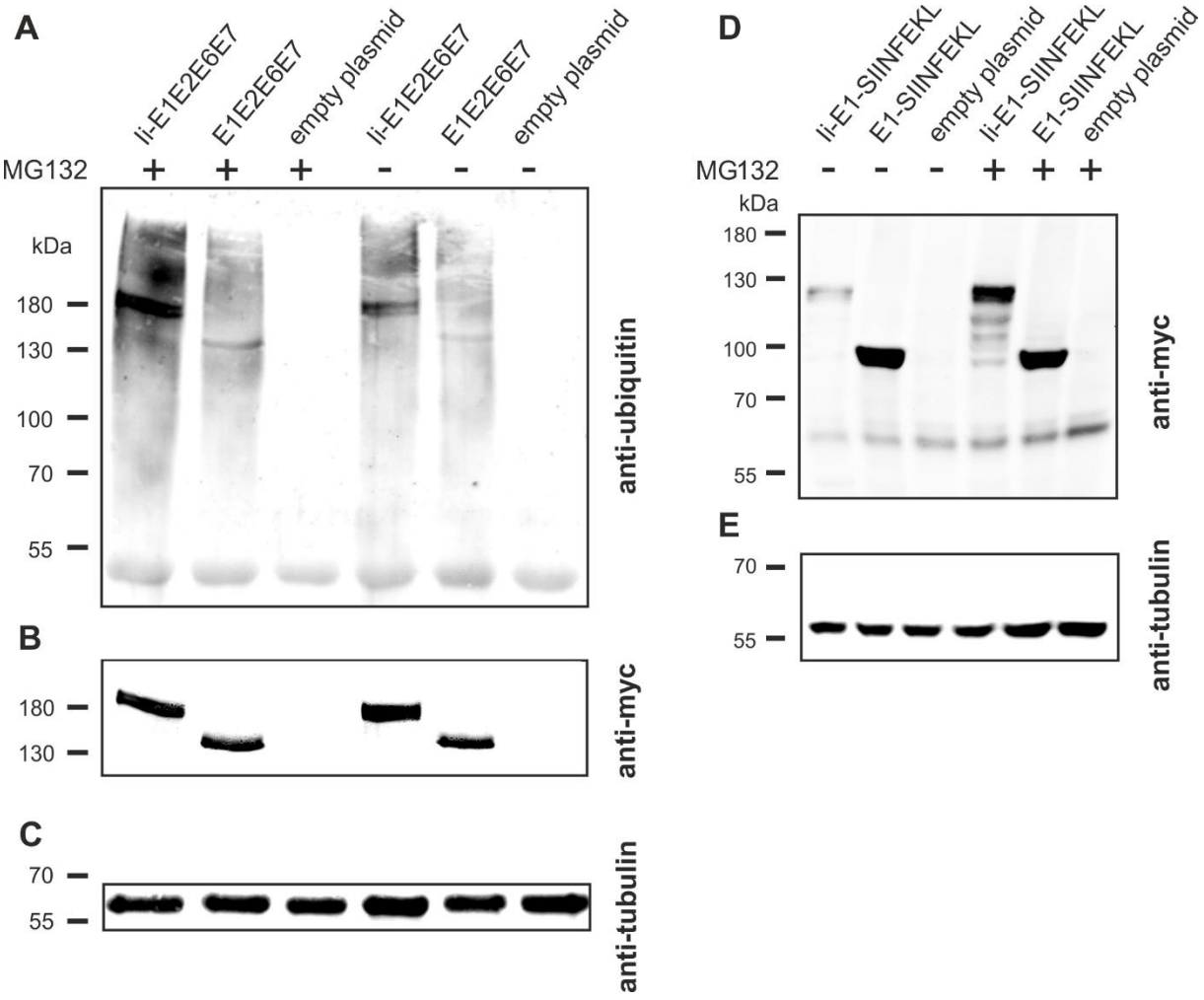

Figure 13: Influence of Ii on ubiquitination and degradation.
(A–C) pURVac Ii-E1E2E6E7, pURVac E1E2E6E7 or the empty plasmid were transfected into HEK293T cells. 24 h after transfection, cells were treated with MG132 or DMSO as control for 6 h. Myc-tagged proteins were immunoprecipitated and analyzed by western blot using an anti-ubiquitin antibody (A) and anti-myc antibody (B). Tubulin levels were monitored using an anti-tubulin antibody as loading control (C). (D, E) pURVac Ii-E1-SIINFEKL, pURVac E1-SIINFEKL or empty plasmid were transfected into HEK293T cells. 24 h after transfection, cells were treated with MG132 or DMSO for 6 h. The samples were analysed by western blot using anti-myc antibody (D) and anti-tubulin antibody (E).

5.2.5 Discussion

Despite the availability of prophylactic vaccines against HPV infections there is an urgent need for an efficient therapeutic HPV vaccine. Currently, there are different vaccine development approaches focusing either on early stages (197,201,255,342) of cervical lesions or late stages such as invasive cervical cancer (313,343–346) or on all stages of pre-malignant cervical lesions (192).

Macaca fascicularis papillomavirus type 3 (MfPV3) infects cynomolgus macaques and infection is associated with persistence and cervical intraepithelial neoplasia (196,199). Moreover, MfPV3 is phylogenetically closely related to HPV16 deriving from a shared most recent common ancestor and both viruses possess a similar mechanism of oncogenesis (198). The closely related pathogenesis of MfPV3 in *Macaca fascicularis* and the use of MfPV3 as antigen source, opens a perspective towards testing therapeutic vaccination concepts in naturally infected macaques and evaluate the correlates of protection under almost natural conditions (201).

Here, ten different antigens were designed comprising the viral early proteins E1, E2, E6 and E7 of MfPV3 in different configurations. These constructs combine antigens against early and late stages of papillomavirus persistence and should be capable of inducing T cell responses against both asymptomatic infections, LSIL as well as HSIL and cancers. All antigens were properly expressed, and their expression levels were similar, despite being artificially fused polypeptides.

Notwithstanding the limited immunogenicity of DNA vaccines, pURVac plasmid immunization of CD1 mice allowed for fast immunological evaluation in an outbred mouse model. Based on this initial *in vivo* screening, a refined antigen (Ii-E1E6E7-p2a-Ii-E2, and as reference Ii-E1E6E7) was devised in order to separate E2 from the readthrough protein, and Ii-E6E7E1E2 was excluded for further development of rAd-based vaccine prototypes. Antigen delivery with rAds of serotype 19a/64 confirmed that all antigens were immunogenic, with most of them inducing potent $CD4^+$ and/or $CD8^+$ T cell responses (Figure 11). In general, adenoviral delivery seemed to be overall more immunogenic than DNA vaccination.

Unexpectedly, no responses against E6 and E7 could be measured in these experiments with CD1 mice. Although fewer mice were expected to respond to E6 and E7 as compared to E2 and E1 due to significant differences in size (factor 5) and thus presumably also number of potential epitopes, it was still surprising that none of the 107 outbred CD1 mice in our experiments that were immunized with E6 and/or E7 harboring vaccines were responding. This might be explained by a yet limited number of MHC alleles in CD1 mice. This hypothesis is supported by the fact that this strain descends from only two male and seven female founder mice (341). In a different strain, outbred OF1 mice, we could successfully elicit T-cell responses against MfPV3 E6 confirming the general immunogenicity of this antigen.

Coupling of antigens to certain immune regulatory molecules and T cell adjuvants could be beneficial in terms of breaking the immunosuppressive environment of tumors (343,347). All immunogens expressed *via* rAds contain the T cell adjuvant Ii (except for E1E2E6E7 which serves as reference), which is known to enhance $CD4^+$ and $CD8^+$ T cell responses when delivered by viral vectors (218,221–223,323). A trend towards higher magnitudes of responses against E1 and E2 could be observed in outbred mice when vaccinated with rAd Ii-E1E2E6E7 as compared to E1E2E6E7 (Figure 11) and, importantly, a significantly higher level of specific killing in animals vaccinated with Ii-adjuvanted vaccines has been shown (Figure 12). Whereas enhancement of $CD4^+$ T cell response is believed to be induced by trafficking to endolysosomal compartments (221), far less is known about the mechanism of enhancing $CD8^+$ T cell

response. However, this effect is independent of MHC-II and $CD4^+$ T cell response (222), but possibly depending on enhanced MHC-I loading (221). As shown in Figure 13, Ii-fusion leads to more pronounced ubiquitination and faster degradation of Ii-E1E2E6E7 as compared to E1E2E6E7 lacking Ii and therefore might increase the number of peptides that can be loaded on MHC I. Such a mechanism has recently also been reported by Esposito *et al.* (323), as a mode of action for the Ii adjuvant to increase the level of antigen fragments available for MHC presentation.

Considering the protein expression pattern during early stages of HPV infection, it is reasonable to assume that potent $CD4^+$ and $CD8^+$ T cell responses against E1 and E2 should be sufficient to boost naturally raised T cell immunity against PVs in LSIL, especially as E2 responses correlate with absence of lesion progression (150). Noteworthy, E1 is required for successful PV replication in infected cells, and cellular immune responses against E1 have been detected in PBMCs of some patients with HPV^+ cervical squamous cell carcinoma. The presence of E1 responses strikingly correlated in these patients with improved clinical outcomes, but the responses were of low magnitude, suggesting insufficient APC-mediated activation of T-cells (319). An explanation for this could be that E1 during natural infection, is not abundantly expressed and rapidly degraded through the proteasome as shown for bovine PV (202,203). Therefore, a vaccine delivery format supporting efficient induction of $CD4^+$ and $CD8^+$ specific T cells on the fundament of strong expression and efficient antigen processing and presentation is expected to support elimination of premalignant PV transduced cells - provided that early neoplasias display sufficient amounts of E1/MHC-I complexes on their cell surface. Herein, we demonstrated strong expression of E1 comparable to E2, E6 and also E7, probably attributable to the strong CMV promoter-induced overexpression, and additional Ii-induced accelerated proteasomal degradation (Figure 13) and MHC-I presentation (Figure 8C). Altogether, our E1 containing vaccine constructs gave rise to solid $CD8^+$ and $CD4^+$ responses, which are cytotoxic to E1-peptide-pulsed target cells (Figure 12). This, together with the indication that E1 responses, once induced, are correlated with improved clinical outcome, build a strong case for including E1 in therapeutic HPV vaccine designs.

Our study has limitations regarding weak or absent T-cell responses against E6 and E7 in different mouse strains used in this study. This could potentially be due to immunodominance of E1 and E2 competing with E6 and E7 antigen processing, presentation and induction of specific T-cell responses. Alternatively, we cannot exclude that inactivation of E6- and E7-transforming potential has destroyed relevant epitopes. Ongoing preclinical analysis of viral vector-delivered MfPV3 antigens in macaques and comparable HPV16-derived immunogen designs in selected mouse models will provide further insights regarding the capacity of such immunogens to raise broad T-cell responses to the delivered early antigens including E6 and E7. The latter will also reveal to which extent the antigen design will be transferable to HPV16 and other high-risk HPV types. Given the phylogenetically close relationship and similar mechanisms underlying oncogenesis of the two papillomaviruses (198), similar immunological properties would be assumed.

Taken together, we developed ten immunogens that target the early proteins of MfPV3. These artificially fused polypeptides share similar biochemical and immunological properties without loss of individual antigen responses. Two polypeptides, Ii-E1E2E6E7 and Ii-E1E2-p2a-Ii-E6E7, elicited vigorous T cell responses, in particular, these two antigens were able to induce robust T cell responses against E1, E2 and E6, and to kill peptide-pulsed cells *in vivo*. Due to lower complexity, antigen size and non-inferior immunogenicity, Ii-E1E2E6E7 was chosen for further studies. Ad19a/64 proved to be a suitable vector to deliver Ii-E1E2E6E7 and is currently being validated as a therapeutic vaccine in persistently MfPV3-infected cynomolgus macaques. Moreover, the configuration of this immunogen will serve as template to

generate novel vaccine candidates for therapeutic vaccination against high-risk human papillomavirus types.

5.2.6 Supplement

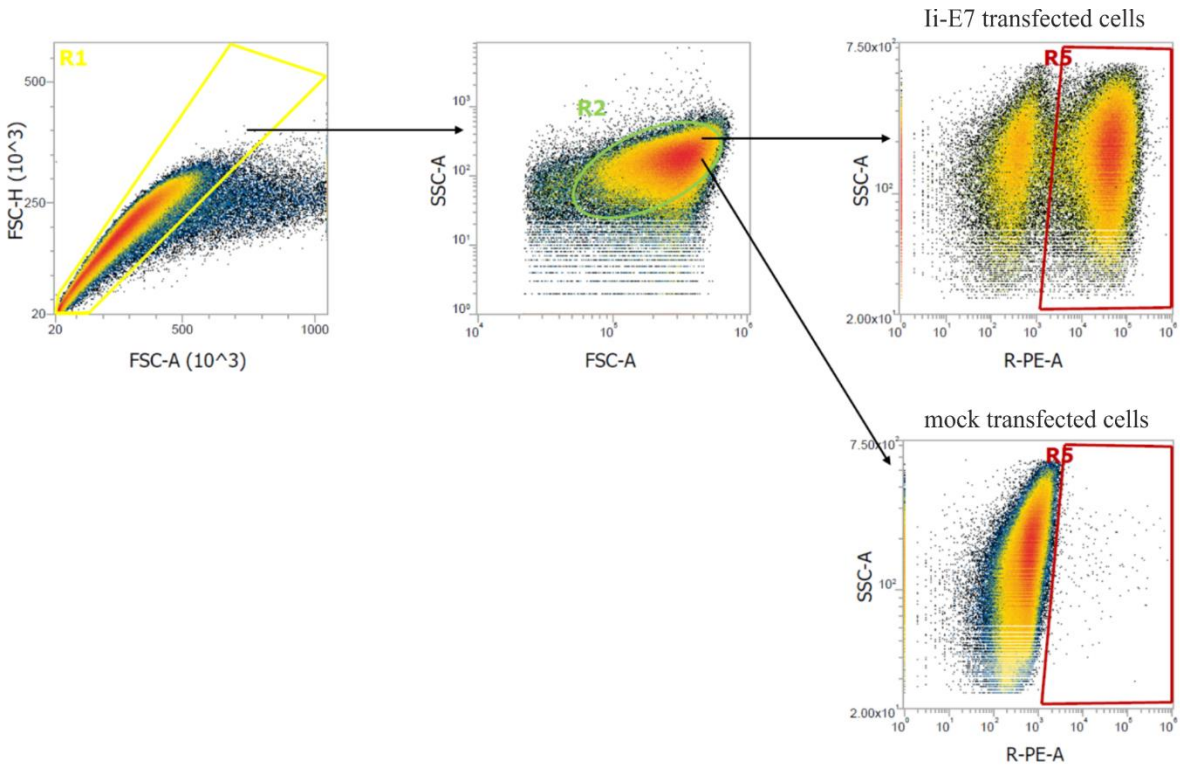

Supplementary Figure 1.
Gating strategy for flow cytometry analysis of pURVac transfected HEK293T cells 48 h post transfection.

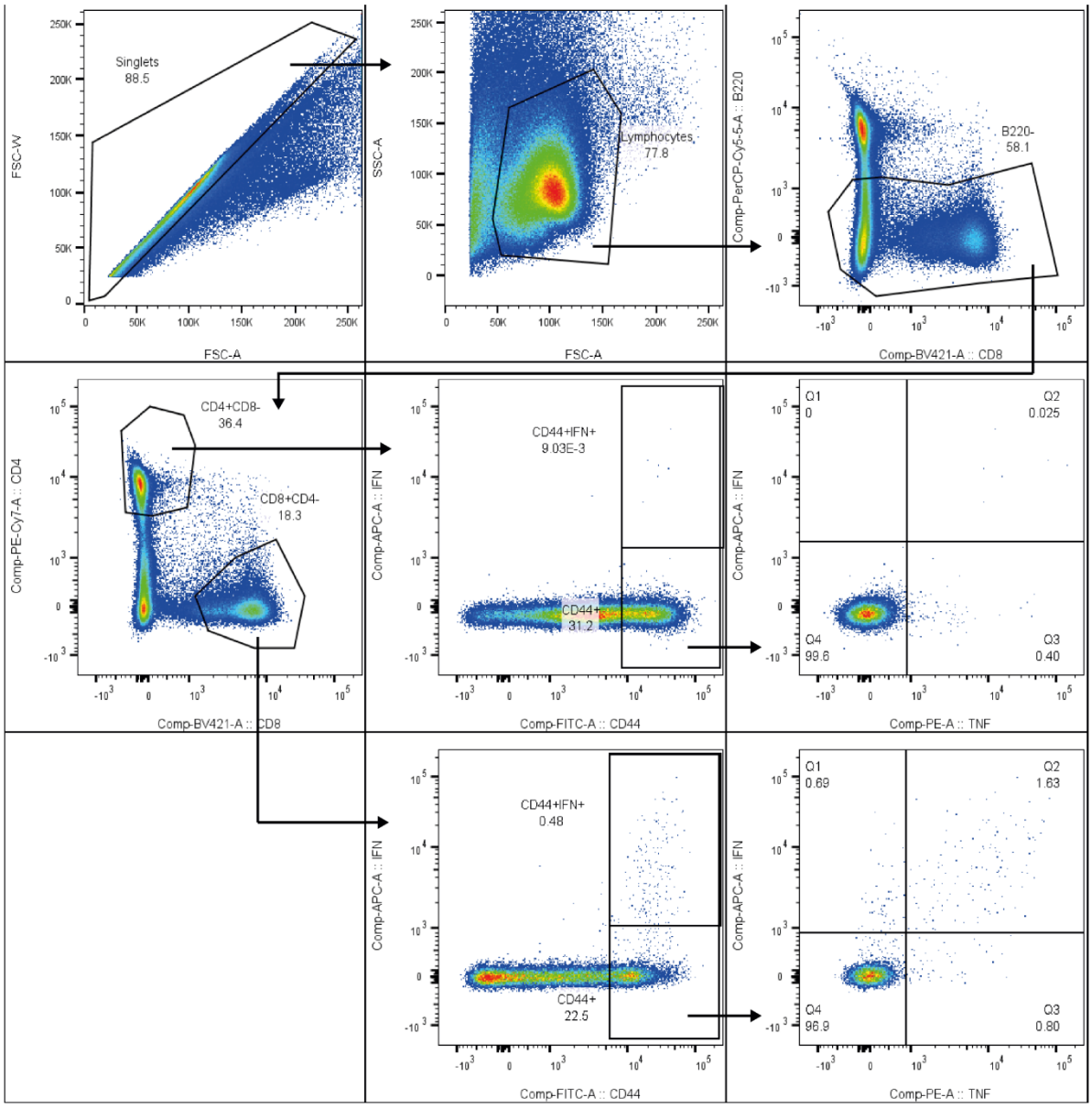

Supplementary Figure 2.
Gating of spleen samples of a representative animal 14 days after vaccination with rAd-Ii_E1E2E6E7, stimulated with E1 peptide pool. The total number of IFN- γ^+/CD44$^+$/CD8$^+$ or CD4$^+$/B220$^-$ cells reported as the CD8$^+$ and CD4$^+$ responses throughout the article, has been gated this way.

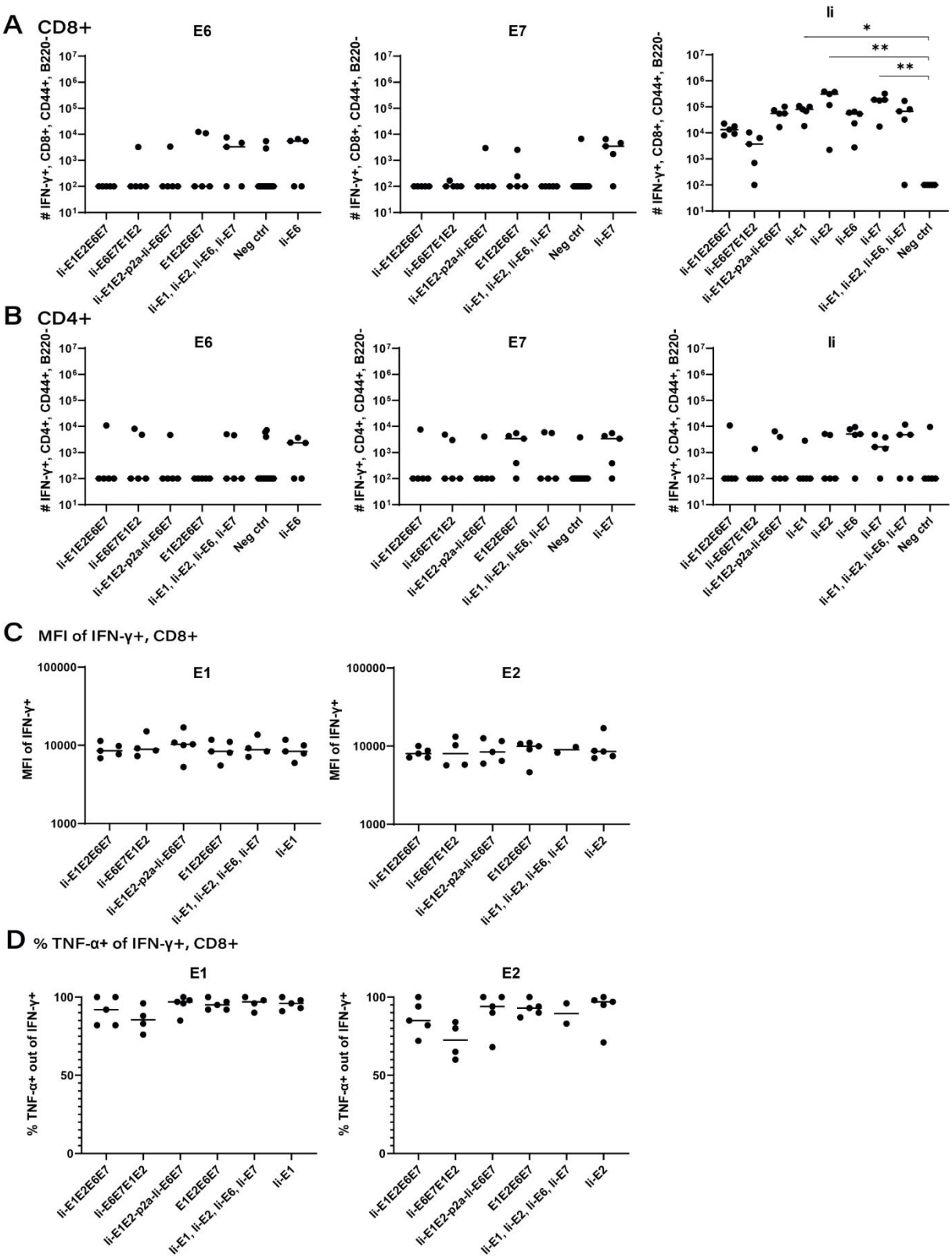

Supplementary Figure 3.

(A-D) CD1 mice (5 per group) were immunized 4 times with 0.5 µg DNA of pURVac DNA encoding the indicated MfPV3 early antigens. Mice were sacrificed 7 days post last immunization, spleens were harvested. (A-B) $CD8^+$ and $CD4^+$ T-cell immune responses against li were measured using ICS and flow cytometry. (C-D) The quality of the $CD8^+$ antigen specific cells was assessed by the MFI of IFN-γ and by the fraction of IFN-$γ^+$ T cells capable of also producing TNF-α. Negative control groups consist of all mice immunized with a pURVac DNA vaccine encoding antigens not covered by the peptide pools used for *in vitro* restimulation. Asterisks between groups

indicate significant differences in response-levels after subtraction of background responses. Each symbol represents one mouse.

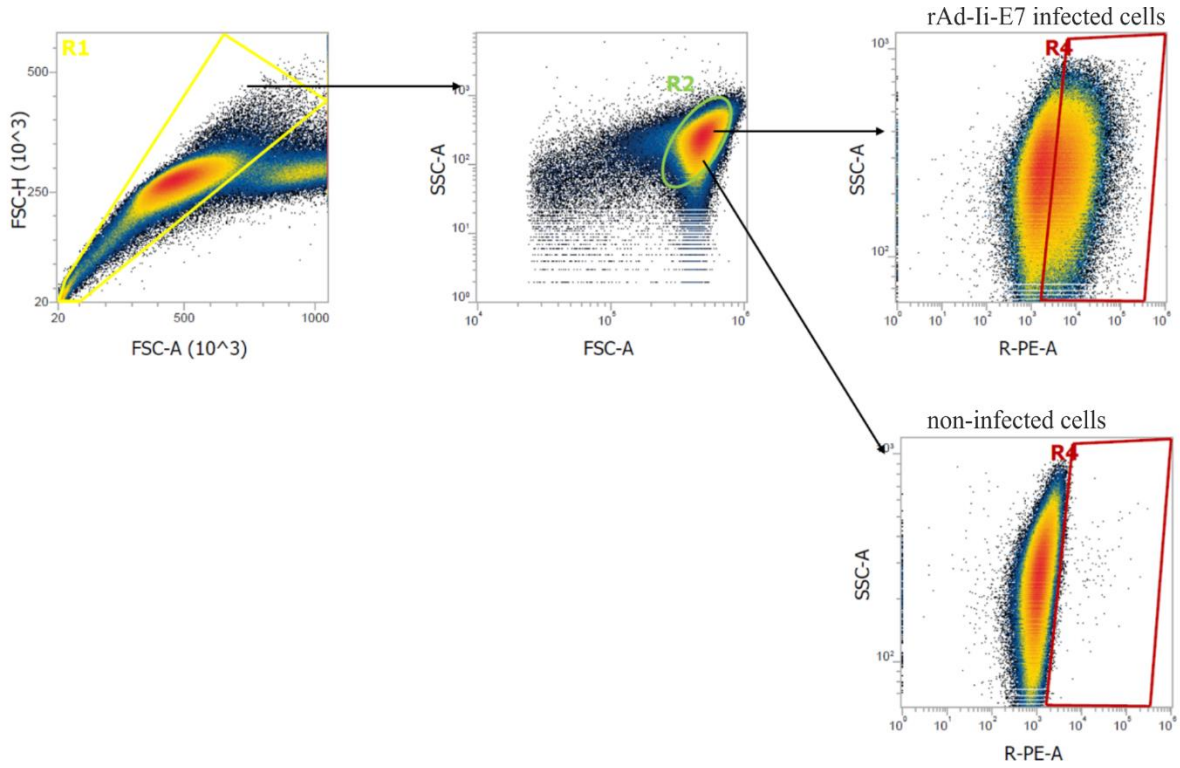

Supplementary Figure 4.
Gating strategy for flow cytometry analysis of rAd-infected A549 cells 48 h post infection.

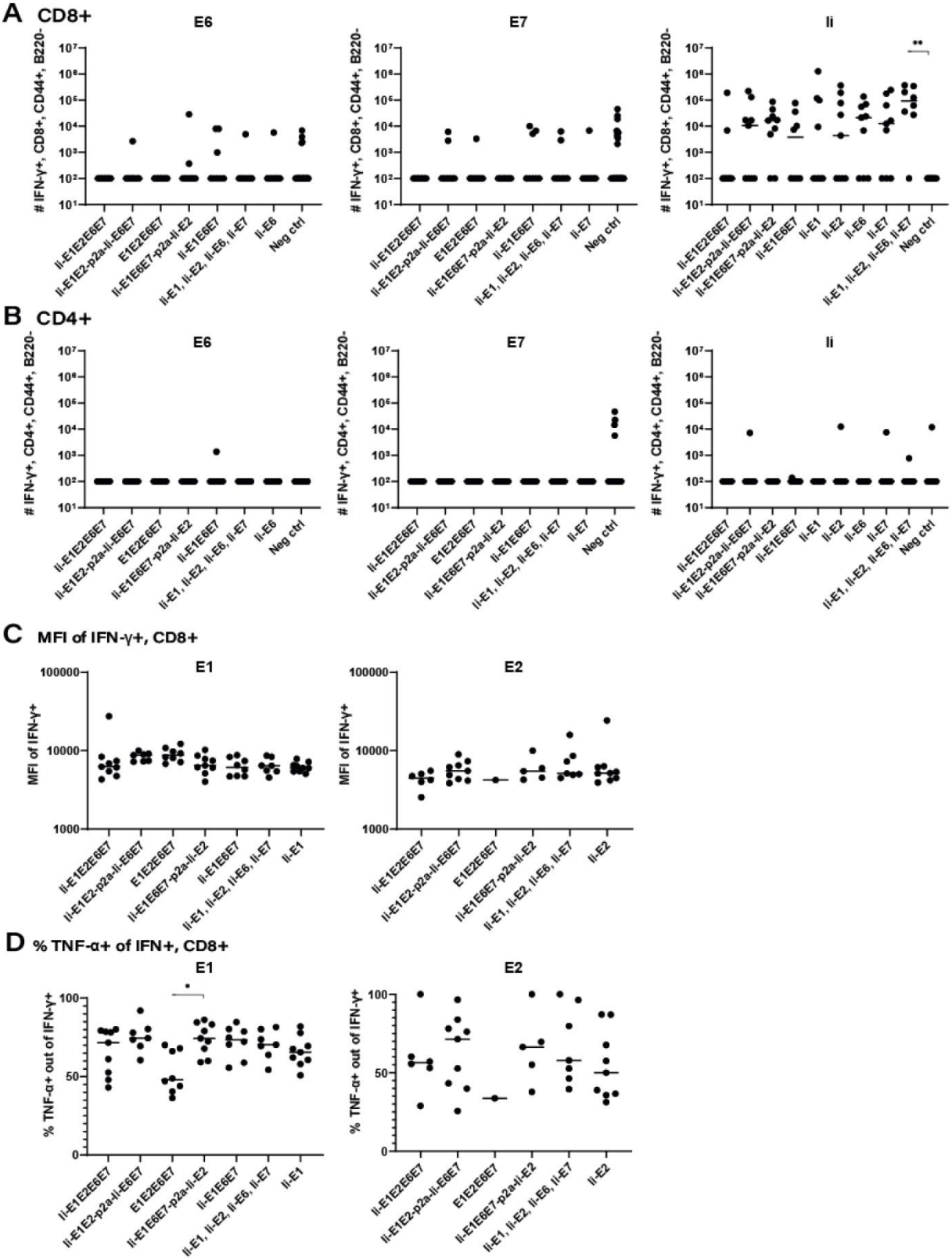

Supplementary Figure 5.

(A-D) CD1 mice were immunized with rAd vectored vaccine (2×10^7 IFU) encoding the various MfPV3 early antigens as indicated. Mice were sacrificed on day 14 and spleens were harvested. (A-B) CD8$^+$ and CD4$^+$ T-cell immune responses against Ii were measured using ICS and flow cytometry. (C-D) The quality of the CD8$^+$ antigen specific cells was assessed by the MFI IFN-γ and by the fraction of IFN-γ$^+$ T cells capable of also producing TNF-α. Negative control groups consist of all mice immunized with rAd encoding antigens not covered by the peptide pools used for *in vitro* restimulation. Each symbol represents one mouse. Asterisks between groups indicate significant differences in response-levels after subtraction of background responses.

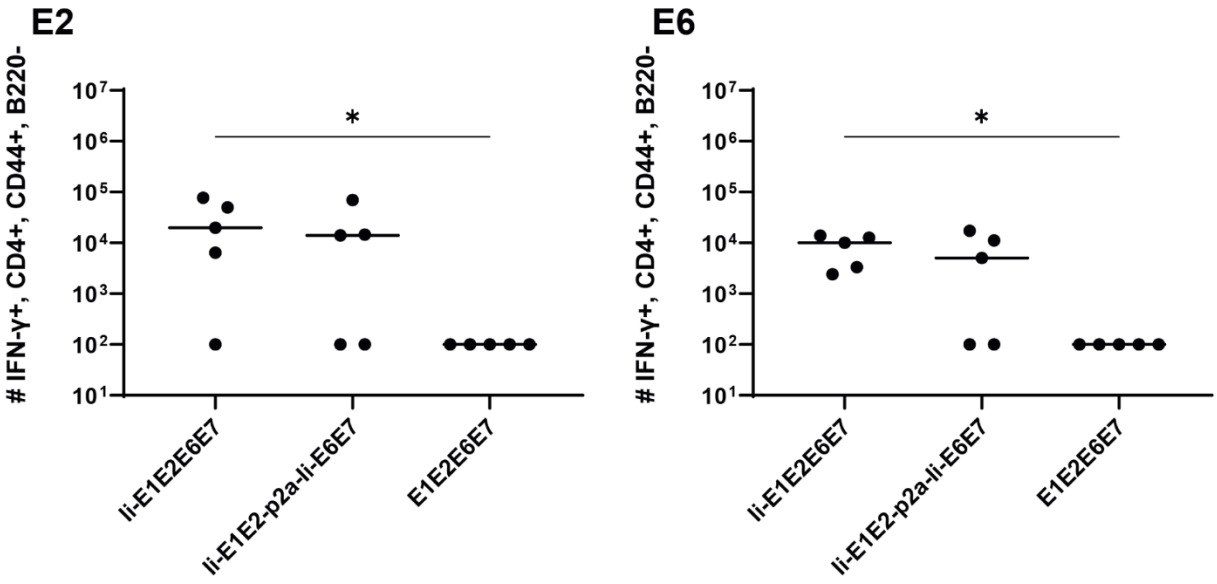

Supplementary Figure 6.
BALB/c mice were immunized with (2×10^7 IFU) rAd vectored vaccine encoding the various MfPV3 early antigens. Mice were sacrificed on day 14, spleens were harvested and $CD4^+$ T-cell immune responses against E2 and E6 were measured using ICS and flow cytometry. Each symbol represents one mouse.

5.2.7 Ethics Statement

The animal study was reviewed and approved by National Animal Experiments Inspectorate (Dyreforsøgstilsynet, license no. 2016-15-0201-01131).

5.2.8 Funding

This project has received funding from the Eurostars-2 joint programme with co-funding from the European Union Horizon 2020 research and innovation programme (E!12151). The project E!12151 was carried out within the framework of the European funding program “Eurostars” and the German partners were funded by the Federal Ministry of Education and Research. The manuscript reflects only the authors’ view and the European Commission is not responsible for any use that may be made of the information it contains. The funders had no influence on study design, data collection and analysis, decision to publish, or preparation of the manuscript.

5.2.9 Acknowledgments

We kindly thank Eurostars-2 joint programme, the European Union Horizon 2020 research and innovation programme and the German Federal Ministry of Education and Research for funding this work. We would like to thank Jan Pravsgaard Christensen, UCPH, for advice on the *in vivo* cytotoxicity experiments, and Anette Stryhn Buus, UCPH, for assistance with peptides for *ex vivo* stimulation.

5.3 Manuscript 2

"Efficacy and Synergy with Cisplatin of an Adenovirus Vectored Therapeutic E1E2E6E7 Vaccine against HPV Genome-Positive C3 Cancers in Mice"

Ditte Rahbaek Boilesen [1 2 #], Patrick Neckermann [3 #], Torsten Willert [4], Mikkel Dons Müller [1 2], Silke Schrödel [4], Cordula Pertl [4], Christian Thirion [4], Benedikt Asbach [3], Ralf Wagner [3 5 *], Peter Johannes Holst [1 2 *]

[1] Centre for Medical Parasitology, The Panum Institute, Department of Immunology and Microbiology, University of Copenhagen, Copenhagen, Denmark.

[2] InProTher ApS, Copenhagen, Denmark.

[3] Institute of Medical Microbiology and Hygiene, Molecular Microbiology (Virology), University of Regensburg, Regensburg, Germany.

[4] SIRION Biotech GmbH, Planegg-Martinsried, Germany.

[5] Institute of Clinical Microbiology and Hygiene, University Hospital Regensburg, Regensburg, Germany.

[#]These authors have contributed equally to this work and share first authorship

*Correspondence: Ralf Wagner, ralf.wagner@ur.de; Peter Johannes Holst, pholst@sund.ku.dk

Published in Cancer Immunology Research, ©2022 American Association for Cancer Research

DOI: 10.1158/2326-6066.CIR-22-0174

Received: 06th of March 2022

Revision received: 25th of August 2022

Accepted: 14th of December 2022

Published: 03rd of February 2023

5.3.1 Abstract

Human papillomavirus (HPV) infections are the main cause of cervical and oropharyngeal cancers. As prophylactic vaccines have no curative effect, an efficient therapy would be highly desired. Most therapeutic vaccine candidates target only a small subset of HPV regulatory proteins, namely, E6 and E7, and are therefore restricted in the breadth of their immune response. However, research has suggested E1 and E2 as promising targets to fight HPV$^+$ cancer. Here, we report the design of adenoviral vectors efficiently expressing HPV16 E1 and E2 in addition to transformation-deficient E6 and E7. Vaccination elicited vigorous CD4$^+$ and CD8$^+$ T-cell responses against all encoded HPV16 proteins in outbred mice and against E1 and E7 in C57BL/6 mice. Therapeutic vaccination of C3 tumor-bearing mice led to significantly reduced tumor growth and enhanced survival for both small and established tumors. Tumor biopsies revealed increased numbers of tumor-infiltrating CD8$^+$ T cells in treated mice. Cisplatin enhanced the effect of therapeutic vaccination, accompanied by enhanced infiltration of dendritic cells into the tumor. CD8$^+$ T cells were identified as effector cells in T-cell depletion assays, seemingly under regulation by FoxP3$^+$CD4$^+$ regulatory T cells. Finally, therapeutic vaccination with Ad-Ii-E1E2E6E7 exhibited significantly enhanced survival compared with vaccination with two peptides each harboring a known E6/E7 epitope. We hypothesize that this difference could be due to the induction of additional T-cell responses against E1. These results support the use of this novel vaccine candidate targeting an extended set of antigens (Ad-Ii-E1E2E6E7), in combination with cisplatin, as an advanced strategy to combat HPV$^+$ cancers.

5.3.2 Introduction

Infections with high-risk human papillomavirus (HPV) typically resolve spontaneously, yet some progress into a chronic stage and have been associated with a large fraction of cervical, oropharyngeal, penile, anal, vaginal, and vulvar cancers (348).

Despite efficient prophylactic vaccines, the worldwide HPV-associated disease burden remains substantial. Cervical cancer is the most common HPV-associated cancer globally, whereas the incidence of HPV-associated oropharyngeal squamous cell carcinoma (OPSCC) has increased markedly, in the United States by 225% from 1988 to 2004 (35) and has in some countries surpassed cervical cancer in terms of annual deaths (349).

Cure rates from cervical cancer and OPSCC are high (350), but the treatments cause substantial morbidity, and the patients who experience treatment failure or relapse are left with few treatment options and a poor long-term prognosis. Checkpoint inhibitors, such as anti–PD-1, provide some life-prolonging effects against advanced oropharyngeal cancer (296,351,352) and when administered post initial chemotherapy against metastatic or recurrent cervical cancers (353).

Accordingly, new therapeutic strategies to combat HPV$^+$ cancers are needed. Therapeutic vaccines inducing cytotoxic T cells that eradicate the HPV-infected cells are promising candidates for HPV$^+$ lesions and cancer therapy. However, although a number of therapeutic vaccines show improvements in clinical outcomes for HPV$^+$ cancer patients, this is typically seen only in about 20% to 50% of patients (166). Common for most therapeutic vaccine candidates is that they target the small HPV oncogenes E6 and/or E7 only (166). However, expression and immune responses against other HPV antigens, such as E1 and E2, have been detected in cervical cancer and OPSCC and could broaden the immunopeptidome available for HPV vaccines. In support, E1-specific T-cell responses have been correlated with improved progression-free survival and overall survival in cervical cancer (319), and E2 remains intact in a substantial fraction of cervical cancers (123,135). Furthermore, most OPSCC contain

a high copy number of HPV16 genomes with intact E2 (136,180), and both E1 and E2 are immunogenic in OPSCC (188,354). The high prevalence and possible immunogenicity of E1 and E2 in HPV-associated malignancies demand a reconsideration of antigen selection in HPV therapeutics.

A problem for many E6- and E7-based therapeutic vaccines in clinical testing is that only a fraction of patients responds (166). Incorporation of E1 and E2 into the fusion-gene vaccine antigen increases the immunogen size 5-fold, compared with E6 and E7 alone, and a larger antigen increases the likelihood of inducing an anti-HPV response in more individuals across HLA types (217). Janssen tested a vaccine encoding E2, E6, and E7, where E2, the largest of the three antigens, was the only antigen toward which all patients had $CD8^+$ T-cell responses (355). A large antigen may also increase the number of anti-HPV specificities induced in a vaccinated individual, thereby potentially increasing the magnitude of the total T-cell response.

Here, we present an immunogen design, which encompasses the full-length HPV16 antigens E1, E2, E6, and E7. The selection of antigen, adjuvant, and order of antigens was influenced by previous work on *Macaca fascicularis* papillomavirus type 3 (MfPV3) vaccines, which proved highly immunogenic in various outbred mouse strains and confirmed a general superiority of E1 and E2 over E6 and E7 in terms of immunogenicity (356). The two oncoproteins were inactivated by selected point mutations and characterized *in vitro* to confirm the lack of transforming capacity. To enhance the magnitude of the vaccine-induced $CD8^+$ T-cell activation, antigens were genetically linked to the T-cell adjuvant major histocompatibility complex (MHC) class II–associated invariant chain (Ii; (323)).

For antigen delivery, an adenovirus vector platform was chosen as the most potent clinically validated T cell–inducing technology (323). In the context of SARS-CoV-2, it was shown that using a heterologous prime–boost strategy to bypass vector immunity is superior to a homologous regimen in terms of inducing strong T-cell responses (357). For that purpose, we implemented a heterologous prime–boost regimen of the human adenovirus serotype 19a/64 (Ad19a/64) and serotype 5 (Ad5; (255)).

Herein, we assessed the immunogenicity in outbred and inbred mice and antitumor efficacy of such vaccines in mice, using the hard-to-treat C57BL/6 murine $HPV16^+$ tumor model C3 (195,358,359). Outbred mice with a larger diversity in MHC haplotypes were used to better simulate immunogenicity in the outbred human population, before moving into inbred mice for antitumor efficacy studies. All four antigens in the vaccine were immunogenic in at least one outbred mouse strain, and E1 was the only antigen capable of consistently inducing immune responses across all used outbred models. The vaccine showed single-agent therapeutic efficacy and synergy with cisplatin and performed well compared with vaccination with two selected synthetic long E6/E7 peptides that have previously been efficacious against C3 tumors (302,359,360). A similar peptide vaccination approach comprising altogether 13 synthetic long peptides has also been validated in patients (300).

To our knowledge, no previously published studies have evaluated the immunogenicity and antitumor efficacy of a vaccine encoding full-length E1 and E2 in addition to E6 and E7.

5.3.3 Materials and Methods

5.3.3.1 Antigen sequences

The antigen sequences were designed as previously described (356). Sequences encoding E1, E2, E6, and E7 of HPV16 (gi|333031|lcl|HPV16REF.1|HPV16REF) were gene-optimized and synthesized at Geneart/Thermo Fisher (324).

Further sequence elements that were optionally used to build the prototype vaccine inserts (Figure 14) comprised (i) the human MHC-II–associated invariant chain (Ii; (323); molecular adjuvant; NM_004355.3), (ii) a 2 amino acid GS-linker connecting the viral early proteins in the respective fusion proteins, as well as (iii) the porcine teschovirus-1 p2a sequence (325) to support coexpression of two fusion proteins when relevant. Vaccine inserts were assembled in adenoviral vectors and lentiviral vectors either with fusion PCR or using type II exocutter sites. Nucleotide sequences are shown in Supplementary Figure 7.

5.3.3.2 *In silico* MHC-I binding prediction

MHC-I epitope prediction was performed on May 16, 2022, using IEDB analysis resource v2.24 with the ANN4.0/NetMHC4.0 prediction method (361–363) for the E1, E2, E6, and E7 antigen sequences. A number of 49 HLA types were selected that together cover at least 75% of the worldwide population for HLA-A, -B, and -C, respectively. Only epitopes with a calculated IC_{50} below 5,000 nmol/L were further analyzed. For visualization, calculated epitopes were aligned on the E1E2E6E7 fusion protein at their respective position.

5.3.3.3 Cell culture, transfection, and viral infection

HEK293T (ATCC, CRL-11268/2007, number of passages not monitored), A549 (from Marian Wiegand/Amvac Research GmbH), and NIH-3T3 (from Martin Ehrenschwender/IMHR, maximum 20 passages) cells were maintained and grown in Dulbecco's MEM (DMEM, Gibco) supplemented with 10% fetal calf serum (FCS), 100 units/mL penicillin, and 0.1 mg/mL streptomycin (penicillin/streptomycin, Gibco). The NIH-3T3 cells were maintained between 10% and 70% confluence to prevent maturation and differentiation. The three cell lines were maintained at 37°C and 5% CO_2 in a nonhumidified incubator. HEK293T cells were transfected using the polyethylenimide (PEI) method (330). Cell line authentication and mycoplasma testing were not performed for the three abovementioned cell lines.

C3 cells ((195); from Prof. Dr. S.H. van der Burg, Leiden University Medical Center) were cultured in Iscove's modified Dulbecco's media (Gibco), 8% FCS (Sigma-Aldrich), 2 mmol/L L-glutamine (Gibco), 100 IU/mL penicillin (BioWhittaker), 100 µg/mL streptomycin (BioWhittaker), and 0.1 mg/mL kanamycin (Sigma-Aldrich). The day before tumor cell injection, the media were changed to one not containing kanamycin. Authentication was done with intracellular staining with anti-HPV16E7 (sc-65711, Santa Cruz Biotechnology) and flow cytometry. Cells were thawed, passaged three times, and tested negative for mycoplasma (Eurofins) before being injected in mice.

5.3.3.4 Generation and titration of adenoviral vectors

E1/E3-deficient adenoviral vectors of serotype Ad19a/64 and serotype Ad5 were generated as previously described (258). Titration was performed using the RapidTiter method by detection of infected HEK293 cells via IHC staining with anti-hexon [Ad19a/64: Novus, Adenovirus Antibody (8C4), Ad5: Santa Cruz, Adenovirus Antibody (1E11)]. Insert integrity was confirmed by PCR amplification from the purified vector DNA followed by DNA sequencing.

5.3.3.5 Western blot analysis

Western blot analysis was performed as previously described (258). Protein was detected using anti-E2 (TVG-271, 1:200, Santa Cruz Biotechnology), anti-E6 (for western blots only, GTX132686, 1:2,000, Biozol), anti-E7 (NM2, 1:200, Santa Cruz Biotechnology), mouse anti-tubulin (DM1α, 1:1,000, Santa Cruz), goat anti-mouse-HRP (115-036-003, 1:5,000, Jackson), goat anti-rabbit-HRP (P0448, 1:2,000, Dako), and enhanced chemiluminescence substrate or Femto ECL (Thermo Fisher), and read on Chemilux Pro (Intas).

5.3.3.6 Flow cytometry analysis of transfected and transduced cell lines

Intracellular staining of antigens was performed using standard methods (258). Cells were stained with anti-E2, anti-E7 (see Western blot section, 1:50), anti-E6 (orb557164, 1:50, Biozol), anti-p53 (7F5, 1:800, Cell Signaling Technology), goat anti-mouse-PE (550589, 1:200, BD), goat anti-rabbit Alexa Fluor 647 (A21244, 1:200, Life Technologies), rabbit mAb IgG XP isotype control (DA1E, Cell Signaling Technology), or mouse IgG1 κ isotype control (MG1-45, BioLegend). Flow cytometry was performed on Attune NxT (Thermo Fisher) and analyzed using Attune NxT software.

5.3.3.7 Production of VSV-G-pseudotyped lentiviral vectors

The designed HPV16 antigens and HPV16 E6 wild-type (wt) were cloned into pLV-CMV-MCS-IRES-Puro (Sirion Biotech), and HPV16 E7wt was cloned into pLV-CMV-MCS-IRES-Neo (Sirion Biotech), using AgeI-HF and NotI-HF (New England Biolabs). 3.9×10^6 HEK293T cells were seeded, and after 24 hours transfected with 3.75 µg of pLV containing the antigen and 3.75 µg of lentivirus packaging mix (1:1:1; pMDL-Gag:pVSV-G:pREV, supplied by Sirion Biotech) using the PEI (Sigma-Aldrich) method (330) in a final volume of 9 mL, and harvested after 48 hours.

5.3.3.8 Transduction of NIH-3T3 cells and antibiotic selection

NIH-3T3 cells (1×10^5) were seeded, and after 24 hours transduced with 2 mL of each supernatant containing the respective lentiviral vector in the presence of 10 µg/mL polybrene (TR-1003-G, Sigma-Aldrich). After 72 hours, transduced cells were selected via 1 mg/mL G418 (CP11.3, Roth) and/or 2 µg/mL puromycin (ant-pr-1, InVivoGen). The cells were under antibiotic selection for at least 2 weeks, until all untransduced cells had died.

5.3.3.9 Soft-agar transformation assay

The soft-agar transformation assay was performed as described previously (364) with minor modifications as follows. Six-well plates were filled with 2 mL DMEM (D2902, Sigma-Aldrich) containing 10% FCS, penicillin/streptomycin, 3.7 g/L $NaHCO_3$, 3.8 g/L D-glucose, 0.5% low melt agarose (6351.2, Roth), 1 mg/mL G418, and/or 2 µg/mL puromycin. Once solidified, 5×10^3 lentivirally transduced polyclonal NIH-3T3 cells were seeded in 37°C-prewarmed DMEM containing 10% FCS, penicillin/streptomycin, 3.7 g/L $NaHCO_3$, 3.8 g/L D-glucose, 0.35% low melt agarose, 1 mg/mL G418, and/or 2 µg/mL puromycin. The plates were incubated at 37°C and 5% CO_2 for 21 days. 200 µL medium (DMEM, FCS, penicillin/streptomycin) was added twice weekly for 21 days. Cells were then fixed in 4% PFA (w/v, cat. no.: P6148-500G, Sigma-Aldrich) and stained with 0.005% crystal violet (w/v, cat. no.: C-6158, Sigma-Aldrich) in 10% methanol (v/v, M/4000/17, Fisher Scientific) for 1 hour at room temperature. Pictures were taken on an alphaimager HP (Proteinsimple) at an aperture of 5.6 and focus of 2.88. The colonies were counted with ImageJ (365). Representative picture sections were taken with a BZ 9000 inverted microscope (Keyence).

5.3.3.10 Animals

C57BL/6 and CD1 mice were obtained from Envigo, OF1 mice from Charles River, and HSd-Ola mice from Envigo. All animals were females, 6 to 8 weeks old, and were housed at the Panum Institute, University of Copenhagen. All experiments were initiated after allowing the mice to acclimatize for at least 1 week. Experiments were approved by the National Animal Experiments Inspectorate (Dyreforsøgstilsynet, license no. 2016-15-0201-01131) and performed according to national guidelines. Animals were sacrificed by cervical dislocation once the tumor exceeded 1,000 mm^3 or at the time points indicated.

5.3.3.11 Tumors and immunizations

C3 tumor cells (1×10^6) in 200 µL PBS were injected subcutaneously (s.c.) into the flank of C57BL/6 mice. Tumor size was measured in length and width three times weekly, and the tumor volume was calculated as: length × width^2 × 0.5236 (366). For the treatment of established tumors, mice were randomized by tumor volume prior to treatment. Groups of treated tumor-bearing mice were terminated when all mice in the corresponding control group or 50% of the mice within the treatment group had died.

Immunizations with adenoviral vectors were performed intramuscular (i.m.) in the thigh with 2×10^7 infectious units (IFU) in 50 µL PBS. Negative controls contained vectors with Ii-linked HIV or SIV antigens (Supplementary Figure 7). Immunization with two peptides, HPV16 $E6_{41–65}$ (KQQLLRREVYDFAFRDLCIVYRDGN), harboring the H2-Kb epitope $E6_{48–57}$ (EVYDFAFRDL; (367)), and $E7_{43–77}$ (GQAEPDRAHYNIVTFCCKCDSTLRLCVQSTHVDIR) harboring the H2-Db epitope $E7_{49–57}$ (RAHYNIVTF; (195); Schafer), was performed s.c. in the flank with 50 µg of each peptide in Incomplete Freund's adjuvant (Sigma-Aldrich) as previously described (302,359). The peptides correspond to synthetic long peptides E6.2 and E7.2 of the ISA101 vaccine used in clinical testing (see Melief and colleagues Supplementary Table S10; (300)) and were selected as they harbor the only known $CD8^+$ T-cell epitopes in C57BL/6 mice. Peptides for immunization were prepared according to previous studies (302,359) and advice from T. van Hall and C. Melief of Leiden University Medical Centre. Lyophilized peptide was dissolved to 0.5 mg/mL in PBS and 0.5% DMSO and then emulsified 1:1 in Incomplete Freund's adjuvant (Sigma-Aldrich). 200 µL was injected per mouse.

Cisplatin (Sigma-Aldrich) was dissolved to 1 mg/mL in 0.9% NaCl (Honeywell) solution, and 3 mg/kg mouse body weight was injected intraperitoneally (i.p.) once weekly three times.

$CD4^+$ and $CD8^+$ T-cell depletion was done by i.p. injection of 0.25 mg anti-mouse CD4 (GK1.5; #BE0003-1; Bio X Cell), 0.1 mg anti-mouse CD8 (2.43; #BE0061; Bio X Cell), or 0.1 mg rat IgG2b isotype control (LTF-2; #BE0090; Bio X Cell) per mouse in 100 µL PBS. Depletion antibodies were given on days 20, 23, and 26 after C3 tumor challenge. Depletion was verified in blood samples on day 28 using BV421 CD8 (53-6.7, 1:200, BD), PerCP/Cy5.5 CD4 (RM4-5, 1:100, BD), PE/Cy7 CD45.2 (104, 1:100 BD), and Fixable Viability Dye eFluor 780 (1:1,000, eBioscience) and is shown in Supplementary Figure 8A (representative mice).

5.3.3.12 Intracellular staining and flow cytometry analysis of splenic, lymph node, blood, and intratumoral immune cells

Splenocytes and lymph nodes were harvested and prepared as previously described (356). Tumor tissue was weighed after harvesting and processed using the Miltenyi mouse tumor dissociation kit (cat. no. 130-096-730) and the gentleMACS Dissociator using the manufacturer's protocol. Blood was harvested in EDTA Microvette tubes (Sarstedt), and red blood cells were lysed using ACK lysing buffer (Gibco).

Stimulation with peptide (JPT HPV16 pepmix), intracellular staining, and flow cytometry were performed as previously described (356) using the following antibodies: BV421 CD8 (53-6.7, 1:200, BioLegend), PE-Cy7 CD4 (RM4-5, 1:800, BD), FITC CD44 (IM7, 1:100, BioLegend), PerCP-Cy5.5 B220 (RA3-6B2, 1:200, BioLegend), APC IFNγ (XMG1.2, 1:100, BioLegend), PE TNFα (MP6-XT22, 1:100, BioLegend), and Fixable Viability Dye eFluor 780 (eBioscience). HPV16-specific $CD8^+$ T-cell responses were measured as B220-, $CD8^+$ or $CD4^+$, $CD44^+$, $IFN\gamma^+$ cells and are presented in total number of cells per spleen, total number of cells per mL blood, total number of cells per gram tumor, or as fractions

of populations as described in the respective figures. The gating strategy is shown in Supplementary Figure 8B.

5.3.3.13 Lineage staining and flow cytometry analysis of intratumoral immune cells

Tumor tissue was prepared as above, and cells were stained against surface markers (all 1:100, BD unless otherwise noted): BV650 CD8 (53-6.7), PerCP/Cy5.5 CD4 (RM4-5), PE/Cy7 CD45.2 (104), APC F4/80 (BM8, BioLegend), AF488 CD11c (N418, BioLegend), AF700 TER119 (TER-119), and Fixable Viability Dye eFluor 780 (1:1,000, eBioscience). After surface staining, cells were fixed and permeabilized using the eBioscience Foxp3/Transcription Factor Staining Buffer Set, and stained intracellularly using PE FoxP3 (FJK-16s, 1:100, Invitrogen).

Flow cytometry was performed on the Fortessa 5 (BD) flow cytometer, and data analysis was performed using FlowJo V10 software. The gating strategy is shown in Supplementary Figure 8C.

5.3.3.14 IHC staining of tumor tissue

Tumor tissue was carefully harvested at the time of sacrifice and fixated in 4% cold PFA (Alfa Aesar). The fixative was exchanged with 70% ethanol after approximately 24 hours. Fixated tissues were embedded in paraffin and slides were stained with PE and with DAB for CD8α (D4W2Z, 1:600, pH = 9, Cell Signaling Technology).

Tissues were scanned using Axio Scan.Z1 (Zeiss) and analyzed using Zen 3.4 software (cutoff area: 10–180 μm^2. Cutoff circularity: 0.5–1.0).

5.3.3.15 Statistical analyses and graphical representation

Statistical analysis was done using GraphPad Prism 8 software (GraphPad Software).

For ICS of cell lines and soft-agar transformations, individual groups were compared using a two-sided, parameterized, unpaired t test. Each symbol represents one replicate, bars indicate the mean with standard error of the mean (SEM).

For immune responses and tumor infiltration studies, the Mann–Whitney test (nonparametric rank-sum test) was used when comparing only two groups, and the Kruskal–Wallis test (nonparametric one-way ANOVA on ranks) using Bonferroni adjustment when comparing three or more groups. Negative control groups were not included in multiple comparison tests. Tumor growth curves were analyzed by a mixed-effects model for matched values with Geisser-Greenhouse correction of sphericity comparing the entire course of the curves, including all values in the statistical analysis up to the last time point where more than 50% of mice in one group were alive. Survival curves were analyzed by a log-rank (Mantel–Cox) test.

For analysis of intracellular staining results, nonstimulated samples were used as background controls, and their response values have been subtracted from the peptide-stimulated samples of the corresponding animal before performing statistical analysis and graphical presentation.

Splenic immune responses shown in numbers (indicated by # on the y-axis) are the total number of responding cells in the animal. This is calculated by multiplying the percentage of responding cells out of all lymphocytes with the number of nucleated cells in the spleen. To aid the visual representation of systemic immune responses (spleen or blood), all nonresponders have manually been adjusted to a value of 100, 10, or 1 (as indicated in the figure legends). All statistical analyses were done on nonadjusted values. For splenic immune responses, we applied a threshold for responses based on the average number of B220-, $CD8^+$, $CD44^+$, $IFN\gamma^+$ counts for unstimulated background samples. All samples with fewer counts than the average $^+$ 2 × standard deviation of the background samples were regarded

as nonresponding. The analysis of the fraction of double positive (% TNFα$^+$ IFNγ$^+$ out of all IFNγ$^+$) and mean fluorescence intensity (MFI) of IFNγ$^+$ was performed only on responders.

Each symbol represents one mouse. For tumor growth data, the lines show the mean, and error bars indicate the SEM. For all other data, bars indicate the geometric mean.

Significance levels are marked: *, $p < 0.05$; **, $p < 0.01$; ***, $p < 0.005$; ****, $p < 0.001$.

5.3.3.16 Data availability statement

The original contributions presented in the study are included in the article/Supporting Information. Further inquiries can be directed to the corresponding authors.

5.3.4 Results

5.3.4.1 Design and biochemical characterization of the antigen-expressing Ad19a/64 vectors

The antigens for an HPV16 E1-, E2-, E6-, and E7-containing therapeutic vaccine were designed in analogy to the published homologous MfPV3 antigens (356), which were down-selected in mouse models and are now being tested for efficacy in MfPV3-infected nonhuman primates (NHP; Figure 14A). The different HPV16 early proteins were separated by glycine-serine (GS) linkers and encoded in Ad19a/64 vectors. With one exception (E1E2E6E7), all polypeptides were N-terminally fused to the human MHC class II invariant chain (Ii).

To ensure the safety of the vaccines, transformation-defective variants of the highly potent oncoproteins E6 and E7 were generated. The oncoprotein E6 was inactivated by introducing an L117Q substitution to prevent the binding of E6 to E6BP and subsequent degradation of tumor suppressor p53 (333). Additionally, the C-terminal PDZ domain was deleted (ΔETQL) to abolish the binding of telomerase and other LxxLL motif-containing proteins (334). E7 was inactivated by introducing the substitutions C24G, L67R, and C91A within the central LxCxE motif in order to inhibit dimerization and reduce binding to pRB known to reduce the interaction with Mi2β (334,335). Furthermore, we changed E2 (C300A) to reduce DNA binding. Epitope prediction revealed that E1 and E2 harbor a larger number of potential epitopes (Figure 14B; Supplementary Table 1A) across 75% of the most common human HLA types (Supplementary Table 1B) compared with E6 and E7, supporting our hypothesis of the advantage of including all four antigens in the vaccine design.

The antigen coding sequences were inserted into adenoviral vectors from serotype 19a/64 (Ad19a/64) as described (235).

Proper expression of the encoded antigens was confirmed by western blot analysis following transduction of A549 cells with the indicated Ad19a/64 constructs (Figure 14C). All vectors readily expressed the encoded antigens, and bands running at the expected size were observed when blots were probed with HPV16 early protein-specific antibodies. In most cases, especially for proteins with high signal intensities, bands of lower molecular weight than calculated were observed, presumably caused by partial degradation.

Because proteins of different sizes behave differently during blotting and signal intensities may not reflect expression accurately, HPV16 antigen amounts were quantified by flow cytometry after intracellular staining with anti-E2, anti-E6, and anti-E7 (Figure 14D; Supplementary Figure 9A). The Ad19a/64 transductions yielded comparable expression for the different HPV16 polypeptides except for E1E2E6E7 trending toward slightly higher signals with anti-E6 and anti-E7 (Figure 14D). There is, to our knowledge, no available E1 antibody; hence, E1 expression was not directly assessed. However, E1 is in all analyzed constructs N-terminally fused to either E2 alone, E2E6E7, or E6E7. Western blot

analysis with monoclonal or polyclonal ABs directed against E2, E6, and E7 in all cases proved expression of fusion proteins detected at the calculated molecular weights (including E1; 72.9 KDa on its own). Based on this, and on our previously published homologous MfPV3 vaccine design where E1 expression was confirmed, we anticipated E1 to be properly expressed (this was later supported by the vaccine's ability to induce E1-specific immune responses; see Figure 15).

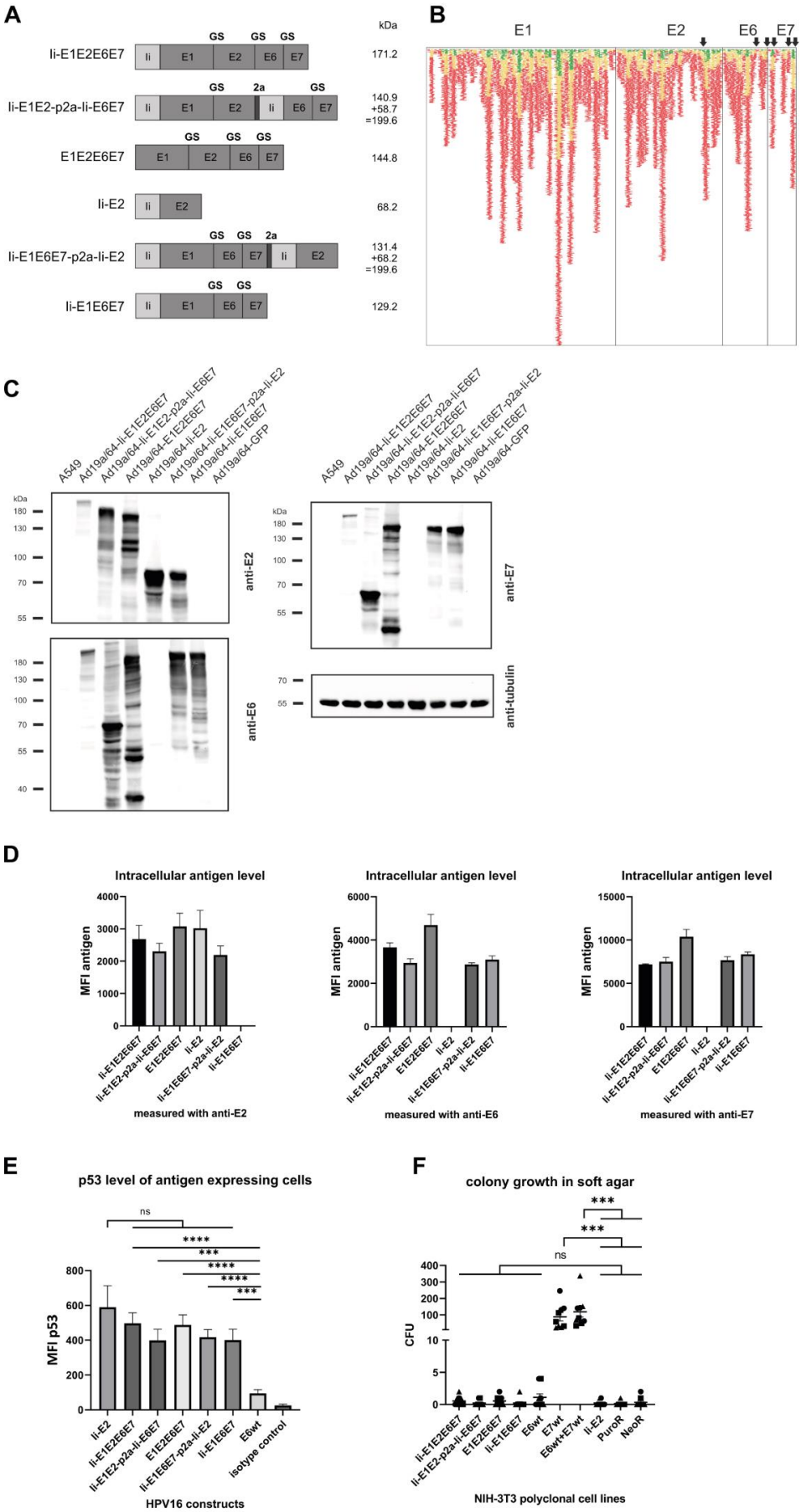

Figure 14: *In vitro* expression and inactivated transforming potential of HPV16 antigen variants.

(A) HPV16 antigens were designed as fusion proteins comprising either E1, E2, E6, and E7 altogether, or fusion proteins partially linked by a p2a peptide, and fused to the MHC-II invariant chain (Ii), respectively. Antigens were fused as single open reading frames without the Ii coding sequence. Calculated molecular weights are indicated (kDa). (B) Predicted MHC-I epitopes of HPV16 early protein antigens E1, E2, E6, and E7 identified by IEDB analysis and mapped on the E1E2E6E7 fusion protein. Arrows mark the point mutations introduced for inactivation of the oncoproteins. Each of the colored horizontal lines corresponds to one predicted epitope, and the vertical axis thereby indicates epitope density. Colors indicate the affinity of the predicted epitopes (green: high affinity, 0–50 nmol/L calculated IC50; yellow: medium affinity, 50–500 nmol/L calculated IC50; red: low affinity, 500–5,000 nmol/L calculated IC50). (C) Western blot analysis of A549 cell lysates 48 hours following transduction with Ad19a/64 encoding the indicated polypeptides at an MOI of 100. Antigens were detected with anti-E2 (left top), anti-E6 (left bottom), and anti-E7 (right top) antibodies. As a loading control, tubulin was monitored using an anti-tubulin antibody (right bottom). (D) Flow cytometry analysis of A549 cells 48 hours following transduction with Ad19a/64 expressing the various MfPV3 antigens, at an MOI of 100. Intracellular staining was performed with anti-E2 (left), anti-E6 (middle), and anti-E7 (right). Depicted is the MFI of the average of 3 independent experiments. Error bars indicate SEM. (E) Flow cytometry analysis of p53 in antigen-expressing HEK293T cells upon transfection with pURVac plasmids containing the respective antigens. Intracellular staining was performed with anti-p53 together with anti-E6 (all E6 containing antigens) or anti-E2 (Ii-E2 only). Depicted is the MFI of the average of 3 independent experiments. Error bars, SEM. Individual groups were compared using two-sided, parameterized, unpaired t test. (F) Anchorage-independent colony growth in soft-agar transformation assay in the NIH-3T3 cell line. The number of colony-forming units (CFU) in the assay is shown. Depicted is the mean with SEM of 3 technical replicates from 3 independent experiments. Individual groups were compared using two-sided, parameterized, unpaired t test. Ii: MHC II–associated invariant chain, GS: glycine–serine–linker, 2a: p2a peptide for cotranslational separation.

5.3.4.2 Virally delivered antigens induce less p53 degradation and colony-forming potential

Next, we determined the extent of p53 degradation, known as the main tumor suppressor protein, by E6wt and the engineered fusion-polypeptides. We saw that our modifications maintained high p53 in transfected cells compared with E6wt (Figure 14E; Supplementary Figure 9B), suggesting functional inactivation of the E6 oncoprotein.

To further test for the ability to promote anchorage-independent growth (364), NIH-3T3 cells were transduced with VSV-G-pseudotyped lentiviral vectors encoding the engineered fusion-antigens, or E6wt and E7wt alone or in combination as positive controls. As negative controls, NIH-3T3 cells were transduced with VSV-G-pseudotyped lentiviral vectors encoding Ii-E2 or lentiviral vectors lacking a transgene, respectively.

Transgene expression of polyclonal NIH-3T3 cell lines was verified by western blot analysis (Supplementary Figure 9C). For all cell lines, the expected bands at the correct sizes were detected, except for Ii-E1E6E7-p2a-Ii-E2, which failed to be generated even after repeated attempts. Cell lines expressing the mutated E6 and E7 proteins performed as control antigens, whereas E7wt- and E6wt$^+$E7wt-transduced cells readily formed high numbers of colonies in the soft agar (Figure 14E; Supplementary Figure 9D). Taken together, this confirms the functional inactivation of the transforming potential of HPV16 antigens.

5.3.4.3 Ad19a/64-vectored vaccination induces robust CD8$^+$ and CD4$^+$ T-cell responses in both outbred and inbred mice which can be boosted by Ad5

Intramuscular immunization of outbred CD1 mice with a single dose of Ad19a/64-vectored vaccines confirmed immunogenicity of the different antigen constructs *in vivo*, as CD8$^+$ T-cell responses were detected against E1 (Figure 15A) and CD4$^+$ responses were detected against E1 (Figure 15B) and E2 (Figure 15C).

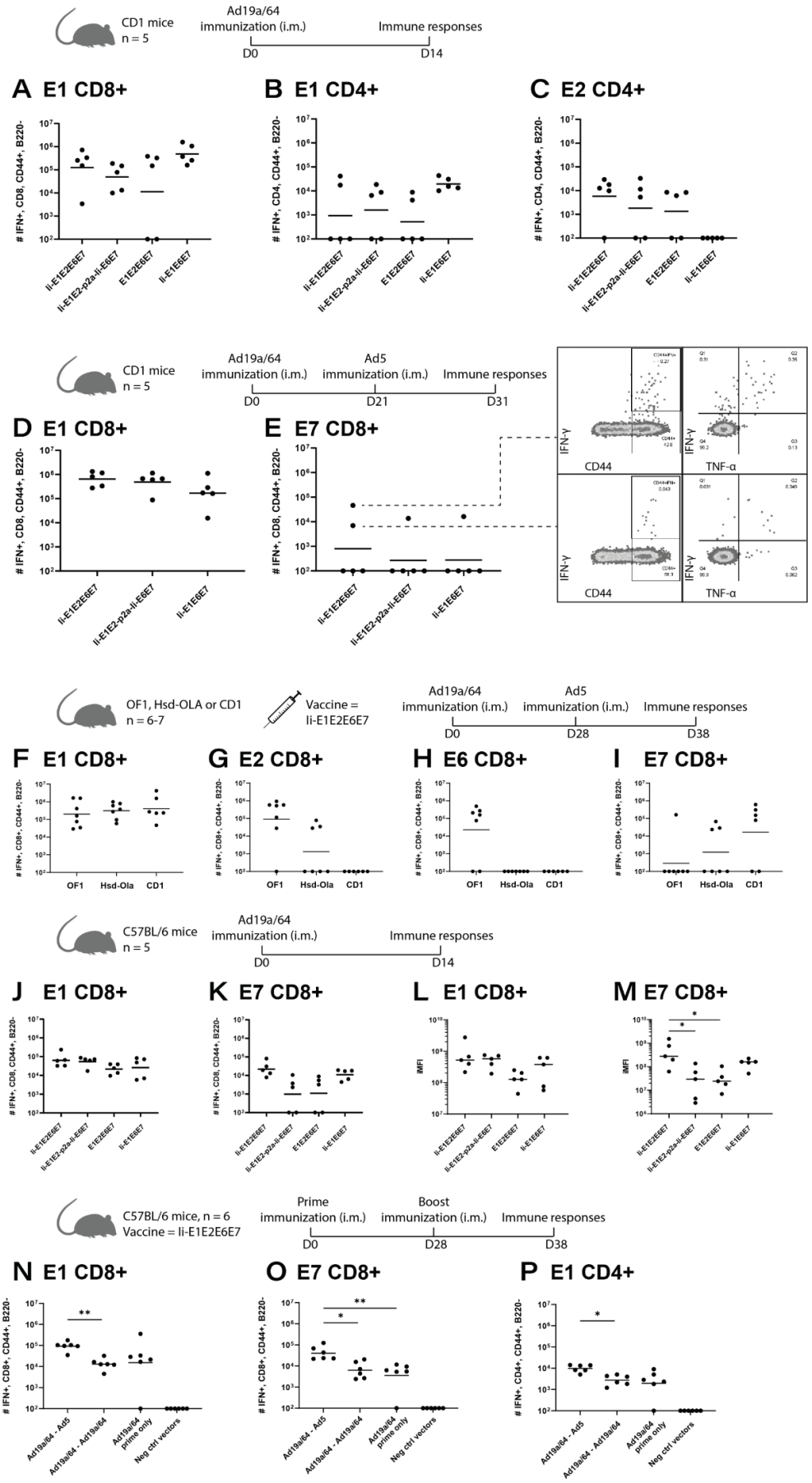

Figure 15: Ad19a/64 vectored vaccination induces robust CD8⁺ and CD4⁺ T-cell responses in both outbred and inbred mice.

CD1 mice (A–E), different outbred mice as indicated (F–I), or C57BL/6 mice (J–P) were immunized with Ad vaccines (2×10^7 IFU) encoding the various HPV16 early antigens as indicated.

To enhance immune responses further, a heterologous prime–boost immunization was applied delivering human Ad5-encoded Ii-E1E2E6E7 as a booster vaccine (Supplementary Figure 10). This increased $CD8^+$ T-cell responses to E1 (Figure 15D as compared with Figure 15A) and induced some responses against E7 as well (Figure 15E). $CD4^+$ T-cell responses were consistently detected against E1 and E2 and sporadically detected against E6 and E7 (Supplementary Figure 11A-D). We never detected $CD8^+$ T-cell responses to E2 or E6 in CD1 mice, potentially reflecting limited MHC diversity in the supposedly outbred CD1 mouse model due to a rather small number of founder mice (341). We, therefore, chose to evaluate the Ii-E1E2E6E7 vaccine in an Ad19a/64-Ad5 prime–boost regimen in selected other outbred mouse strains derived independently from CD1 (OF1 and Hsd-Ola; (341)). Here, we detected vaccine-induced $CD8^+$ responses against all four antigens in at least one of the mouse strains (Figure 15F-I) and $CD4^+$ responses against E1, E2, and E7 (Supplementary Figure 11E-G).

Lastly, we wanted to confirm immunogenicity in the C57BL/6 mouse, which is the standard mouse model in the field of HPV16 therapeutic vaccines. We found responding $CD8^+$ T cells against E1 for all antigen designs (Figure 15J) and detected E7-specific $CD8^+$ T cells (Figure 15K) and $CD4^+$ responses against E1 (Supplementary Figure 11H). The Ii-E1E2E6E7 gave significantly stronger E7 responses than the Ii-E1E6E7-p2a-Ii-E2 vaccine, and Ii-E1E2E6E7 also seemed to give stronger E7 responses than the vaccine not encoding Ii ($p = 0.077$). This advantage of the Ii-E1E2E6E7 was further supported when looking at the integrated MFI (iMFI) of IFNγ-positive cells combining the magnitude and quality of the induced T-cell response (368). In this analysis, the E1 response was by trend higher for Ii-E1E2E6E7 compared with the non Ii vaccine as well (Figure 15L, $p = 0.06$). Notably, Ii-E1E2E6E7 significantly enhanced the response against E7 compared with the vaccine not encoding Ii and the vaccine encoding E7 directly linked to the p2a-Ii (Figure 15M). We did not detect any E2- or E6-specific CD8+ T-cell responses despite a previously reported E6 epitope (aa48–57, EVYDFAFRDL; (367)). This could be due to immunodominance, as responses against the E6 epitope have previously been described only for vaccines encoding E6 alone, and the E6 epitope has been reported as less immunogenic than the dominant E7 epitope (aa49–57, RAHYNIVTF; (195)).

Based on the superior $CD8^+$ T-cell responses in the C57BL/6 mice, and the lack of inferiority and positive trends in the outbred mouse models, we decided to move forward with the Ii-E1E2E6E7 antigen design.

Lastly, we confirmed that heterologous Ad5-vectored boosting after Ad19a/64 priming induced a recall vaccine-specific response compared with Ad19a/64 priming alone, whereas homologous boosting with Ad19a/64 did not (Figure 15N-P). A negative control group of Ad19a/64 and Ad5 vectors containing no antigen was included to confirm that the responses were vaccine specific.

5.3.4.4 Ad-vector vaccination shortly after tumor inoculation provides single-agent tumor control and increased survival

To investigate the therapeutic effect of our HPV vaccine, C57BL/6 mice were injected with syngeneic C3 tumor cells. The C3 cell line was established by transfection of mouse embryonic cells with the HPV16 genome and an activated ras oncogene (195), and the tumors can express all HPV16 antigens (369), in contrast to the commonly used TC-1 tumor model containing only HPV16 E6 and E7 (194). It is worth mentioning that the C3 tumor cell line is generally slower-growing and more treatment-resistant than the TC-1 model, as shown by Sluis and colleagues (cf. their Supplementary Fig. S1; (359)), making it more challenging to show therapeutic effect in the C3 model.

In the first experiments, mice were treated with A19a/64 vectors encoding Ii-E1E2E6E7 or an irrelevant antigen (neg ctrl, see Supplementary Figure 7) 2 days after tumor challenge. On day 20, another treatment with Ad5 vectors containing the same antigens was done to boost responses. Ii-E1E2E6E7 treatment significantly reduced tumor growth (Figure 16A), completely cleared tumors in 3 of 10 mice (Figure 16B) and significantly increased survival (Figure 16C, 3/10 vs. 10/10 dead at day 41), indicating that the treatment is effective against small tumors.

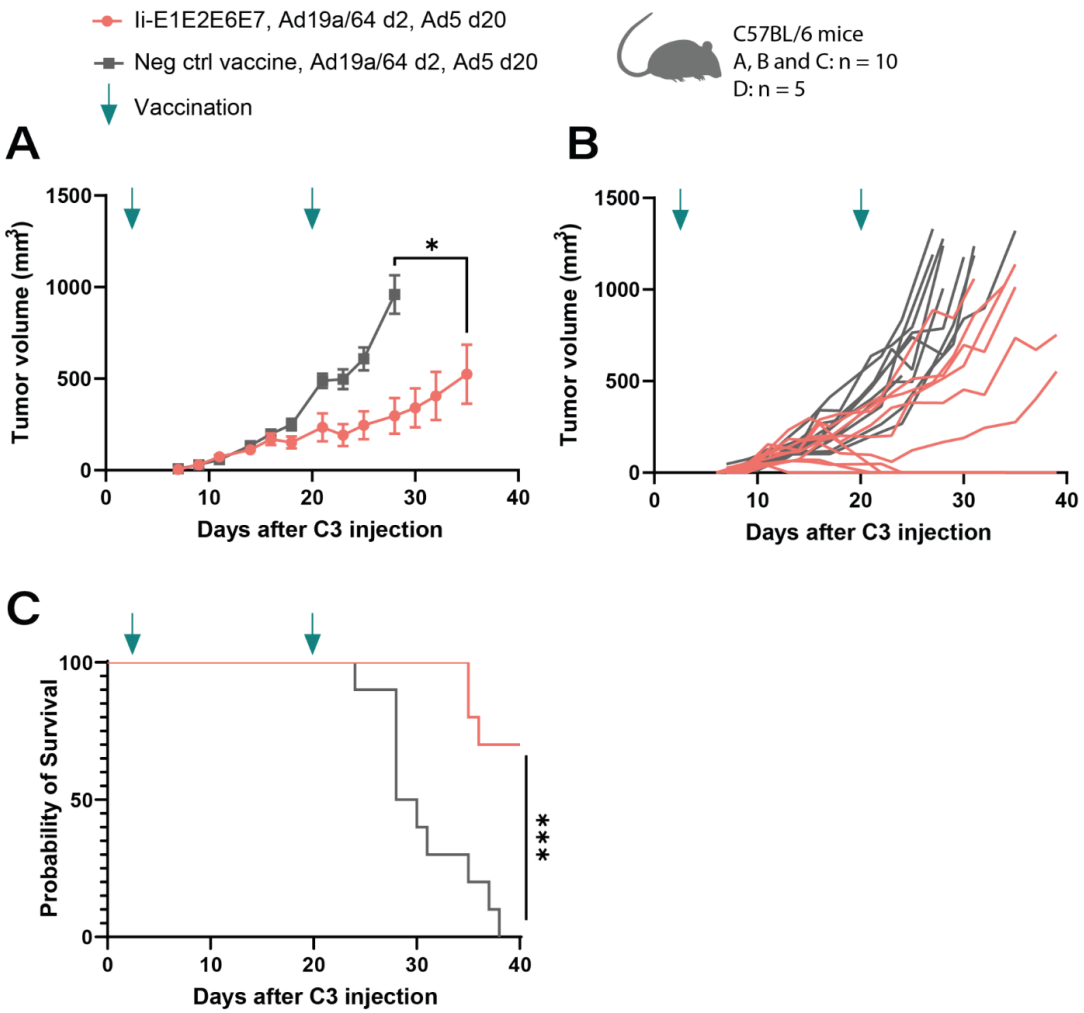

Figure 16: Ad-vectored delivery provides single-agent tumor control and increased survival by vaccination shortly after tumor inoculation 1×10^6 C3 cells were injected s.c. into the flank of C57BL/6 mice, and the mice received Ad19a/64- and Ad5-vectored vaccines i.m. in the same side as the tumor on days 2 and 20, respectively.
Tumor growth (A and B) and survival (C). Pink curves with circles represent the therapeutic vaccine group. Gray lines with squares depict negative control vaccinated mice. Green arrows indicate the time of vaccination. Statistical analysis was performed using the mixed-effects model for matched values with Geisser-Greenhouse correction of sphericity (A, comparing the entire course of the curves) and log-rank (Mantel–Cox) test (C). *, p < 0.05; ***, p < 0.005.

5.3.4.5 Ad-vectored vaccination provides single-agent control of established tumors and synergizes with cisplatin

Having confirmed that the early treatment of C3 tumors with therapeutic vaccination had a good effect as vaccine regimen monotherapy, we went on to investigate the potency of established tumors. Once palpable tumors were present (day 10), mice were treated with therapeutic vaccination, which showed

a reduction of tumor growth in some animals (Figure 17A and B) and significantly increased survival (Figure 17C). Cisplatin is the standard treatment of HPV$^+$ cancers in the clinic and has previously shown synergy with HPV-targeting therapeutic vaccines (359). Combining the therapeutic vaccination with three once-weekly cisplatin injections, as previously described by Nejad and colleagues (302), dramatically increased the tumor control (Figure 17D and E) and survival (Figure 17F) compared with cisplatin treatment and control vaccination, and compared with therapeutic vaccination alone (Supplementary Figure 12A).

IHC staining of tumor tissues revealed that the therapeutic vaccination significantly increased the number of CD8$^+$ T cells (Figure 17G) and even more importantly the infiltration of these CD8$^+$ T cells into the central tumor parenchyma (Figure 17H). Representative pictures of the IHC anti-CD8 staining are shown in Figure 17I. Cotreatment with cisplatin did not seem to have any obvious effect on the infiltration of CD8$^+$ T cells visualized by IHC (Supplementary Figure 12B).

To further investigate the cause of the observed therapeutic effect, we harvested tumors and lymphoid organs at the time points where the therapeutic effect had only just started to kick in for the respective treatment combinations. Organ harvest was performed on day 24 for mice treated with vaccine and cisplatin combined (Figure 17D) and on day 30 for mice treated with the vaccine alone (Figure 17A). Analysis of the tumor-infiltrating CD8$^+$ T cells showed that the vaccinated mice had more tumor-reactive CD8$^+$ T cells producing IFNγ when incubated with tumor cells *ex vivo* at both time points (Figure 17J). Looking at the splenic responses, the vaccine specifically induced E1- and E7-specific CD8$^+$ T-cell responses in these tumor-bearing mice (Figure 17K), corresponding to the nontumor challenged mice previously analyzed (Figure 15). Cisplatin treatment alone (neg ctrl $^+$ cisplatin, d24, Figure 17K, left, gray squares) seemed to induce some anti-HPV responding CD8$^+$ T cells, primarily to E7 and in some mice toward E1, but the amount of IFNγ per cell (Figure 17L), and the amount of IFNγ producing CD8$^+$ T cells, also capable of producing TNF was clearly inferior compared with Ii-E1E2E6E7-treated mice (Figure 17M).

Surface staining analysis revealed that cisplatin treatment did not seem to have an effect on the amount of CD8$^+$ T cells in the tumor, supporting the IHC findings (Supplementary Figure 12C), but that the therapeutic vaccination significantly increased the proportion of antigen-presenting CD11c-positive cells in the tumor both on days 24 and 30 (Figure 17N). We also saw a tendency of higher infiltration of dendritic cells (DC) in the tumor of mice who received cisplatin treatment, similar to what was reported by Nejad and colleagues (302), but this difference could also be attributed to the fact that the analysis was done on days 24 and 30, respectively.

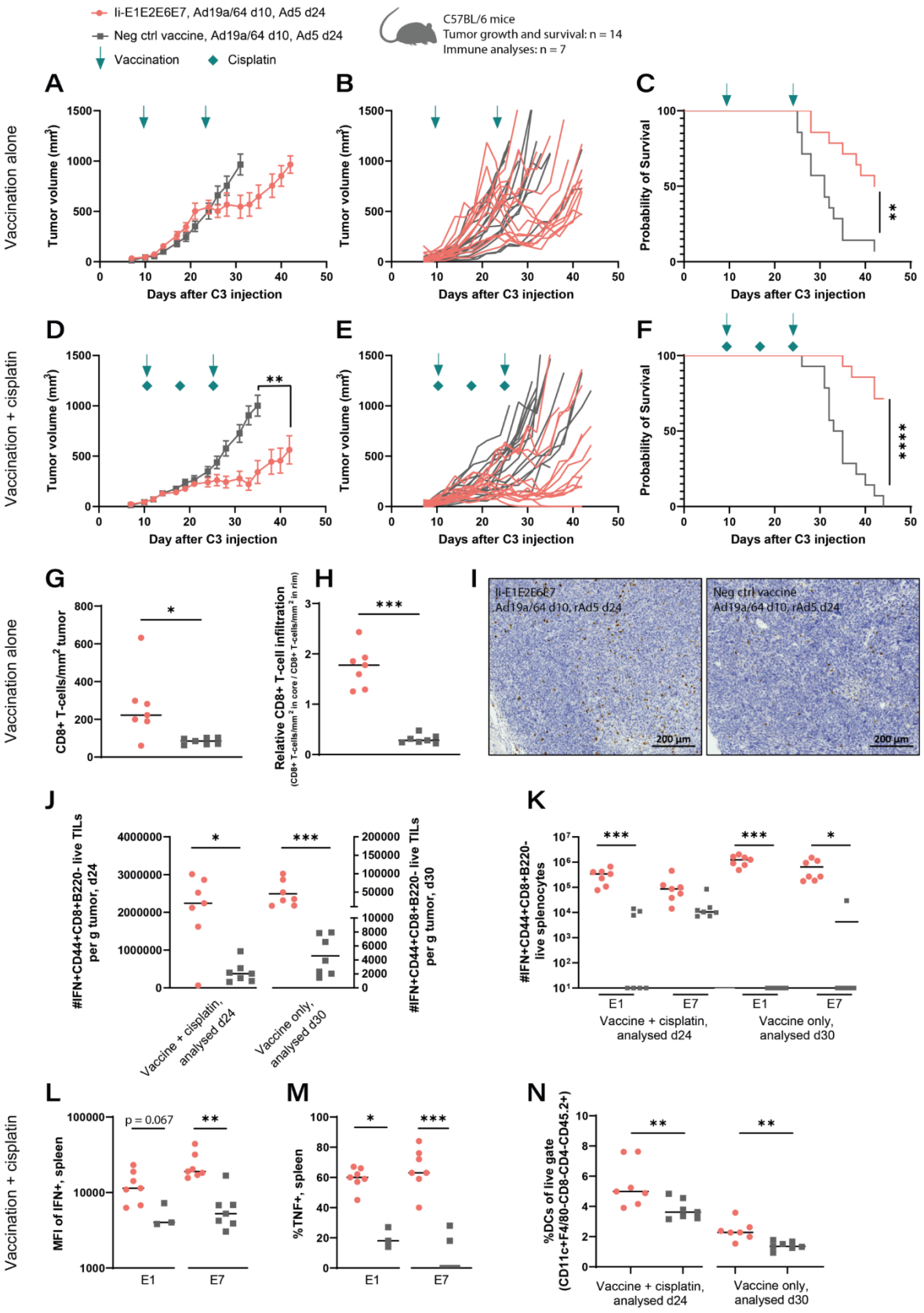

Figure 17: Ad-vectored vaccination provides single-agent control of established tumors and works in synergy with cisplatin cotreatment.

1 × 10^6 C3 cells were injected s.c. into the flank of C57BL/6 mice, and the mice received Ad19a/64- and Ad5-vectored vaccines i.m. in the same side as the tumor on days 10 and 24, respectively. Mean tumor growth with SEM (A), tumor growth for individual mice (B), and survival (C) were assessed. In (D–F) all mice were

additionally treated with cisplatin on days 10, 17, and 24 (green diamonds). Tumors of mice receiving therapeutic vaccine or negative control vaccine alone were harvested either once the tumor exceeded 1,000 mm^3 or at the end of the trial (day 42) and $CD8^+$ cells were detected by IHC. (G) Total number of $CD8^+$ spots per mm^2 tumor. (H) Ratio of $CD8^+$ spots per mm^2 tumor in the core vs. the rim of the tumor. (I) representative images of IHC staining of a tumor from either a vaccinated (left) or a negative control vaccinated (right) mouse. The pictures show the rim (bottom left side of the pictures) and a bit of the core (top right side of the pictures). (J) Mice were sacrificed at the time points indicated, tumors were harvested, and the resulting single-cell suspension of a mix of tumor and immune cells was incubated for 5 hours without the presence of additional HPV16 peptides. IFNγ producing $CD8^+$ T cells were detected by intracellular staining and flow cytometry. (K) Mice were sacrificed at the time points indicated, spleens were harvested and $CD8^+$ T-cell immune responses following E1 and E7 peptide stimulation were measured using intracellular staining and flow cytometry. (L and M) MFI of IFNγ (L), and the percentage of $TNF\alpha^+$ of all $CD8^+CD44^+IFN\gamma^+$ splenocytes (M), for mice treated with cisplatin and vaccinated with a therapeutic vaccine of a negative control vaccine. (N) Tumors were harvested at the time indicated, single-cell suspensions were prepared, and the fraction of DCs ($CD11c^+F4/80^-CD8^-CD4^-CD45.2^+$TER119-live) was assessed by surface staining and flow cytometry. Pink circles represent the therapeutic vaccine group. Gray squares depict negative control vaccinated mice. Green arrows indicate the time of vaccination. Green diamonds indicate the time point of cisplatin injections. (G–N) Black bars indicate geometric mean. (A–F) Data pooled from two independent experiments. Statistical analysis was performed using the mixed-effects model for matched values with Geisser-Greenhouse correction of sphericity (A and D, comparing the entire course of the curves), log-rank (Mantel–Cox) test (C and F), or the Mann–Whitney test (G–N). *, $p < 0.05$; **, $p < 0.01$; ***, $p < 0.005$; ****, $p < 0.001$. To aid the visual representation of splenic immune responses, all nonresponders have manually been adjusted to a value of 10.

5.3.4.6 Tumor control is mediated by $CD8^+$ T cells

As $CD8^+$ T cells seemed to be associated with therapeutic vaccination and tumor-therapeutic effect, we wanted to confirm whether $CD8^+$ T cells were in fact the principal effector cell type. Mice with palpable tumors (day 10) were treated with the therapeutic vaccine and cisplatin and subsequently treated with antibody-cell-depleting antibodies from day 20 to primarily address the effector phase of the antitumor response. We saw that CD8 depletion completely abolished the antitumor effect of the therapeutic vaccination (Figure 18A). In contrast, we saw a tendency of $CD4^+$ T-cell depletion leading to increased tumor control (Figure 18A), potentially indicating an immune-suppressive phenotype of $CD4^+$ T cells in the tumor microenvironment. Indeed, we found that the tumor-infiltrating $CD4^+$ population was largely composed of the $FoxP3^+$ subtype, indicating a substantial presence of regulatory T cells (Treg), and this was increased by the therapeutic vaccination (although only significant in the cisplatin cotreatment setting; Figure 18B).

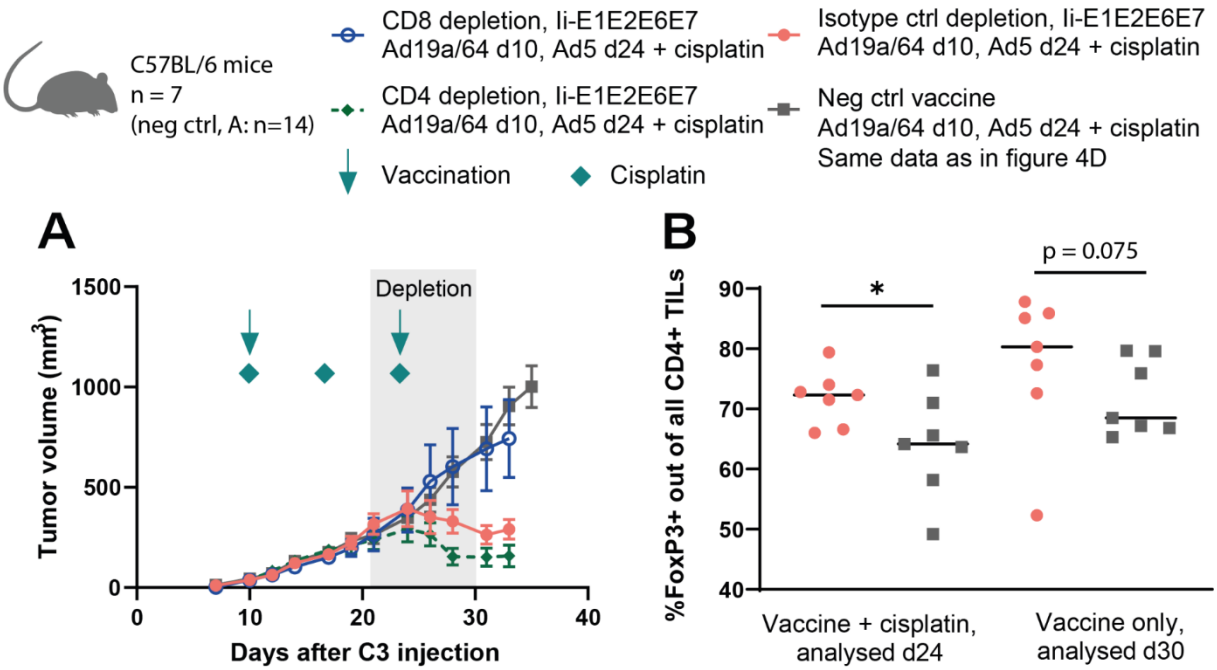

Figure 18: Tumor control is mediated by CD8⁺ T cells and regulated by tumor-resident FoxP3⁺ Tregs.
1×10^6 C3 cells were injected s.c. into the flank of C57BL/6 mice, and the mice received Ad19a/64- and Ad5-vectored vaccines i.m. in the same side as the tumor on days 10 and 24, respectively. Cisplatin treatment was given i.p. on days 10, 17, and 24. (A) Mean tumor growth with SEM of mice treated i.p. with CD4- (green dashed, diamonds), or CD8-depleting (blue, open cicles) or isotype-control antibodies (pink, circles) on days 20, 23, and 26. The gray curve shows neg ctrl vaccinated mice for comparison (note that these are the same mice depicted in Figure 17D, and pooled from two independent experiments). Green arrows indicate the time of vaccination. Green diamonds indicate time point of cisplatin injections. (B) FoxP3 expression on tumor-infiltrating $CD4^+CD8^-CD45.2^+TER119$ live cells in mice Ii-E1E2E6E7 (pink circles) or neg ctrl (gray squares) vaccination with or without cotreatment with cisplatin. Tumor-infiltrating cells were analyzed on day 24 (combination treatment groups) or day 30 (vaccination alone) by intracellular staining and flow cytometry. Statistical analysis was performed using the Mann–Whitney test. *, $p < 0.05$.

5.3.4.7 The Ad-vectored Ii-E1E2E6E7 vaccine provides enhanced survival compared with two E6/E7 synthetic long reference peptides in combination with cisplatin

Previous studies have shown efficacy against C3 tumors by immunization with an E7 peptide, $E7_{43–77}$, formulated in Incomplete Freund's Adjuvant (IFA; (302,359,360,370)). This peptide includes a well-established E7 epitope that is immunodominant in C57BL/6 mice (195). Another epitope is also reported in E6 (367), though it is less dominant. Although the previously published studies on peptide vaccines against HPV⁺ C3 tumors include only the $E7_{43–77}$ peptide, we chose to include an $E6_{41–65}$ peptide in our vaccination comparison as well. The two peptides are also part of a complex synthetic long peptide vaccine (under the clinical development name ISA101), consisting of 13 peptides covering the entire HPV16 E6 and E7 (300) and were selected (i) due to their compatibility with the inbred mouse strain and (ii) for reference purposes (302,359,360,370)).

Mice were treated with cisplatin and therapeutic vaccination by either the two peptides formulated in IFA or our Ad-vectored Ii-E1E2E6E7 once palpable tumors were present (day 10). The Ii-E1E2E6E7 vaccine reduced the tumor growth to a larger extent than the peptide vaccine (Figure 19A; Supplementary Figure 13A) and led to significantly better survival (Figure 19B). CD8⁺ T-cell responses against E1 were detected after vaccination with Ii-E1E2E6E7 but not after vaccination with the two

E6/E7 peptides (Figure 19C). Both vaccines induced E7-specific $CD8^+$ T cells similarly (Figure 19D) without detectable $CD4^+$ T-cell responses (Supplementary Figure 13B).

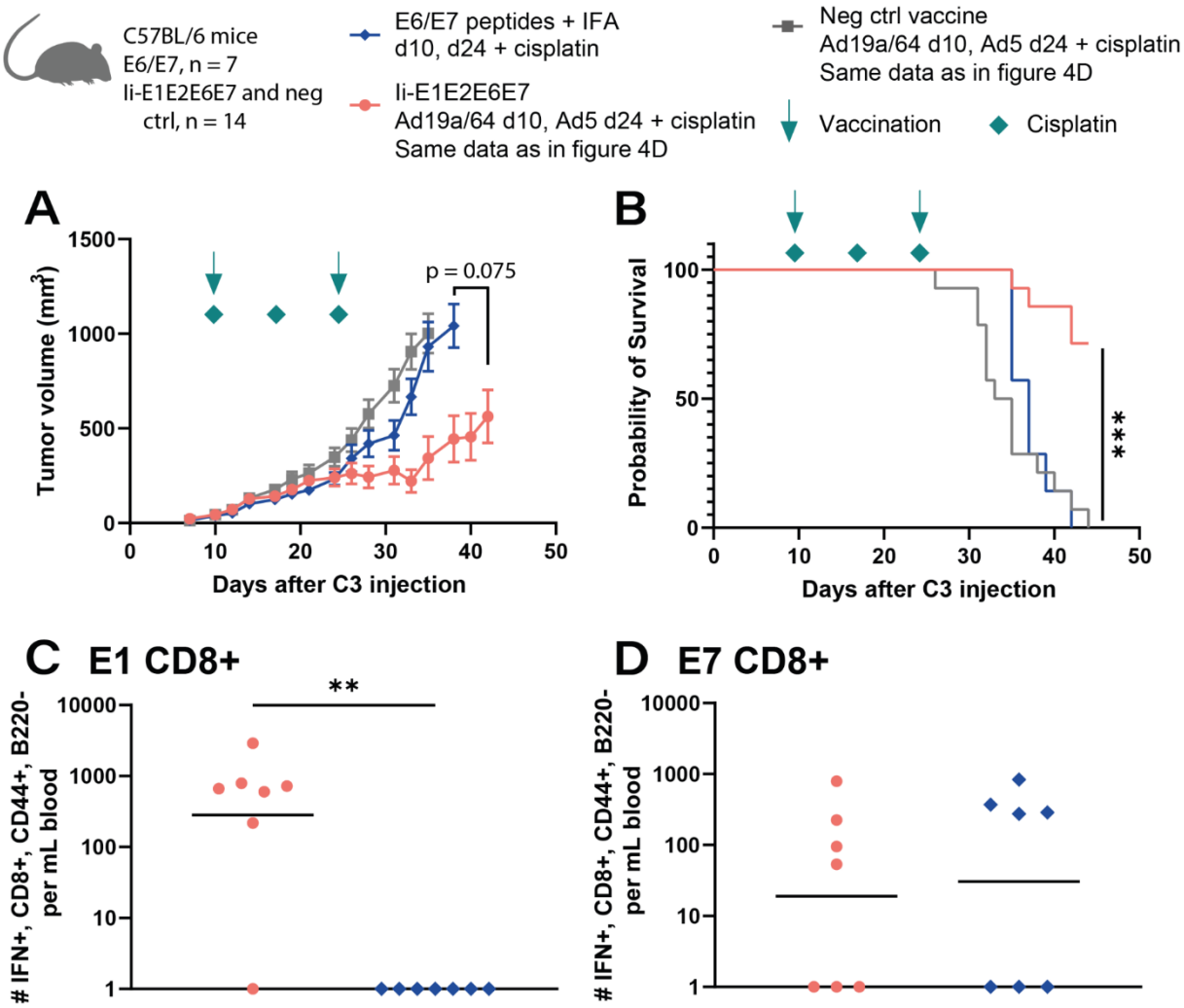

Figure 19: The Ad-vectored Ii-E1E2E6E7 vaccine provides enhanced tumor control and survival compared with an E6E7 peptide-based vaccine in combination with cisplatin 1×10^6 C3 cells were injected s.c. into the flank of C57BL/6 mice, and the mice received Ad19a/64- and Ad5-vectored vaccines i.m. in the same side as the tumor, or peptide-based vaccine s.c. in the opposite flank on days 10 and 24.
Cisplatin treatment was given i.p. on days 10, 17, and 24. (A and B) Mean tumor growth with SEM (A) and survival curves (B) of peptide vaccine (blue, diamonds), Ii-E1E2E6E7* (pink, circles) or neg ctrl* (gray, squares). *, Same mice as depicted in Figure 17D and pooled from two independent experiments. Green arrows indicate the time of vaccination. Green diamonds indicate the time point of cisplatin injections. (C and D) $CD8^+$ T-cell responses ($IFN\gamma^+CD44^+CD8^+CD4^-B220^-$ live cells) against E1 (C) and E7 (D) measured in the blood of Ii-E1E2E6E7 (pink circles) or peptide (blue diamonds) vaccinated mice on day 22 using intracellular staining and flow cytometry. Statistical analysis was performed using the mixed-effects model for matched values with Geisser-Greenhouse correction of sphericity (A, comparing the entire course of the curves), log-rank (Mantel–Cox) test (B), or the Mann–Whitney test (C). **, $p < 0.01$; ***, $p < 0.005$. To aid the visual representation of blood immune responses, all nonresponders have manually been adjusted to a value of 1.

5.3.5 Discussion

Here, we describe a therapeutic vaccine candidate that encodes the two HPV16 oncogenes E6 and E7, representing classic targets of therapeutic HPV vaccines, together with two other nonstructural HPV16 proteins, E1 and E2, to enhance the range of potential target epitopes in the HPV^+ infected or

cancerous cells. We encode these in adenoviral vectors and apply a heterologous prime–boost regimen, a principle which in combination with the genetic adjuvant, Ii, has previously generated unprecedented antiviral T-cell responses in humans (323).

The vaccine antigens were properly expressed, and successful inactivation of the transformation potential of E6 and E7 was verified *in vitro*. The vaccine constructs were immunogenic in both inbred and outbred mice, and it was shown that Ii enhanced the magnitude and cytokine-producing competence of the T-cell responses. In the HPV16$^+$ murine C3 tumor model, the Ii-E1E2E6E7 vaccine regimen proved capable of reducing tumor growth and increasing survival on small tumors as monotherapy and on established tumors when coadministered with cisplatin. Monotherapy of established tumors also showed a tendency of tumor control (not significant) and significantly extended survival. Notably, and of relevance for the clinical translation of the Ad-vectored Ii-E1E2E6E7 vaccine, we observed no vaccine-related safety concerns in any of the vaccinated mice.

Immunogenicity and depletion studies indicate that the vaccine efficacy is due to vaccine-induced E1- and E7-specific CD8$^+$ T cells, and IHC showed a vaccine-augmented higher degree of CD8$^+$ T-cell infiltration into the central areas of the tumor, which is known to be important for antitumor efficacy (299,371,372). We also saw that vaccination increased the presence of DCs in the tumor microenvironment, a finding potentially augmented by cisplatin as previously reported for the C3 tumor model (302). This increased DC infiltration may be important as mouse studies with clinical correlates suggest that recurrent tumors remained insensitive to treatment in spite of CD8$^+$ T-cell presence, presumably because of a lack of myeloid cell infiltration (303). However, with T cells and DCs present in the tumors, it is likely that regulatory mechanisms are active to diminish T-cell effectiveness. One likely regulatory mechanism is CD4$^+$ Tregs, as we observed improved tumor control after CD4 depletion and vaccine-enhanced infiltration of FoxP3-expressing CD4$^+$ T cells (Figure 18A and B).

The literature, and our data, argue for the advantage of including more HPV antigens than E6 and E7 (166). In our vaccine design, we prioritized E1 and E2, due to their constitutive expression profile during HPV infection lifecycle, including in the stem cells maintaining viral infection (55,373). There is evidence that T-cell responses against E1 and E2 are correlated with improved clinical outcomes in cancer patients (319) and resolving of persistent HPV lesions (149), respectively, and increased E1 expression has been associated with carcinogenesis (374). Importantly, a larger antigen comprising a broader spectrum of MHC class I–restricted T-cell epitopes increases the likelihood of effect across individuals in a population with large HLA-variation. This is supported by the better prognosis of cervical cancer patients mounting spontaneous E1-specific T-cell responses and was exemplified here by E1 being the only antigen that induced CD8$^+$ T-cell responses in all tested outbred mice (Figure 15F-I).

A challenge for the translation of therapeutic HPV vaccines from preclinical studies to clinical efficacy is the availability of good animal models. The murine models are all based on the inbred C57BL/6 mouse, harboring one immunodominant epitope in HPV16 E7 (195) and a nondominant epitope in E6 (367), with the E7 epitope being the driver of the effect seen in most preclinical therapeutic vaccine studies. Although the TC-1 tumor model is more commonly used, it was not used here, as it only encodes E6 and E7, and not E1 and E2. Compared with the C3 model, the TC-1 model is more sensitive to treatment ((359); presumably due to higher HPV16 antigen expression (358)) and more aggressive in nontreated mice, leading to a higher risk of overestimation of the therapeutic effect of treatment.

Among the long list of therapeutic vaccines in clinical testing, far from all show clinical efficacy, and only a few have been validated in the C3 model. However, a complex peptide-based vaccine consisting of 13 synthetic long peptides covering the complete HPV16 E6 and E7 formulated in IFA (ISA101) has

shown efficacy in the clinic (175,299,300,375). Two of the 13 peptides ($E6_{41–65}$ and $E7_{43–77}$) harbor epitopes that have shown to be immunogenic in C57BL/6 mice (195,367), and particularly $E7_{43–77}$ has been tested multiple times in the C3 model (302,359,360). The Ad-vectored Ii-E1E2E6E7 vaccine presented here performed on par in terms of tumor control and better in terms of survival, when compared with the coadministered E7 and E6 peptides. Compared with previously published results (359), the coformulated E6/E7 peptides performed less efficiently with regard to tumor growth reduction and survival, most probably due to a higher tumor inoculum used in our study to ensure consistent engraftment of tumors. Although the two coformulated E6/E7 peptides and the Ad-vectored Ii-E1E2E6E7 vaccine approaches are fundamentally different in terms of both platform, adjuvant and vaccination route, they gave rise to similar E7-specific responses (and no $CD8^+$ T cells against E6 nor any $CD4^+$ T-cell responses). This may suggest that the inclusion of E1 could at least in part explain the observed superior survival. Extrapolated to clinical settings, this may also suggest that for patients with cancers expressing more HPV antigens than E6 and E7, as is often the case for OPSCC (136,180,188), a therapeutic vaccine including additional antigens such as E1 and E2 could induce more antitumor T cells and hence provide better treatment.

In the present work, we utilize a heterologous prime–boost consisting of Ad19a/64 for priming and Ad5 for boosting vaccinations. A very similar regimen is used in the Sputnik V vaccine, which has yielded cellular immune responses unmatched by other vectored vaccines applied in the current SARS-COV-2 pandemic (249). Although this is clearly applicable for human use, strong arguments exist that hAd5 vector immunity could reduce the translational efficacy. However, not only does practical experience speak against this, the use of the Ii adjuvant has a further demonstrated ability to increase booster effect, even in the face of anti-Ad5 immunity that would block a priming vaccine (376).

Another consideration for the design of future HPV therapeutic vaccines with a translational scope is whether to target multiple HPV types or not. Our Ii-E1E2E6E7 vaccine encodes only HPV16 antigens and will have limited or no effect against other HPV types (197). Alternatively, a multigenotype therapeutic vaccine has been published by Hancock and colleagues (192) and is now in clinical testing in patients with early cervical HPV^+ lesions (377). Broad genotype coverage is desirable, but the selection of specific parts of the HPV antigens may be at the cost of suboptimal responses against the type present in any given patient. Furthermore, more and more countries begin to implement HPV detection instead of cytology in their national cervical cancer screening programs (209), which means an effective type-specific vaccine could outcompete a broad vaccine against prevalent infection that may have suboptimal efficacy.

Altogether, we find that the presented adenoviral vectored Ii-E1E2E6E7 vaccine shows promising antitumor efficacy in mice. A similar vaccine design encoding MfPV3 Ii-E1E2E6E7 (356) is currently being tested in NHPs for efficacy against prevalent cervical infection in the *Macaca fascicularis* papillomavirus type 3 model (201). We believe that the combination of a strong vaccine platform and the inclusion of a broader range of HPV antigens than most other published therapeutic vaccines brings distinct benefits and warrants the clinical development of this therapeutic vaccine candidate.

5.3.6 Supplement

5.3.6.1 Supplementary Tables

Supplementary Table 1: Number of predicted epitopes

HPV 16 early protein	high affinitiy	medium affinity	low affinity	total
E1	452	1652	2632	4736
E2	166	696	1334	2196
E6	52	278	489	819
E7	44	132	263	439

Number of HLA types covered (of the 49 most frequent HLA types)

HPV 16 early protein	high affinitiy	medium affinity	low affinity	total
E1	37	42	44	44
E2	34	40	44	44
E6	26	37	43	43
E7	16	30	35	39

Predicted MHC-I epitopes of HPV16 early protein antigens E1, E2, E6 and E7 were aligned on the E1E2E6E7 fusion protein. Epitope prediction was performed using IEDB analysis resource v2.24 with ANN4.0 prediction method. The most frequent HLA types that together cover at least 75% of the human population (individually for HLA A, B, and C) were selected (49 in total). High affinity (0 - 50 nM calculated IC50) epitopes are depicted in green, medium affinity (50 - 500 nM calculated IC50) in yellow and low affinity (500 - 5000 nM calculated IC50) in red.

5.3.6.2 Supplementary Figures

li:

Atgcacagaaggcggagcagaagctgccgcgaggatcagaaacccgtgatggacgaccagcgggacctgatcagcaacaacgagcagctgcctatgctcggcagaaggcctggcgctcctgagagca
aatgttctagaggcgccctgtacaccggcttcagcatcctggttacactgctgctggccggacaggctaccacgcctactttctgtatcagcagcagggcagactggacaagctgaccgtgaccagccag
aacctgcagctggaaaacctgcggatgaagctgcccaagcctcctaagcctgtgtccaagatgcggatggccacacctctgctgatgcaggctttgcctatgggagcactgcctcagggccctatgca
gaacgccaccaaatacggcaacatgaccgaggaccacgtgatgcatctgctgcagaatgccgatcctctgaaggtgtaccctccactgaagggcagctttccgagaacctgcggcacctgaagaacaccat
ggaaaccatcgactggaaggtgttcgagagctggatgcaccactggctgctgttcgagatgagccggcacagcctggaacagaagcctacagacgcccctcctaaagagtccctggaactggaagatcccag
ctctggcctgggcgtgacaaagcaagatctgggccctgtgcctatg

E1:

ATGGCCGATCCTGCTGGCACAAACGGCGAAGAAGGCACAGGCTGCAACGGCTGGTTTTACGTGGAAGCCGTGGTGGAAAAGAAAACCGGCGACGCCATCAGCGACG
ACGAGAACGAGAATGACAGCGACACCGGCGAGGACCTGGTGGACTTCATCGTGAACGACAACGACTACCTGACACAGGCCGAGACAGAGACAGCCCACGCTCTGTTT
ACAGCCCAAGAGGCCAAGCAGCACAGAGATGCCGTTCAGGTGCTGAAGAGAAAGTACCTGGGCAGCCCTCTGAGCGACATCAGCGGCTGTGTGGACAACAACATCAG
CCCCAGACTGAAGGCCATCTGCATCGAGAAGCAGAGCAGAGCCGCCAAGCGGAGACTGTTTGAGAGCGAGGATAGCGGCTACGGCAATACCGAGGTGGAAACCCAG
CAAATGCTGCAGGTCGAGGGCAGACACGAAACCGAGACACCTTGCAGCCAGTACAGCGGAGGATCTGGCGGAGGCTGTAGCCAGTACTCTTCTGGAAGTGGCGGAG
AGGGCGTGTCCGAGAGACACACCATTTGTCAGACCCCTCTGACCAACATCCTGAACGTGCTGAAAACCAGCAACGCCAAGGCCGCCATGCTGGCCAAGTTCAAAGAGC
TGTACGGCGTCAGCTTCAGCGAACTCGTGCGGCCCTTCAAGAGCAACAAGTCCACCTGTTGCGACTGGTGCATTGCCGCCTTTGGCCTGACACCTTCTATCGCCGACAGC
ATCAAGACCCTGCTCCAGCAGTACTGTCTGTACCTGCACATTCAGAGCCTGGCCTGCTCTTGGGGAATGGTGGTGCTGCTGCTCGTGCGGTACAAGTGCGGCAAGAACA
GAGAGACAATTGAGAAGCTGCTGAGCAAACTGCTGTGCGTGTCCCCTATGTGCATGATGATCGAGCCTCCAAAGCTGCGGTCTACAGCCGCCGCTCTGTACTGGTACAA
GACCGGCATCAGCAATATCTCCGAGGTGTACGGCGACACCCCTGAGTGGATTCAGAGACAGACCGTCCTGCAGCACAGCTTCAACGACTGCACCTTCGAGCTGTCCCAG
ATGGTGCAGTGGGCCTACGACAATGACATCGTGGACGACTCCGAGATCGCCTATAAGTACGCCCAGCTGGCCGACACCAACAGCAATGCCAGCGCCTTCCTGAAGTCC
AACAGCCAGGCCAAGATCGTGAAGGACTGCGCCACCATGTGCAGACACTACAAGCGGGCCGAGAAGAAACAGATGAGCATGAGCCAGTGGATCAAGTACAGATGCG
ACAGAGTGGACGACGGCGGCGATTGGAAGCAGATCGTGATGTTCCTGAGATACCAGGGCGTCGAGTTCATGAGCTTTCTGACAGCCCTGAAGCGGTTCCTGCAGGGC
ATCCCCAAGAAGAACTGCATCCTGCTGTATGGCGCCGCTAACACCGGCAAGAGCCTGTTCGGAATGAGCCTGATGAAGTTTCTGCAGGGCTCCGTGATCTGCTTTGTGA
ACAGCAAGAGCCACTTCTGGCTCCAGCCACTGGCCGATGCCAAGATTGGCATGCTGGACGATGCCACCGTGCCTTGCTGGAACTACATCGACGACAACCTGAGAAACGCCCTG
GACGGCAACCTGGTTTCTATGGACGTGAAGCACAGACCCCTGGTGCAGCTGAAGTGTCCTCCACTGCTGATCACCAGCAACATCAACGCCGGCACCGATTCCAGATGGC
CCTATCTGCACAACCGGCTGGTGGTGTTTACCTTTCCTAACGAGTTCCCCTTCGACGAAAACGGCAACCCCGTGTACGAGCTGAACGATAAGAATTGGAAGTCCTTCTTC
AGCCGGACCTGGTCCAGACTGAGCCTGCACGAGGATGAGGACAAAGAGAACGACGGCGACAGCCTGCCTACCTTCAAATGTGTCAGCGGCCAGAACACCAACACACT
G

E2:

ATGGAAACACTGTGCCAGCGGCTGAACGTGTGCCAGGACAAGATTCTGACCCACTATGAGAACGACAGCACCGACCTGAGGGACCACATCGACTACTGGAAGCACAT
GCGGCTGGAATGCGCCATCTACTACAAGGCTAGAGAGATGGGCTTCAAGCACATCAACCACCAGGTGGTGCCTACACTGGCCGTGTCTAAGAACAAGGCTCTGCAGGC
CATCGAACTGCAGCTGACCCTGGAAACAATCTACAACTCCCAGTACTCCAACGAGAAGTGGACCCTCCAGGACGTGTCACTGGAAGTGTACCTGACCGCTCCTACCGGC
TGCATCAAGAAACACGGCTACACCGTGGAAGTGCAGTTTGACGGCGATATCTGCAATACCATGCACTACACCAACTGGACCCACATCTACATCTGCGAAGAGGCCAGC
GTGACAGTGGTGGAAGGCCAGGTCGACTACTACGGCCTGTACTACGTGCACGAGGGCATCAGAACCTACTTCGTGCAGTTCAAGGATGACGCCGAGAAGTACAGCAA
GAACAAAGTGTGGGAAGTGCACGCTGGCGGCCAAGTGATCCTGTGTCCTACAAGCGTGTTCAGCAGCAACGAAGTGTCTAGCCCCGAGATCATCAGACAGCACCTGGC
CAATCATCCTGCCGCCACACACACAAAAGCTGTGGCCCTGGGCACCGAGGAAACACAGACCACAATTCAGAGGCCCAGAAGCGAGCCCGATACCGGCAATCCTTGTCA
CACCACCAAGCTGCTGCACCGGGATTCCGTGGATTCTGCCCCTATCCTGACCGCCTTCAACAGCTCCCACAAAGGCCGGATCAACTGCAACAGCAACACCACACTATCGTGCA
CCTGAAAGGGGACGCCAACACTCTGAAGGCCCTGCGGTACAGATTCAAGAAGCACTGTACCCTGTATACCGCCGTGTCCAGCACATGGCACTGGACCGGACACAACGT
GAAACACAAGAGCGCCATCGTGACCCTGACCTACGATAGCGAGTGGCAGAGGGACCAGTTCCTGAGCCAAGTGAAGATCCCTAAGACCATCACCGTGTCCACCGGCTT
T ATGAGCATT

E6:

ATGCACCAGAAACGGACAGCCATGTTCCAGGATCCTCAAGAGCGGCCACGGAAGCTGCCTCAGCTGTGTACAGAACTGCAGACCACCATCCACGACATCATCCTCGAG
TGCGTGTACTGCAAGCAGCAGCTCCTGCGGAGAGAAGTGTACGACTTCGCCTTCCGGGATCTGTGCATCGTGTACAGAGATGGCAACCCCTACGCCGTGTGCGACAAG
TGCCTGAAGTTCTACTCCAAGATCAGCGAGTACCGGCACTACTGCTACTCCCTGTACGGCACCACACTTGAGCAGCAGTACAACAAGCCCCTGTGCGATCTGCTGATCCG
GTGCATCAACTGCCAGAAACCTCAGTGCCCCGAGGAAAAGCAGAGACACCTGGACAAGAAGCAGCGGTTCCACAACATTAGAGGCAGATGGACAGGCCGGTGCATGA
G CTGCTGTAGAAGCAGCAGAACAAGACGG

E7:

ATGCACGGCGATACCCCAACACTGCACGAGTACATGCTGGATCTGCAGCCCGAGACAACCGATCTGTACGGCTATGAGCAGCTGAATGACTCCAGCGAGGAAGAGGA
CGAGATCGACGGACCTGCTGGACAGGCTGAACCTGATAGAGCCCACTACAATATCGTGACCTTCTGCTGCAAGTGCGATAGCACCCTGAGAAGATGCGTGCAGAGCAC
CCACGTGGACATCAGGACCCTCGAGGATCTGCTCATGGGCACCCTGGGAATTGTGGCCCCAATCTGCTCTCAGAA GCCT

p2a-li:

gccaccaatttcagtctgcttaaacaggccggggacgtcgaagagaaccccggacctatgcatcggcgcagatctcggtcttgtagagaagaccaaaagcctgtcatggatgatcaaagagattt
aatttctaataatgaacaattacccatgttgggacggcgccccggagcccccgaatctaagtgcagccggggagctttatatacaggattttctattttagtgaccttattattagctggccaagcca
caacagcttatttcttataccaacaacaaggacggttagataaattaacagtcacatctcaaaatttacaattagagaatttaagaatgaaattacctaaaccacccaaacccgtcagtaaaatgaga
atggctacccccttattaatgcaagccctccccatgggcgccttaccccaaggacccatgcaaaatgctacaaagtatggaaatatgacagaagatcatgtcatgcacttattacaaaacgctgacccct
taaaagtctatcccccctttaaaaggatctttccctgaaaatttaagacatttaaaaaatacaatggagacaattgattggaaagtctttgaatcttggatgcatcattggttattatttgaaatgtcta
ggcattctttagagcaaaaacccaccgatgctccacccaaggaaagtttagagttagaggacccttctagcggattaggagtcaccaaacaggacttaggacccgtccccatg

Supplementary Figure 7.
DNA sequences of the designed antigens.

Negative control antigens used in mouse tumor model experiments

SIV (vif, rev and vpr): used for Ad19a negative control

ATGGAGGAGGAGAAGAGGTGGATCGCAGTGCCAACATGGAGGATCCCTGAGCGGCTGGAGAGATGGCACTCTCTGATCAAGTACCTGAAGTATAAGACCAAGGACC
TGCAGAAGGTGTGCTACGTGCCCCACTTCAAGGTCGGCTGGGCCTGGTGGACATGTTCCAGAGTGATCTTTCCTCTGCAGGAGGGCTCTCACCTGGAGGTGCAGGGCT
ATTGGCACCTGACCCCAGAGAAGGGCTGGCTGAGCACCTACGCCGTGAGAATCACATGGTATTCCAAGAACTTCTGGACCGATGTGACACCAAATTACGCCGACATCCT
GCTGCACTCCACCTATTTCCCCTGTTTTACAGCAGGAGAGGTGAGGAGGGCAATCAGGGGAGAGCAGCTGCTGTCTTGCTGTAGGTTTCCTCGCGCCCACAAGTACCAG
GTGCCAAGCCTGCAGTATCTGGCCCTGAAGGTGGTGTCTGACGTGAGGAGCCAGGGCGAGAACCCAACCTGGAAGCAGTGGCGGAGAGACAATAGGCGCGGCCTGC
GCATGGCCAAGCAGAACAGCAGGGGCGATAAGCAGAGGGGAGGCAAGCCACCAACAAAGGGAGCCAATTTCCCAGGCCTGGCAAAGGTGCTGGGAATCCTGGCCAT
GTCCAACCACGAGAGGGAGGAGGAGCTGAGGAAGCGGCTGAGACTGATCCACCTGCTGCACCAGACCAATCCATACCCTACCGGACCAGGAACAGCAAACCAGCGGA
GACAGAGGAAGAGGCGCTGGCGGAGAAGGTGGCAGCAGCTGCTGGCCCTGGCAGACCGCATCTATTCCTTTCCAGACCCTCCAACCGATACACCCCTGGACCTGGCCAT
CCAGCAGCTGCAGAATCTGGCCATCGAGTCTATCCCCGATCCCCCTACCAACACACCAGAGGCCCTGTGCGATCCCACCGAGGACTCTCGGAGCCCTCAGGACATGGAGGA
GCGGCCCCCAGAGAATGAGGGACCACAGAGAGAGCCCTGGGATGAGTGGGTGGTGGAGGTGCTGGAGGAGCTGAAGGAGGAGGCCCTGAAGCACTTTGACCCTAG
GCTGCTGACCGCCCTGGGCAACCACATCTACAATAGGCACGGCGATACACTGGAGGGAGCAGGAGAGCTGATCAGGATCCTGCAGAGAGCCCTGTTCATGCACTTCGGC
GCGGCTGTATCCACAGCAGAATCGGCCAGCCCGGCGGCGGCAATCCACTGAGCGCAATCCCCCCATCCAGATCCATGCTG

HIV (rev, vif, vpr and gag/pol fragments): used for Ad5 negative control

ATGGCAGGCAGGAGCGGCGACTCCGATGAGGCCCTGCTGCAGGCCGTGCGCATCATCAAGATCCTGTACCAGAGCAACCCATATCCAAAGCCTGAGGGAACCAGGCA
GGCAAGAAAGAATAGAAGGCGCCGGTGGAGGGCAAGGCAGAGACAGATCCACTCTATCAGCGAGCGGATCCTGTCCACATGCCTGGGCAGACCAGCAGAGCCAGTG
CCACTGCAGCTGCCACCTATCGAGAGGCTGCACATCGGATGTTCCGAGTCTGGAGGCACCAGCGGAACACAGCAGTCCCAGGGAACCACAGAGGGAGTGGGATCTCC
CGTGAGCGGCAAGTCCTGCGCCGTGCTGGGAAGCGGCGCCAAGAAGGAGATGGAGAACCGCTGGCAGGTGCTGATCGTGTGGCAGGTGGACAGGATGAAGATCCG
CACCTGGAACAGCCTGGTGAAGCACCACATGTACATCTCCAGAAGGGCCAATGGCTGGTTTTACCGGCACCACTATGAGTCCAGACACCCAAAGGTGTCTAGCGAGGT
GCACATCCCACTGGGCGACGCAAGGCTGGTCATCAAGACCTATTGGGGACTGCAGACAGGAGAGAGGGATTGGCACCTGGGACACGGCGTGTCTATCGAGTGGAGA
CTGCGCCGGTACAGCACCCAGGTGGACCCAGGCCTGGCCGATCAGCTGATCCACATGCACTATTTCGACTGCTTTGCCGATAGCGCCATCCGGAAGGCCATCCTGGGCCACAT
CGTGATCCCTAGATGTGATTACCAGGCCGGCCACAACAAGGTCGGCAGCCTGCAGTATCTGGCCCTGACAGCCCTGATCAAGCCCAAGAAGATCAAGCCACCCCTGCCT
TCCGTGAGGAAGCTGGTGGAGGACCGCTGGAATAAGCCTCAGAAGACCAGGGGCAGAAGGGGCAACCACACAATGAATGGCCACATGGAGCAGGCACCAGAGGAT
CAGGGACCACAGCGCGAGCCTTACAACGAGTGGACCCTGGAGCTGCTGGAGGAGCTGAAGCAGGAGGCCGTGCGGCACTTCCCTAGACCATGGCTGCACTCCCTGGG
CCAGTACATCTATGAGACATATGGCGACACCTGGACAGGCGTGGAGGCCATCATCCGGATCCTGCAGCAGCTGCTGTTCATCCACTTTCGGATCGGCTGCCAGCACAGC
AGAATCGGCATCCTGCAGAGGAGGGCAAGGAATGGAGCAAGCCGCTCCGGCGACGATGGCAAGGTGTCCCAGAACTACCCCATCGTGCAGAATCTGCAGGGACCTCC
ACCATCCCACAAGGCAAGAGTGCTGGCCGAGGCCATGTCTCAGGCCAACAATACCAACATCATGATGCAGAGGTCTAATTTCAAGGGCGGCAGCACCGATTGTACAGA
GCGCCAGGCCAACTTTCTGGGCAAGATCTGGCCATCCCACAAGGGCAGGCCCGGCAACTTTCTGCAGAATAGGCCAGAGCCTACCGCACCTCCAGCAGAGTCTTTCAG
GTTTGAGGAGACCACACCAGCCCCCAAGCAGGAGCCTAAGGACCGCGAGCCACTGACATCTCTGAAGAGCCTGTTCGGCTCTGATCCACTGTCCCAGGGATCTACCCAGCTG
GGATGTACACTGAACTTTCCAATCAGCCCCATCGAGACCGTGCCACCTCCAATCGCAGGAGCCGAGACATTCTACGTGGACGGAGCAGCAAATAGGGGATCCTCTAGCGGCAT
CCGCAAGGTGCTGTTCCTGGACGGCATCGATAAGGCCGGCAGCACC

Supplementary Figure 7. continued.
DNA sequences of the designed antigens.

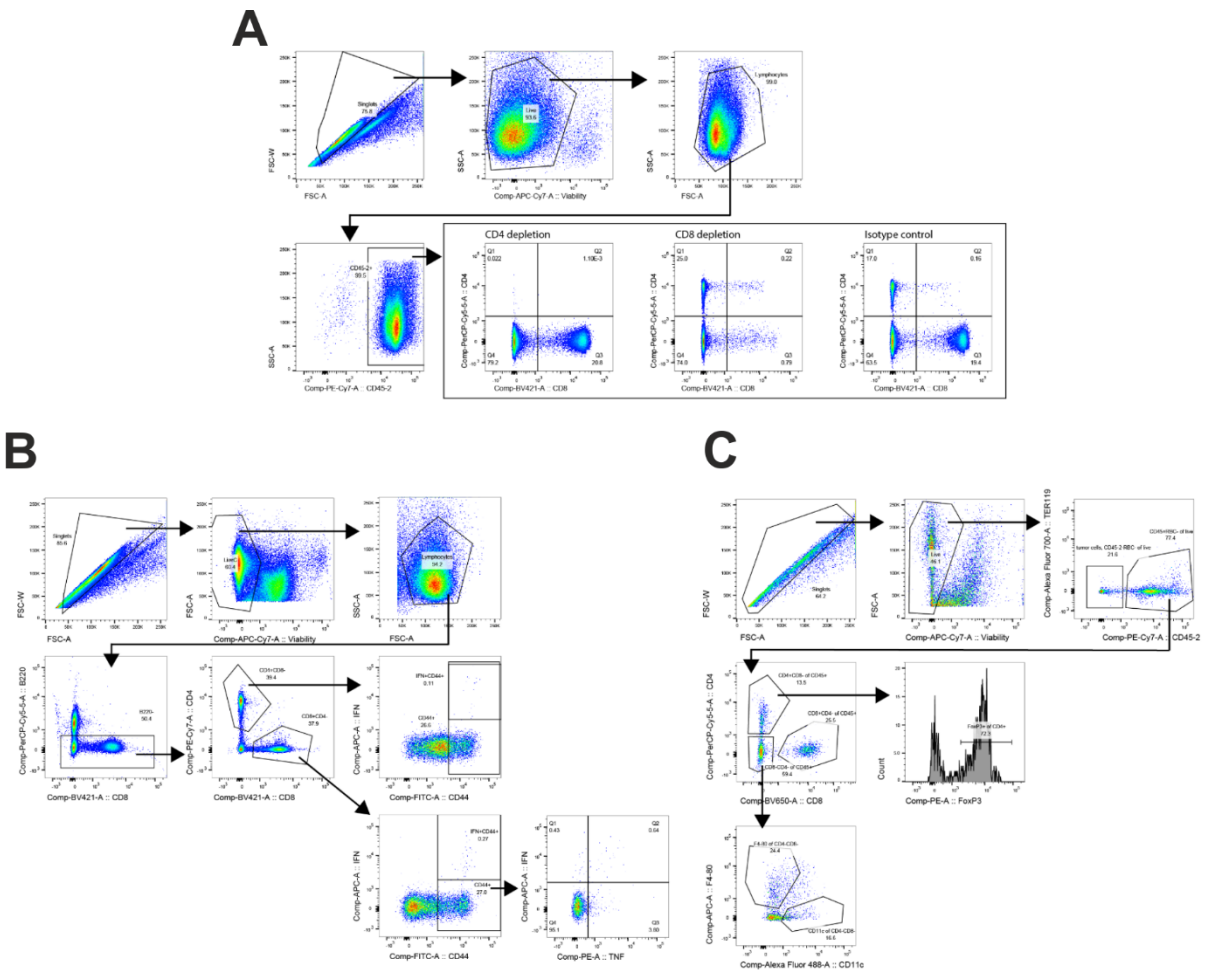

Supplementary Figure 8.
(A) Representative images of verification of depletion of $CD8^+$ and $CD4^+$ T-cells. (B) Gating strategy for immune response analysis by intracellular staining. C: Gating strategy for tumor lineage staining.

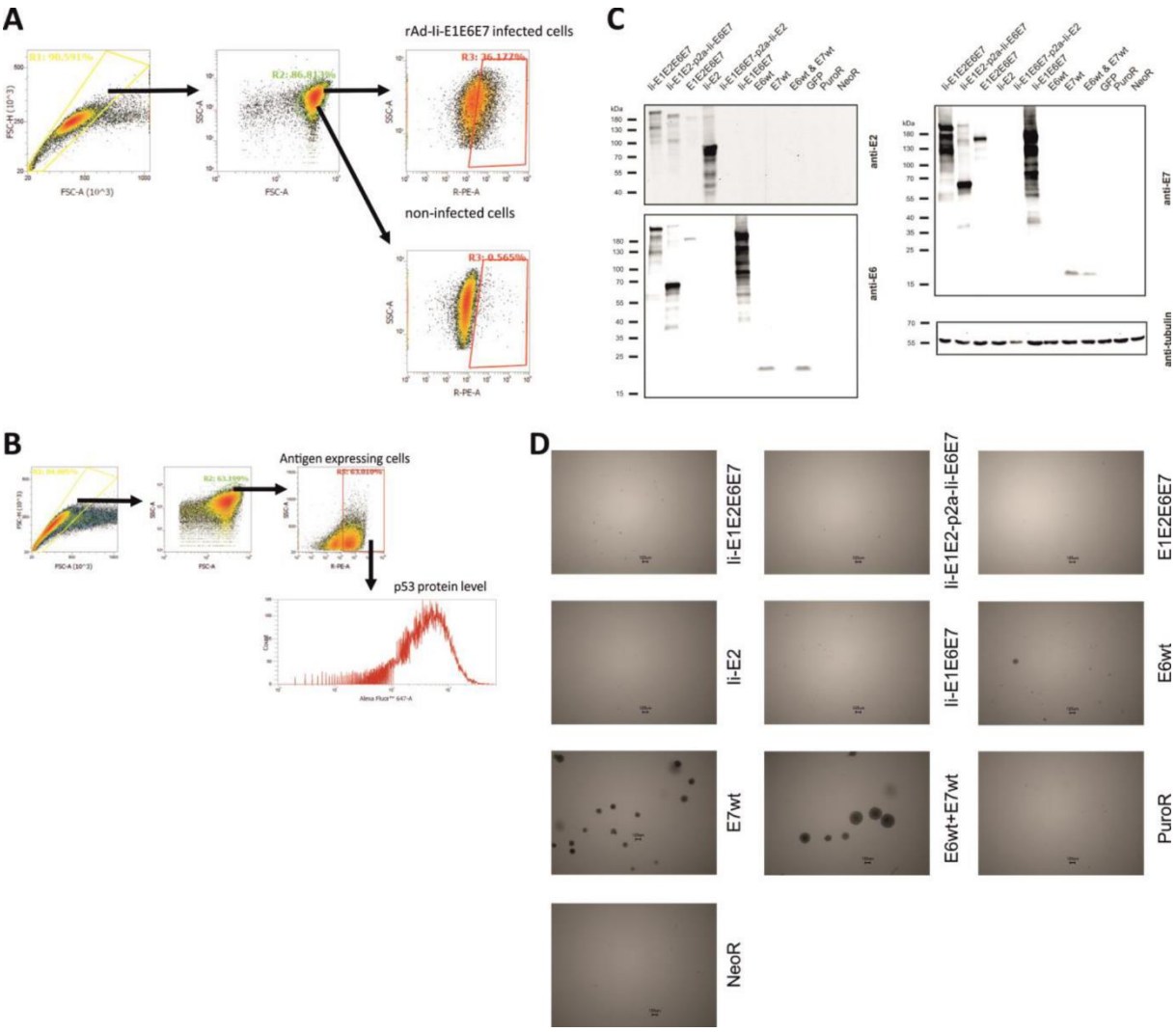

Supplementary Figure 9.
(A) Gating strategy for flow cytometry analysis of rAd-infected A549 cells 48 h post infection. (B) Gating strategy for flow cytometry analysis of p53 level of antigen-expressing HEK293T cells 48 h post infection. (C) Western blot analysis of cell lysates of lentivirally transduced NIH 3T3 cells after antibiotic selection. Antigens were detected with anti-E2 (left upper panel), anti-E6 (left lower panel) and anti-E7 (right upper panel) antibodies. As loading control, tubulin levels were monitored using an anti-tubulin antibody (right lower panel). (D) Representative microscopy images of lentivirally transduced NIH 3T3 cells in soft agar assay 3 weeks after seeding in soft agar. The colonies were stained with crystal violet. Images were taken at 4x optical magnification.

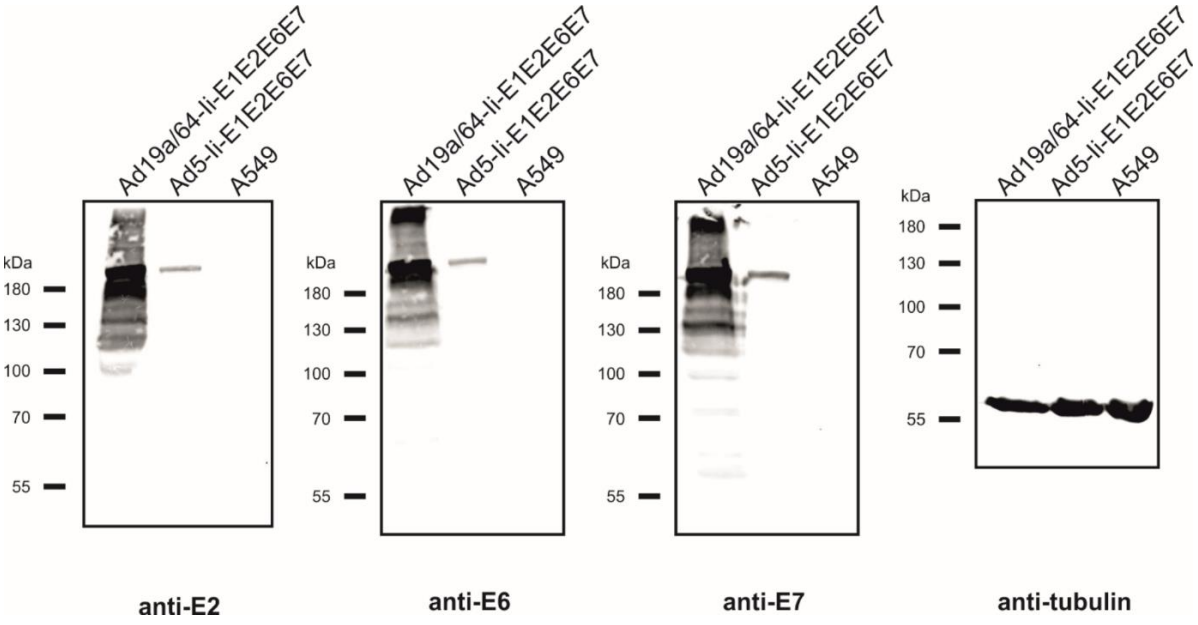

Supplementary Figure 10.
Western blot analysis of A549 cell lysates 48 h following transduction with Ad19a/64 or Ad5 encoding li-E1E2E6E7 at an MOI of 100. Antigens were detected with anti-E2 (first panel), anti-E6 (second panel) and anti-E7 (third panel) antibodies. As loading control, tubulin levels were monitored using an anti- tubulin antibody (fourth panel).

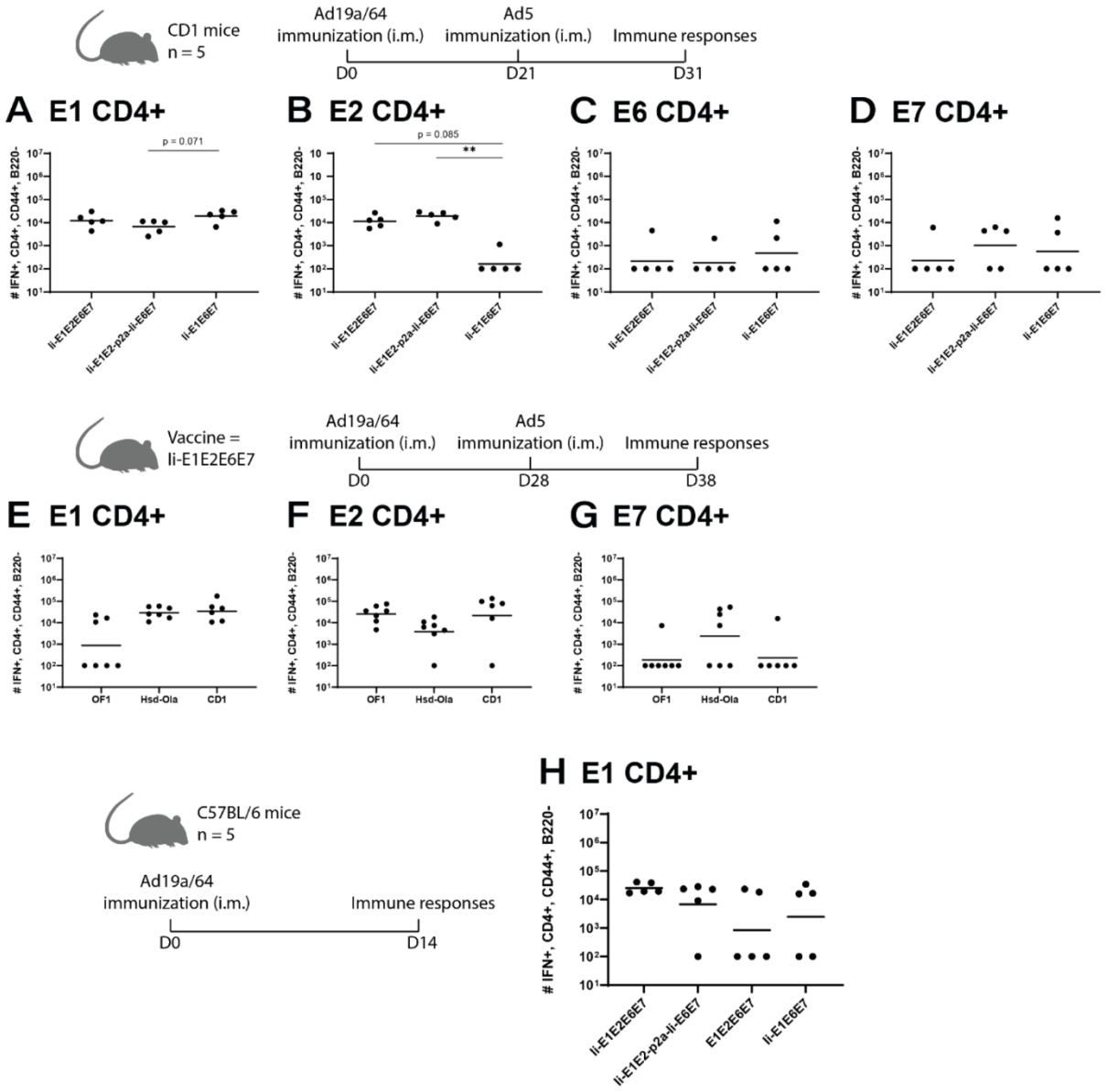

Supplementary Figure 11.
CD1 mice (A-D), different outbred mice as indicated (E-G) or C57BL/6 mice (H) were immunized with Ad vaccine(s) (2×10^7 IFU) encoding the various HPV16 early antigens as indicated. Mice were sacrificed at the timepoints indicated, spleens were harvested and $CD4^+$ T-cell immune responses against E1, E2, E6, and E7 were measured using intracellular staining and flow cytometry. Each symbol represents one mouse, bars represent the geometric mean.

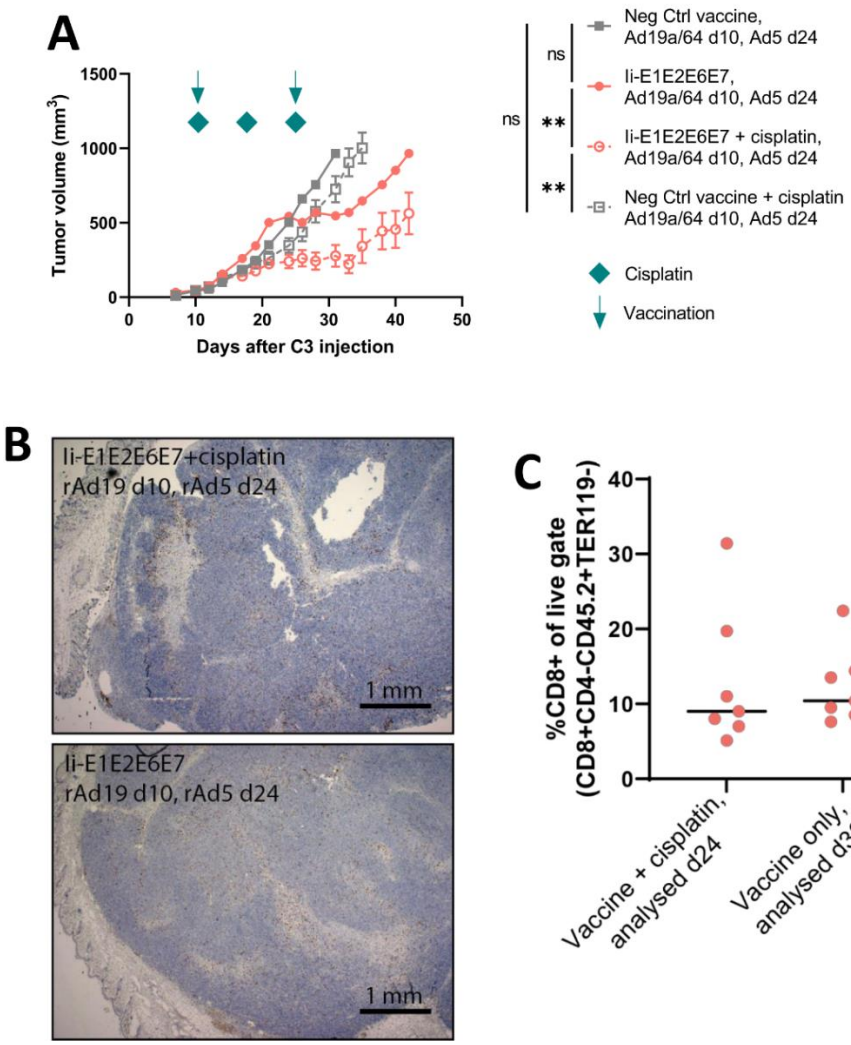

Supplementary Figure 12.
1×10^6 C3 cells were injected s.c. into the flank of C57BL/6 mice, and the mice received Ad19a/64- and Ad5-vectored vaccines i.m. in the same side as the tumor on day 10 and day 24, respectively. Cisplatin treatment was given i.p. on days 10, 17 and 24. (A) Mean tumor growth with SEM was assessed. Pink circles represent the therapeutic vaccine group. Gray squares depict negative control vaccinated mice. Open icons/dashed lines depicts cisplatin treated mice. Green arrows indicate time of vaccination. Green diamonds indicate time-point of cisplatin injections. The figure shows data pooled from two independent experiments. (B) Representative images of immunohistochemistry staining of a tumor from either vaccinated mice with (top) or without (bottom) cisplatin co-treatment. Pictures are taken with the same magnification. (C) tumors were harvested at the time indicated, single cell suspensions were prepared, and the fraction of $CD8^+$ cells ($CD8^+CD4^-CD45.2^-$live) was assessed by surface staining and flow cytometry.

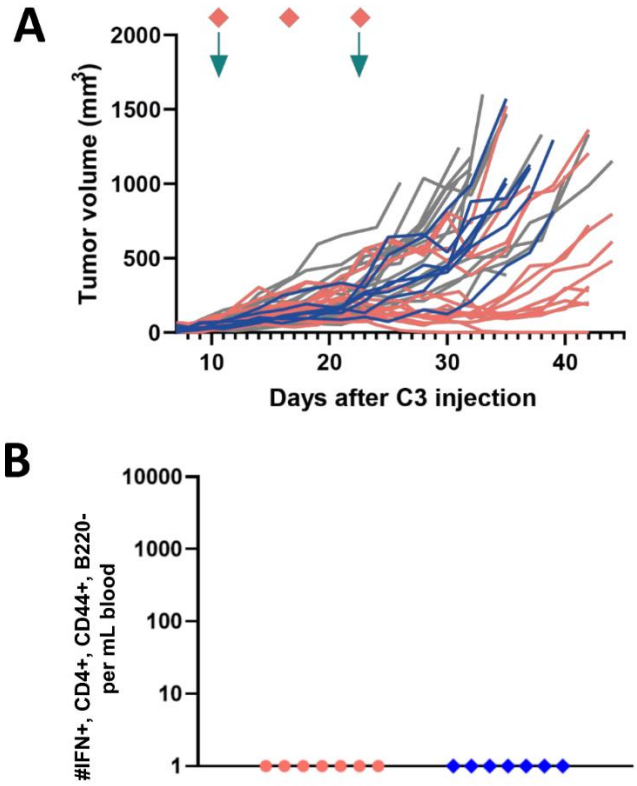

Supplementary Figure 13.
1×10^6 C3 cells were injected s.c. into the flank of C57BL/6 mice, and the mice received Ad19a/64- and Ad5-vectored vaccines i.m. in the same side as the tumor, or peptide- based vaccine s.c. in the opposite flank on day 10 and day 24. Cisplatin treatment was given i.p. on days 10, 17 and 24. (A) Curves show the measured tumor size for the individual mice. Ii-E1E2E6E7 vaccinated in pink, neg ctrl vaccinated in gray, peptide vaccinated in blue. (B) No detectable E1 specific $CD4^+$ T-cell immune responses were measured in the blood on day 22 using intracellular staining and flow cytometry. Each symbol represents one mouse.

5.3.7 Ethical statement

The animal study was reviewed and approved by National Animal Experiments Inspectorate (Dyreforsøgstilsynet, license no. 2016-15-0201-01131).

5.3.8 Funding

This project has received funding from the Eurostars-2 joint programme with co-funding from the European Union Horizon 2020 research and innovation programme (E!12151). The project E!12151 was carried out within the framework of the European funding program “Eurostars” and the German partners were funded by the Federal Ministry of Education and Research. The manuscript reflects only the authors’ view and the European Commission is not responsible for any use that may be made of the information it contains. The funders had no influence on study design, data collection and analysis, decision to publish, or preparation of the manuscript.

5.3.9 Acknowledgments

This project has received funding from the Eurostars-2 joint program with cofunding from the European Union Horizon 2020 research and innovation program (E!12151). The project E!12151 was carried out within the framework of the European funding program "Eurostars," and the German partners were funded by the Federal Ministry of Education and Research. The manuscript reflects only the authors' view and the European Commission is not responsible for any use that may be made of

the information it contains. The funders had no influence on study design, data collection and analysis, decision to publish, or preparation of the manuscript. A549 cells were kindly provided by Marian Wiegand/Amvac Research GmbH. NIH-3T3 cells (passage 3) were a gift from Martin Ehrenschwender/IMHR. C3 cells were a kind gift from S.J. van der Burg, Leiden University Medical Centre, and E. Nejad was very helpful with advice on handling the cells. We would like to thank T. van Hall and C. Melief for advice on using the E6/E7 peptides and colleague K. Orfin for assistance with tumor-model experiments. J.C. Brings and C. Ørskov of the Biomedical Institute, University of Copenhagen, have provided very valuable input on the IHC analysis.

5.4 Manuscript 3

"Transgene expression knock-down in recombinant Modified Vaccinia virus Ankara vectors improves genetic stability and sustained transgene maintenance across multiple passages"

Patrick Neckermann[1], Madlen Mohr[1], Martina Billmeier[1], Alexander Karlas[2], Ditte R. Boilesen[3,4], Christian Thirion[5], Peter J. Holst[3,4], Ingo Jordan[2], Volker Sandig[2], Benedikt Asbach[1] and Ralf Wagner[1,6*]

[1]University of Regensburg, Institute of Medical Microbiology & Hygiene, Molecular Microbiology (Virology), Franz-Josef-Strauß-Allee 11, 93053 Regensburg, Germany

[2]ProBioGen AG, Herbert-Bayer-Straße 8, 13086 Berlin, Germany

[3]University of Copenhagen, department of Immunology and Microbiology, center for medical parasitology, the Panum Institute, Blegdamsvej 38, 2200 Copenhagen N, Denmark

[4]InProTher APS, Ole Maaløes vej 3, 2200 Copenhagen, Denmark

[5]SIRION Biotech GmbH, Am Klopferspitz 19, 82152 Planegg-Martinsried, Germany

[6]Institue of Clinical Microbiology and Hygiene, University Hospital Regensburg, Franz-Josef-Strauß-Allee 11, 93053 Regensburg, Germany

*correspondence to Ralf Wagner, ralf.wagner@ur.de

Manuscript submitted on 14th of November 2023 to Frontiers in Immunology

5.4.1 Abstract

Modified vaccinia virus Ankara is a versatile vaccine vector, well suited for transgene delivery, with an excellent safety profile. However, certain transgenes render recombinant MVA (rMVA) genetically unstable, leading to the accumulation of mutated rMVA with impaired transgene expression. This represents a major challenge for upscaling and manufacturing of rMVA vaccines. To prevent transgene-mediated negative selection, the continuous avian cell line AGE1.CR pIX (CR pIX) was modified to suppress transgene expression during rMVA generation and amplification. This was achieved by constitutively expressing a tetracycline repressor (TetR) together with a rat-derived shRNA in engineered CR pIX PRO suppressor cells targeting an operator element (tetO) and 3' untranslated sequence motif on a chimeric poxviral promoter and the transgene mRNA, respectively. This cell line was instrumental in generating two rMVA (isolate CR19) expressing a *Macaca fascicularis* papillomavirus type 3 (MfPV3) E1E2E6E7 artificially-fused polyprotein following recombination-mediated integration of the coding sequences into the DelIII (CR19 M-DelIII) or TK locus (CR19 M-TK), respectively. Characterization of rMVA on parental CR pIX or engineered CR pIX PRO suppressor cells revealed enhanced replication kinetics, higher virus titers and a plaque morphology equaling wild-type MVA, when transgene expression was suppressed. Serially passaging both rMVA ten times on parental CR pIX cells and tracking E1E2E6E7 expression by flow cytometry revealed a rapid loss of transgene product after only few passages. PCR analysis and next-generation sequencing demonstrated that rMVA accumulated mutations within the E1E2E6E7 open reading frame (CR19 M-TK) or deletions of the whole transgene cassette (CR19 M-DelIII). In contrast, CR pIX PRO suppressor cells preserved robust transgene expression for up to 10 passages, however, rMVAs were more stable when E1E2E6E7 was integrated into the TK as compared to the DelIII locus. In conclusion, sustained knock-down of transgene expression in CR pIX PRO suppressor cells facilitates the generation, propagation and large-scale manufacturing of rMVA with transgenes hampering viral replication.

5.4.2 Introduction

Modified Vaccinia virus Ankara (MVA) is a highly attenuated poxvirus strain which has been derived from Chorioallantois Vaccinia virus Ankara (CVA) by over 500 passages on primary chicken embryo fibroblasts (269,270). Because of its extensive passaging, MVA differs from CVA by the loss of about 30 kb of genomic DNA in 6 major deletion sites (271) and several smaller mutations (272). As a consequence, replication of MVA is restricted to avian cells and very few mammalian cells (273–276). MVA has a proven clinical track record and a high safety profile (277). Therefore, MVA can also be used in immunocompromised animals (378) and humans (280). MVA-BN is an approved prophylactic vaccine against smallpox and monkeypox in the European Union (379) and the USA (380). Moreover, MVA is a versatile vector to deliver vaccine payloads because of its ability to express large and multiple transgenes and the capacity to elicit robust T-cell and antibody responses (282,283). Since 2020, the recombinant MVA (rMVA) MVA-BN-Filo (284) is approved in combination with Zabdeno as a prophylactic vaccine against Zaire ebolavirus (285). Additionally, multiple MVA based vaccine candidates are under clinical development (381), including more recently candidates targeting e.g. SARS-CoV2 and MERS (286,382). Apart from prophylactic vaccines, rMVA is also investigated as a potential vector platform for immunotherapeutics (287,288).

Instability of rMVA, i. e. the tendency to spontaneously loose transgene expression, is a common issue in the field (306–308,383,384). While generating rMVA vaccines against different viruses, e.g. Ebola, HIV, SARS-CoV-2, and also immunotherapeutics against HPV- and HERV-induced cancers, we and others commonly found mutated rMVA (mrMVA) that had lost expression of their recombinant antigen

after tissue culture passage (306–308,383,384). As described by Wyatt *et al.*, although unstable rMVA may be present in virus stocks at concentrations too low for detection unless extensive plaque screening or deep-sequencing is performed, they are able to rapidly overgrow the desired rMVA if loss of transgene expression leads to a replication advantage (306). Since production of clinical GMP-grade rMVA for large vaccine seed stocks requires vector expansion, it is important to maintain genetic stability of the transgene over a sufficient number of replication cycles in order to preserve immunogenicity and efficacy of the vaccine. Wang and colleagues showed that rMVA encoding CMV IE1 and pp65 propagated for 10 passages exhibited lower induction of antigen specific T cell responses in preclinical analysis, and detailed characterization of this passaged rMVA revealed frequent loss of the CMV transgenes (308). Even though stability of rMVA is crucial, only few studies systematically investigated the stability of rMVA. Three factors seem to contribute to the instability of some rMVA: the integration locus (306,307), promotor usage controlling recombinant transgene expression (308), and harmful transgene products (306,384).

We previously have generated adenoviral vectors as therapeutic vaccine candidates encoding various combinations of optimized *Macaca fascicularis* papillomavirus 3 (MfPV3) and human papillomavirus type 16 early antigens (E1, E2, E6, E7) (356,385). For a heterologous prime-boost regimen, we aimed towards complementing our vector suite with rMVA (MVA-CR19 (291)) expressing a corresponding set of antigens. Despite our serious efforts we failed to generate these rMVA on the continuous avian AGEI.CR pIX (CR pIX) cell line, regardless of the integration locus and the poxviral promoter usage (290).

Here, we provide evidence that the expression of the papillomavirus early antigens was associated with genetic instability and selection of rMVA mutants escaping transgene expression alongside with replication. Loss of transgene expression was mainly caused by early translation terminations or large deletions depending on the locus of the integrated transgene in the rMVA genome. Suppression of transgene expression in an engineered suppressor cell line (CR pIX PRO) by targeting an operator element on chimeric poxviral promoters via a constitutively expressed tetracycline repressor (TetR) together with a shRNA (Plin-2) targeting a rat perilipin-2 derived 3’ untranslated sequence element (P2TS) on the transgene mRNA restored genetic stability of the rMVA and stabilized transgene expression across several passages. Our data suggest that sustained transgene suppression during generation and amplification of rMVA mitigates the risk for transgene mediated genetic instability and strongly enhances production yields of otherwise hard to produce rMVA.

5.4.3 Methods

5.4.3.1 Antigen sequence

Antigen Ii-E1E2E6E7 was generated as previously described (356). For codon optimization, canonical vaccinia transcription termination signal T_5NT (386) and the known instability motifs - runs of G_5 and C_5 (306) - were excluded.

5.4.3.2 Cell lines

Adherent AGEI.CR pIX (CR pIX) cells were cultivated in DMEM/F-12 containing 5% fetal calf serum (FCS) as previously described (290). CR pIX cells in suspension were cultivated as previously described (290). Modified AGEI.CR pIX (CR pIX PRO) suppressor cells were generated by transduction of CR pIX cells with a VSV-G pseudotyped lentiviral vector at MOI 1 in the presence of 8 µg/ml polybrene (hexadimethrine bromide, Cat. H9268, Sigma-Aldrich, Germany) coding for the ProVector expression cassette. In detail, the ProVector expression cassette contains Plin2 shRNA under control of a U6 promoter, the tetracyclin repressor gene (tetR) controlled by a CMV promoter, and a puromycin

resistance marker gene under the EF1α core promoter. CR pIX PRO cells were cultivated in respective growth medium additionally containing 1 µg/ml puromycin for selection purposes.

5.4.3.3 Generation of recombinant viruses

Recombinant MVA-CR19 vectors were generated as previously described (292). Briefly, MfPV3 Ii-E1E2E6E7 (356) or GFP was cloned into the shuttle vector SP-CR19III, suitable for integration into MVA's deletion site III (DelIII) under the control of the MVA E/L-promoter (SSP with one point mutation (292)) or cloned into the shuttle vector pLZAW1, suitable for integration into MVA's thymidine kinase locus (TK) under the control of the MVA SSP-promoter (387). The shuttle vectors were modified further by inserting two copies of the tetracycline operator sequence (tetO) directly downstream of the MVA promoter and by adding the Plin2 target sequence (P2TS) at the 3'-UTR of the GOI. Recombinant MVA encoding the different genes-of-interest (GOI) were generated by homologous recombination in adherent parental CR pIX or CR pIX PRO suppressor cells that prevent the undesirable expression of the GOI during generation and propagation of the recombinant MVA. To this end, the culture monolayers seeded in a six-well plate were infected with MVA-CR19 with an MOI of 0.05 and transfected with 2 µg of the individual shuttle vector by using the Effectene Transfection Reagent (Qiagen, Hilden, Germany) according to the manufacturer's instructions. The infected/transfected culture was harvested 2-3 days post-infection/transfection, sonicated, and used for infection of a cell monolayer in a six-well plate format. Resulting plaques were validated by PCR and an iterative plaque purification procedure was initiated until MVA without the correct GOI expression cassette were absent (usually within 5–8 rounds of plaque purification).

For the propagation of plaque-purified rMVA, the cell harvest material was sonicated by using a Vial Tweeter (set to 20 s of 100% cycle and 90% amplitude, Hielscher, Germany), and CR pIX PRO cells (grown in suspension at 2×10^6 cells per ml in 1:1 mixtures of CD-U4 and CD-VP4 media (Merck-Millipore, Darmstadt, Germany)) were inoculated with the individual recombinant MVA vectors at MOI 0.05. Finally, rMVA were harvested 48 h - 72 h post-infection and the TCID50 titer was determined. 3 propagation cycles were needed to generate the viral stocks.

5.4.3.4 Virus titration

Virus titers were measured by using the tissue-culture-infectious-dose 50 (TCID50) assay. Briefly, 3×10^4 CR pIX PRO suppressor cells per well were seeded in 96-well plates. Virus-containing material was serially diluted 1:10 in 8 technical replicates and added to the cells. 72 h post-infection the cells were screened for CPE by optical inspection under the microscope. TCID50 was calculated with the Spearman-Karber formula (388).

5.4.3.5 Antibodies

The following antibodies were used in this study: monoclonal mouse anti-myc antibody (9B11, 1:1000 in western blot, 1:500 in flow cytometry, Cell Signaling Technologies, Danvers, USA), polyclonal rabbit anti-vaccinia (1-VA003-07, 1:5000 in western blot, 1:1000 in flow cytometry and immunostaining, Quartett, Berlin, Germany), monoclonal mouse anti-tubulin (DM1α, 1:1000 in western blot, Santa Cruz Biotechnologies, Heidelberg, Germany), polyclonal goat anti-mouse-HRP (115-036-003, 1:5000, Jackson, West Grove, USA), polyclonal goat anti-rabbit-HRP (P0448, 1:2000 in western blot and immunostaining, Dako, Santa Clara, USA), polyclonal goat anti-mouse-PE (550589, 1:200 in flow cytometry, BD, Franklin Lakes, USA), goat anti-rabbit Alexa Fluor 647 (A21244, 1:200 in flow cytometry, Life Technologies, Eugene, USA).

5.4.3.6 Western blot

Western blot analysis was performed as previously described (258). Briefly, cells of interest were lysed in TDLB buffer (50 mM Tris, pH 8.0, 150 mM NaCl, 0.1% SDS, 1% Nonidet P-40 and 0.5% sodium deoxycholate) supplemented with protease inhibitors (Complete Mini, Roche, Basel, Switzerland). Total protein concentration of the supernatants was measured by the Bradford method (Protein Assay, BioRad, Feldkirchen, Germany). The proteins were separated on 10% SDS-PAGE under reducing conditions and blotted on a nitrocellulose membrane for western blot analysis. Targets were probed with primary and secondary antibodies as listed above. HRP-labeled secondary antibodies and enhanced chemiluminescence substrate or Femto ECL (Thermo Fisher, Waltham, USA) were used for detection in a Chemilux Pro device (Intas, Göttingen, Germany).

5.4.3.7 Flow cytometry

Intracellular staining of antigens was performed by using standard methods (258). Cells were fixed and permeabilized with cytofix/cytoperm-Buffer (4% PFA, 1% saponine, in PBS). All washing steps were done with perm/wash-buffer (PBS containing 0.1% saponine). All antibodies were diluted in perm/wash-buffer and incubated for 30 min each. Flow cytometry was performed by using an Attune NxT device (Thermo Fisher, Waltham, USA) with 488 nm and 638 nm excitation and 574/26 nm and 670/14 nm emission filters. Cells were gated on stained, uninfected, and stained mock-MVA-infected cells. Evaluation of data was performed by using Attune NxT software.

5.4.3.8 Quantification of transgene expression

$3x10^4$ CR pIX and CR pIX PRO cells were seeded and infected with the indicated MVA strain at an MOI of 1. After 6 and 24 hpi, cells were harvested into PBS. Total RNA was prepared with RNeasy Mini kit (Cat. 74106, Qiagen, Hilden, Germany) according to manufacturer's instructions. Impurities from genomic DNA were digested with Turbo DNA-*free* kit (Cat. AM1907, Thermo Fisher, Waltham, USA). Reverse transcription quantitative PCR (RT-qPCR) was performed with Luna Universal Probe One-Step RT-qPCR kit (E3006L, NEB, Ipswich, USA) according to manufacturer's instructions. 2 µl of total RNA extract were used on a StepOnePlus qPCR cycler (Thermo Fisher, Waltham, USA) with the following protocol: Initial reverse transcription at 55°C for 10 min, followed by initial denaturation at 95°C for 1 min, followed by 40 cycles of denaturation for 15 s at 95°C and annealing/extension for 30 s at 60°C.

Following primer and probes were used: To amplify the transgene, E2 forward primer GATACAGGCTGGGACAAAGTG and E2 reverse primer GATCACTGTTCTGCCGATATGC were used together with the E2 probe Fam-CCTGTACTATGTGCTGCACGGCCT-BHQ1. For normalization on virus infection MVA128L was amplified with MVA128L forward primer CGTTTTGCATCATACCTCCATCTT and the MVA128L reverse primer GCGGGTGCTGGAGTGCTT, together with the MVA128L probe Fam-AGGCATAAACGATTGCTGCTGTTCCTCTGT-BHQ1.

For relative quantification of the transgene expression, Ct values were normalized according the following equation (389), using the primer efficiency calculated by the StepOnePlus software:

$$fold\ reduction\ of\ transgene\ expression\ = \ {}^{1}\Big/\frac{eff_{E2}{}^{Ct_{CR\ pIX}-Ct_{CR\ pIX\ PRO}}}{eff_{MVA128L}{}^{Ct_{CR\ pIX}-Ct_{CR\ pIX\ PRO}}}$$

5.4.3.9 Immunostaining of plaques

Immunostaining was used to visualize plaques, as described previously (390). 3×10^5 CR pIX or CR pIX PRO cells per well were seeded in 24-well plates. Cells were infected with an MOI of 0.01 in 1 ml DMEM/F-12 without additives. 2 h post-infection, medium was exchanged to DMEM/F-12 with 5% FCS. 48 h post-infection, cells were fixed with ice-cold acetone/methanol solution (1:1, v/v) and blocked

with blocking buffer (PBS containing 3% BSA) overnight at 4°C. Cells were sequentially stained by using an anti-vaccinia antibody and anti-rabbit-HRP, both incubated for 1 h at RT with gentle agitation. All wash steps and antibody dilution steps were conducted in blocking buffer. Finally, plaques were stained with TrueBlue Peroxidase Substrate (5510-0030, Seracare, Milford, USA) until plaques were visible (usually 5-10 min); subsequently the reaction was stopped with water. Pictures were taken with an inverted microscope (BZ-9000, Keyence, Frankfurt, Germany)

5.4.3.10 Multistep growth curve

To analyze virus replication, a multi-step growth curve was conducted as described previously (273). 3×10^5 CR pIX and CR pIX PRO cells per well were seeded in 24-well plates. Cells were infected at an MOI of 0.05 in 200 µl DMEM/F-12 without additives. 45 min post-infection, cells were carefully washed once with PBS and incubated with a medium containing 5% FCS. Cells and supernatant were harvested at 0, 24, 48, and 72 h after adsorption, freeze-thawed thrice, sonicated for 1 min, and titrated as mentioned above.

5.4.3.11 Passaging of rMVA

For analysis of genetic stability of rMVA, the viruses were passaged on parental CR pIX and CR pIX PRO suppressor cells, similar to the protocol of Kremer and colleagues (390). 1.2×10^6 cells per well were seeded in a 6-well plate 24 h before infection. Cells were infected at an MOI of 0.05 in 1 ml DMEM/F-12 without additives. 2 h post-infection, medium was exchanged to DMEM/F-12 with 5% FCS. 48 h post-infection, cells and supernatant were harvested (=passage 1), freeze-thawed three times, and additionally sonicated three times for 1 min in a cup sonifier. New cells were again infected with 1 ml of a 1:1000 dilution of the virus material from the previous passage. This was repeated to a maximum number of 10 passages. All obtained virus material was stored at -80°C.

To obtain single plaques, cell monolayers were infected with different dilutions and covered with growth medium containing 0.8% low melting agarose. 72 h post-infection, plaques were picked in 300 µl DMEM/F-12, freeze-thawed three times, sonicated for 1 min, and amplified by infection of 3×10^5 cells per well in 24-well plates.

5.4.3.12 Genotyping of MVA

For genotyping of transgene insertion loci, PCR was utilized. Genomic DNA of either plaque-purified or bulk material of virus-infected cells or virus stocks was prepared with a Quick-DNA MiniPrep kit (D3025, Zymo, Freiburg, Germany) according to the manufacturer's instructions. PCR was conducted with Q5 High-fidelity DNA polymerase (M0491L, NEB, Ipswich, USA) according to standard protocols. Primers were taken from literature (292,390) and are listed in Table 1. Analysis was done by electrophoresis in 0.5%, 0.8% or 1.5% agarose TBE gels, depending on the amplicon size.

For Sanger sequencing analysis, PCR amplicons of bulk material were purified from agarose gel by using QIAquick Gel Extraction Kit (28706X4, QIAGEN, Hilden, Germany), ligated into pJET1.2/blunt (K1231, Thermo Fisher Scientific, Waltham, USA) and used for transformation of E. coli. Plasmids were isolated from single clones and sequenced.

Table 1: Primers for genotyping of MVA

Primer	Primer sequence	Expected size	T_M and elongation time
DelIII f x r	GATGAGTGTAGATGCTGTTATTTTG GCAGCTAAAAGAATAATGGAATTG	Wildtype: 446 bp With transgene: 5143 bp	61°C 3.5 min
TK f x r	CTCTCTAGCTACCACCGCAA CACTACGGTGGCACCATCTAA	Wildtype: 920 bp With transgene: 5094 bp	67°C 4.33 min
DelVI f x r	CGTCATCGATAACTGTAGTCTTG TACCCTTCGAATAAATAAAGACG	702 bp	60°C 0.5 min
DelIII wide III3-f x III2-r	GCCGGTATTGGCATACAGTTC GCAATTGTCAGTTAACACAAGTCC	Wildtype: 9471 bp With transgene: 14169 bp	65°C 11.5 min

5.4.3.13 Next-generation sequencing (NGS)

Exogenous cellular gDNA was depleted from virus-containing material as described previously (291). Briefly, virus stock or virus-containing material was precipitated by the addition of polyethylene glycol to a final concentration of 8% (w/w), incubated for 30 min on ice, and subsequently centrifuged at 6600 g for 1 h. The translucent pellet was dissolved in PBS and exogenous gDNA was digested with 8 units of TurboDNAse for 1 h, followed by adding 20 mM EDTA and heat-inactivation at 80°C for 10 min. Viral gDNA was prepared with a Quick-DNA MiniPrep kit (D3025, Zymo, Freiburg, Germany) according to the manufacturer's instructions. 10 µl of each gDNA were barcoded for NGS with the Nextera XT DNA library Prep kit (FC-131-1096, Illumina, San Diego, USA) according to the manufacturer's instructions. NGS was performed with the NextSeq500 system by using a NextSeq500/550 High Output Kit v2.5 with 300 cycles (20024905, Illumina, San Diego, USA). FastQ files were evaluated with CLC Genomics Workbench 22 (Qiagen, Hilden, Germany). Obtained sequences were assembled by using derivatives of the MVA-CR19 genome sequence (GenBank accession number KY633487.1) with Ii-E1E2E6E7 transgene integrated into DelIII or TK locus. Normalized transgene coverage was calculated with the formula:

$$\% = \frac{\frac{read\ coverage\ transgene\ of\ passage\ x}{read\ coverage\ of\ MVA056L\ of\ passage\ x}}{\frac{read\ coverage\ transgene\ of\ seed\ stock}{read\ coverage\ of\ MVA056L\ of\ seed\ stock}}$$

5.4.4 Results

5.4.4.1 Tet repressor- and shRNA-mediated knock-down of MVA transgene expression

We have demonstrated previously that a fusion protein comprising the early antigens E1, E2, E6 and E7 of *Macaca fascicularis* papillomavirus type 3 (MfPV3) are well suited to induce potent T cell responses in outbred CD1 and OF1 mice when delivered via DNA or adenoviral vectors (356). Repeated attempts to generate a recombinant MVA (rMVA-CR19) expressing the corresponding Ii-E1E2E6E7 fusion protein for booster immunization purposes was hampered by the stepwise loss of transgene positive plaques alongside the plaque selection process. This led us to hypothesize that expression of the transgene Ii-E1E2E6E7 imposed a disadvantage on rMVA propagation.

Hence, we herein aimed to develop a system to suppress transgene expression during the generation, selection and amplification of the rMVA. For this purpose, we first modified the AGEI.CR pIX cell line (CR pIX) by means of lentiviral transduction to constitutively express the tetracycline repressor (TetR) together with a rat perilipin-2 (Plin2) shRNA yielding AGEI.CR pIX PRO (CR pIX PRO). Complementary, two tetracycline operator sequences (tetO) and a Plin2 shRNA target sequence (P2TS) were integrated into the 5' and the 3' UTR of the transgene expression module of the transfer plasmid used to generate rMVA via *in vitro* recombination (IVR). According to these design features, residual mRNAs possibly resulting from incomplete TetR/tetO-mediated transcription repression will be degraded via binding of Plin2 shRNA to the 3' PT2S on the transcript, collectively resulting in a sustained knock-down of toxic transgene expression. The CR pIX PRO suppressor cell line used in conjunction with the tetO/Plin2 transfer plasmids for IVR, rMVA plaque selection and subsequent rMVA amplification is in the following referred to as ProVector system (Figure 20A).

Performing the IVR with the transfer plasmids encoding the presumably toxic MfPV3 Ii-E1E2E6E7 fusion protein, now flanked by the tetO/P2TS control elements, in the CR pIX PRO suppressor cells and applying the ProVector system for subsequent rMVA selection, we eventually succeeded to generate two rMVA: MVA-CR19-TK (short CR19 M-TK) and MVA-CR19-DelIII (CR19 M-DelIII) with the MfPV3 Ii-E1E2E6E7 transgene sequence integrated either into the thymidine kinase (TK) locus or, alternatively, in the deletion III (DelIII) locus, respectively (Supplementary Figure 14). Virus stocks for the subsequent experiments were produced starting from single plaques via 3 rounds of expansion on CR pIX PRO suppressor cells.

Specific knock-down of Ii-E1E2E6E7 expression by CR pIX PRO suppressor cells was initially proven via western blot analysis and quantified by flow cytometry using a C-terminally fused myc-tag for expression monitoring of the fusion protein (Figure 20B and C). Expression of Ii-E1E2E6E7 was clearly reduced in CR pIX PRO suppressor cells as compared to parental CR pIX cells, when infected with CR19 M-TK and CR19 M-DelIII, respectively, suggesting successful suppression of transgene expression (Figure 20B). GFP expression was comparable in parental CR pIX cells and CR pIX PRO suppressor cells following infection with rMVA-GFP lacking tetO and P2TS, respectively. This demonstrates that the presence of the TetR and Plin2 shRNAs do not impact transgene expression per se. Flow cytometry analysis confirmed approximately 4.3-fold and 6-fold suppression of Ii-E1E2E6E7 expression in CR pIX PRO suppressor cells compared with the parental CR pIX cells 48 hpi with CR19 M-TK and CR19 M-DelIII (Figure 20C, Supplementary Figure 15). Ii-E1E2E6E7 mRNA levels were determined by RT-qPCR and shown to be reduced in CR pIX PRO suppressor cells by a factor of 5.8 (CR19 M-DelIII) or 1.98 (CR19 M-TK) at 6 hpi, respectively, and by a factor of 11.43 (CR19 M-DelIII) or 2.96 (CR19 M-TK) after 24 h (Supplementary Figure 16). The observed reduction of Ii-E1E2E6E7 transcripts level in the CR pIX PRO suppressor cells might be underestimated, and mainly capture the impact of TetR-mediated suppression of transcription, as exact quantification of siRNA-mediated mRNA degradation is hard to achieve by means of RT-qPCR (391).

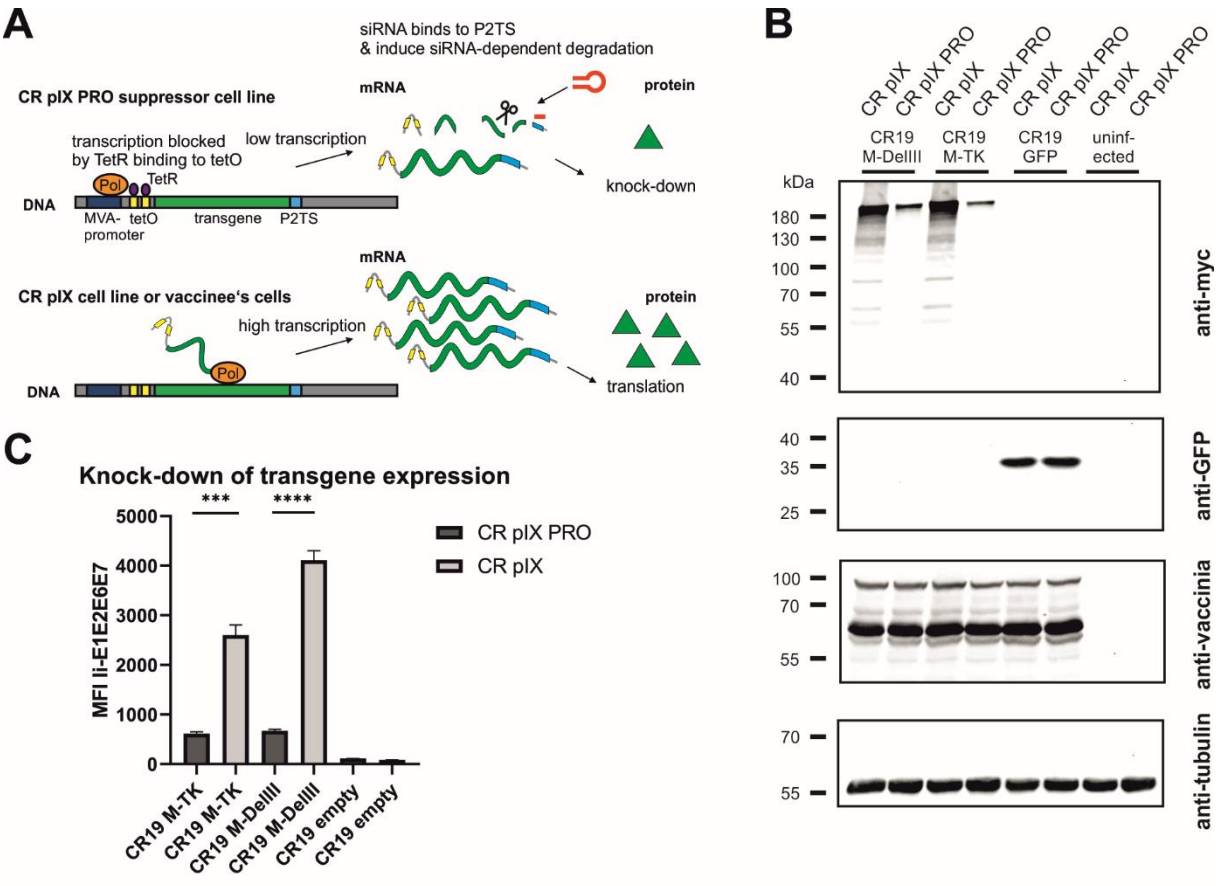

Figure 20: Transgene expression of CR19 M-TK and CR19 M-DelIII on parental CR pIX and CR pIX PRO suppressor cell line.
(A) Schematic overview of TetR/tetO and Plin2 shRNA/P2TS mediated transgene suppression. Colors and shapes resemble the following: orange: MVA RNA polymerase; dark blue: MVA promoter; yellow: tetO; violet: TetR; light blue: P2TS; green: transgene DNA/mRNA; red hairpin: Plin2 shRNA; green triangle: transgene product (B) Western blot analysis of CR pIX PRO suppressor cells and CR pIX cells infected with rMVA coding for MfPV3 Ii-E1E2E6E7 (integrated into DelIII or TK locus) controlled by tetO and P2TS, or infected with rMVA coding for GFP lacking tetO and PT2S. Cells were infected at an MOI of 0.5 and harvested 48 hours post infection (hpi). Antibodies used are indicated on the right. (C) Expression analysis of CR pIX PRO and CR pIX cells infected with rMVA coding for MfPV3 Ii-E1E2E6E7 controlled by tetO and P2TS. Cells were infected at an MOI of 0.1 and harvested 48 hpi. Cells were stained with rabbit anti-vaccinia and goat anti-rabbit AF647 for MVA infection and mouse anti-myc and goat anti-mouse PE for transgene expression. Cells were gated on vaccinia-positive cells using the fluorescence background of cells infected with MVA without any antigen. MFI of PE out of AF647 positive cells is represented as mean with SEM, Statistical analysis was done with an unpaired t-test. **: p<0.005; ***: p< 0.0005; ****: p<0.00005; n=3 biological replicates.

5.4.4.2 rMVA expressing MfPV3 Ii-E1E2E6E7 has a replication disadvantage on parental CR pIX cells which can be rescued on CR pIX PRO suppressor cells

Following successful generation of an rMVA-MfPV3-Ii-E1E2E6E7 virus stock on CR pIX PRO suppressor cells, we set out to test the hypothesis that (i) expression of certain potentially harmful transgenes can have a detrimental impact on virus replication and that (ii) replicative capacity can be restored in such cases by restricting expression of such transgenes. For this purpose, replication kinetics of CR19 M-DelIII and, for comparison, CR19 GFP, and CR19 empty were measured under restricting and non-restricting conditions. CR pIX PRO suppressor cells and non-modified parental CR pIX cells were infected with the respective rMVA at an MOI of 0.05, and a multistep growth curve was generated by harvesting infected cells together with cell supernatant after 0, 24, 48, and 72 hpi. Titration on CR pIX

PRO suppressor cells showed that the titer of CR19 M-DelIII was significantly reduced by a factor of approximately 10 when propagated on CR pIX cells compared with CR pIX PRO suppressor cells at all time points (Figure 21A). As a reference, virus titer of CR19 M-DelIII on CR pIX PRO cells was equal to the titers of both control viruses CR19 empty and CR19 GFP that in turn displayed no differences on both cell lines. Consistent results were obtained when comparing the plaque size of the rMVA at 48 hpi (MOI of 0.01) (Figure 21B). Immunostaining with a vaccinia-specific antibody revealed comparable plaques sizes formed by CR19 empty, CR19 GFP, and CR19 M-DelIII on CR pIX PRO suppressor cells. In contrast, smaller sized plaques with less intense staining were notified following infection of the parental CR pIX cells CR19 M-DelIII expressing the Ii-E1E2E6E7 transgene, but not for CR19 GFP and CR19 empty.

Taken together, this suggests that unrestricted expression of the MfPV3 Ii-E1E2E6E7 antigen results in a replication disadvantage for CR19 M-DelIII and, consequently, reduced virus titers and mitigated virus spread. This replication deficit can be restored when Ii-E1E2E6E7 expression is knocked-down in CR pIX PRO suppressor cells.

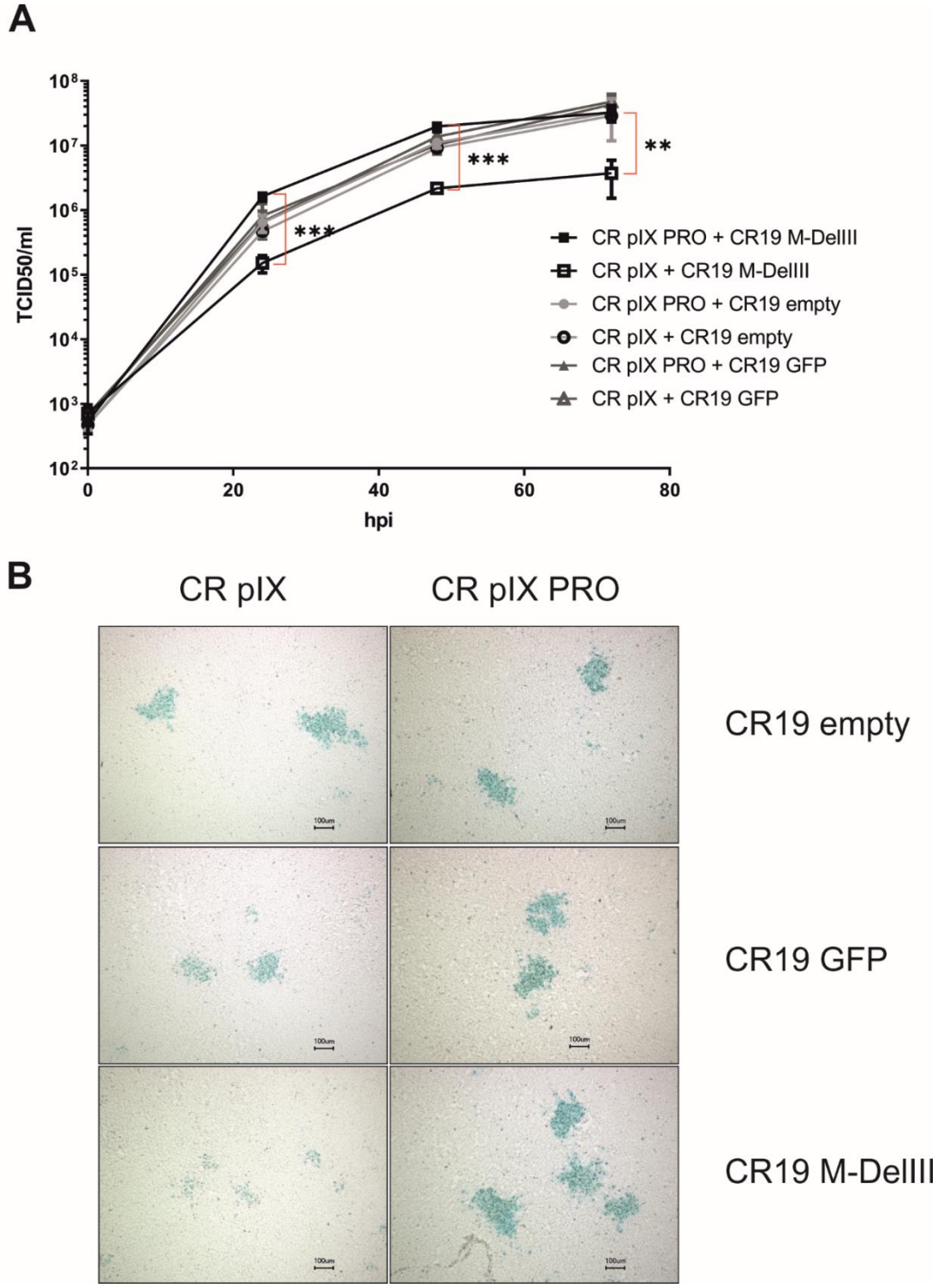

Figure 21: Replication kinetics and plaque morphology of CR19 empty, CR19 GFP and CR19 M-DelIII on parental CR pIX and CR pIX PRO suppressor cell line.
(A) Multiple growth step curves for the indicated CR19 variants on CR pIX and CR pIX PRO cells. Cells were infected at an MOI of 0.05 Samples taken at 0, 24, 48, and 72 hpi were titrated on CR pIX PRO suppressor cells using the $TCID_{50}$ method. Statistical analysis was done with an unpaired t-test. Data points represent mean with SEM, **: p< 0.005; ***: p<0.0005 n=3 independent biological replicates. (B) CR pIX and CR pIX PRO suppressor cells were infected at an MOI of 0.01 with the indicated rMVA-CR19. 48 hpi, cells were fixed and stained with an anti-vaccinia antibody, an HRP-coupled secondary antibody and KPL Trublue substrate. Photos were taken on a Keyence inverted microscope at a magnification of 10. Bar represents 100 µm. Shown plaques are representative for the respective conditions.

5.4.4.3 Replication of CR19 M-DelIII, but not of CR19 M-TK, is restored upon passaging on parental CR pIX cells

Provided the MfPV3-Ii-E1E2E67 transgene has negative impact on the MVA replicative capacity under non-restricting conditions, the transgene might also have an influence on the genetic stability of the rMVA by imposing a strong negative selection on such transgene-expressing rMVA. To test this, we first generated a CR19 M-DelIII and CR19 M-TK seed virus stock (defined as passage 0) by expanding the originally selected, positive plaques (i.e. passage -3) in three consecutive amplification steps on CR pIX PRO suppressor cells, respectively. Such seed virus stocks were then serially passaged side-by-side on the parental CR pIX cells and on CR pIX PRO suppressor cells for 10 passages as described by Kremer *et al.* (390). Harvested virus samples were subsequently titrated under restricting conditions on CR pIX PRO suppressor cells (Supplementary Figure 17).

Titration of CR19 M-DelIII virus samples harvested after each passage on CR pIX PRO suppressor cells yielded similar titers across all passages with a trend towards marginally higher titers in later passages, which did, however, not reach statistical significance (Figure 22A). Starting from the same seed virus stock (passage 0), CR19 M-DelIII lost already after 1 passage on the parental CR pIX cells one order of magnitude in virus titer as compared to the same virus passaged on CR pIX PRO suppressor cells (Figure 21A). This observation was in line with previous findings suggesting a replication disadvantage of CR19 M-DelIII under non-restricting conditions in the parental CR pIX cells (Figure 21). Beginning with passage 3, the titers of CR pIX-passaged CR19 M-DelIII increased and reached the same level as CR-pIX-PRO-passaged CR19 M-DelIII from passage 5 onwards.

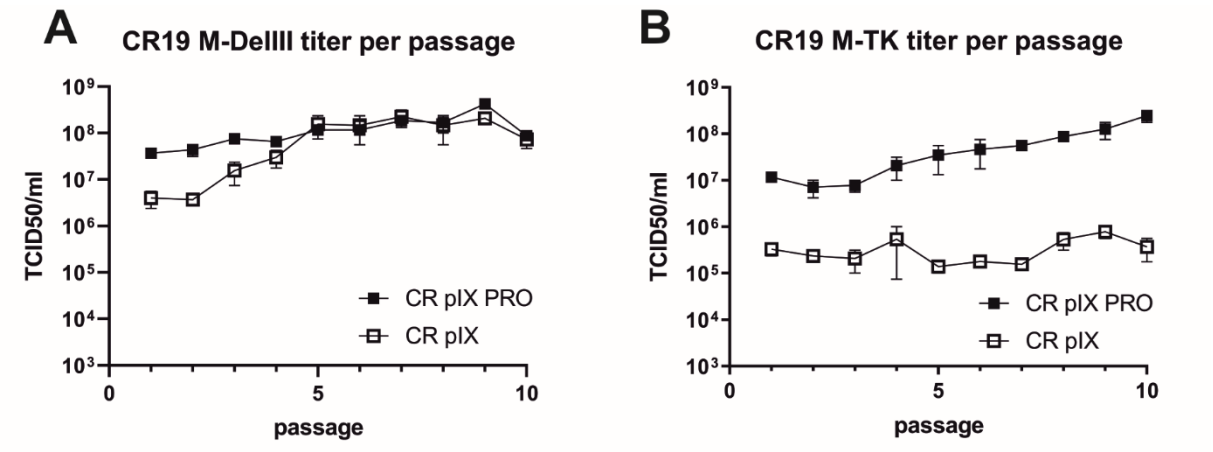

Figure 22: Growth kinetic (titer per passage) of CR19 M-DelIII (A) and CR19 M-TK (B) passaged on either parental CR pIX or CR pIX PRO suppressor cells.
Samples of each passage were titrated on CR pIX PRO suppressor cells by using the $TCID_{50}$ method. TCID50s for each passage are indicated. Data points represent the mean with SEM, n=2 independent biological replicates.

A different effect was observed when CR19 M-TK was passaged on the two cell lines: Whilst CR19 M-TK, similar to CR19 M-DelIII, experienced a significant loss in titer after a single passage on the parental CR pIX cells, the titers of CR19 M-TK did - unlike notified for CR19 M-DelIII - not increase while being passaged on the parental CR pIX cells and consistently remained approximately 100-fold below the levels obtained for CR19 M-TK passaged on CR pIX PRO suppressor cells (Figure 22B). In general, CR19 M-TK exhibited slightly lower virus titers as compared with CR19 M-DelIII across all passages on both cell lines.

5.4.4.4 Passaging on CR pIX cells leads to rapid loss of Ii-E1E2E6E7 expression

We next quantified Ii-E1E2E6E7 transgene expression under non-restricting conditions in parental CR pIX cells of CR19 M-DelIII samples harvested after each passage on either CR pIX or CR pIX PRO suppressor cells, respectively, in a high-throughput flow-cytometry-based assay. Infected CR pIX cells were co-stained to monitor intracellular expression of Ii-E1E2E6E7 (via its myc-tag) and vaccinia proteins (polyclonal anti-vaccinia-antibody) 48 hpi (Figure 23). As controls, uninfected cells and CR19-empty-infected cells were used to gate for CR19-infected cells (vac$^+$), and CR19 M-DelIII to gate for Ii-E1E2E6E7 expression out of vac$^+$ cells (Supplementary Figure 18). A rapid reduction in the frequency of Ii-E1E2E6E7 expressing cells among the CR19 M-DelIII-infected cells was observed. This was already apparent with virus samples derived from passage 1 on CR pIX cells (Figure 23A). After only 3 passages on the parental CR pIX cells, expression of Ii-E1E2E6E7 was lost. In contrast, expression of Ii-E1E2E6E7 could be observed with CR19 M-DelIII passaged on CR pIX PRO suppressor cells throughout all 10 passages. However, even suppression of transgene expression in the ProVector system could not prevent a continuously decreasing fraction of Ii-E1E2E6E7 expressing cells amongst vaccinia virus positive cells with passages from 70% to only 10%. A rapid reduction in the frequency of Ii-E1E2E6E7$^+$ cells amongst vaccinia virus antigen positive cells was also observed for CR19 M-TK passaged on CR pIX cells (Figure 23B). Interestingly, no significant difference in the fraction of Ii-E1E2E6E7 expressing cells was observed with passage level of CR19 M-TK grown on CR pIX PRO suppressor cells.

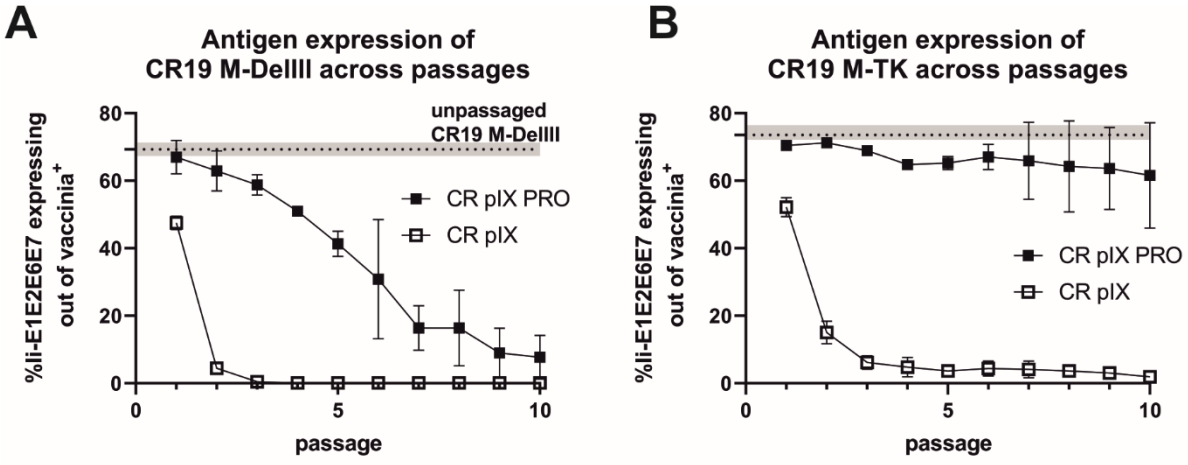

Figure 23: Expression analysis of CR19 M-DelIII (A) and CR19 M-TK (B) passaged on either parental CR pIX or CR pIX PRO suppressor cells by using flow cytometry.
CR pIX cells were infected at an MOI of 0.1 (CR19 M-DelIII) or MOI of 0.01 (CR19 M-TK) with virus samples obtained after each passage and were harvested 48 hpi. Cells were stained with rabbit anti-vaccinia and goat anti-rabbit AF647 for MVA infection and mouse anti-myc and goat anti-mouse PE for transgene expression. Cells were gated on vaccinia-positive cells using cells infected with MVA without any antigen. %gated Ii-E1E2E6E7 expressing cells out of vaccinia antigen positive cells represents myc-positive cells out of vaccinia-positive cells. Dashed line represents Ii-E1E2E6E7-expressing out of vac$^+$ cells of passage 0 of CR19 M-DelIII or CR19 M-TK used as starting material for passaging on both cell lines. Data points represent mean with SEM, n=2 independent biological replicates.

In conclusion, this experiment suggests a strong negative selection on rMVA expressing Ii-E1E2E6E7. Suppression of transgene expression by CR19 pIX PRO suppressor cells led to prolonged production of Ii-E1E2E6E7. Remarkably, the integration site had a major impact on the stability of transgene expression: Whereas expression of the DelIII-inserted transgene continuously declined upon passaging, even when the virus was passaged under restricting conditions, the TK-locus-inserted

transgene appeared to be maintained more stably, but was strictly dependent on passaging on CR19 pIX PRO suppressor cells.

5.4.4.5 Loss of Ii-E1E2E6E7 expression from the DelIII locus is mainly caused by transgene deletions (CR19-M-DelIII)

We next investigated whether the reduction of Ii-E1E2E6E7-expressing CR19-M-DelIII- and CR19-M-TK-infected cells is caused by alterations in the DNA sequence of the transgene expression cassette. PCR analyses on single plaques from selected passages were performed with primers that bind in the flanking regions of the DelIII and TK locus, respectively (390). In line with the transgene expression analysis above, the fraction of correctly sized PCR amplicons for CR19 M-DelIII quickly declined with the number of passages on CR pIX cells (Supplementary Table 2). Some plaques, which proved positive with vaccinia-specific primers, showed no specific DelIII amplicon, neither the full length, not a shortened PCR product. This may be explained by acquisition of mutations or deletions in the primer binding sites. In contrast, the expected PCR amplicon could be detected in almost all plaques of CR19 M-DelIII passaged on CR pIX PRO.

However, this analysis does not exclude short deletions, point mutations or insertions/deletions of few bases that might result in frame shifts or truncated products. Thus, next-generation sequencing (NGS) was employed as an unbiased method to deeply characterize the genetic integrity of the passaged rMVA. Predominantly viral DNA was isolated from CR-pIX- and CR-pIX-PRO-passaged CR19 M-DelIII and CR19 M-TK by depleting cellular gDNA, and subjected to Illumina NextSeq500 deep-sequencing. The resulting reads were aligned to the CR19 M-DelIII guiding sequence (Supplementary Table 3). The obtained coverage maps revealed a wide deletion at the DelIII locus when CR19 M-DelIII had been passaged on parental CR pIX cells (Supplementary Figure 19A). To quantify the fraction of the DelIII locus deletion along the passages, the mean read coverage of the transgene Ii-E1E2E6E7 was normalized to the mean read coverage of the essential MVA-DNA polymerase gene locus (MVA056L) (Figure 24A, Supplementary Table 3). The normalized Ii-E1E2E6E7 mean read coverage of CR19 M-DelIII rapidly dropped to almost 0% within three passages on CR pIX cells, whereas normalized mean read coverage of Ii-E1E2E6E7 of CR–pIX-PRO-passaged CR19 M-DelIII was overall high with a trend towards some decline at later passages.

Aligning the NGS reads of CR pIX-passaged CR19 M-DelIII with the expected CR19 M-DelIII genome sequence also showed a reduction in read coverage upstream of the transgene (Supplementary Figure 19A) spanning from MVA157L to MVA164R, and also a complete absence of MVA165R and parts of MVA166R, both downstream of the transgene. Thus, this comprises not only the deletion of the transgene but also large sequence parts flanking the DelIII locus and extending beyond the flanking sites used for homologous recombination during generation of the recombinant virus (Figure 24B).

CR-pIX-PRO-passaged CR19 M-DelIII exhibited a slight reduction in read coverage in passages 5-10. Detailed analysis revealed reduced read coverage spanning from the middle of the E2 gene within the transgene until MVA165R (nucleotide position 161317 to 165771, Supplementary Figure 19B and C), indicative for a truncation of the transgene. This may explain the continuously decreasing fraction of Ii-E1E2E6E7 expressing cells amongst vaccinia virus positive cells from 70% (passage 1) to only 10% (passage 10).

To confirm the deletions found by NGS, a PCR analysis with a primer pair spanning from MVA155R to MVA167R was done with the same DNA preparation used for NGS (Figure 24C and D). This PCR analysis confirmed fast deletion of the transgene from the DelIII locus when passaged on parental CR pIX cells (Figure 24D), resulting in bands of a lower molecular weight than the expected full-length PCR

amplicon of 14169 bp (CR19 M-DelIII; black arrow, Figure 24D). Moreover, frequent detection of bands of a lower molecular weight than the expected empty DelIII integration site were observed (< 9471 bp, white arrow). These bands resemble deletions not only of the transgene itself but also of neighboring genes upstream and downstream of the DelIII locus. This PCR analysis was repeated for an independent replicate of the passaging experiment (without depletion of cellular gDNA) with similar results (Supplementary Figure 20).

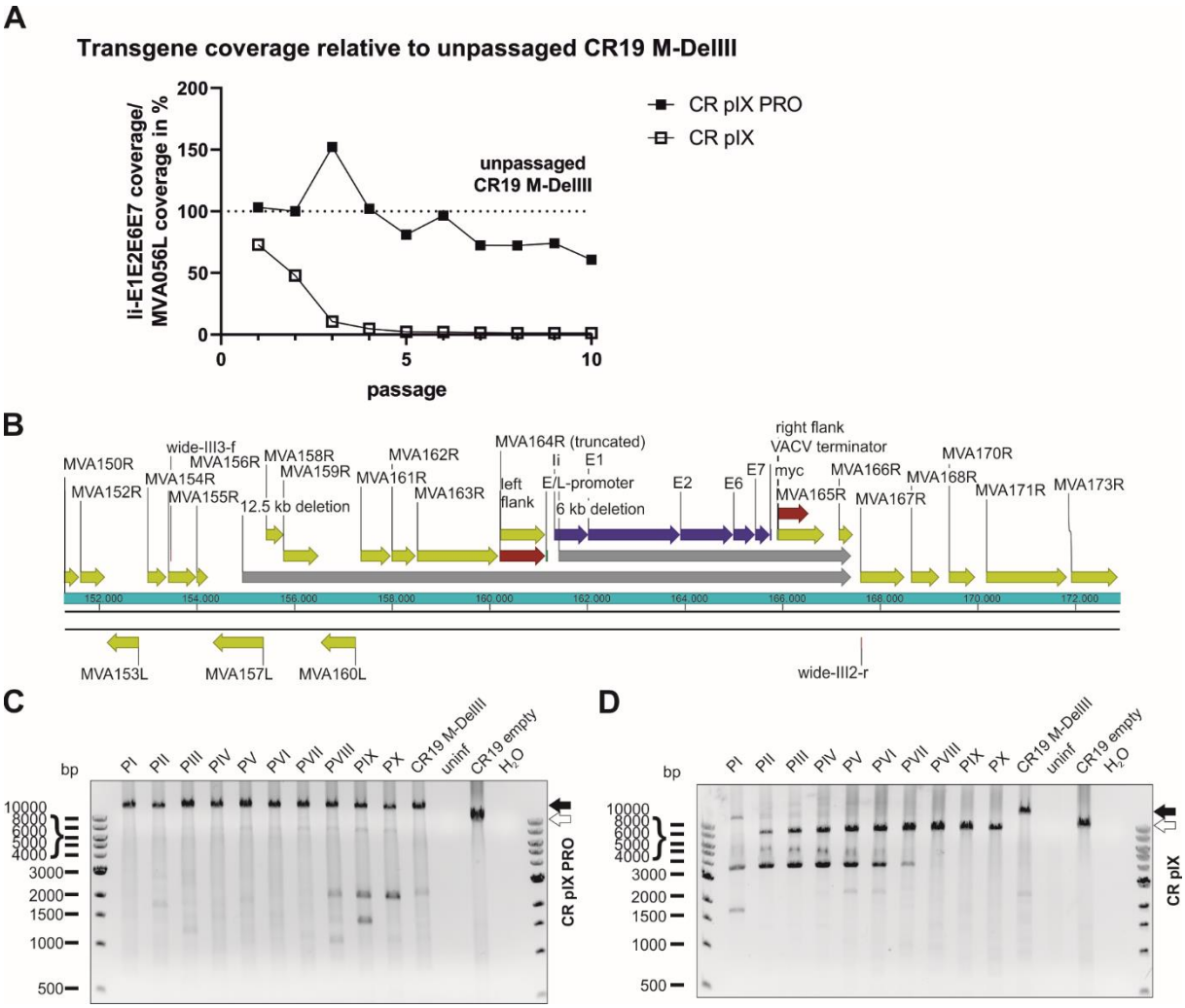

Figure 24: Deletions in the context of the DelIII integration locus across passaging.
(A) Depicted is the quotient of the mean read coverage of the entire li-E1E2E6E7 transgene integrated into DelIII and the mean read coverage of the essential MVA056L gene (MVA DNA polymerase, E9L) of CR19 M-DelIII passaged on parental CR pIX cells or CR pIX PRO suppressor cells, normalized to the unpassaged rMVA. Dashed line represents normalized read coverage of unpassaged rMVA used as starting material for passaging on both cell lines. (B) Schematic overview of DelIII integration locus. Yellow marks MVA genes; red marks homologous sequence flanks used for integration into DelIII locus; blue marks the transgene; grey marks potential deletions postulated by NGS. Genotyping of rMVA passaged on CR pIX PRO suppressor cells (C) and parental CR pIX cells (D) cells by agarose gel analysis of PCR products obtained with the primer pair wide-III3-f and wide-III2-r. Expected size of CR19 M-DelIII: 14169 bp (black arrow); expected size of CR19 empty: 9471 bp (white arrow).

5.4.4.6 Early translational stop as a result of mutations impair transgene expression from the TK locus under non-restricting conditions (CR19 M-TK)

In contrast to CR19 M-DelIII passaged on CR pIX, CR19 M-TK bands resembling shortened PCR products as a result of deletions represented only a minor fraction in the PCR analysis (Figure 25A and B,

Supplementary Table 2). This PCR analysis was repeated for an independent replicate of the passaging experiment and the results were similar (Supplementary Figure 21). This was also confirmed by the deep-sequencing analysis of the passaged CR19 M-TK that revealed no difference in normalized transgene coverage between the two cell lines (not shown). However, instead of deletions, specific mutations within the transgene could be observed (Figure 25C and D). Passaging of CR19 M-TK on parental CR pIX cells led to the early accumulation of a virus variant harboring a specific guanine to thymidine exchange resulting in the transition of E265 (GAG) to an early stop codon (TAG; referred to as E265*). The fraction of the E265* rMVA mutant among all rMVA peaked at passage 5, but then declined again until passage 9. Furthermore, during passaging on CR pIX, a variant carrying an insertion of guanine after nucleotide position 893 emerged. This insertion results in a frameshift beginning at L299 leading to an early translational stop at position 342 and thus to a truncated protein, referred to as L299Tfs*342. L299Tfs*342 could already be detected in about 5% of the recovered reads of passage 1 on CR pIX cells and accumulated until all recovered reads in passage 9 exhibited this mutation. Both mutations found by deep-sequencing could be verified by Sanger sequencing of pJET1.2/blunt-subcloned PCR amplicons of passage 3 and 10 (Supplementary Figure 22). L299Tfs*342 could also be observed among CR19 M-TK passaged on CR pIX PRO cells, albeit only in a very small fraction of the recovered reads. The frequency of this mutant increased only gradually so that at passage 10 the fraction of reads without the L299Tfs*342 was still approximately 90%.

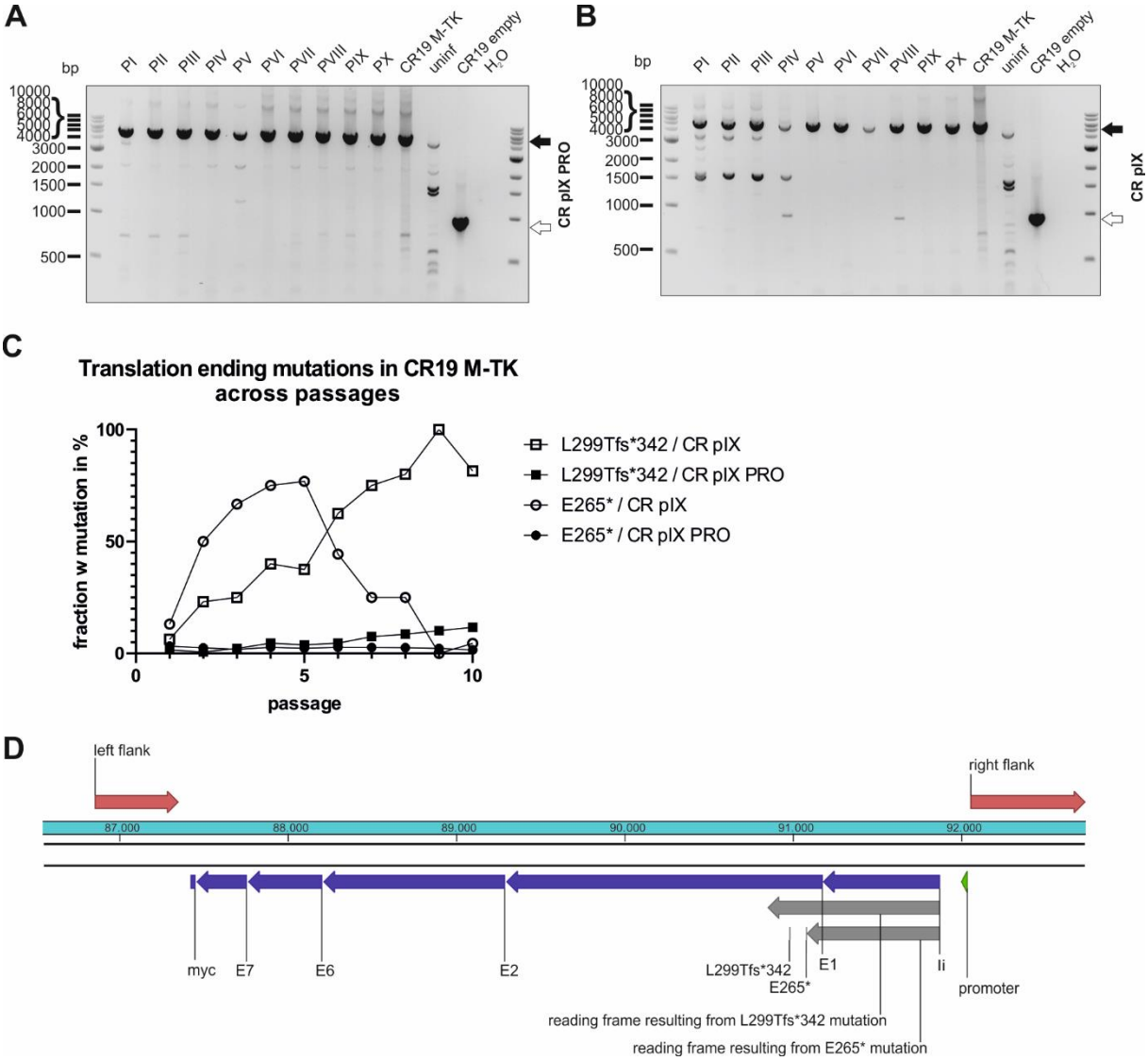

Figure 25: Mutations leading to truncated proteins in the context of TK integration locus across passages. Genotyping of rMVA generated by passaging on CR pIX PRO suppressor (A) and parental CR pIX (B) cells by using PCR and primer pair TK f and TK r. Expected size of CR19 M-TK of 5094 bp (black arrow) and expected size of CR19 empty of 920 bp (white arrow). (C) The fraction of rMVA mutants among CR19 M-TK carrying the early translational stop mutations L299Tfs*342 or E265* across the passages on either CR pIX or CR pIX PRO cells is plotted against the passage number. (D) Schematic overview of the transgene in the TK locus. Red marks homologous sequences used for integration into TK locus; blue marks the transgene's subunits; grey marks reading frames resulting from mutations that lead to early translational stops.

5.4.5 Discussion

Several recombinant viral vectors have been licensed as vaccines since 2010, among them, in 2020, the recombinant MVA-based Ebolavirus vaccine Mvabea carrying filovirus antigens (392). These recent advancements underscore the potential of viral vector vaccines. Conventionally recombinant MVA are generated by means of homologous recombination between the poxviral genome and a shuttle vector (281). However, depending on the design of the antigen expression cassette, generation may be difficult or even unsuccessful, as we have experienced for an artificial papillomavirus antigen, MfPV3 Ii-E1E2E6E7. Others have reported similar observations (306–308,383,384,393,394) but only few comparative studies were conducted to analyze this systematically (306–308). Even in cases when generation of recombinant MVA is successful, their propagation and the generation of bulk material

for larger preclinical studies or GMP-grade drug substance or drug product for clinical trials may suffer from transgene instability leading to the emergence of mutated recombinant MVA (mrMVA) with reduced or abrogated antigen expression or modification of the transgene product.

To address this limitation we have implemented a system that conditionally represses MVA-driven transgene expression in an engineered production cell line (CR pIX PRO) and thus supports the generation and expansion of rMVA encoding otherwise difficult to express transgene products. Remarkably, the tetracycline repressor (TetR) in combination with a functional shRNA, both provided from the engineered CR pIX PRO suppressor cell line, was capable to clearly reduce the MVA-mediated transgene expression. In the specific case of the MfPV3-derived Ii-E1E2E6E7 antigen this system eventually enabled the generation of the rMVA, that had failed using unmodified CR pIX cells in earlier attempts.

When e.g. CR19 M-DelII was propagated in non-restricting CR pIX cells, it replicated to lower titers, plaques were phenotypically smaller, and more than 90% of the virus had lost antigen expression within three passages. Detailed sequence analysis showed that concomitantly with the loss of antigen expression, mrMVA variants emerged that quickly outcompeted the original rMVA within only few passages. One explanation is that expression of the foreign antigen may be harmful to the host cell. Impaired replication leads to fewer progeny of rMVA expressing the desired antigen compared to mrMVA. Antigen expression thus exerts a negative selection pressure leading to reduced viral fitness in a classical Darwinian "survival of the fittest" competition.

The loss of rMVA within few rounds of passaging for two different rMVA (TK- and DelIII-integration) carrying the same transgene confirms the general conclusion of negative selection within the virus population. Side-by-side comparison of viruses led to the interesting observation that the mode of antigen suppression can follow different pathways. In the case of DelIII integration site, the transgene is removed by deletions that range from partial transgene deletion to complete deletion even extending into flanking non-essential viral genes, similar to results reported by Wyatt *et al.* (306). In contrast, in the case of TK insertion, no deletions but rather mutations within the transgene occurred. Here, we observed either a premature stop codon or insertion of a single base causing a frameshift leading to a stop codon in the shifted frame. As a result, a considerably shortened protein variant was expressed that presumably is less toxic to the infected cell. It is plausible that the presence of an essential viral gene next to the TK locus, i.e. MVA085R (Copenhagen J1R) (395), hinders the emergence of viable deletions mutants, thus leading to a genetically more stable region within the genome (396). Interestingly, this leads to the emergence of variants avoiding transgene expression by subtle point mutations, leading to truncated Ii-E1E2E6E7 antigen variants, which seems not to mitigate the fitness loss to the degree achieved by full deletion.

The observed replication capacity of the CR19 M-DelIII-virus population reached wild-type levels once the population was dominated by mrMVA, but this was not the case for the CR19 M-TK-virus population. In line with this, the initially prevalent CR19 M-TK mutant virus, E265*, was subsequently replaced by the L299Tfs*342 variant that (by inference) seems to have a fitness advantage over E265*. The slightly quicker appearance of mrMVA in the case of DelIII-integrations suggests that poxviruses tend to preferably acquire deletions over specific mutations, though this remains speculative given the low number of studied examples. Nevertheless, these observations argue for rather selecting the TK locus over DelIII as more stable integration site when generating rMVA or even more stable integration sites e.g. IGR3 or between I8R and G1L (306,397).

The TetR/tetO system has been described earlier to conditionally regulate transgene expression in adenoviral vectors (398), and was shown to enhance the genetic stability (399). The concerted action of a production cell line expressing the TetR/Plin2 shRNA (CR pIX PRO suppressor cells) and the transgene expression cassette flanked by a 5' tetO and a 3' shRNA target sequence (P2TS) not only augmented generation of the rMVA, but also led to a considerable increase in stability upon propagation and expansion of the virus.

In the repressing CR pIX PRO suppressor cell line, higher virus titers, larger plaques, and prolonged retention of the transgene upon passaging were observed. However, suppression was not complete and mrMVA also arose during the passaging experiment, though with a certain delay and, if at all, at much lower frequencies, especially for CR19 M-TK. More than 90% correct virus even after 10 passages constitutes a promising potency for use of such an rMVA as a vaccine, depending on the number of passages that are required in a large-scale manufacturing process.

Another strategy to reduce the expression of harmful transgenes in the producer cells would be choosing a weaker promoter. For instance, by using p7.5 instead of the strong promoters mH5 or SSP helped to stabilize the measles virus fusion protein as transgene (383). However, this strategy also leads to reduced expression of the antigen upon vaccination (400). Importantly, as the suppressed transgene expression system used in this work is artificially engineered into the virus producer cell line, antigen expression will not be suppressed in the vaccinees' cells upon administration of the rMVA.

There are also some limitations to our study. First, in concordance with Kremer *et al.* (390), we have not used a defined MOI for each passage of the passaging experiment which might have biased our results to an even accelerated negative selection of the rMVA. Furthermore, our results regarding M-DelIII stability in a CR19 background may not be completely translatable to conventional MVA since CR19 underwent a recombination that duplicated the genes MVA167 to the right ITR (291,292). This might influence the proximal DelIII locus and also explain the appearance of large deletions in the context of the DelIII locus that have not been reported previously (306–308). On the other hand, it was shown that CR19 containing GFP and mCherry as a dual expression cassette in the DelIII locus is stable for at least 20 passages (292). Others used a genetically engineered and restructured DelIII site for integration of their inserts by removing non-essential MVA164R, 165R and 166R. In that case the transgene is integrated between the MVA163R (A50R) and MVA167R (B1R) to enhance the stability of the modified DelIII integration site in MVA (401). The obviously non-essential character of MVA165R and MVA166R flanking our demanding transgene in MVA-CR19 may favor larger deletions in DelIII and concomitant loss of transgene expression.

In summary, by suppressing the transgene expression we could obtain sustained transgene maintenance of an otherwise instable antigen, MfPV3 Ii-E1E2E6E7, for a considerable number of passages. The system was further improved by integration of the transgene into the more stable TK locus. This confirms that knock-down of transgene expression during MVA expansion can enhance virus yield, genetic stability, and transgene expression levels.

These data emphasize the importance of rigorous quality controls regarding correctness of the expression cassette's sequence and protein production levels during all steps of rMVA generation and production. This should comprise characterization of bulk virus batches but also methods that allow detection of minority mrMVA populations, such as analysis of sufficient numbers of plaques or deep-sequencing of the MVA population. As demonstrated herein, depending on the transgene, mutations may occur quickly and vary in nature depending to the transgene integration site. The novel MVA-

adapted transgene expression suppression system can be employed to rescue the generation of otherwise hard-to-generate rMVA.

5.4.6 Supplement

5.4.6.1 Supplementary Figures

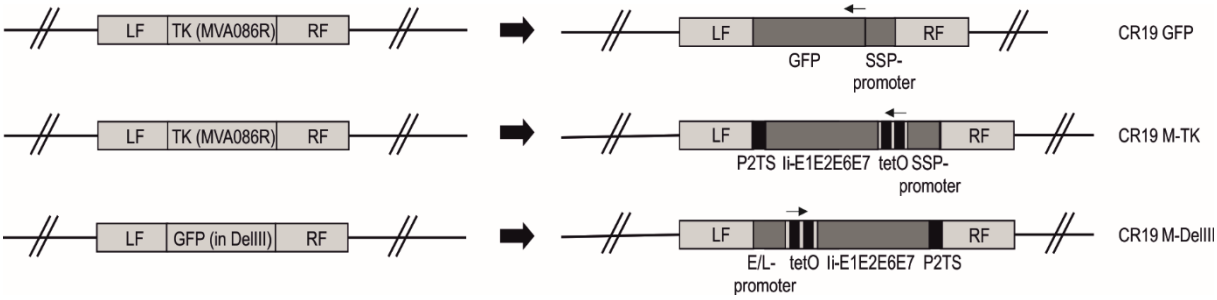

Supplementary Figure 14.
Generation of rMVA. Schematic representation of the generated rMVA. Abbreviations: RF: right flank, LF: left flank, TK: thymidine kinase locus (MVA086R), GFP: green fluorescent protein, SSP-promoter: short synthetic promoter, tetO: tetracyclin operator, P2TS: Plin2 target sequence, DelIII: Deletion site III. Arrow indicates orf reading direction.

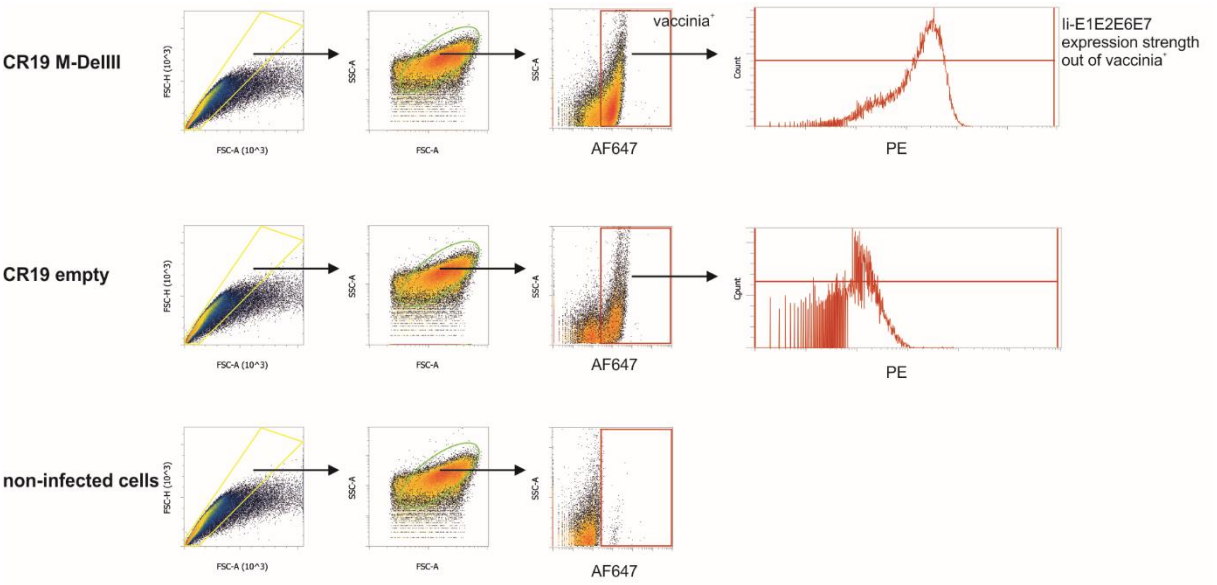

Supplementary Figure 15.
Gating strategy to analyze transgene expression strength. Cells were gated on single cells using forward and side scatter. Vaccinia-infected cells (via rabbit anti-vaccinia and goat anti-rabbit AF647) were gated using non-infected CR pIX cells. MFI of li-E1E2E6E7 (via mouse anti-myc and goat anti-mouse PE) was measured from vaccinia-positive cells.

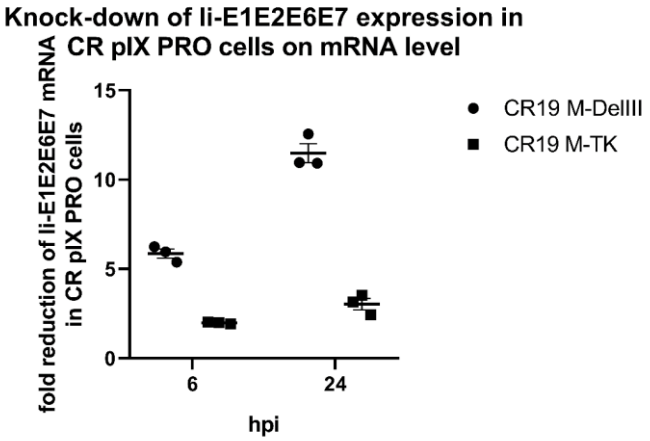

Supplementary Figure 16.
Quantification of Ii-E1E2E6E7 transcript knock-down with RT-qPCR. Depicted is the fold reduction of Ii-E1E2E6E7 transcript level in CR pIX PRO suppressor cells compared to parental CR pIX cells of CR19 M-DelIII and CR19 M-TK after 6 and 24 hpi measured by RT-qPCR. Relative comparison of transcript levels between cell lines was normalized with the housekeeping gene MVA128L and calculated with the Pfaffl method. N=3 biological replicates, bars represent mean with SEM.

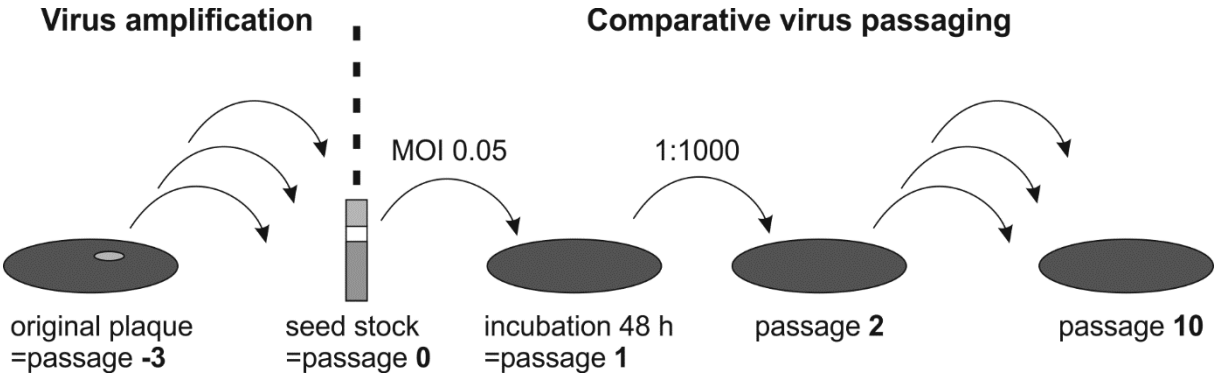

Supplementary Figure 17.
Schematic representation of comparative passaging on parental CR pIX and CR pIX PRO suppressor cell lines. Initially, 3 expansion rounds on CR pIX PRO suppressor cells were needed to generate both seed stocks from the original plaque-purified rMVA. Passaging was conducted from virus seed stocks of CR19 M-DelIII and CR19 M-TK (defined as passage 0). CR pIX and CR pIX PRO cells were infected with an MOI of 0.05 and incubated for 48 h. Cells were harvested with supernatant (passage 1), freeze-thawed for virus release and a dilution of 1:1000 was reinfected on CR pIX or CR pIX PRO cells, respectively. This was repeated until 10 passages were obtained.

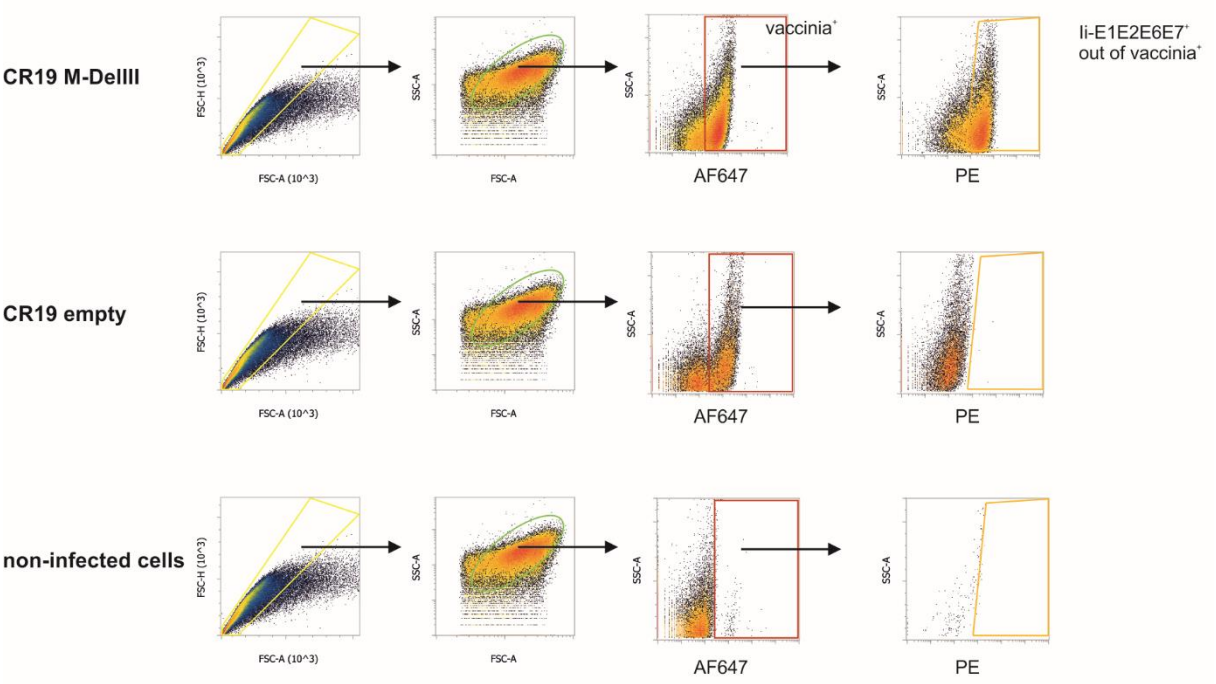

Supplementary Figure 18.
Gating strategy to analyze the fraction of transgene-expressing MVA-infected cells. Cells were gated on single cells using forward and side scatter. Vaccinia-infected cells (via rabbit anti-vaccinia and goat anti-rabbit AF647) were gated using non-infected CR pIX cells. Vaccinia$^+$ cells were then gated for Ii-E1E2E6E7 expression (via mouse anti-myc and goat anti-mouse PE) based on CR19-empty-infected control cells.

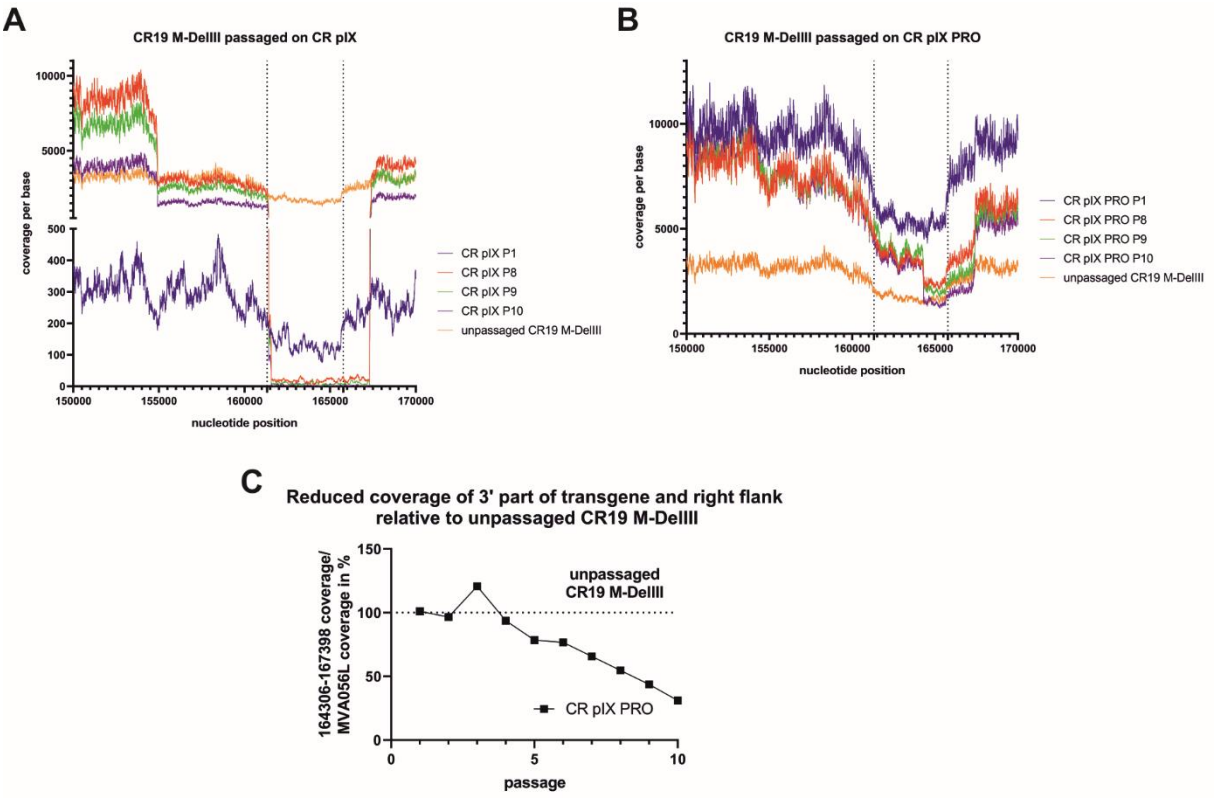

Supplementary Figure 19.
Coverage maps and relative coverage of selected CR19 M-DelIII-derived samples. Depicted is the read coverage per nucleotide from the nucleotide position 150000 to 170000 of CR19 M-DelIII passaged on parental CR pIX (A) and CR pIX PRO suppressor (B) cells from selected passages. Dotted lines represent the position of the

transgene (nucleotide position 161317 to 165771). (C) Depicted is the quotient of the mean read coverage of nucleotide position 164306 to 167398 (3' part of Ii-E1E2E6E7 and right flank) and the mean read coverage of the essential MVA056L gene (MVA DNA polymerase, E9L) of CR19 M-DelIII passaged on CR pIX PRO cells, normalized to the unpassaged rMVA. Dashed line represents normalized read coverage of unpassaged rMVA used as starting material for passaging on both cell lines.

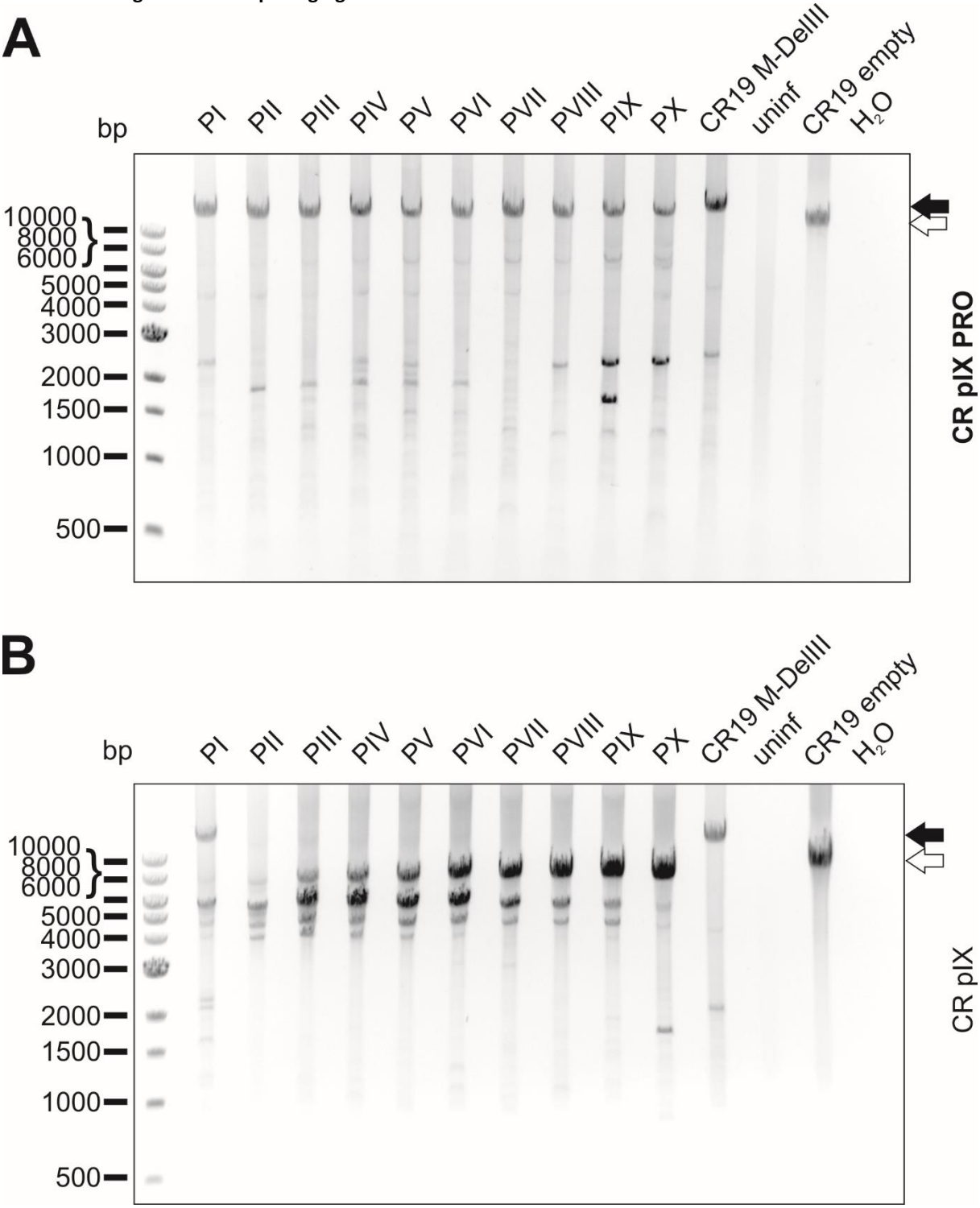

Supplementary Figure 20.
Genotyping of CR19 M-DelIII passaged on CR pIX PRO suppressor (A) and parental CR pIX (B) cells by agarose gel analysis of PCR products obtained with the primer pair wide-III3-f and wide-III2-r. Expected size of CR19 M-DelIII: 14169 bp (black arrow); expected size of CR19 empty: 9471 bp (white arrow).

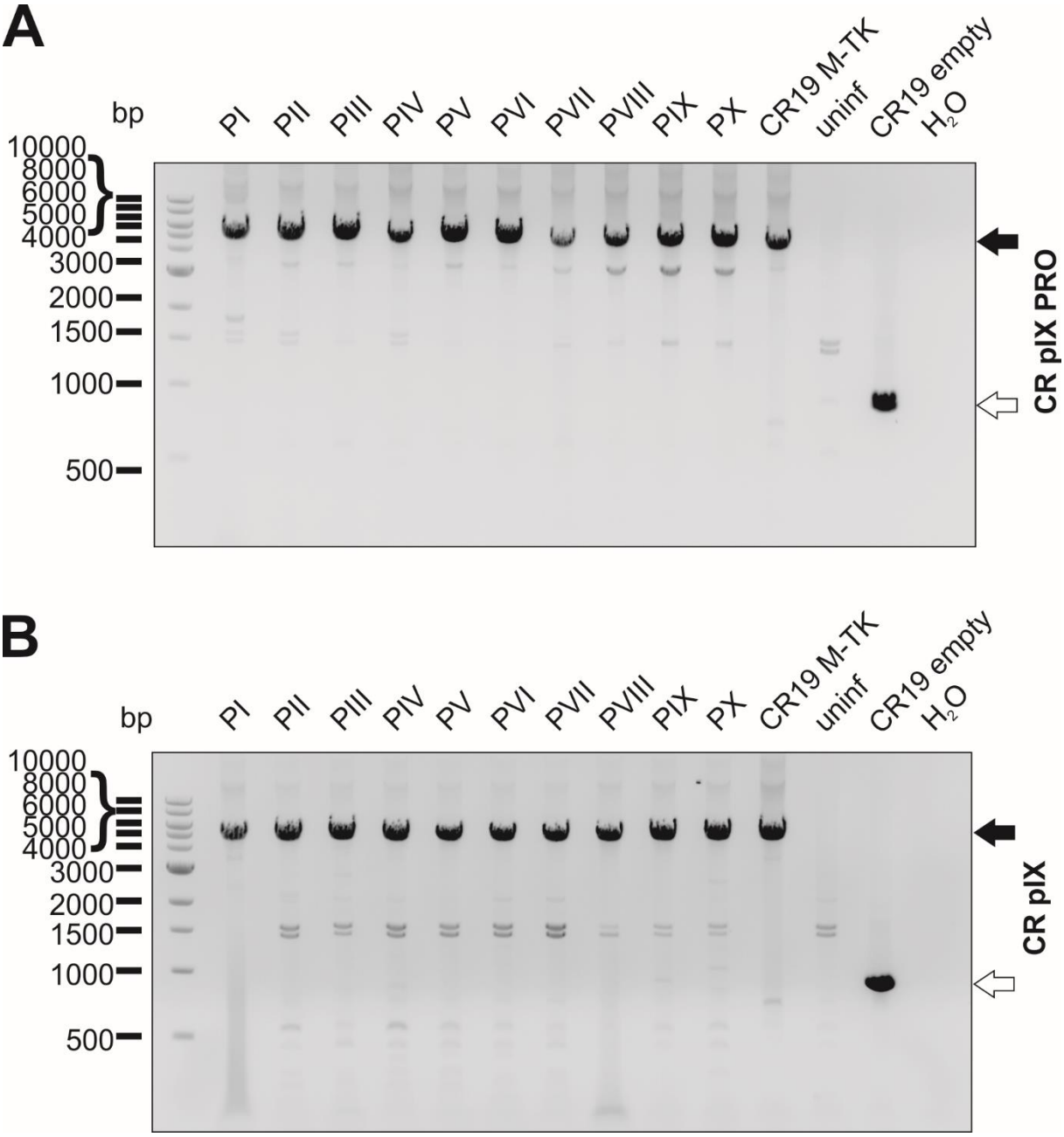

Supplementary Figure 21.
Genotyping of CR19 M-TK passaged on CR pIX PRO suppressor (A) and parental CR pIX (B) cells by agarose gel analysis of PCR products obtained with the primer pair TK f and TK r. Expected size of CR19 M-TK of 5094 bp (black arrow) and expected size of CR19 empty of 920 bp (white arrow).

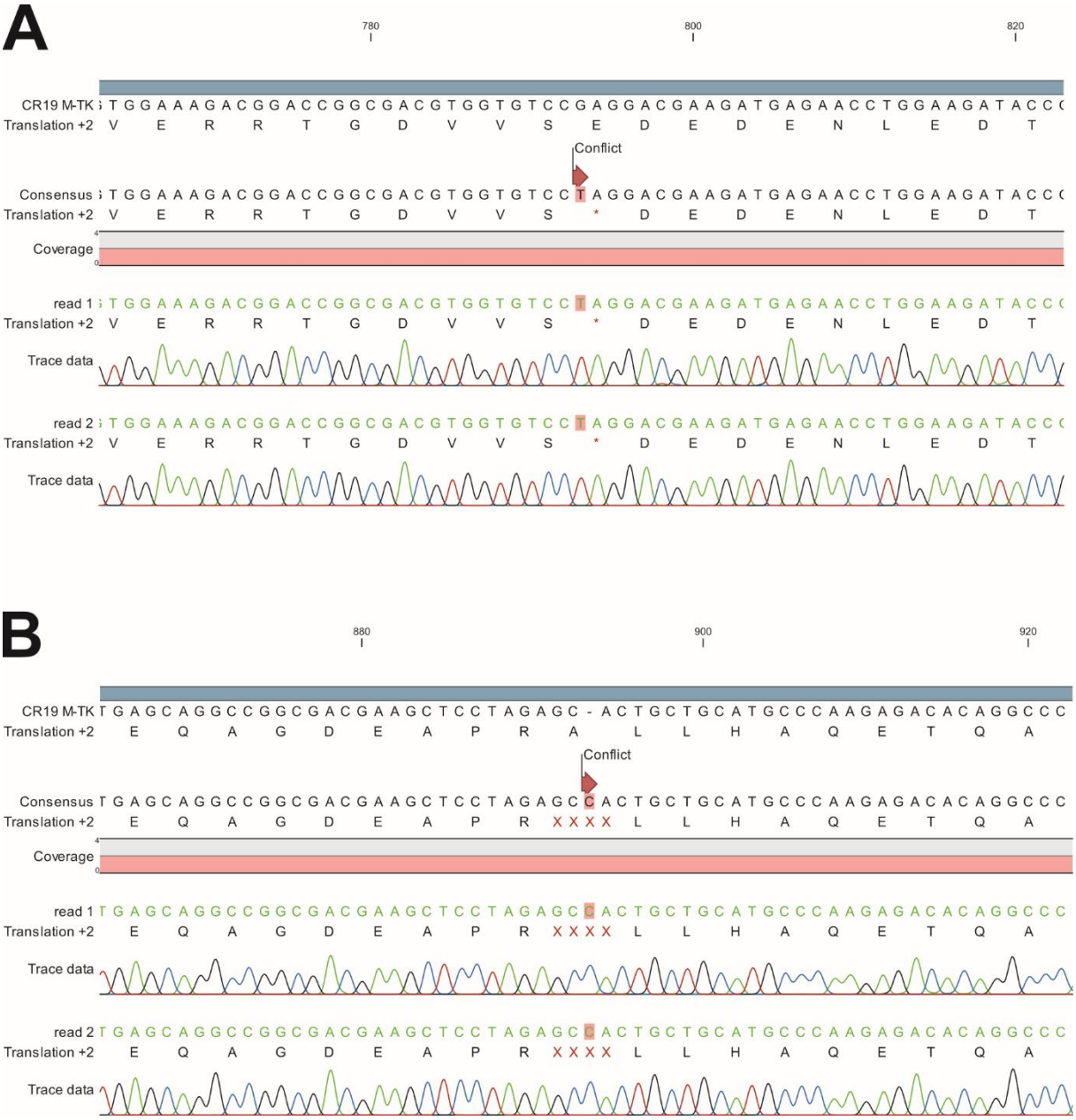

Supplementary Figure 22.
Sanger sequencing on pJET1.2/blunt-subcloned PCR amplicons of passaged CR19 M-TK. The gDNA was prepared from bulk material of passage 3 (A) or passage 10 (B) and used as template in a PCR using the primer pair TK f and TK r flanking the transgene within the TK locus. The amplicons were cloned into pJET1.2/blunt and Sanger-sequenced. Both mutations E265*(A) and L299Tfs342* (B) could be observed when the sequencing results were aligned with the transgene.

5.4.6.2 Supplementary Tables

Supplementary Table 2: PCR analysis of plaque isolated rMVA

Virus	passage	CR pIX PRO		CR pIX	
		transgene	DelVI	transgene	DelVI
CR19 M-DelIII	0	20*	20	13	20
	3	19	20	3	20
	10	18	20	2	20
CR19 M-TK	0	20	20	20	20
	3	20	20	18	20
	10	20	20	20	20

*numbers indicate the number of plaque isolated rMVA, which showed an amplicon at the expected size. For each condition 20 plaque-isolated rMVA were tested. DelVI served as sampling control.

Supplementary Table 3: coordinates of rMVA gene and transgene locations (based on KY633487.1)

Virus	Gene	5’ start	3’ end
CR19 M-DelIII	Ii-E1E2E6E7	161317	165771
	DelIII locus incl. flanks	160201	166525
	MVA056L	63330	60310
	Whole genome	1	194409
CR19 M-TK	Ii-E1E2E6E7	91871	87417
	TK locus incl. flanks	92734	86851
	MVA056L	63330	60310
	Whole genome	1	193884

5.4.7 Funding

This project has received funding from the Eurostars-2 joint program with co-funding from the European Union Horizon 2020 research and innovation program (E!12151). The project E!12151 was carried out within the framework of the European funding program “Eurostars” and the German partners were funded by the Federal Ministry of Education and Research. The manuscript reflects only the authors’ view and the European Commission is not responsible for any use that may be made of the information it contains. The funders had no influence on the study design, data collection, and analysis, decision to publish, or preparation of the manuscript.

5.4.8 Acknowledgements

We kindly thank the Eurostars-2 joint program, the European Union Horizon 2020 research and innovation program, and the German Federal Ministry of Education and Research for funding this work. We would like to thank Wulf Schneider and Jürgen Fritsch, from University Hospital Regensburg, for the use of their NextSeq500 device and their advice on these experiments.

6 Summary of findings

6.1 Manuscript 1

A set of up to 10 antigen constructs, based on MfPV3, was designed, and certain modifications were introduced in the oncoproteins according to literature in order to inactivate the transformation activity. Characterization of DNA vaccine and adenoviral vectors regarding expression and immunogenicity in outbred mice revealed that the artificial fusion of E1, E2, E6, and E7 is not inferior compared to the single proteins. Fusion of the molecular T cell adjuvant Ii enhanced the functionality of induced T cells by increasing antigen-specific T cell cytotoxicity *in vivo*. The fusion of Ii led to enhanced ubiquitination and proteasomal degradation of the antigen constructs, which might be the molecular mechanism of Ii for improving $CD8^+$ T cell responses. The results of the biochemical, cell-biological and immunological analysis in CD1, OF1 and BALB/c mice using DNA and recombinant adenoviruses for antigen delivery led to the down-selection to the best-in-class antigen (Ii-E1E2E6E7), which opened up future testing of this antigen construct in persistently MfPV3-infected macaques.

6.2 Manuscript 2

Based on the previous MfPV3 vaccine designs, a set of HPV16 antigens was generated. *In vitro* characterization of adenoviral vectors comprising these antigens proved proper expression. Sufficient inactivation of the oncoproteins was shown in a flow cytometry-based p53-degradation assay using DNA-transfected human cells and in a soft-agar-transformation assay using lentivirally-transduced embryonic mouse cells. Immunization of outbred and inbred mice proved rigid T cell responses, especially against E1 and E7. Moreover, the efficacy of the Ii-E1E2E6E7 therapeutic vaccine candidate was shown in a translational C57BL/6 mouse model against HPV16-positive tumors in different settings, simulating small and advanced tumors. The therapeutic effect was enhanced by cisplatin, which increased the amount of HPV16-specific TIL. $CD8^+$ T cells were found to be the primary effector cells to reduce tumor growth. Finally, the Ii-E1E2E6E7 was benchmarked with promising results against a preclinical derivative of a peptide-based therapeutic vaccine candidate currently in clinical evaluation. Altogether, an HPV16-specific therapeutic vaccine candidate was generated and pre-clinically evaluated, which showed promising results and thus might be a good candidate for clinical evaluation.

6.3 Manuscript 3

Two recombinant MVA, coding for MfPV3 Ii-E1E2E6E7, were generated using a modified avian cell line that aimed to reduce the transgene expression. It was shown that the modified cell line (CR pIX PRO) indeed reduced the transgene expression of the rMVA using western blot, flow cytometry, and RT-qPCR analysis. Moreover, growth kinetics analysis and plaque staining revealed that the knock-down of the transgene expression in the CR pIX PRO cell line enhanced the virus yield. In contrast, replication on unmodified CR pIX cells exhibited reduced replication by a factor of approximately 10. Therefore, the expression of the Ii-E1E2E6E7 seemed to induce a negative selection pressure. Serial passaging of both rMVA on both cell lines and subsequent expression analysis using flow cytometry proved enhanced transgene stability across the passages for viruses passaged on the CR pIX PRO suppressor cell line. Finally, PCR-analysis and next-generation sequencing revealed that the mode of action that leads to abrogated transgene expression under non-suppressive passaging (CR pIX) differs depending on the integration locus: deletions of the whole DelIII locus could be observed, whereas transgenes in TK locus underwent translation-distorted mutations. In conclusion, the knock-down of transgene

expression within the generation and production of rMVA comprising a demanding transgene can increase the virus yields and stability.

7 General Discussion

7.1 Antigen and Vaccine Candidate Design

7.1.1 Impact of the Inclusion of E1 and E2

For all generated constructs, Ii-E1E2E6E7 turned out to be the lead candidate, mainly due to similar expression compared to others in combination with the most consistent T cell responses in different mouse strains and strikingly enhanced cytotoxicity. The rigid detection of induced T cell responses against E1 and E2 of MfPV3 (Manuscript 1), as well as HPV16 (Manuscript 2) in different mouse strains, proved the immunogenicity of these antigens in the Ii-E1E2E6E7 vaccine construct. Especially the consistent detection in the context of outbred mice provides information that the bigger antigens indeed increased the breadth of induced immune responses because more potential epitopes are included, which fit the MHC alleles of the individual mice. Thus, the inclusion of E1 and E2 may overcome the limited responder rate for E6 and E7-based vaccine candidates in humans (161,166,190,191).

A limitation is that no direct comparison of viral vector-encoded Ii-E6E7 versus Ii-E1E2E6E7 in the C3 tumor challenge was made based on the same vector backbone, which prohibits the ultimate proof of the superiority of the inclusion of E1 and E2 in an E6 and E7-based vaccine candidate compared to a vaccine with E6 and E7 alone. Ii-E1E2E6E7 had to be benchmarked against an Ii-E6E7 construct, delivered with the same heterologous prime and boost vectors to achieve this.

7.1.2 Ii-Induced Rapid Proteasomal Degradation as a Possible Driving Force of $CD8^+$ T Cell Response Enhancement

As observed throughout the experiments, the N-terminal fusion of Ii to the antigen resulted in a trend towards enhanced $CD8^+$ T cell responses (Manuscript 1 and Manuscript 2) and T cell functionality. Investigating the mechanism behind this effect led to the observation that the Ii-fused construct indicated enhanced ubiquitination and accelerated proteasomal degradation. Others also found similar results (220), and it is presumed that this enhanced degradation provides more peptides for MHC-I loading (221). A hypothesis for this might be that the direct fusion of Ii leads to misfolding of the proteins, which triggers unfolded protein response (UPR) that lead to enhanced ubiquitination (402) and further result in enhanced degradation via the endoplasmic reticulum-associated protein degradation (ERAD) (403). Therefore, the fusion of Ii might be introducing a similar effect as the hypothesized defective ribosomal products (DRiPs), which also contribute vastly to the MHC-I-presented peptidome (404–406).

7.1.3 Viral Vectors as a Delivery Platform

DNA vaccine vectors have several benefits regarding easy and fast generation, cost-efficiency, thermostability, and display the method of choice for initial evaluation of a broad panel of antigens (216,224). Furthermore, DNA vaccine vectors can also be directly used in clinical development, which is reflected by several vaccine candidates currently in clinical trials (407–409).

However, DNA vaccine vectors inferior in the strength of immune responses compared to viral vectors, especially in the context of therapeutic vaccines (216,217,225–228). Delivering the generated MfPV3 constructs with adenoviral vectors showed superior T cell responses compared to DNA vaccination (Manuscript 1), similar to those seen by others (192). Furthermore, the adenoviral vector-shuttled antigens showed promising efficacy in the C3 tumor challenge (Manuscript 2), highlighting these viral

vectors' value. The heterologous adenoviral prime with MVA boost scheme is shown to induce potent T cell responses in NHPs and humans (255,410–412), and this combination is also used in the VTP-200 therapeutic HPV vaccine candidate, which is currently evaluated in 1b/2 phase clinical trial (NCT04607850). In order to enhance the potency of a viral vector-based vaccination regimen, the construction of rMVA with MfPV3 vaccine constructs was done (Manuscript 3), but unfortunately, the immunological characterization is pending. This might be done in the future, together with the upcoming efficacy trial in macaques.

7.1.4 Safety of Vaccine Candidates

The use of adenoviral vectors (and also DNA vaccine vectors) as vector delivery platforms inhabits the risk of spontaneous integration of the vector genome and their transgene into the vaccinee's genome (413–415). Although the frequency of these events is relatively low compared to spontaneous mutations, this has a tremendous implication if an adenoviral vector comprises oncoproteins like E6 and E7, since a single integration event might lead to the transformation of the cell and inflict a novel source of cancer. Therefore, only modified PV antigens without risk must be used in adenoviral vectors (334). It could be shown that the vaccine constructs with the modified HPV16 E6 antigen are unable to degrade p53 *in vitro*. Moreover, vaccine constructs with the modified HPV16 E7 are rendered transformation-incompetent, which is proven in the soft agar transformation assay (364). These results are in accordance with others (333–335,416–421) and verify the safety of the generated antigens in the context of antigen-derived oncogenic transformation (Manuscript 2). This is also bolstered by the safety profiles of the DNA vaccine candidates comprising E6 and E7 of hrHPV, VGX-3100, and GX-188E. Both DNA vaccines are shown to be safe (345,407,422,423), but the mechanisms of oncoprotein inactivation are different. Whereas the oncoproteins in GX-188E are shuffled, and therefore their activities are disturbed (424), the oncoproteins in VGX-3100 are mutated (425). In terms of induced autoimmunity by therapeutic vaccination, the use of foreign virus-derived TSA might be considered safe since TSA are expressed solely in HPV-infected or transformed cells (161,163).

The extensive enrollment of adenoviral vectors as prophylactic vaccines against SARS-CoV-2 led to the detection of the ultra-rare phenomenon of VITT (230,426–428). VITT seems to correlate with the occurrence of autoantibodies against platelet factor 4 (PF4) (427). Against initial assumptions, it was shown that the coronavirus spike protein is not inducing VITT by cross-reactivity to PF4 (429). More recent studies instead suggested impurities from the production process of the adenoviral vectors as a possible origin of VITT (430,431), and meanwhile, strategies to combat VITT are in place (432). More research on the use of adenoviral vectors might be needed in the future. Nevertheless, in the case of therapeutic vaccination, where potential patients are already suffering from HPV-induced malignancies, the delivery of antigens via adenoviral vectors might be more relaxed in terms of risk-benefit analysis, which is also reflected in the ongoing VTP-200 trial (NCT04607850).

The use of MVA as a vaccine as well as a vector for recombinant genes might be considered safe due to its long clinical track record. MVA was already tested in a large study at the end of the smallpox vaccination campaign (262,277) and is currently used as a licensed vaccine against monkey poxvirus (278,279). Additionally, rMVA is licensed in combination with Zabdeno as a prophylactic vaccine against Zaire ebolavirus (284,285). In both cases, no major MVA-induced adverse events could be observed (59–62). This reemphasizes the future development of an MVA-based therapeutic vaccine with the designed PV antigens for therapeutic vaccination.

7.2 Aspects of rMVA Manufacturing and Upscaling

As outlined before, using rMVA as a potential vaccine delivery vehicle for therapeutic vaccination might be advantageous, although the generation process of such poxviral vectors is quite laborious. It was observed that the homologous recombination of the vaccine candidate into CR19 was not feasible until the production cell line and transfer vectors were modified to knock down the transgene expression while rMVA generation (Manuscript 3). This was most probably induced by a strong negative selection against the rMVA, leading to instability of the recombinant poxviral vector, which was also shown for some other transgenes (306–308,383,384). Others hypothesized that UPR might induce such negative selection (306), a phenomenon that might be connectable to the Ii adjuvant. No evidence for UPR could be found for Ii-E1E2E6E7 (data not shown), but also, a construct without Ii (E1E2E6E7) was hard to generate (data not shown). Interestingly, others could generate rMVA encoding either Ii together with other transgenes, or E1, or E2, or E6, or E7, respectively (219,220,255,289,433–435), which leads to the hypothesis that the artificially fused polyprotein itself (Ii-E1E2E6E7) is the cause of the negative selection.

The knock-down of transgene during repeated passaging, which simulated the process of generating master virus seed stocks and amounts of virus for vaccination purposes, led to enhanced stability and improved virus yields (as thoroughly discussed in Manuscript 3), an essential criterion for the production of a vaccine and often neglected by scientific researchers. Multiple rounds of propagation are needed to produce a commercial vaccine. Enhanced stability and high viru titers over these propagation rounds are tremendous for its use as a vaccine, especially when the number of amplification rounds is limited due to stability issues. These aspects are not only restricted to rMVA but are also crucial in the production of adenoviral vectors, where genetic stability is characterized to ensure vector integrity throughout the manufacturing process (436). In particular, it could be found that some transgenes in adenoviral vectors tend to be unstable, and the vectors could be rescued using transgene expression knockdown (399). The improved yield elicited by transgene expression knock-down is significant for rMVA since replication-deficient viral vectors require higher amounts per vaccination to achieve the desired immune response (437). Although the required doses of a therapeutic vaccine against HPV-induced malignancies might be smaller than prophylactic vaccines against malaria, HIV, or other infectious diseases (436), the production process still needs to be highly efficient.

In general, while generating the rMVA, a particular focus has been directed towards compliance with good manufacturing procedure (GMP) compliance. Usually, rMVA are generated on primary CEF cells. In contrast, the rMVA presented in Manuscript 3 were generated in the continuous cell line AGE1.CR pIX (CR pIX). This continuous cell line has several advantages compared to primary cells, including avian origin, GMP compliance, low amount of integrated endogenous retroviruses, high MVA replication, and improved suspension culture for scalable industrial processes (290,438). Moreover, using a continuous cell line allowed cell line modification to facilitate transgene knock-down during rMVA generation and propagation, which perhaps would be impossible in primary cells. Additionally, CR19 replicates to higher titers and is released from the CR pIX cell surface when amplified in CR pIX suspension culture in a chemically defined medium, which not only yields higher virus titers (290–292,438) but also reduces the risk of cellular contaminants in the final vaccine that might be the cause of VITT by adenoviral vectors against SARS-CoV-2 (430,431).

More efficient viral vector manufacturing is an essential key point to address in the future. Enhancing vector stability and production yields by knock-down of the transgene might be a first step regarding

the upscaling of viral vectors with demanding transgenes. However, future research also has to clarify whether the transgene knock-down components influence the elicited immune responses, especially in humans.

7.3 Clinical Potential of the Novel HPV16 Ii-E1E2E6E7 Vaccine Candidate

A type-specific therapeutic vaccine candidate against HPV16 is highly restricted to treat only HPV16-derived disease, whereas the candidate VTP-200, based on 5GHPV3, comprises conserved elements of multiple early proteins of five different HPV genotypes (192). In terms of genotypes, VTP-200 might be covering more genotypes and thus can be used to treat more HPV-derived malignancies. However, the direct fusion of many epitopes into one antigen construct increases the risk of artificial epitopes formed by the junction of fused epitopes. Hellner and colleagues reported the frequent detection of T cell responses against the junctions of epitopes in VTP-200 at the IPVC conference (439). T cell responses against these neoepitopes might not result in effective T cell responses against HPV-infected cells. In contrast to the multiple genotype candidate, it can be hypothesized that a type-specific therapeutic vaccine against HPV16, which comprises the full-length early proteins, might prove superiority if directly compared with a candidate that only consists of conserved epitopes of several early proteins (VTP-200) when targeting HPV16-derived malignancies. Targeting HPV16 is of the highest clinical relevance since this genotype is connected to at least 61% of HPV-derived cervical cancer (8), more than 85% of HPV-positive OPSCCs (39), and 80% of HPV-derived anal carcinomas (440). Additionally, HPV16 is involved in the majority of other HPV-derived anogenital cancers (64), thus reflecting the importance of this genotype in therapeutic vaccine research. A possibility for future development of the here-described HPV16 Ii-E1E2E6E7 might be the expansion towards a bivalent vaccine candidate by including, for example, an HPV18 Ii-E1E2E6E7 in the same viral vectors in the case of cervical cancer (64). This might be achieved by using the antigen design as a blueprint for other important HPV genotypes, similar to what was already done by using the antigen design from MfPV3 to generate the HPV16 vaccine candidate (Manuscript 2). The role model for such an extension of the antigens are the prophylactic vaccines, which started initially as bivalent (Cervarix™) or tetravalent (Gardasil® 4) vaccine, where the latter hereafter was extended towards a nonavalent prophylactic vaccine (Gardasil® 9) (71).

Currently tested therapeutic vaccine candidates against HPV-induced malignancies are primarily focused on the oncoproteins E6 and E7, thus limiting the vaccine candidates' efficacy to (pre-) cancerous entities, where both oncoproteins are highly expressed. In contrast, the inclusion of E1 and E2 side-by-side with E6 and E7 might increase the range of stages where such an improved therapeutic vaccine candidate could work. To be more precise, the Ii-E1E2E6E7 could target all stages between (persistent) infection, precancerous lesions, and advanced cancer, induced by HPV16. Additionally, the extension of antigen range by adding E1 and E2 might also be superior in conditions where E6- and E7-based vaccine candidates already have shown efficacy due to the increased number of potential immunogenic peptides (166). It could be hypothesized that such a broader response against HPV16-derived proteins might increase the clinical response rate of therapeutic vaccine candidates in advanced cancer, mainly since at least some of these advanced cancers still express residual E1 and E2 peptides (191).

Due to the concept of the designed HPV16 Ii-E1E2E6E7, multiple groups of patients might be attractive targets for a novel therapeutic vaccine to combat HPV16-derived malignancies: (i) female patients in HICs with persistent HPV16 infection before the onset of CIN or within CIN1, (ii) female patients in

LMICs with advanced CIN and cervical cancer, (iii) patients with OPSCCs as part of a de-intensification strategy and (iv) male patients with enhanced risk of HPV-induced malignancies.

First of all, the group of female patients with persistent HPV16 infection before the onset of CIN or in CIN1 might benefit most of all patient groups. This can be only achieved by changing the screening method from the detection of HPV dysplasia to the detection of hrHPV infection. This transition in the screening method is currently done in some HICs with the aim of improving risk assessment of disease progression (209–212). By this date, there is no treatment for persistent HPV infection before the onset of CIN or for CIN1, but just intensified screening for progression (210). It can be hypothesized that therapeutic vaccination within this stage of disease might be promising, especially since HPV-specific T cell responses against the early proteins correlate with lack of progression, CIN regression, and HPV clearance (146–154). Furthermore, most therapeutic vaccine candidates are not tested in such early stages, presumably because of their reliance on E6 and E7, which are only expressed at low levels in this stage of disease (43,441). In contrast, Ii-E1E2E6E7 also comprises E1 and E2, which might be beneficial determinants. Evaluating the efficacy of the MfPV3 Ii-E1E2E6E7 in persistently infected macaques will probably give information about the potency against CIN1-like lesions. The sole therapeutic vaccine tested for efficacy against CIN1 is VTP-200 (NCT04607850), but only immunogenicity results without the efficacy data have been presented so far (439). These results might be leading the path for future tests in CIN1 patients but also for persistently HPV-infected patients without CIN.

The next patient group, which might benefit from the novel HPV16-specific Ii-E1E2E6E7 therapeutic vaccine candidate, might be women in advanced CIN and cervical cancer in LMICs. These countries have the highest burden for cervical cancer (33,34,38), probably due to the reduced number of vaccinated individuals (442), which therefore prolongs the high infection rates and high loads of cervical cancer (29,30,443). Additionally, LMICs often have limited access to screening procedures as well as expensive cancer treatment medication and surgery, thus increasing the burden and mortality of cancer (443,444). Easy and cheap therapy strategies might be needed to overcome this. Therefore, viral vector-based therapeutic vaccinations are perhaps more feasible in area-wide distribution than expensive peptide-based therapeutic vaccine candidates or surgery with follow-up treatment. The production of adenoviral vectors is cost-efficient (445), which is currently seen for large-scale use of adenoviral vector-based vaccines against SARS-CoV-2. The use of MVA genotype CR19 facilitates replication in GMP-compatible CR pIX suspension culture, yielding high titers of the poxviral vector (290–292,438). Moreover, the knock-down of transgene expression in the production cell line (CR pIX PRO, Manuscript 3) further enhanced the yield and stability of rMVA, which perhaps lead to cheap large-scale production of the poxviral vector compared to conventional production of such vectors on primary CEF cells. A similar viral-vectored vaccine approach based on recombinant Ad26 and MVA-BN is currently used as a prophylactic vaccine against Ebolavirus in LMICs (284,285), which endorses the feasibility of area-wide administration of viral vector-based (therapeutic) vaccination in such countries.

The treatment of HPV-positive OPSCCs with SOC therapy is highly successful (38,161,166,446) but often leads to severe therapy-induced side effects, which exhibit a high burden for these patients (161,167). OPSCCs resulting from HPV infection have a better prognosis compared to HPV-negative OPSCCs (167). Therefore, current efforts are undertaken to de-intensify the treatment of HPV-positive OPSCCs without compromising the efficacy (38,447,448). Therapeutic vaccination, which comprises more antigens than both oncoproteins, is perhaps a method of choice to reduce the duration and dose of radiation and chemotherapy (38,449). Several studies provided information about the high

relevance of E1 and E2 in HPV-positive OPSCCs (188–190), thus encouraging the use of Ii-E1E2E6E7 in combination with reduced loads of SOC therapy in these patient groups to reduce the burden of therapy-induced sickness. Most E6- and E7-based therapeutic vaccines are tested either in curative or recurrent/metastatic settings, usually combined with CPI or chemotherapy (449). An even more interesting stage of OPSCC treatment might be the application of the therapeutic vaccine in patients with remitting cancers, thus reducing the risk of tumor recurrence, which is often correlated with poor prognosis (296,351,352). The need for additional intervention in this remitting stage of the disease is reflected by the PepCan study (NCT03821272), where OPSCC patients in remission after curative therapy were immunized with E6 peptides screened for reduced recurrence within two years. The results of this trial are perhaps groundbreaking for further clinical trials of therapeutic vaccines in this patient group.

Last but not least, it should be addressed that men represent a relevant target group for the generated Ii-E1E2E6E7 vaccine. Several anogenital but non-cervical, -vulvar and -vaginal carcinomas linked to HPV apply to either both sexes or men only (440). Additionally, male individuals exhibit oral HPV infection and HPV-positive OPSCCs more frequently than female individuals (450,451). This is probably due to the reduced vaccination coverage among men compared to women, due to the later vaccination recommendation for men in most HICs, which can also be seen in the increased incidence of HPV-positive OPSCCs, predominantly in the male population, which have already exceeded the incidence of cervical cancer in HICs (452). Since the availability of the prophylactic vaccines, 110 nations introduced HPV as a target in their vaccination schedule for females, but only 40 countries have included male individuals (453). Therefore, approximately 15% of eligible girls globally received the full course vaccination compared to only 4% of eligible boys (454). Moreover, this is even exacerbated since there is no FDA-approved diagnostic test or screening method for male individuals (453,455), which puts men at a higher risk for developing HPV-induced malignancies. HPV-positive OPSCCs have the highest incidence in middle-old, white men, which, in combination with the increased incidence of oral HPV infection and low vaccination rates, will even lead to higher incidences of virus-induced OPSCCs in the near future, which reemphasizes the necessity of improved therapy (452).

8 Conclusion and Outlook

Within this thesis, a set of type-specific antigens encoding full-length E1, E2, E6, and E7 of MfPV3 and HPV16, respectively, was designed. Moreover, suitable vectors for the designed antigens were constructed, and systems were implemented to produce these vectors efficiently with reduced risk of genetic instability. The data obtained here argue that Ii-E1E2E6E7 is the best-in-class antigen within the designed antigens. Furthermore, this antigen is safe, immunogenic, and has anti-tumor efficacy. In addition, the inclusion of E1 and E2 enhanced the breadth of the potential T cell responses, which is seen consistently throughout the experiments.

On the basis of the so far obtained data, also taking data obtained from others for competing vaccine candidates into consideration, it can be argued that the viral vector-delivered HPV16 Ii-E1E2E6E7 construct might be a promising and superior novel therapeutic HPV16 vaccine candidate, with the potential to successfully tackle HPV16-derived malignancies in all stages of the disease. Therefore, this therapeutic vaccine candidate might be the optimal treatment for patients with persistent HPV16 infection in a low-grade or early stage of disease. Still, it can also be used against advanced stages of disease in resource-poor settings or to de-intensify current SOC treatments and thus can help potentially all patients at risk of HPV16-derived disease.

A currently ongoing pre-clinical efficacy trial in persistently MfPV3-infected macaques will determine the efficacy of therapeutic vaccination with an adenoviral-prime and MVA-boost regimen using MfPV3 Ii-E1E2E6E7 against persistent infection and low-grade dysplasia. These results will pave the future clinical development of the type-specific HPV16 Ii-E1E2E6E7 therapeutic vaccine candidate.

Moreover, in the future, the principle of transgene expression knock-down within the generation of rMVA shall be used to generate additional poxviral vectors, which can express HPV16 Ii-E1E2E6E7, to reconstruct the vaccination regimen used in the above-mentioned efficacy trial in macaques also in humans.

Finally, despite HPV16 being responsible for most HPV-derived diseases, there are still other HPV types that contribute to the high amount of HPV-induced morbidity and mortality. Hence, additional antigen constructs should be designed using sequences of other important types, e.g., HPV18, HPV31, or HPV58, using the MfPV3 and HPV16 Ii-E1E2E6E7 as a blueprint. Moreover, monovalent vaccine vectors against these types might be mixed into a multivalent therapeutic vaccine, similar to the prophylactic vaccines, to cover multiple genotypes. Additionally, ways should be explored to combine several HPV types in one viral vector in order to generate bivalent (HPV16 and HPV18) or even multivalent candidates, similar to VTP-200, but with reliance on the full-length sequences of the antigens.

9 Appendix

9.1 Contribution in SARS-CoV-2-Related Research Due to Research Restrictions During the Pandemic

This PhD thesis was carried out between October 2018 and December 2023 and, therefore, was executed during the SARS-CoV-2 pandemic. Due to these research restrictions in parts of this time, research institutions had to conduct SARS-CoV-2-related research. Additionally, the research group of Ralf Wagner has received funding from international (EU H2020, Virofight), national (BMBF, German ministry of education and research) and local (Bavarian StmWK, states ministry of science and arts) and obliged to collect data supporting political measures to fight the epidemic. Hence, the PhD candidate Patrick Neckermann participated in SARS-CoV-2-related research, mainly by generating and producing critical reagents for the detection of immune responses against SARS-CoV-2. This led to five co-authorships in publications in peer-reviewed journals. Hereafter, several abstracts of these publications and the contribution within the research work are mentioned.

The emergence of the severe acute respiratory syndrome coronavirus 2 (SARS-CoV-2) in late 2019 (456) and its subsequent transmission across the globe led to more than 770.000.000 confirmed infections and nearly 7.000.000 confirmed deaths within the time frame of about four years (457). SARS-CoV-2 shares high sequence homology with SARS-CoV and RaTG13 (456). The infection with SARS-CoV-2 led to the clinical symptoms of corona-virus-induced disease (COVID-19), which are fever, dyspnea, headache, pneumonia, cough up to severe alveolar damage, multiple organ failure, and death (1), similar to symptoms induced by SARS-CoV (458). Due to the fast spread of the virus throughout the population, contact restrictions and lockdowns were exempted to reduce the transmission rates (459,460). Only “system-relevant” institutions were still allowed to perform their work, and research institutions were obliged to conduct research dedicated to SARS-CoV-2.

SARS-CoV-2 infects the host cell by the engagement of the host cell receptor angiotensin-converting-enzyme-2 (Ace2) via the viral trimeric spike (S) protein (461,462). This interaction is facilitated by the binding of the receptor-binding-domain (RBD) to the Ace2 (461–464). After binding to Ace2, the S protein is cleaved by the cellular protease TMPRSS2, which leads to subsequent membrane fusion and internalization of the virus (465).

Simultaneous with the pandemic's beginning, various efforts were consolidated to streamline the generation of prophylactic vaccines against COVID-19. In this process, multiple approaches were used to induce a potent immune response against SARS-CoV-2, e.g. mRNA-encoded S protein (Comirnaty, Spikevax), adenoviral-delivered S protein (Vaxzevria, JCOVDEN, GAM-COVID-Vac), protein-based vaccines (Nuvaxovid) and inactivated virus vaccines (CoronaVac) (247–249,466–469). These vaccines induce proper antibody responses and protect from severe COVID-19. Additionally, SARS-CoV-2-infected persons can be treated with monoclonal antibodies to prevent severe COVID-19 (470). Unfortunately, the constant evolution of SARS-CoV-2 during the pandemic led to the emergence of variants of concern (VOC), which display immune evasion capabilities and enhanced transmission within the population (471–474). The immune evasion of the VOCs reduced the efficacy of the vaccine-induced immune response and monoclonal antibody therapy (473,475–479). Hence, adapted booster vaccines targeting the different VOCs are needed to broaden the immune response towards protection against VOCs.

Monitoring immune responses against SARS-CoV-2, especially of S protein-specific antibodies, is an important determinant for the retrospective assessment of the real incidence of infection and infection

fatality ratio, for the detection of the amount of underreported SARS-CoV-2 infections and for the measurement of the durability of antibody responses (480–482). Additionally, the analysis of both, binding and neutralizing antibody titers, to determine correlates of protection and the breadth of antibody responses upon infection are important characteristics for novel vaccine designs (483–485). Neutralizing antibodies against SARS-CoV-2 S protein can be detected either by 50% plaque-reduction neutralization assay ($PRNT_{50}$) or pseudovirus neutralization assay (pVNT) (486–488). Practically, lentivirus- or vesicular stomatitis virus-based pVNT are often chosen over $PRNT_{50}$ since these pVNT assays are high-throughput capabilities but still require cell-based assays and pseudotyped viruses, thus require at least laboratories of biosafety level 1/2. The RBD contains multiple epitopes for neutralizing antibodies, which renders RBD a vulnerable site of the S protein (489). Antibodies against RBD correlate with neutralization titers against the virus (490) and thus are also used as possible vaccine candidates in preclinical models (491). Multiple assays use recombinant RBD, conditionally supported by the use of recombinant Ace2, to detect antibody responses against SARS-CoV-2 as a surrogate for neutralization and the detection of seroconversion (490,492–494), which emphasizes the importance of these proteins as valuable tools in epidemiological studies and the development of vaccine candidates to analyze immune responses against SARS-CoV-2.

9.1.1 Appendix publication 1

Title: “Symptoms, SARS-CoV-2 Antibodies, and Neutralization Capacity in a Cross Sectional-Population of German Children”

Authors: Otto Laub, Georg Leipold, Antoaneta A Toncheva, David Peterhoff, Sebastian Einhauser, **Patrick Neckermann**, Natascha Borchers, Elisangela Santos-Valente, Parastoo Kheiroddin, Heike Buntrock-Döpke, Sarah Laub, Patricia Schöberl, Andrea Schweiger-Kabesch, Dominik Ewald, Michael Horn, Jakob Niggel, Andreas Ambrosch, Klaus Überla, Stephan Gerling, Susanne Brandstetter, Ralf Wagner, Michael Kabesch; Corona Virus Antibodies in Children from Bavaria (CoKiBa) Study Group

Published on 4th of October 2021 in Frontier in Pediatrics

DOI: 10.3389/fped.2021.678937

Abstract: Background: Children and youth are affected rather mildly in the acute phase of COVID-19 and thus, SARS-CoV-2 infection infection may easily be overlooked. In the light of current discussions on the vaccinations of children it seems necessary to better identify children who are immune against SARS-CoV-2 due to a previous infection and to better understand COVID-19 related immune reactions in children. Methods: In a cross-sectional design, children aged 1-17 were recruited through primary care pediatricians for the study (a) randomly, if they had an appointment for a regular health check-up or (b) if parents and children volunteered and actively wanted to participate in the study. Symptoms were recorded and two antibody tests were performed in parallel directed against S (in house test) and N (Roche Elecsys) viral proteins. In children with antibody response in either test, neutralization activity was determined. Results: We identified antibodies against SARS-CoV-2 in 162 of 2,832 eligible children (5.7%) between end of May and end of July 2020 in three, in part strongly affected regions of Bavaria in the first wave of the pandemic. Approximately 60% of antibody positive children (*n* = 97) showed high levels (>97th percentile) of antibodies against N-protein, and for the S-protein, similar results were found. Sufficient neutralizing activity was detected for only 135 antibody positive children (86%), irrespective of age and sex. Initial COVID-19 symptoms were unspecific in children except for the loss of smell and taste and unrelated to antibody responses or neutralization capacity. Approximately 30% of PCR positive children did not show seroconversion in our small subsample in which PCR tests were performed. Conclusions: Symptoms of SARS-CoV-2 infections are unspecific in children and antibody responses show a dichotomous structure with strong responses in many and no detectable antibodies in PCR positive children and missing neutralization activity in a relevant proportion of the young population.

Author contribution: OL, GL, SG, KÜ, RW, and MK were responsible for the study design. OL, GL, HB-D, SL, AS-K, DE, MH, JN, and MK performed the data collection. AT, DP, SE, **PN**, NB, ES-V, PK, PS, RW, and AA carried out the laboratory analysis and the data interpretation. Data Analysis was performed by DP, SE, **PN**, SB, RW, and MK. OL, GL, DP, SE, SB, RW, and MK wrote this manuscript.

Personal contribution: PN supervised and supported the Master’s thesis of student Sebastian Einhauser, who established a pseudovirus-based assay for the quantification of neutralizing antibodies against SARS-CoV-2. PN further evaluated, analyzed and interpreted the data.

9.1.2 Appendix publication 2

"Analysis of Serological Biomarkers of SARS-CoV-2 Infection in Convalescent Samples From Severe, Moderate and Mild COVID-19 Cases"

Authors: Javier Castillo-Olivares, David A Wells, Matteo Ferrari, Andrew C Y Chan, Peter Smith, Angalee Nadesalingam, Minna Paloniemi, George W Carnell, Luis Ohlendorf, Diego Cantoni, Martin Mayora-Neto, Phil Palmer, Paul Tonks, Nigel J Temperton, David Peterhoff, **Patrick Neckermann**, Ralf Wagner, Rainer Doffinger, Sarah Kempster, Ashley D Otter, Amanda Semper, Tim Brooks, Anna Albecka, Leo C James, Mark Page, Wilhelm Schwaeble, Helen Baxendale, Jonathan L Heeney

Published on 19th of November 2021 in Frontiers in Immunology

DOI: 10.3389/fimmu.2021.748291

Abstract: Precision monitoring of antibody responses during the COVID-19 pandemic is increasingly important during large scale vaccine rollout and rise in prevalence of *Severe Acute Respiratory Syndrome-related Coronavirus-2* (SARS-CoV-2) variants of concern (VOC). Equally important is defining Correlates of Protection (CoP) for SARS-CoV-2 infection and COVID-19 disease. Data from epidemiological studies and vaccine trials identified virus neutralising antibodies (Nab) and SARS-CoV-2 antigen-specific (notably RBD and S) binding antibodies as candidate CoP. In this study, we used the World Health Organisation (WHO) international standard to benchmark neutralising antibody responses and a large panel of binding antibody assays to compare convalescent sera obtained from: a) COVID-19 patients; b) SARS-CoV-2 seropositive healthcare workers (HCW) and c) seronegative HCW. The ultimate aim of this study is to identify biomarkers of humoral immunity that could be used to differentiate severe from mild or asymptomatic SARS-CoV-2 infections. Some of these biomarkers could be used to define CoP in further serological studies using samples from vaccination breakthrough and/or re-infection cases. Whenever suitable, the antibody levels of the samples studied were expressed in International Units (IU) for virus neutralisation assays or in Binding Antibody Units (BAU) for ELISA tests. In this work we used commercial and non-commercial antibody binding assays; a lateral flow test for detection of SARS-CoV-2-specific IgG/IgM; a high throughput multiplexed particle flow cytometry assay for SARS-CoV-2 Spike (S), Nucleocapsid (N) and Receptor Binding Domain (RBD) proteins); a multiplex antigen semi-automated immuno-blotting assay measuring IgM, IgA and IgG; a pseudotyped microneutralisation test (pMN) and an electroporation-dependent neutralisation assay (EDNA). Our results indicate that overall, severe COVID-19 patients showed statistically significantly higher levels of SARS-CoV-2-specific neutralising antibodies (average 1029 IU/ml) than those observed in seropositive HCW with mild or asymptomatic infections (379 IU/ml) and that clinical severity scoring, based on WHO guidelines was tightly correlated with neutralisation and RBD/S antibodies. In addition, there was a positive correlation between severity, N-antibody assays and intracellular virus neutralisation.

Author contribution: JC-O: Coordinating the laboratory work; analysis of results; conception of the manuscript; writing the manuscript. DW: Statistical analysis. MF: Semiautomated immunology-blotting; analysis of results. AC: ELISA, Lateral flow testing; sample processing; analysis off results; PS: Blood processing, samples archiving, ELISA testing. AN: ELISA set up; pseudo neutralisation assay. MiP: Laboratory set up; ELISA set up. LO: Semi-automated immunoblotting. DC: pseudoneutralization assays. MMN: pseudoneutralization assay. PP: Statistical analysis. NJT: pseudoneutralization. DP: Design constructs, expression and purification of recombinant RBD. **PN**: Design constructs, expression and purification of recombinant RBD. RW: Design constructs, expression and purification of

recombinant RBD. RD: Luminex assay. SK: Sample selection and provision pre-pandemic sera. AO: Electrochemiluminescence assays. AS: Electrochemiluminescence assays. AS: Electrochemiluminescence assays. TB: Electrochemiluminescence assays. AA: EDNA assay. LCJ: EDNA assay. MaP: Consultation on Standardization of serological assays. WS: Grant holder; assessing manuscript; scientific direction. HB: Clinical Lead; clinical assessment; coordination clinical work. JLH: Scientific direction.

Personal contribution: PN contributed to this publication by the supply of critical reagents. He designed expression constructs for the recombinant expression of the receptor-binding domain of SARS-CoV-2 Spike protein (RBD). PN further cloned the constructs, expressed the recombinant proteins in human cell culture, purified and quality-controlled the recombinant proteins by ELISA. These proteins were used to analyze RBD-binding antibodies in reconvalescent COVID-19 patients and SARS-CoV-2-positive and -negative health care workers.

9.1.3 Appendix publication 3

"Liposome-based high-throughput and point-of-care assays toward the quick, simple, and sensitive detection of neutralizing antibodies against SARS-CoV-2 in patient sera"

Authors: Simon Streif, **Patrick Neckermann**, Clemens Spitzenberg, Katharina Weiss, Kilian Hoecherl, Kacper Kulikowski, Sonja Hahner, Christina Noelting, Sebastian Einhauser, David Peterhoff, Claudia Asam, Ralf Wagner, and Antje J. Baeumner

Published on 9th of February 2023 in Analytical and Bioanalytical Chemistry

DOI: 10.1007/s00216-023-04548-3

Abstract: The emergence of severe acute respiratory syndrome-related coronavirus 2 (SARS-CoV-2) in 2019 caused an increased interest in neutralizing antibody tests to determine the immune status of the population. Standard live-virus-based neutralization assays such as plaque-reduction assays or pseudovirus neutralization tests cannot be adapted to the point-of-care (POC). Accordingly, tests quantifying competitive binding inhibition of the angiotensin-converting enzyme 2 (ACE2) receptor to the receptor-binding domain (RBD) of SARS-CoV-2 by neutralizing antibodies have been developed. Here, we present a new platform using sulforhodamine B encapsulating liposomes decorated with RBD as foundation for the development of both a fluorescent, highly feasible high-throughput (HTS) and a POC-ready neutralizing antibody assay. RBD-conjugated liposomes are incubated with serum and subsequently immobilized in an ACE2-coated plate or mixed with biotinylated ACE2 and used in test strip with streptavidin test line, respectively. Polyclonal neutralizing human antibodies were shown to cause complete binding inhibition, while S309 and CR3022 human monoclonal antibodies only caused partial inhibition, proving the functionality of the assay. Both formats, the HTS and POC assay, were then tested using 20 sera containing varying titers of neutralizing antibodies, and a control panel of sera including prepandemic sera and reconvalescent sera from respiratory infections other than SARS-CoV-2. Both assays correlated well with a standard pseudovirus neutralization test (r = 0.847 for HTS and r = 0.614 for POC format). Furthermore, excellent correlation (r = 0.868) between HTS and POC formats was observed. The flexibility afforded by liposomes as signaling agents using different dyes and sizes can hence be utilized in the future for a broad range of multianalyte neutralizing antibody diagnostics.

Author contribution: Conceptualization, AJB, RW, and SS; performed HTS experiments, SS; performed POC experiments, SS and KW; liposome synthesis and optimization, SS, KH, CS, KK; cloning of recombinant protein expression plasmids, **PN** and CA; expression, purification, and quality control of recombinant ACE2 and RBD, **PN**, CA, DP, SH; pseudovirus neutralization assays, SE; RBD binding antibody test, CN; writing — original draft, SS; writing — review and editing, SE, **PN**, RW, AJB.

Personal contribution: PN contributed to this publication by the supply of critical reagents, in particular antigens suitable for the immobilization on liposomes. For this, PN designed expression constructs for the recombinant expression of the SARS-CoV-2 receptor Angiotensin-converting-enzyme-2 (Ace2) and multiple variants of the receptor-binding domain of SARS-CoV-2 Spike protein (RBD) suitable for either side-specific or non-directional immobilization on particles. He further cloned the constructs, expressed the recombinant proteins in human cell culture, purified and quality-controlled the recombinant proteins regarding their antigenicity and accessibility of the domains used for immobilization by ELISA. These proteins were used for the development of a liposome-based assay to detect neutralizing antibodies against SARS-CoV-2.

9.1.4 Appendix publication 4

"Glycan masking of a non-neutralising epitope enhances neutralising antibodies targeting the RBD of SARS-CoV-2 and its variants"

Authors: George W Carnell, Martina Billmeier, Sneha Vishwanath, Maria Suau Sans, Hannah Wein, Charlotte L George, **Patrick Neckermann**, Joanne Marie M Del Rosario, Alexander T Sampson, Sebastian Einhauser, Ernest T Aguinam, Matteo Ferrari, Paul Tonks, Angalee Nadesalingam, Anja Schütz, Chloe Qingzhou Huang, David A Wells, Minna Paloniemi, Ingo Jordan, Diego Cantoni, David Peterhoff, Benedikt Asbach, Volker Sandig, Nigel Temperton, Rebecca Kinsley, Ralf Wagner, Jonathan L Heeney

Published on 23rd of February 2023 in Frontiers in Immunology

DOI: 10.3389/fimmu.2023.1118523

Abstract: The accelerated development of the first generation COVID-19 vaccines has saved millions of lives, and potentially more from the long-term sequelae of SARS-CoV-2 infection. The most successful vaccine candidates have used the full-length SARS-CoV-2 spike protein as an immunogen. As expected of RNA viruses, new variants have evolved and quickly replaced the original wild-type SARS-CoV-2, leading to escape from natural infection or vaccine induced immunity provided by the original SARS-CoV-2 spike sequence. Next generation vaccines that confer specific and targeted immunity to broadly neutralising epitopes on the SARS-CoV-2 spike protein against different variants of concern (VOC) offer an advance on current booster shots of previously used vaccines. Here, we present a targeted approach to elicit antibodies that neutralise both the ancestral SARS-CoV-2, and the VOCs, by introducing a specific glycosylation site on a non-neutralising epitope of the RBD. The addition of a specific glycosylation site in the RBD based vaccine candidate focused the immune response towards other broadly neutralising epitopes on the RBD. We further observed enhanced cross-neutralisation and cross-binding using a DNA-MVA CR19 prime-boost regime, thus demonstrating the superiority of the glycan engineered RBD vaccine candidate across two platforms and a promising candidate as a broad variant booster vaccine.

Author contribution: Conceptualization, JH, RW, RK. Data curation: GC, MB, SV. Investigation: GC, MB, SV, BA, JH, RK, RW. Methodology: GC, MB, SV, HW, AS, MSS, CG, JDR, ATS, AN, CH, DW, MF, MP, PT, DP. Critical reagents: SE, **PN**, DC, NT, IJ, VS. Project administration: JH, RW. Resources: JH, RW. Supervision: JH, RW, RK. Visualization: GC, MB, SV. Writing—original draft: GC, MB, SV. Writing—review and editing: GC, MB, SV, JH, RW, IJ.

Personal contribution: For this publication, PN supplied critical reagents to detect binding antibodies and distinguish between binding and neutralizing antibody titers. In order to develop vaccine candidates targeting not only the wild-type but also different virus variants (e.g. VOCs) and measuring their humoral immune responses, PN designed and cloned expression constructs for the recombinant expression of RBD proteins of different VOCs, e.g. alpha, beta, gamma, delta, omicron BA1. PN further expressed the recombinant VOC-RBD proteins in human cell culture, purified and quality-controlled the antigenicity of recombinant proteins by ELISA. These proteins were used for the evaluation of binding antibody responses in DNA vaccine vector-immunized mice, DNA-MVA-immunized mice, DNA-MVA-immunized mice pre- and post-challenge with SARS-CoV-2 live virus. These binding antibody titers were instrumental for the comparison of binding antibody titers with neutralization titers.

9.1.5 Appendix publication 5

"A computationally designed antigen eliciting broad humoral responses against SARS-CoV-2 and related sarbecoviruses"

Authors: Sneha Vishwanath, George William Carnell, Matteo Ferrari, Benedikt Asbach, Martina Billmeier, Charlotte George, Maria Suau Sans, Angalee Nadesalingam, Chloe Qingzhou Huang, Minna Paloniemi, Hazel Stewart, Andrew Chan, David Arthur Wells, **Patrick Neckermann**, David Peterhoff, Sebastian Einhauser, Diego Cantoni, Martin Mayora Neto, Ingo Jordan, Volker Sandig, Paul Tonks, Nigel Temperton, Simon Frost, Katharina Sohr, Maria Teresa Lluesma Ballesteros, Farzad Arbabi, Johannes Geiger, Christian Dohmen, Christian Plank, Rebecca Kinsley, Ralf Wagner, Jonathan Luke Heeney

Published on 25th September 2023 in Nature Biomedical Engineering

DOI: 10.1038/s41551-023-01094-2

Abstract: The threat of spillovers of coronaviruses associated with the severe acute respiratory syndrome (SARS) from animals to humans necessitates vaccines that offer broader protection from sarbecoviruses. By leveraging a viral-genome-informed computational method for selecting immune-optimized and structurally engineered antigens, here we show that a single antigen based on the receptor binding domain of the spike protein of sarbecoviruses elicits broad humoral responses against SARS-CoV-1, SARS-CoV-2, WIV16 and RaTG13 in mice, rabbits and guinea pigs. When administered as a DNA immunogen or by a vector based on a modified vaccinia virus Ankara, the optimized antigen induced vaccine protection from the Delta variant of SARS-CoV-2 in mice genetically engineered to express angiotensin-converting enzyme 2 and primed by a viral-vector vaccine (AZD1222) against SARS-CoV-2. A vaccine formulation incorporating mRNA coding for the optimized antigen further validated its broad immunogenicity. Vaccines that elicit broad immune responses across subgroups of coronaviruses may counteract the threat of zoonotic spillovers of betacoronaviruses.

Author contribution: S.V., D.A.W. and S.F. developed the computational pipeline. G.W.C., M.F., C.G., M.S.S., A.N., C.Q.H., M.P., H.S. and A.C. performed the *in vitro* assays. G.W.C. and P.T. performed the animal experiments. B.A., M.B., **P.N.**, D.P. and S.E. performed DNA purification and preparation. M.B., I.J. and V.S. performed MVA production and purification. K.S., M.T.L.B., F.A., J.G., C.D. and C.P. performed mRNA production and purification. D.C., M.M.N. and N.T. provided key reagents. S.V. and G.W.C. analysed and visualized the data. R.K., R.W. and J.L.H. acquired funding, conceptualized the investigation, reviewed data and administered the project. R.W. and J.L.H. supervised the project. S.V. wrote the original draft. S.V., G.W.C. and J.L.H. reviewed and edited the manuscript.

Personal contribution: PN contributed to this publication by the supply of critical reagents for the characterization of novel vaccine candidates against SARS-CoV-2 VOCs. PN purified LPS-free DNA vaccine vector constructs of novel SARS-CoV-2 antigens, computationally-designed to elicit broad antibody responses against multiple SARS-CoV-2 VOCs, for the immunization of BALB/c mice, guinea pigs and K18-hACE2 mice. Further, PN controlled the quality of the vaccine plasmids by restriction digests, sequencing and expression analysis.

9.2 List of Abbreviations

Ad	human adenovirus
AIN	anal intraepithelial neoplasia
APC	antigen-presenting cell
BM	basement membrane
BPV	bovine papillomavirus
Cdk	cyclin-dependent kinase
CEF	chicken embryonic fibroblasts
CIN	cervical intraepithelial neoplasia
CPI	checkpoint inhibitor
CTL	cytotoxic T lymphocyte
cycD	cyclin D
DC	dendritic cell
DelIII	deletion site III
DNA	deoxyribonucleic acid
DNMT	DNA methyltransferase
DRiPs	defective ribosomal products
EGFR	epidermal growth factor receptor
ELISA	enzyme-linked immunosorbent assay
ERAD	endoplasmic reticulum-associated protein degradation
GFP	green fluorescent protein
GLOBOCAN	global cancer observatory
GMP	good manufacturing procedure
HDAC	histone deacetylase
HIC	high-income country
HLA	human leukocyte antigen
HNC	heck and neck cancer
HPV	human papillomavirus
hrHPV	high-risk HPV
HSIL	high-grade squamous cell intraepithelial lesion
HSPG	heparin sulfate proteoglycan
IFN	interferon
IFU	infectious units
Ii	invariant chain
IL	interleukin
LCR	long control region
LMIC	low- and middle-income country
lrHPV	low-risk HPV
LSIL	low-grade squamous cell intraepithelial lesion
MDSC	myeloid-derived suppressor cell
MFI	mean fluorescence intensity
MfPV3	*Macaca fascicularis* papillomavirus type 3
MHC	major histocompatibility complex

MOI	moiety of infection
NGS	next-generation sequencing
NHP	non-human primate
OPSCC	oropharyngeal squamous cell cancer
ORF	open reading frame
ORI	origin of replication
PBMC	peripheral blood mononuclear cell
PD-1	programmed cell death 1
PIN	penile intraepithelial neoplasia
PML bodies	promyelocytic leukemia nuclear bodies
POC	point-of-care
pRb	retinoblastoma protein
PV	papillomavirus
pVNT	pseudovirus neutralization assay
rAd	adenoviral vector
RBD	receptor-binding-domain
rMVA	recombinant Modified Vaccinia virus Ankara
SARS-CoV-2	severe acute respiratory syndrome corona virus 2
SLP	synthetic long peptide
SOC	standard-of-care
TAA	tumor-associated antigen
TAM	tumor-associated macrophage
TCID50	tissue culture infectious dose 50
TetO	tetracycline operator
TetR	tetracycline repressor
TIL	tumor infiltrating lymphocyte
TK	thymidine kinase
TNF	tumor necrosis factor
Treg/T_{reg}	regulatory T cell
TSA	tumor-specific antigen
UPR	unfolded protein response
VaIN	vaginal intraepithelial neoplasia
VIN	vulvar intraepithelial neoplasia
VITT	vector-induced thrombotic thrombocytopenia
VLP	virus-like particle
VOC	variant of concern

9.3 References

1. zur Hausen H. Papillomaviruses and cancer: from basic studies to clinical application. *Nat Rev Cancer* (2002) 2:342–350. doi:10.1038/nrc798
2. de Villiers E-M. Cross-roads in the classification of papillomaviruses. *Virology* (2013) 445:2–10. doi:10.1016/j.virol.2013.04.023
3. Kjaer SK et al. High-risk human papillomavirus is sexually transmitted: evidence from a follow-up study of virgins starting sexual activity (intercourse). *Cancer Epidemiol biomarkers Prev a Publ Am Assoc Cancer Res cosponsored by Am Soc Prev Oncol* (2001) 10:101–106.
4. Winer RL et al. Genital human papillomavirus infection: incidence and risk factors in a cohort of female university students. *Am J Epidemiol* (2003) 157:218–226. doi:10.1093/aje/kwf180
5. Burchell AN et al. Epidemiology and transmission dynamics of genital HPV infection. *Vaccine* (2006) 24:S52–S61.
6. Chesson HW et al. The estimated lifetime probability of acquiring human papillomavirus in the United States. *Sex Transm Dis* (2014) 41:660–664. doi:10.1097/OLQ.0000000000000193
7. Walboomers JMM et al. Human papillomavirus is a necessary cause of invasive cervical cancer worldwide. *J Pathol* (1999) 189:12–19.
8. Doorbar J et al. The biology and life-cycle of human papillomaviruses. *Vaccine* (2012) 30 Suppl 5:F55-70. doi:10.1016/j.vaccine.2012.06.083
9. zur Hausen H. Papillomaviruses in the causation of human cancers - a brief historical account. *Virology* (2009) 384:260–265. doi:10.1016/j.virol.2008.11.046
10. Chen XS et al. Structure of small virus-like particles assembled from the L1 protein of human papillomavirus 16. *Mol Cell* (2000) 5:557–567. doi:10.1016/s1097-2765(00)80449-9
11. Schiller JT et al. Understanding and learning from the success of prophylactic human papillomavirus vaccines. *Nat Rev Microbiol* (2012) 10:681–692. doi:10.1038/nrmicro2872
12. Modis Y et al. Atomic model of the papillomavirus capsid. *EMBO J* (2002) 21:4754–4762. doi:10.1093/emboj/cdf494
13. Van Doorslaer K et al. ICTV Virus Taxonomy Profile: Papillomaviridae. *J Gen Virol* (2018) 99:989–990. doi:10.1099/jgv.0.001105
14. Rubio I et al. The N-terminal region of the human papillomavirus L2 protein contains overlapping binding sites for neutralizing, cross-neutralizing and non-neutralizing antibodies. *Virology* (2011) 409:348–359. doi:10.1016/j.virol.2010.10.017
15. Kines RC et al. The initial steps leading to papillomavirus infection occur on the basement membrane prior to cell surface binding. *Proc Natl Acad Sci U S A* (2009) 106:20458–20463. doi:10.1073/pnas.0908502106
16. Schwartz S. Papillomavirus transcripts and posttranscriptional regulation. *Virology* (2013) 445:187–196. doi:10.1016/j.virol.2013.04.034
17. Johansson C et al. Regulation of human papillomavirus gene expression by splicing and polyadenylation. *Nat Rev Microbiol* (2013) 11:239–251. doi:10.1038/nrmicro2984
18. Bravo IG et al. Papillomaviruses: Viral evolution, cancer and evolutionary medicine. *Evol Med Public Heal* (2015) 2015:32–51. doi:10.1093/emph/eov003
19. Kraberger S et al. Discovery of novel fish papillomaviruses: From the Antarctic to the commercial fish market. *Virology* (2022) 565:65–72. doi:10.1016/j.virol.2021.10.007
20. Antonsson A et al. Papillomavirus in healthy skin of Australian animals. *J Gen Virol* (2006) 87:3195–3200. doi:10.1099/vir.0.82195-0
21. Antonsson A et al. The ubiquity and impressive genomic diversity of human skin papillomaviruses suggest a commensalic nature of these viruses. *J Virol* (2000) 74:11636–11641. doi:10.1128/jvi.74.24.11636-11641.2000
22. Antonsson A et al. General acquisition of human papillomavirus infections of skin occurs in early infancy. *J Clin Microbiol* (2003) 41:2509–2514. doi:10.1128/JCM.41.6.2509-2514.2003
23. Duffy S et al. Rates of evolutionary change in viruses: patterns and determinants. *Nat Rev Genet* (2008) 9:267–276. doi:10.1038/nrg2323
24. Sanjuán R et al. Viral mutation rates. *J Virol* (2010) 84:9733–9748. doi:10.1128/JVI.00694-10
25. Doorslaer K Van. Evolution of the Papillomaviridae. *Virology* (2013) 445:11–20. doi:10.1016/j.virol.2013.05.012
26. de Villiers E-M et al. Classification of papillomaviruses. *Virology* (2004) 324:17–27. doi:10.1016/j.virol.2004.03.033
27. Bernard H-U et al. Classification of papillomaviruses (PVs) based on 189 PV types and proposal of taxonomic amendments. *Virology* (2010) 401:70–79. doi:10.1016/j.virol.2010.02.002
28. Bravo IG et al. Phylogeny and evolution of papillomaviruses based on the E1 and E2 proteins. *Virus Genes* (2007) 34:249–262. doi:10.1007/s11262-006-0017-4
29. de Sanjosé S et al. Worldwide prevalence and genotype distribution of cervical human papillomavirus DNA in women with normal cytology: a meta-analysis. *Lancet Infect Dis* (2007) 7:453–459. doi:10.1016/S1473-3099(07)70158-5
30. Bruni L et al. Cervical human papillomavirus prevalence in 5 continents: meta-analysis of 1 million women with normal cytological findings. *J Infect Dis* (2010) 202:1789–1799. doi:10.1086/657321
31. Kombe Kombe AJ et al. Epidemiology and Burden of Human Papillomavirus and Related Diseases, Molecular Pathogenesis, and Vaccine Evaluation. *Front public Heal* (2020) 8:552028. doi:10.3389/fpubh.2020.552028
32. Guan P et al. Human papillomavirus types in 115,789 HPV-positive women: a meta-analysis from cervical infection to cancer. *Int J cancer* (2012) 131:2349–2359. doi:10.1002/ijc.27485
33. Sung H et al. Global Cancer Statistics 2020: GLOBOCAN Estimates of Incidence and Mortality Worldwide for 36

Cancers in 185 Countries. *CA Cancer J Clin* (2021) 71:209–249. doi:https://doi.org/10.3322/caac.21660
34. Hull R et al. Cervical cancer in low and middle-income countries. *Oncol Lett* (2020) 20:2058–2074. doi:10.3892/ol.2020.11754
35. Chaturvedi AK et al. Human Papillomavirus and Rising Oropharyngeal Cancer Incidence in the United States. *J Clin Oncol* (2011) 29:4294–4301. doi:10.1200/JCO.2011.36.4596
36. de Martel C et al. Global burden of cancer attributable to infections in 2018: a worldwide incidence analysis. *Lancet Glob Heal* (2020) 8:e180–e190. doi:10.1016/S2214-109X(19)30488-7
37. Chaturvedi AK et al. Worldwide trends in incidence rates for oral cavity and oropharyngeal cancers. *J Clin Oncol Off J Am Soc Clin Oncol* (2013) 31:4550–4559. doi:10.1200/JCO.2013.50.3870
38. Lechner M et al. HPV-associated oropharyngeal cancer: epidemiology, molecular biology and clinical management. *Nat Rev Clin Oncol* (2022) 19:306–327. doi:10.1038/s41571-022-00603-7
39. Kreimer AR et al. Human papillomavirus types in head and neck squamous cell carcinomas worldwide: a systematic review. *Cancer Epidemiol Biomarkers Prev* (2005) 14:467–475.
40. Lechner M et al. Gender-neutral HPV vaccination in the UK, rising male oropharyngeal cancer rates, and lack of HPV awareness. *Lancet Infect Dis* (2019) 19:131–132. doi:10.1016/S1473-3099(18)30802-8
41. Faraji F et al. The prevalence of human papillomavirus in oropharyngeal cancer is increasing regardless of sex or race, and the influence of sex and race on survival is modified by human papillomavirus tumor status. *Cancer* (2019) 125:761–769. doi:10.1002/cncr.31841
42. Zwolinska K et al. Experimental Support for Human Papillomavirus Genome Amplification Early after Infectious Delivery. *J Virol* (2023) 97:e00214-23. doi:10.1128/jvi.00214-23
43. Middleton K et al. Organization of human papillomavirus productive cycle during neoplastic progression provides a basis for selection of diagnostic markers. *J Virol* (2003) 77:10186–10201. doi:10.1128/jvi.77.19.10186-10201.2003
44. Doorbar J. Molecular biology of human papillomavirus infection and cervical cancer. *Clin Sci* (2006) 110:525–541. doi:10.1042/CS20050369
45. Schiller JT et al. Current understanding of the mechanism of HPV infection. *Gynecol Oncol* (2010) 118:S12-7. doi:10.1016/j.ygyno.2010.04.004
46. Bienkowska-Haba M et al. Cyclophilins Facilitate Dissociation of the Human Papillomavirus Type 16 Capsid Protein L1 from the L2/DNA Complex following Virus Entry. *J Virol* (2012) 86:9875–9887. doi:10.1128/jvi.00980-12
47. Day PM et al. In vivo mechanisms of vaccine-induced protection against HPV infection. *Cell Host Microbe* (2010) 8:260–270. doi:10.1016/j.chom.2010.08.003
48. Day PM et al. Identification of a role for the trans-Golgi network in human papillomavirus 16 pseudovirus infection. *J Virol* (2013) 87:3862–3870. doi:10.1128/JVI.03222-12
49. Pyeon D et al. Establishment of human papillomavirus infection requires cell cycle progression. *PLoS Pathog* (2009) 5:e1000318. doi:10.1371/journal.ppat.1000318
50. Day PM et al. Establishment of papillomavirus infection is enhanced by promyelocytic leukemia protein (PML) expression. *Proc Natl Acad Sci U S A* (2004) 101:14252–14257. doi:10.1073/pnas.0404229101
51. Bienkowska-Haba M et al. Incoming human papillomavirus 16 genome is lost in PML protein-deficient HaCaT keratinocytes. *Cell Microbiol* (2017) 19: doi:10.1111/cmi.12708
52. Day PM et al. The papillomavirus minor capsid protein, L2, induces localization of the major capsid protein, L1, and the viral transcription/replication protein, E2, to PML oncogenic domains. *J Virol* (1998) 72:142–150. doi:10.1128/JVI.72.1.142-150.1998
53. Parish JL et al. ChlR1 is required for loading papillomavirus E2 onto mitotic chromosomes and viral genome maintenance. *Mol Cell* (2006) 24:867–876. doi:10.1016/j.molcel.2006.11.005
54. McBride AA. The papillomavirus E2 proteins. *Virology* (2013) 445:57–79. doi:10.1016/j.virol.2013.06.006
55. Bergvall M et al. The E1 proteins. *Virology* (2013) 445:35–56. doi:10.1016/j.virol.2013.07.020
56. Maglennon GA et al. Persistence of viral DNA in the epithelial basal layer suggests a model for papillomavirus latency following immune regression. *Virology* (2011) 414:153–163. doi:10.1016/j.virol.2011.03.019
57. You J et al. Interaction of the bovine papillomavirus E2 protein with Brd4 tethers the viral DNA to host mitotic chromosomes. *Cell* (2004) 117:349–360. doi:10.1016/s0092-8674(04)00402-7
58. Wang X et al. Recruitment of Brd4 to the human papillomavirus type 16 DNA replication complex is essential for replication of viral DNA. *J Virol* (2013) 87:3871–3884. doi:10.1128/JVI.03068-12
59. McBride AA et al. Multiple Roles of Brd4 in the Infectious Cycle of Human Papillomaviruses . *Front Mol Biosci* (2021) 8: Available at: https://www.frontiersin.org/articles/10.3389/fmolb.2021.725794
60. Medda A et al. Human Papillomavirus and Cellular Pathways: Hits and Targets. *Pathog (Basel, Switzerland)* (2021) 10: doi:10.3390/pathogens10030262
61. Lane DP. Cancer. p53, guardian of the genome. *Nature* (1992) 358:15–16. doi:10.1038/358015a0
62. Zilfou JT et al. Tumor suppressive functions of p53. *Cold Spring Harb Perspect Biol* (2009) 1:a001883. doi:10.1101/cshperspect.a001883
63. Krawczyk E et al. Koilocytosis: a cooperative interaction between the human papillomavirus E5 and E6 oncoproteins. *Am J Pathol* (2008) 173:682–688. doi:10.2353/ajpath.2008.080280
64. Doorbar J et al. Human papillomavirus molecular biology and disease association. *Rev Med Virol* (2015) 25 Suppl 1:2–23. doi:10.1002/rmv.1822
65. DiMaio D et al. The E5 proteins. *Virology* (2013) 445:99–114. doi:10.1016/j.virol.2013.05.006
66. Doorbar J. The E4 protein; structure, function and patterns of expression. *Virology* (2013) 445:80–98.

doi:10.1016/j.virol.2013.07.008
67. Wang Q et al. Functional analysis of the human papillomavirus type 16 E1=E4 protein provides a mechanism for in vivo and in vitro keratin filament reorganization. *J Virol* (2004) 78:821–833. doi:10.1128/jvi.78.2.821-833.2004
68. Doorbar J et al. Specific interaction between HPV-16 E1–E4 and cytokeratins results in collapse of the epithelial cell intermediate filament network. *Nature* (1991) 352:824–827. doi:10.1038/352824a0
69. Doorbar J. The papillomavirus life cycle. *J Clin Virol Off Publ Pan Am Soc Clin Virol* (2005) 32 Suppl 1:S7-15. doi:10.1016/j.jcv.2004.12.006
70. Johansson C et al. HPV-16 E2 contributes to induction of HPV-16 late gene expression by inhibiting early polyadenylation. *EMBO J* (2012) 31:3212–3227. doi:10.1038/emboj.2012.147
71. Roden RBS et al. Opportunities and challenges for human papillomavirus vaccination in cancer. *Nat Rev Cancer* (2018) 18:240–254. doi:10.1038/nrc.2018.13
72. Steinbach A et al. Immune evasion mechanisms of human papillomavirus: An update. *Int J Cancer* (2018) 142:224–229. doi:https://doi.org/10.1002/ijc.31027
73. Fields BN et al. *Fields virology*. 6th ed. Philadelphia SE -: Wolters Kluwer Health/Lippincott Williams & Wilkins Philadelphia (2013). doi:LK - https://worldcat.org/title/825740706
74. Hanahan D et al. Hallmarks of cancer: the next generation. *Cell* (2011) 144:646–674. doi:10.1016/j.cell.2011.02.013
75. Tomaić V et al. The stability of the human papillomavirus E6 oncoprotein is E6AP dependent. *Virology* (2009) 393:7–10. doi:10.1016/j.virol.2009.07.029
76. Pim D et al. Interaction of viral oncoproteins with cellular target molecules: infection with high-risk vs low-risk human papillomaviruses. *APMIS* (2010) 118:471–493. doi:10.1111/j.1600-0463.2010.02618.x
77. Werness BA et al. Association of human papillomavirus types 16 and 18 E6 proteins with p53. *Science* (1990) 248:76–79. doi:10.1126/science.2157286
78. Crook T et al. Degradation of p53 can be targeted by HPV E6 sequences distinct from those required for p53 binding and trans-activation. *Cell* (1991) 67:547–556. doi:10.1016/0092-8674(91)90529-8
79. Boyer SN et al. E7 protein of human papilloma virus-16 induces degradation of retinoblastoma protein through the ubiquitin-proteasome pathway. *Cancer Res* (1996) 56:4620–4624.
80. Münger K et al. Biological activities and molecular targets of the human papillomavirus E7 oncoprotein. *Oncogene* (2001) 20:7888–7898.
81. Galloway DA et al. Regulation of telomerase by human papillomaviruses. *Cold Spring Harb Symp Quant Biol* (2005) 70:209–215. doi:10.1101/sqb.2005.70.041
82. Gewin L et al. E box-dependent activation of telomerase by human papillomavirus type 16 E6 does not require induction of c-myc. *J Virol* (2001) 75:7198–7201. doi:10.1128/JVI.75.15.7198-7201.2001
83. Klingelhutz AJ et al. Telomerase activation by the E6 gene product of human papillomavirus type 16. *Nature* (1996) 380:79–82. doi:10.1038/380079a0
84. Veldman T et al. Transcriptional activation of the telomerase hTERT gene by human papillomavirus type 16 E6 oncoprotein. *J Virol* (2001) 75:4467–4472. doi:10.1128/JVI.75.9.4467-4472.2001
85. Elsum I et al. The Scribble-Dlg-Lgl polarity module in development and cancer: from flies to man. *Essays Biochem* (2012) 53:141–168. doi:10.1042/bse0530141
86. Koskimaa HM. *Human Papillomavirus Infections in Early Childhood – Immune Response and Disease Outcome in the Finnish*. (2016).
87. Kranjec C et al. A systematic analysis of human papillomavirus (HPV) E6 PDZ substrates identifies MAGI-1 as a major target of HPV type 16 (HPV-16) and HPV-18 whose loss accompanies disruption of tight junctions. *J Virol* (2011) 85:1757–1764. doi:10.1128/JVI.01756-10
88. Massimi P et al. Regulation of the hDlg/hScrib/Hugl-1 tumour suppressor complex. *Exp Cell Res* (2008) 314:3306–3317. doi:10.1016/j.yexcr.2008.08.016
89. Brehm A et al. The E7 oncoprotein associates with Mi2 and histone deacetylase activity to promote cell growth. *EMBO J* (1999) 18:2449–2458. doi:10.1093/emboj/18.9.2449
90. Nguyen DX et al. Human papillomavirus type 16 E7 maintains elevated levels of the cdc25A tyrosine phosphatase during deregulation of cell cycle arrest. *J Virol* (2002) 76:619–632. doi:10.1128/jvi.76.2.619-632.2002
91. McLaughlin-Drubin ME et al. Human papillomavirus E7 oncoprotein induces KDM6A and KDM6B histone demethylase expression and causes epigenetic reprogramming. *Proc Natl Acad Sci U S A* (2011) 108:2130–2135. doi:10.1073/pnas.1009933108
92. Roskoski RJ. The ErbB/HER family of protein-tyrosine kinases and cancer. *Pharmacol Res* (2014) 79:34–74. doi:10.1016/j.phrs.2013.11.002
93. Ashrafi GH et al. E5 protein of human papillomavirus 16 downregulates HLA class I and interacts with the heavy chain via its first hydrophobic domain. *Int J cancer* (2006) 119:2105–2112. doi:10.1002/ijc.22089
94. Campo MS et al. HPV-16 E5 down-regulates expression of surface HLA class I and reduces recognition by CD8 T cells. *Virology* (2010) 407:137–142. doi:https://doi.org/10.1016/j.virol.2010.07.044
95. McLaughlin-Drubin ME et al. The human papillomavirus E7 oncoprotein. *Virology* (2009) 384:335–344. doi:10.1016/j.virol.2008.10.006
96. Isaacson Wechsler E et al. Reconstruction of human papillomavirus type 16-mediated early-stage neoplasia implicates E6/E7 deregulation and the loss of contact inhibition in neoplastic progression. *J Virol* (2012) 86:6358–6364. doi:10.1128/JVI.07069-11
97. Nees M et al. Papillomavirus type 16 oncogenes downregulate expression of interferon-responsive genes and

upregulate proliferation-associated and NF-kappaB-responsive genes in cervical keratinocytes. *J Virol* (2001) 75:4283–4296. doi:10.1128/JVI.75.9.4283-4296.2001

98. Li S et al. The human papilloma virus (HPV)-18 E6 oncoprotein physically associates with Tyk2 and impairs Jak-STAT activation by interferon-alpha. *Oncogene* (1999) 18:5727–5737. doi:10.1038/sj.onc.1202960
99. Zhou F et al. Human papillomavirus 16-encoded E7 protein inhibits IFN-γ-mediated MHC class I antigen presentation and CTL-induced lysis by blocking IRF-1 expression in mouse keratinocytes. *J Gen Virol* (2013) 94:2504–2514. doi:10.1099/vir.0.054486-0
100. Schiller JT et al. A review of clinical trials of human papillomavirus prophylactic vaccines. *Vaccine* (2012) 30 Suppl 5:F123-38. doi:10.1016/j.vaccine.2012.04.108
101. Schiller J et al. Explanations for the high potency of HPV prophylactic vaccines. *Vaccine* (2018) 36:4768–4773. doi:10.1016/j.vaccine.2017.12.079
102. Katz J. The impact of HPV vaccination on the prevalence of oropharyngeal cancer (OPC) in a hospital-based population: A cross-sectional study of patient's registry. *J oral Pathol Med Off Publ Int Assoc Oral Pathol Am Acad Oral Pathol* (2021) 50:47–51. doi:10.1111/jop.13091
103. Bruni L et al. HPV vaccination introduction worldwide and WHO and UNICEF estimates of national HPV immunization coverage 2010–2019. *Prev Med (Baltim)* (2021) 144:106399. doi:https://doi.org/10.1016/j.ypmed.2020.106399
104. Spayne J et al. Estimate of global human papillomavirus vaccination coverage: analysis of country-level indicators. *BMJ Open* (2021) 11:e052016. doi:10.1136/bmjopen-2021-052016
105. Radisic G et al. Factors associated with parents' attitudes to the HPV vaccination of their adolescent sons : A systematic review. *Prev Med (Baltim)* (2017) 95:26–37. doi:10.1016/j.ypmed.2016.11.019
106. Sonawane K et al. Parental intent to initiate and complete the human papillomavirus vaccine series in the USA: a nationwide, cross-sectional survey. *Lancet Public Heal* (2020) 5:e484–e492.
107. Gottvall M et al. Parents' views of including young boys in the Swedish national school-based HPV vaccination programme: a qualitative study. *BMJ Open* (2017) 7:e014255.
108. Hildesheim A et al. Impact of human papillomavirus (HPV) 16 and 18 vaccination on prevalent infections and rates of cervical lesions after excisional treatment. *Am J Obstet Gynecol* (2016) 215:212.e1-212.e15. doi:10.1016/j.ajog.2016.02.021
109. Karimi-Zarchi M et al. Can the prophylactic quadrivalent HPV vaccine be used as a therapeutic agent in women with CIN? A randomized trial. *BMC Public Health* (2020) 20:274. doi:10.1186/s12889-020-8371-z
110. Gillison ML et al. Epidemiology of Human Papillomavirus-Positive Head and Neck Squamous Cell Carcinoma. *J Clin Oncol Off J Am Soc Clin Oncol* (2015) 33:3235–3242. doi:10.1200/JCO.2015.61.6995
111. Schiffman M et al. Chapter 2: Natural history of anogenital human papillomavirus infection and neoplasia. *J Natl Cancer Inst Monogr* (2003)14–19. doi:10.1093/oxfordjournals.jncimonographs.a003476
112. Kjær SK et al. Long-term absolute risk of cervical intraepithelial neoplasia grade 3 or worse following human papillomavirus infection: role of persistence. *J Natl Cancer Inst* (2010) 102:1478–1488. doi:10.1093/jnci/djq356
113. Steenbergen RDM et al. HPV-mediated transformation of the anogenital tract. *J Clin Virol* (2005) 32:25–33.
114. Peto J et al. The cervical cancer epidemic that screening has prevented in the UK. *Lancet* (2004) 364:249–256.
115. Jenkins D. Histopathology and cytopathology of cervical cancer. *Dis Markers* (2007) 23:199–212. doi:10.1155/2007/874795
116. Solomon D et al. The 2001 Bethesda System: terminology for reporting results of cervical cytology. *JAMA* (2002) 287:2114–2119. doi:10.1001/jama.287.16.2114
117. Crosbie EJ et al. Human papillomavirus and cervical cancer. *Lancet* (2013) 382:889–899. doi:10.1016/S0140-6736(13)60022-7
118. von Knebel Doeberitz M. New markers for cervical dysplasia to visualise the genomic chaos created by aberrant oncogenic papillomavirus infections. *Eur J Cancer* (2002) 38:2229–2242.
119. Ojesina AI et al. Landscape of genomic alterations in cervical carcinomas. *Nature* (2014) 506:371–375. doi:10.1038/nature12881
120. Vinokurova S et al. Differential methylation of the HPV 16 upstream regulatory region during epithelial differentiation and neoplastic transformation. *PLoS One* (2011) 6:e24451. doi:10.1371/journal.pone.0024451
121. Jeon S et al. Integration of human papillomavirus type 16 DNA into the human genome leads to increased stability of E6 and E7 mRNAs: implications for cervical carcinogenesis. *Proc Natl Acad Sci U S A* (1995) 92:1654–1658. doi:10.1073/pnas.92.5.1654
122. Marongiu L et al. Human Papillomavirus 16, 18, 31 and 45 viral load, integration and methylation status stratified by cervical disease stage. *BMC Cancer* (2014) 14:384. doi:10.1186/1471-2407-14-384
123. Vinokurova S et al. Type-Dependent Integration Frequency of Human Papillomavirus Genomes in Cervical Lesions. *Cancer Res* (2008) 68:307–313. doi:10.1158/0008-5472.CAN-07-2754
124. Fehrmann F et al. Human papillomaviruses: targeting differentiating epithelial cells for malignant transformation. *Oncogene* (2003) 22:5201–5207. doi:10.1038/sj.onc.1206554
125. Badaracco G et al. HPV16 and HPV18 in genital tumors: Significantly different levels of viral integration and correlation to tumor invasiveness. *J Med Virol* (2002) 67:574–582. doi:10.1002/jmv.10141
126. Woodman CBJ et al. Human papillomavirus type 18 and rapidly progressing cervical intraepithelial neoplasia. *Lancet (London, England)* (2003) 361:40–43. doi:10.1016/S0140-6736(03)12120-4
127. Cullen AP et al. Analysis of the physical state of different human papillomavirus DNAs in intraepithelial and invasive cervical neoplasm. *J Virol* (1991) 65:606–612. doi:10.1128/JVI.65.2.606-612.1991

128. Matsukura T et al. Both episomal and integrated forms of human papillomavirus type 16 are involved in invasive cervical cancers. *Virology* (1989) 172:63–72. doi:10.1016/0042-6822(89)90107-4
129. Pett M et al. Integration of high-risk human papillomavirus: a key event in cervical carcinogenesis? *J Pathol* (2007) 212:356–367. doi:10.1002/path.2192
130. Moscicki A-B et al. Updating the natural history of human papillomavirus and anogenital cancers. *Vaccine* (2012) 30 Suppl 5:F24-33. doi:10.1016/j.vaccine.2012.05.089
131. Salcedo MP et al. "29 - Intraepithelial neoplasia of the lower genital tract (cervix, vagina, vulva): Etiology, Screening, Diagnosis, Management," in, ed. D. M. Gershenson (St. Louis (MO): Elsevier), 637-647.e2. doi:https://doi.org/10.1016/B978-0-323-65399-2.00038-3
132. Pan C et al. HPV-driven oropharyngeal cancer: current knowledge of molecular biology and mechanisms of carcinogenesis. *Cancers Head Neck* (2018) 3:12. doi:10.1186/s41199-018-0039-3
133. Gelwan E et al. Nonuniform Distribution of High-risk Human Papillomavirus in Squamous Cell Carcinomas of the Oropharynx: Rethinking the Anatomic Boundaries of Oral and Oropharyngeal Carcinoma From an Oncologic HPV Perspective. *Am J Surg Pathol* (2017) 41: Available at: https://journals.lww.com/ajsp/fulltext/2017/12000/nonuniform_distribution_of_high_risk_human.14.aspx
134. Parfenov M et al. Characterization of HPV and host genome interactions in primary head and neck cancers. *Proc Natl Acad Sci U S A* (2014) 111:15544–15549. doi:10.1073/pnas.1416074111
135. Arias-Pulido H et al. Human Papillomavirus Type 16 Integration in Cervical Carcinoma In Situ and in Invasive Cervical Cancer. *J Clin Microbiol* (2006) 44:1755–1762. doi:10.1128/JCM.44.5.1755-1762.2006
136. Morgan I et al. Integration of Human Papillomavirus Genomes in Head and Neck Cancer: Is It Time to Consider a Paradigm Shift? *Viruses* (2017) 9:208. doi:10.3390/v9080208
137. Nulton TJ et al. Analysis of The Cancer Genome Atlas sequencing data reveals novel properties of the human papillomavirus 16 genome in head and neck squamous cell carcinoma. *Oncotarget* (2017) 8:17684–17699. doi:10.18632/oncotarget.15179
138. Ostör AG. Natural history of cervical intraepithelial neoplasia: a critical review. *Int J Gynecol Pathol Off J Int Soc Gynecol Pathol* (1993) 12:186–192.
139. Herrero R et al. Population-based study of human papillomavirus infection and cervical neoplasia in rural Costa Rica. *J Natl Cancer Inst* (2000) 92:464–474. doi:10.1093/jnci/92.6.464
140. McCredie MRE et al. Natural history of cervical neoplasia and risk of invasive cancer in women with cervical intraepithelial neoplasia 3: a retrospective cohort study. *Lancet Oncol* (2008) 9:425–434. doi:10.1016/S1470-2045(08)70103-7
141. Schiffman M et al. A population-based prospective study of carcinogenic human papillomavirus variant lineages, viral persistence, and cervical neoplasia. *Cancer Res* (2010) 70:3159–3169. doi:10.1158/0008-5472.CAN-09-4179
142. Senba M et al. Mechanisms of virus immune evasion lead to development from chronic inflammation to cancer formation associated with human papillomavirus infection. *Oncol Rev* (2012) 6:e17. doi:10.4081/oncol.2012.e17
143. Nicholls PK et al. Naturally occurring, nonregressing canine oral papillomavirus infection: host immunity, virus characterization, and experimental infection. *Virology* (1999) 265:365–374. doi:10.1006/viro.1999.0060
144. Nicholls PK et al. Regression of canine oral papillomas is associated with infiltration of CD4+ and CD8+ lymphocytes. *Virology* (2001) 283:31–39. doi:10.1006/viro.2000.0789
145. Wilgenburg BJ et al. Characterization of immune responses during regression of rabbit oral papillomavirus infections. *Comp Med* (2005) 55:431–439.
146. Nakagawa M et al. Persistence of human papillomavirus type 16 infection is associated with lack of cytotoxic T lymphocyte response to the E6 antigens. *J Infect Dis* (2000) 182:595–598. doi:10.1086/315706
147. Nakagawa M et al. Cytotoxic T lymphocyte responses to E6 and E7 proteins of human papillomavirus type 16: relationship to cervical intraepithelial neoplasia. *J Infect Dis* (1997) 175:927–931. doi:10.1086/513992
148. Steele JC et al. T-cell responses to human papillomavirus type 16 among women with different grades of cervical neoplasia. *Br J Cancer* (2005) 93:248–259. doi:10.1038/sj.bjc.6602679
149. Dillon S et al. Resolution of cervical dysplasia is associated with T-cell proliferative responses to human papillomavirus type 16 E2. *J Gen Virol* (2007) 88:803–813. doi:10.1099/vir.0.82678-0
150. Woo YL et al. A prospective study on the natural course of low-grade squamous intraepithelial lesions and the presence of HPV16 E2-, E6- and E7-specific T-cell responses. *Int J cancer* (2010) 126:133–141. doi:10.1002/ijc.24804
151. de Jong A et al. Frequent detection of human papillomavirus 16 E2-specific T-helper immunity in healthy subjects. *Cancer Res* (2002) 62:472–479.
152. de Jong A et al. Human Papillomavirus Type 16-Positive Cervical Cancer Is Associated with Impaired CD4+ T-Cell Immunity against Early Antigens E2 and E6. *Cancer Res* (2004) 64:5449 LP – 5455. doi:10.1158/0008-5472.CAN-04-0831
153. Welters MJP et al. Frequent display of human papillomavirus type 16 E6-specific memory t-Helper cells in the healthy population as witness of previous viral encounter. *Cancer Res* (2003) 63:636–641.
154. Jacobelli S et al. Anti-HPV16 E2 protein T-cell responses and viral control in women with usual vulvar intraepithelial neoplasia and their healthy partners. *PLoS One* (2012) 7:e36651. doi:10.1371/journal.pone.0036651
155. Ghosh AK et al. Tumour-infiltrating lymphocytes in cervical carcinoma. *Eur J Cancer* (1992) 28A:1910–1916. doi:10.1016/0959-8049(92)90034-y
156. Ohno A et al. Tumor-infiltrating lymphocytes predict survival outcomes in patients with cervical cancer treated with concurrent chemoradiotherapy. *Gynecol Oncol* (2020) 159:329–334. doi:10.1016/j.ygyno.2020.07.106

157. de Vos van Steenwijk PJ et al. Tumor-infiltrating CD14-positive myeloid cells and CD8-positive T-cells prolong survival in patients with cervical carcinoma. *Int J cancer* (2013) 133:2884–2894. doi:10.1002/ijc.28309
158. Santegoets SJ et al. The Anatomical Location Shapes the Immune Infiltrate in Tumors of Same Etiology and Affects Survival. *Clin cancer Res an Off J Am Assoc Cancer Res* (2019) 25:240–252. doi:10.1158/1078-0432.CCR-18-1749
159. Masterson L et al. CD8(+) T cell response to human papillomavirus 16 E7 is able to predict survival outcome in oropharyngeal cancer. *Eur J Cancer* (2016) 67:141–151. doi:10.1016/j.ejca.2016.08.012
160. Welters MJP et al. Intratumoral HPV16-Specific T Cells Constitute a Type I-Oriented Tumor Microenvironment to Improve Survival in HPV16-Driven Oropharyngeal Cancer. *Clin cancer Res an Off J Am Assoc Cancer Res* (2018) 24:634–647. doi:10.1158/1078-0432.CCR-17-2140
161. Yan F et al. Therapeutic Vaccination for HPV-Mediated Cancers. *Curr Otorhinolaryngol Rep* (2023) 11:44–61. doi:10.1007/s40136-023-00443-8
162. Slifka MK et al. Role of Multivalency and Antigenic Threshold in Generating Protective Antibody Responses. *Front Immunol* (2019) 10:956. doi:10.3389/fimmu.2019.00956
163. van der Burg SH et al. Therapeutic vaccination against human papilloma virus induced malignancies. *Curr Opin Immunol* (2011) 23:252–257. doi:https://doi.org/10.1016/j.coi.2010.12.010
164. Dudley ME et al. Adoptive transfer of cloned melanoma-reactive T lymphocytes for the treatment of patients with metastatic melanoma. *J Immunother* (2001) 24:363–373. doi:10.1097/00002371-200107000-00012
165. Borst J et al. CD4(+) T cell help in cancer immunology and immunotherapy. *Nat Rev Immunol* (2018) 18:635–647. doi:10.1038/s41577-018-0044-0
166. Boilesen DR et al. Novel Antigenic Targets of HPV Therapeutic Vaccines. *Vaccines* (2021) 9:1262. doi:10.3390/vaccines9111262
167. Vokes EE et al. HPV-Associated Head and Neck Cancer. *J Natl Cancer Inst* (2015) 107:djv344. doi:10.1093/jnci/djv344
168. Singh A et al. LEEP Verses Cryotherapy in CIN. *J Obstet Gynaecol India* (2011) 61:431–435. doi:10.1007/s13224-011-0048-1
169. Cai S et al. Effectiveness and Safety of Therapeutic Vaccines for Precancerous Cervical Lesions: A Systematic Review and Meta-Analysis . *Front Oncol* (2022) 12: Available at: https://www.frontiersin.org/articles/10.3389/fonc.2022.918331
170. Kyrgiou M et al. Adverse obstetric outcomes after local treatment for cervical preinvasive and early invasive disease according to cone depth: systematic review and meta-analysis. *BMJ* (2016) 354: doi:10.1136/bmj.i3633
171. Kyrgiou M et al. Fertility and early pregnancy outcomes after treatment for cervical intraepithelial neoplasia: systematic review and meta-analysis. *BMJ* (2014) 349:g6192. doi:10.1136/bmj.g6192
172. Martin-Hirsch PPL PE et al. Surgery for cervical intraepithelial neoplasia. *Cochrane Database Syst Rev* (1999) doi:10.1002/14651858.CD001318
173. Magaldi TG et al. Primary human cervical carcinoma cells require human papillomavirus E6 and E7 expression for ongoing proliferation. *Virology* (2012) 422:114–124. doi:10.1016/j.virol.2011.10.012
174. Santegoets SJ et al. The common HLA class I-restricted tumor-infiltrating T cell response in HPV16-induced cancer. *Cancer Immunol Immunother* (2023) 72:1553–1565. doi:10.1007/s00262-022-03350-x
175. Kenter GG et al. Vaccination against HPV-16 oncoproteins for vulvar intraepithelial neoplasia. *N Engl J Med* (2009) 361:1838–1847. doi:10.1056/NEJMoa0810097
176. Kenter GG et al. Phase I immunotherapeutic trial with long peptides spanning the E6 and E7 sequences of high-risk human papillomavirus 16 in end-stage cervical cancer patients shows low toxicity and robust immunogenicity. *Clin cancer Res an Off J Am Assoc Cancer Res* (2008) 14:169–177. doi:10.1158/1078-0432.CCR-07-1881
177. Münger K et al. Mechanisms of human papillomavirus-induced oncogenesis. *J Virol* (2004) 78:11451–11460. doi:10.1128/JVI.78.21.11451-11460.2004
178. Stevanović S et al. Landscape of immunogenic tumor antigens in successful immunotherapy of virally induced epithelial cancer. *Science* (2017) 356:200–205. doi:10.1126/science.aak9510
179. Romanczuk H et al. Disruption of either the E1 or the E2 regulatory gene of human papillomavirus type 16 increases viral immortalization capacity. *Proc Natl Acad Sci U S A* (1992) 89:3159–3163. doi:10.1073/pnas.89.7.3159
180. Balaji H et al. Causes and Consequences of HPV Integration in Head and Neck Squamous Cell Carcinomas: State of the Art. *Cancers (Basel)* (2021) 13: doi:10.3390/cancers13164089
181. Anderson KS et al. Biologic predictors of serologic responses to HPV in oropharyngeal cancer: The HOTSPOT study. *Oral Oncol* (2015) 51:751–758. doi:10.1016/j.oraloncology.2015.05.007
182. Gleber-Netto FO et al. Variations in HPV function are associated with survival in squamous cell carcinoma. *JCI insight* (2019) 4: doi:10.1172/jci.insight.124762
183. Krishna S et al. Human Papilloma Virus Specific Immunogenicity and Dysfunction of CD8(+) T Cells in Head and Neck Cancer. *Cancer Res* (2018) 78:6159–6170. doi:10.1158/0008-5472.CAN-18-0163
184. Anayannis N V et al. Association of an intact E2 gene with higher HPV viral load, higher viral oncogene expression, and improved clinical outcome in HPV16 positive head and neck squamous cell carcinoma. *PLoS One* (2018) 13:e0191581. doi:10.1371/journal.pone.0191581
185. Ramqvist T et al. Studies on human papillomavirus (HPV) 16 E2, E5 and E7 mRNA in HPV-positive tonsillar and base of tongue cancer in relation to clinical outcome and immunological parameters. *Oral Oncol* (2015) 51:1126–1131. doi:10.1016/j.oraloncology.2015.09.007
186. Ren S et al. HPV E2, E4, E5 drive alternative carcinogenic pathways in HPV positive cancers. *Oncogene* (2020) 39:6327–6339. doi:10.1038/s41388-020-01431-8

187. Ma M et al. Human papilloma virus E1-specific T cell immune response is associated with the prognosis of cervical cancer patients with squamous cell carcinoma. *Infect Agent Cancer* (2018) 13:35. doi:10.1186/s13027-018-0206-5
188. Bhatt KH et al. Profiling HPV-16-specific T cell responses reveals broad antigen reactivities in oropharyngeal cancer patients. *J Exp Med* (2020) 217: doi:10.1084/jem.20200389
189. Eberhardt CS et al. Functional HPV-specific PD-1(+) stem-like CD8 T cells in head and neck cancer. *Nature* (2021) 597:279–284. doi:10.1038/s41586-021-03862-z
190. McInnis C et al. Identification of HPV16 E1 and E2-specific T cells in the oropharyngeal cancer tumor microenvironment. *J Immunother cancer* (2023) 11: doi:10.1136/jitc-2023-006721
191. Peng X et al. Novel canonical and non-canonical viral antigens extend current targets for immunotherapy of HPV-driven cervical cancer. *iScience* (2023) 26:106101. doi:10.1016/j.isci.2023.106101
192. Hancock G et al. A multi-genotype therapeutic human papillomavirus vaccine elicits potent T cell responses to conserved regions of early proteins. *Sci Rep* (2019) 9:1–12. doi:10.1038/s41598-019-55014-z
193. Doorbar J. Model systems of human papillomavirus-associated disease. *J Pathol* (2016) 238:166–179. doi:10.1002/path.4656
194. Lin K-Y et al. Treatment of Established Tumors with a Novel Vaccine That Enhances Major Histocompatibility Class II Presentation of Tumor Antigen1. *Cancer Res* (1996) 56:21–26.
195. Feltkamp MC et al. Vaccination with cytotoxic T lymphocyte epitope-containing peptide protects against a tumor induced by human papillomavirus type 16-transformed cells. *Eur J Immunol* (1993) 23:2242–9. doi:10.1002/eji.1830230929
196. Wood CE et al. Characterization and Experimental Transmission of an Oncogenic Papillomavirus in Female Macaques. *J Virol* (2007) 81:6339–6345. doi:10.1128/jvi.00233-07
197. Ragonnaud E et al. Breadth of T Cell Responses After Immunization with Adenovirus Vectors Encoding Ancestral Antigens or Polyvalent Papillomavirus Antigens. *Scand J Immunol* (2017) 85:182–190. doi:10.1111/sji.12522
198. Chen Z et al. Non-human Primate Papillomaviruses Share Similar Evolutionary Histories and Niche Adaptation as the Human Counterparts. *Front Microbiol* (2019) 10:2093. doi:10.3389/fmicb.2019.02093
199. Chen Z et al. Genomic diversity and interspecies host infection of alpha12 Macaca fascicularis papillomaviruses (MfPVs). *Virology* (2009) 393:304–310. doi:10.1016/j.virol.2009.07.012
200. Wood CE et al. Cervical and vaginal epithelial neoplasms in cynomolgus monkeys. *Vet Pathol* (2004) 41:108–115. doi:10.1354/vp.41-2-108
201. Ragonnaud E et al. Therapeutic Vaccine Against Primate Papillomavirus Infections of the Cervix. *J Immunother* (2017) 40:51–61. Available at: http://beats.bio.d.ac.uk/Tracer
202. Malcles M-H et al. Regulation of bovine papillomavirus replicative helicase e1 by the ubiquitin-proteasome pathway. *J Virol* (2002) 76:11350–11358. doi:10.1128/jvi.76.22.11350-11358.2002
203. Mechali F et al. Bovine papillomavirus replicative helicase E1 is a target of the ubiquitin ligase APC. *J Virol* (2004) 78:2615–2619. doi:10.1128/jvi.78.5.2615-2619.2004
204. Kedl RM et al. T cells compete for access to antigen-bearing antigen-presenting cells. *J Exp Med* (2000) 192:1105–1113. doi:10.1084/jem.192.8.1105
205. Kedl RM et al. Epitope dominance, competition and T cell affinity maturation. *Curr Opin Immunol* (2003) 15:120–127. doi:https://doi.org/10.1016/S0952-7915(02)00009-2
206. Akram A et al. Immunodominance: A pivotal principle in host response to viral infections. *Clin Immunol* (2012) 143:99–115. doi:https://doi.org/10.1016/j.clim.2012.01.015
207. Lauer KB et al. Multivalent and Multipathogen Viral Vector Vaccines. *Clin Vaccine Immunol* (2017) 24: doi:10.1128/CVI.00298-16
208. Spier RE. Multivalent vaccines: prospects and challenges. *Folia Microbiol (Praha)* (1997) 42:105–112. doi:10.1007/BF02898716
209. Fontham ETH et al. Cervical cancer screening for individuals at average risk: 2020 guideline update from the American Cancer Society. *CA Cancer J Clin* (2020) 70:321–346. doi:10.3322/caac.21628
210. Perkins RB et al. 2019 ASCCP Risk-Based Management Consensus Guidelines for Abnormal Cervical Cancer Screening Tests and Cancer Precursors. *J Low Genit Tract Dis* (2020) 24:102–131. doi:10.1097/LGT.0000000000000525
211. Rijkaart DC et al. Human papillomavirus testing for the detection of high-grade cervical intraepithelial neoplasia and cancer: final results of the POBASCAM randomised controlled trial. *Lancet Oncol* (2012) 13:78–88. doi:10.1016/S1470-2045(11)70296-0
212. Nkwabong E et al. Pap smear accuracy for the diagnosis of cervical precancerous lesions. *Trop Doct* (2019) 49:34–39. doi:10.1177/0049475518798532
213. Facciolà A et al. An Overview of Vaccine Adjuvants: Current Evidence and Future Perspectives. *Vaccines* (2022) 10: doi:10.3390/vaccines10050819
214. Scheerlinck J-PY. Genetic adjuvants for DNA vaccines. *Vaccine* (2001) 19:2647–2656. doi:https://doi.org/10.1016/S0264-410X(00)00495-3
215. Kobiyama K et al. Innate Immune Signaling by, and Genetic Adjuvants for DNA Vaccination. *Vaccines* (2013) 1:278–292. doi:10.3390/vaccines1030278
216. Lopes A et al. Cancer DNA vaccines: current preclinical and clinical developments and future perspectives. *J Exp Clin Cancer Res* (2019) 38:146. doi:10.1186/s13046-019-1154-7
217. Ragonnaud E et al. The rationale of vectored gene-fusion vaccines against cancer: evolving strategies and latest evidence. *Ther Adv vaccines* (2013) 1:33–47. doi:10.1177/2051013613480446

218. Holst PJ et al. MHC Class II-Associated Invariant Chain Linkage of Antigen Dramatically Improves Cell-Mediated Immunity Induced by Adenovirus Vaccines. *J Immunol* (2008) 180:3339–3346. doi:10.4049/jimmunol.180.5.3339
219. Capone S et al. Fusion of HCV nonstructural antigen to MHC class II-associated invariant chain enhances T-cell responses induced by vectored vaccines in nonhuman primates. *Mol Ther* (2014) 22:1039–1047. doi:10.1038/mt.2014.15
220. Esposito I et al. MHC class II invariant chain-adjuvanted viral vectored vaccines enhances T cell responses in humans. *Sci Transl Med* (2020) 12:eaaz7715. doi:10.1126/scitranslmed.aaz7715
221. Fougeroux C et al. Modified MHC Class II–Associated Invariant Chain Induces Increased Antibody Responses against Plasmodium falciparum Antigens after Adenoviral Vaccination . *J Immunol* (2019) 202:2320–2331. doi:10.4049/jimmunol.1801210
222. Holst PJ et al. Vaccination against Lymphocytic Choriomeningitis Virus Infection in MHC Class II-Deficient Mice. *J Immunol* (2011) 186:3997–4007. doi:10.4049/jimmunol.1001251
223. Hobbs SJ et al. Vaccinia Virus Vectors Targeting Peptides for MHC Class II Presentation to CD4(+) T Cells. *ImmunoHorizons* (2020) 4:1–13. doi:10.4049/immunohorizons.1900070
224. Akhatova A et al. The Efficacy of Therapeutic DNA Vaccines Expressing the Human Papillomavirus E6 and E7 Oncoproteins for Treatment of Cervical Cancer: Systematic Review. *Vaccines* (2021) 10: doi:10.3390/vaccines10010053
225. Travieso T et al. The use of viral vectors in vaccine development. *npj Vaccines* (2022) 7:75. doi:10.1038/s41541-022-00503-y
226. Larocca C et al. Viral vector-based therapeutic cancer vaccines. *Cancer J* (2011) 17:359–371. doi:10.1097/PPO.0b013e3182325e63
227. Wang S et al. Viral vectored vaccines: design, development, preventive and therapeutic applications in human diseases. *Signal Transduct Target Ther* (2023) 8:149. doi:10.1038/s41392-023-01408-5
228. McDonald I et al. Comparative systematic review and meta-analysis of reactogenicity, immunogenicity and efficacy of vaccines against SARS-CoV-2. *NPJ vaccines* (2021) 6:74. doi:10.1038/s41541-021-00336-1
229. Wold WSM et al. Adenovirus vectors for gene therapy, vaccination and cancer gene therapy. *Curr Gene Ther* (2013) 13:421–433. doi:10.2174/15665232133666131125095046
230. Sallard E et al. The Adenovirus Vector Platform: Novel Insights into Rational Vector Design and Lessons Learned from the COVID-19 Vaccine. *Viruses* (2023) 15: doi:10.3390/v15010204
231. Liu J et al. Magnitude and phenotype of cellular immune responses elicited by recombinant adenovirus vectors and heterologous prime-boost regimens in rhesus monkeys. *J Virol* (2008) 82:4844–4852. doi:10.1128/JVI.02616-07
232. Hillgenberg M et al. System for efficient helper-dependent minimal adenovirus construction and rescue. *Hum Gene Ther* (2001) 12:643–657. doi:10.1089/104303401300057342
233. Harvey B-G et al. Safety of local delivery of low- and intermediate-dose adenovirus gene transfer vectors to individuals with a spectrum of morbid conditions. *Hum Gene Ther* (2002) 13:15–63. doi:10.1089/10430340152712638
234. Zheng C et al. Genomic integration and gene expression by a modified adenoviral vector. *Nat Biotechnol* (2000) 18:176–180. doi:10.1038/72628
235. Ruzsics Z et al. “Engineering Adenovirus Genome by Bacterial Artificial Chromosome (BAC) Technology BT - Adenovirus: Methods and Protocols,” in, ed. M. Chillón (Totowa, NJ: Humana Press), 143–158. doi:10.1007/978-1-62703-679-5_11
236. Mast TC et al. International epidemiology of human pre-existing adenovirus (Ad) type-5, type-6, type-26 and type-36 neutralizing antibodies: correlates of high Ad5 titers and implications for potential HIV vaccine trials. *Vaccine* (2010) 28:950–957. doi:10.1016/j.vaccine.2009.10.145
237. Barouch DH et al. International seroepidemiology of adenovirus serotypes 5, 26, 35, and 48 in pediatric and adult populations. *Vaccine* (2011) 29:5203–5209. doi:10.1016/j.vaccine.2011.05.025
238. Mastrangeli A et al. “Sero-switch” adenovirus-mediated in vivo gene transfer: circumvention of anti-adenovirus humoral immune defenses against repeat adenovirus vector administration by changing the adenovirus serotype. *Hum Gene Ther* (1996) 7:79–87. doi:10.1089/hum.1996.7.1-79
239. Bergelson JM et al. Isolation of a common receptor for Coxsackie B viruses and adenoviruses 2 and 5. *Science* (1997) 275:1320–1323. doi:10.1126/science.275.5304.1320
240. Milligan ID et al. Safety and Immunogenicity of Novel Adenovirus Type 26- and Modified Vaccinia Ankara-Vectored Ebola Vaccines: A Randomized Clinical Trial. *JAMA* (2016) 315:1610–1623. doi:10.1001/jama.2016.4218
241. Kelly C et al. Chronic hepatitis C viral infection subverts vaccine-induced T-cell immunity in humans. *Hepatology* (2016) 63:1455–1470. doi:10.1002/hep.28294
242. Nyombayire J et al. First-in-Human Evaluation of the Safety and Immunogenicity of an Intranasally Administered Replication-Competent Sendai Virus-Vectored HIV Type 1 Gag Vaccine: Induction of Potent T-Cell or Antibody Responses in Prime-Boost Regimens. *J Infect Dis* (2017) 215:95–104. doi:10.1093/infdis/jiw500
243. Penaloza-MacMaster P et al. Alternative serotype adenovirus vaccine vectors elicit memory T cells with enhanced anamnestic capacity compared to Ad5 vectors. *J Virol* (2013) 87:1373–1384. doi:10.1128/JVI.02058-12
244. Nébié I et al. Assessment of chimpanzee adenovirus serotype 63 neutralizing antibodies prior to evaluation of a candidate malaria vaccine regimen based on viral vectors. *Clin Vaccine Immunol* (2014) 21:901–903. doi:10.1128/CVI.00723-13
245. Ersching J et al. Neutralizing antibodies to human and simian adenoviruses in humans and New-World monkeys.

Virology (2010) 407:1–6. doi:10.1016/j.virol.2010.07.043
246. Ledgerwood JE et al. Chimpanzee Adenovirus Vector Ebola Vaccine. *N Engl J Med* (2017) 376:928–938. doi:10.1056/NEJMoa1410863
247. Sadoff J et al. Safety and Efficacy of Single-Dose Ad26.COV2.S Vaccine against Covid-19. *N Engl J Med* (2021) 384:2187–2201. doi:10.1056/NEJMoa2101544
248. Falsey AR et al. Phase 3 Safety and Efficacy of AZD1222 (ChAdOx1 nCoV-19) Covid-19 Vaccine. *N Engl J Med* (2021) 385:2348–2360. doi:10.1056/NEJMoa2105290
249. Logunov DY et al. Safety and efficacy of an rAd26 and rAd5 vector-based heterologous prime-boost COVID-19 vaccine: an interim analysis of a randomised controlled phase 3 trial in Russia. *Lancet (London, England)* (2021) 397:671–681. doi:10.1016/S0140-6736(21)00234-8
250. Zhou X et al. Analysis of human adenovirus type 19 associated with epidemic keratoconjunctivitis and its reclassification as adenovirus type 64. *Invest Ophthalmol Vis Sci* (2012) 53:2804–2811. doi:10.1167/iovs.12-9656
251. Vogels R et al. Replication-deficient human adenovirus type 35 vectors for gene transfer and vaccination: efficient human cell infection and bypass of preexisting adenovirus immunity. *J Virol* (2003) 77:8263–8271. doi:10.1128/jvi.77.15.8263-8271.2003
252. Aoki K et al. A twenty-one year surveillance of adenoviral conjunctivitis in Sapporo, Japan. *Int Ophthalmol Clin* (2002) 42:49–54. doi:10.1097/00004397-200201000-00008
253. Laibson PR. Adenoviral keratoconjunctivitis. *Int Ophthalmol Clin* (1975) 15:187–201. doi:10.1097/00004397-197501540-00016
254. Ruzsics Z et al. Transposon-assisted cloning and traceless mutagenesis of adenoviruses: Development of a novel vector based on species D. *J Virol* (2006) 80:8100–8113. doi:10.1128/JVI.00687-06
255. Ragonnaud E et al. Replication deficient human adenovirus vector serotype 19a/64: Immunogenicity in mice and female cynomolgus macaques. *Vaccine* (2018) 36:6212–6222. doi:10.1016/j.vaccine.2018.07.075
256. Arnberg N et al. Initial interactions of subgenus D adenoviruses with A549 cellular receptors: sialic acid versus alpha(v) integrins. *J Virol* (2000) 74:7691–7693. doi:10.1128/jvi.74.16.7691-7693.2000
257. Thirion C et al. Adenovirus vectors based on human adenovirus type 19a have high potential for human muscle-directed gene therapy. *Hum Gene Ther* (2006) 17:193–205. doi:10.1089/hum.2006.17.193
258. Kiener R et al. Vaccine vectors based on Adenovirus 19a/64 exhibit broad cellular tropism and potently restimulate HCMV-specific T cell responses ex vivo. *Sci Rep* (2018) 8:1474. doi:10.1038/s41598-018-19874-1
259. Lapuente D et al. Protective mucosal immunity against SARS-CoV-2 after heterologous systemic prime-mucosal boost immunization. *Nat Commun* (2021) 12:6871. doi:10.1038/s41467-021-27063-4
260. Lapuente D et al. Evaluation of adenovirus 19a as a novel vector for mucosal vaccination against influenza A viruses. *Vaccine* (2018) 36:2712–2720. doi:10.1016/j.vaccine.2018.02.075
261. Isaacs SN. "Working Safely with Vaccinia Virus BT - Vaccinia Virus and Poxvirology: Methods and Protocols," in, ed. S. N. Isaacs (Totowa, NJ: Humana Press), 1–13. doi:10.1385/1-59259-789-0:001
262. Volz A et al. Modified Vaccinia Virus Ankara: History, Value in Basic Research, and Current Perspectives for Vaccine Development. *Adv Virus Res* (2017) 97:187–243. doi:10.1016/bs.aivir.2016.07.001
263. Huygelen C. [Jenner's cowpox vaccine in light of current vaccinology]. *Verh K Acad Geneeskd Belg* (1996) 58:478–479.
264. Schramm B et al. Cytoplasmic organization of POXvirus DNA replication. *Traffic* (2005) 6:839–846. doi:10.1111/j.1600-0854.2005.00324.x
265. Haim M et al. Adverse reactions to smallpox vaccine: the Israel Defense Force experience, 1991 to 1996. A comparison with previous surveys. *Mil Med* (2000) 165:287–289.
266. Moussatché N et al. Accidental infection of laboratory worker with vaccinia virus. *Emerg Infect Dis* (2003) 9:724–726. doi:10.3201/eid0906.020732
267. Tartaglia J et al. NYVAC: a highly attenuated strain of vaccinia virus. *Virology* (1992) 188:217–232. doi:10.1016/0042-6822(92)90752-b
268. Mayr A et al. Changes in the vaccinia virus through continuing passages in chick embryo fibroblast cultures. *Zentralbl Bakteriol Orig* (1964) 195:24–35.
269. Mayr A et al. Abstammung, Eigenschaften und Verwendung des attenuierten Vaccinia-Stammes MVA. *Infection* (1975) 3:6–14. doi:10.1007/BF01641272
270. Mayr A et al. [The smallpox vaccination strain MVA: marker, genetic structure, experience gained with the parenteral vaccination and behavior in organisms with a debilitated defence mechanism (author's transl)]. *Zentralblatt fur Bakteriol Parasitenkunde, Infekt und Hyg Erste Abteilung Orig R B Hyg Betriebshygiene, Prav Medizin* (1978) 167:375–390.
271. Meyer H et al. Mapping of deletions in the genome of the highly attenuated vaccinia virus MVA and their influence on virulence. *J Gen Virol* (1991) 72 (Pt 5):1031–1038. doi:10.1099/0022-1317-72-5-1031
272. Antoine G et al. The complete genomic sequence of the modified vaccinia Ankara strain: comparison with other orthopoxviruses. *Virology* (1998) 244:365–396. doi:10.1006/viro.1998.9123
273. Carroll MW et al. Host range and cytopathogenicity of the highly attenuated MVA strain of vaccinia virus: propagation and generation of recombinant viruses in a nonhuman mammalian cell line. *Virology* (1997) 238:198–211. doi:10.1006/viro.1997.8845
274. Drexler I et al. Highly attenuated modified vaccinia virus Ankara replicates in baby hamster kidney cells, a potential host for virus propagation, but not in various human transformed and primary cells. *J Gen Virol* (1998) 79 (Pt 2):347–

352. doi:10.1099/0022-1317-79-2-347
275. Moss B et al. “Host Range Restricted, Non-Replicating Vaccinia Virus Vectors as Vaccine Candidates BT - Novel Strategies in the Design and Production of Vaccines,” in, ed. S. Cohen (Boston, MA: Springer US), 7–13. doi:10.1007/978-1-4899-1382-1_2
276. Jordan I et al. Cell lines from the Egyptian fruit bat are permissive for modified vaccinia Ankara. *Virus Res* (2009) 145:54–62. doi:10.1016/j.virusres.2009.06.007
277. Stickl H et al. MVA vaccination against smallpox: clinical tests with an attenuated live vaccinia virus strain (MVA). *Dtsch Medizinische Wochenschrift* (1974) 99:2386–2392.
278. Agency EM. No Title. *Available online: https://www.ema.europa.eu/en/medicines/human/EPAR/imvanex* Available at: https://www.ema.europa.eu/en/medicines/human/EPAR/imvanex
279. U. S. Food and Drug Administration. No Title. *Available online: https://www.fda.gov/vaccines-blood-biologics/jynneos* Available at: https://www.fda.gov/vaccines-blood-biologics/jynneos
280. Overton ET et al. MVA-BN as monkeypox vaccine for healthy and immunocompromised. *Int J Infect Dis* (2020) 101:464. doi:10.1016/j.ijid.2020.09.1217
281. Mackett M et al. General method for production and selection of infectious vaccinia virus recombinants expressing foreign genes. *J Virol* (1984) 49:857–864. doi:10.1128/JVI.49.3.857-864.1984
282. Sutter G et al. Nonreplicating vaccinia vector efficiently expresses recombinant genes. *Proc Natl Acad Sci U S A* (1992) 89:10847–10851. doi:10.1073/pnas.89.22.10847
283. Sutter G et al. A recombinant vector derived from the host range-restricted and highly attenuated MVA strain of vaccinia virus stimulates protective immunity in mice to influenza virus. *Vaccine* (1994) 12:1032–1040. doi:10.1016/0264-410x(94)90341-7
284. Bockstal V et al. First-in-human study to evaluate safety, tolerability, and immunogenicity of heterologous regimens using the multivalent filovirus vaccines Ad26.Filo and MVA-BN-Filo administered in different sequences and schedules: A randomized, controlled study. *PLoS One* (2022) 17:e0274906. Available at: https://doi.org/10.1371/journal.pone.0274906
285. Mvabea | European Medicines Agency. Available at: https://www.ema.europa.eu/en/medicines/human/EPAR/mvabea [Accessed June 13, 2023]
286. Meyer Zu Natrup C et al. Stabilized recombinant SARS-CoV-2 spike antigen enhances vaccine immunogenicity and protective capacity. *J Clin Invest* (2022) 132: doi:10.1172/JCI159895
287. Gatti-Mays ME et al. A Phase I Dose-Escalation Trial of BN-CV301, a Recombinant Poxviral Vaccine Targeting MUC1 and CEA with Costimulatory Molecules. *Clin cancer Res an Off J Am Assoc Cancer Res* (2019) 25:4933–4944. doi:10.1158/1078-0432.CCR-19-0183
288. Medina-Echeverz J et al. Synergistic cancer immunotherapy combines MVA-CD40L induced innate and adaptive immunity with tumor targeting antibodies. *Nat Commun* (2019) 10:5041. doi:10.1038/s41467-019-12998-6
289. Rosales R et al. Regression of human papillomavirus intraepithelial lesions is induced by MVA E2 therapeutic vaccine. *Hum Gene Ther* (2014) 25:1035–1049. doi:10.1089/hum.2014.024
290. Jordan I et al. An avian cell line designed for production of highly attenuated viruses. *Vaccine* (2009) 27:748–756. doi:10.1016/j.vaccine.2008.11.066
291. Jordan I et al. A genotype of modified vaccinia Ankara (MVA) that facilitates replication in suspension cultures in chemically defined medium. *Viruses* (2013) 5:321–339. doi:10.3390/v5010321
292. Jordan I et al. A Deleted Deletion Site in a New Vector Strain and Exceptional Genomic Stability of Plaque-Purified Modified Vaccinia Ankara (MVA). *Virol Sin* (2020) 35:212–226. doi:10.1007/s12250-019-00176-3
293. Carnell GW et al. Glycan masking of a non-neutralising epitope enhances neutralising antibodies targeting the RBD of SARS-CoV-2 and its variants. *Front Immunol* (2023) 14:1118523. doi:10.3389/fimmu.2023.1118523
294. Vishwanath S et al. A computationally designed antigen eliciting broad humoral responses against SARS-CoV-2 and related sarbecoviruses. *Nat Biomed Eng* (2023) doi:10.1038/s41551-023-01094-2
295. Parikh F et al. Chemoradiotherapy-induced upregulation of PD-1 antagonizes immunity to HPV-related oropharyngeal cancer. *Cancer Res* (2014) 74:7205–7216. doi:10.1158/0008-5472.CAN-14-1913
296. Ferris RL et al. Nivolumab for Recurrent Squamous-Cell Carcinoma of the Head and Neck. *N Engl J Med* (2016) 375:1856–1867. doi:10.1056/NEJMoa1602252
297. Cohen EEW et al. The Society for Immunotherapy of Cancer consensus statement on immunotherapy for the treatment of squamous cell carcinoma of the head and neck (HNSCC). *J Immunother cancer* (2019) 7:184. doi:10.1186/s40425-019-0662-5
298. Burtness B et al. Pembrolizumab alone or with chemotherapy versus cetuximab with chemotherapy for recurrent or metastatic squamous cell carcinoma of the head and neck (KEYNOTE-048): a randomised, open-label, phase 3 study. *Lancet (London, England)* (2019) 394:1915–1928. doi:10.1016/S0140-6736(19)32591-7
299. Sousa LG de et al. ISA101 and nivolumab for HPV-16(+) cancer: updated clinical efficacy and immune correlates of response. *J Immunother cancer* (2022) 10: doi:10.1136/jitc-2021-004232
300. Melief CJM et al. Strong vaccine responses during chemotherapy are associated with prolonged cancer survival. *Sci Transl Med* (2020) 12:eaaz8235. doi:10.1126/scitranslmed.aaz8235
301. Massarelli E et al. Combining Immune Checkpoint Blockade and Tumor-Specific Vaccine for Patients With Incurable Human Papillomavirus 16–Related Cancer. *JAMA Oncol* (2019) 5:67. doi:10.1001/jamaoncol.2018.4051
302. Beyranvand Nejad E et al. Tumor Eradication by Cisplatin Is Sustained by CD80/86-Mediated Costimulation of CD8 + T Cells. *Cancer Res* (2016) 76:6017–6029. doi:10.1158/0008-5472.CAN-16-0881

303. Beyranvand Nejad E et al. Lack of myeloid cell infiltration as an acquired resistance strategy to immunotherapy. *J Immunother cancer* (2020) 8: doi:10.1136/jitc-2020-001326
304. Porchia BFMM et al. Active immunization combined with cisplatin confers enhanced therapeutic protection and prevents relapses of HPV-induced tumors at different anatomical sites. *Int J Biol Sci* (2022) 18:15–29. doi:10.7150/ijbs.56644
305. Wieking BG et al. A non-oncogenic HPV 16 E6/E7 vaccine enhances treatment of HPV expressing tumors. *Cancer Gene Ther* (2012) 19:667–674. doi:10.1038/cgt.2012.55
306. Wyatt LS et al. Elucidating and Minimizing the Loss by Recombinant Vaccinia Virus of Human Immunodeficiency Virus Gene Expression Resulting from Spontaneous Mutations and Positive Selection. *J Virol* (2009) 83:7176 LP – 7184. doi:10.1128/JVI.00687-09
307. Atukorale VN et al. Stability of the HSV-2 US-6 Gene in the del II, del III, CP77, and I8R-G1L Sites in Modified Vaccinia Virus Ankara After Serial Passage of Recombinant Vectors in Cells. *Vaccines* (2020) 8:137. doi:10.3390/vaccines8010137
308. Wang Z et al. Modified H5 promoter improves stability of insert genes while maintaining immunogenicity during extended passage of genetically engineered MVA vaccines. *Vaccine* (2010) 28:1547–1557. doi:10.1016/j.vaccine.2009.11.056
309. Haghshenas M et al. Prevalence and type distribution of high-risk human papillomavirus in patients with cervical cancer: a population-based study. *Infect Agent Cancer* (2013) 8:20. doi:10.1186/1750-9378-8-20
310. Brotherton JML et al. Primary Prevention of HPV through Vaccination: Update on the Current Global Status. *Curr Obstet Gynecol Rep* (2016) 5:210–224. doi:10.1007/s13669-016-0165-z
311. Lehtinen M et al. Overall efficacy of HPV-16/18 AS04-adjuvanted vaccine against grade 3 or greater cervical intraepithelial neoplasia: 4-year end-of-study analysis of the randomised, double-blind PATRICIA trial. *Lancet Oncol* (2012) 13:89–99. doi:10.1016/S1470-2045(11)70286-8
312. Hildesheim A et al. Effect of human papillomavirus 16/18 L1 viruslike particle vaccine among young women with preexisting infection: a randomized trial. *JAMA* (2007) 298:743–753. doi:10.1001/jama.298.7.743
313. Hung C-F et al. Therapeutic human papillomavirus vaccines: current clinical trials and future directions. *Expert Opin Biol Ther* (2008) 8:421–439. doi:10.1517/14712598.8.4.421
314. Ho GY et al. Natural history of cervicovaginal papillomavirus infection in young women. *N Engl J Med* (1998) 338:423–428. doi:10.1056/NEJM199802123380703
315. Xue Y et al. HPV16 E2 is an immediate early marker of viral infection, preceding E7 expression in precursor structures of cervical carcinoma. *Cancer Res* (2010) 70:5316–5325. doi:10.1158/0008-5472.CAN-09-3789
316. Chang L et al. Effectiveness of HPV 16 viral load and the E2/E6 ratio for the prediction of cervical cancer risk among Chinese women. *J Med Virol* (2013) 85:646–654. doi:10.1002/jmv.23490
317. Hibma MH. The Immune Response to Papillomavirus During Infection Persistence and Regression. (2012).
318. Monnier-Benoit S et al. Immunohistochemical analysis of CD4+ and CD8+ T-cell subsets in high risk human papillomavirus-associated pre-malignant and malignant lesions of the uterine cervix. *Gynecol Oncol* (2006) 102:22–31. doi:10.1016/j.ygyno.2005.11.039
319. Ma M et al. Human papilloma virus E1-specific T cell immune response is associated with the prognosis of cervical cancer patients with squamous cell carcinoma. *Infect Agent Cancer* (2018) 13:35. doi:10.1186/s13027-018-0206-5
320. Koskimaa HM et al. Human papillomavirus 16-specific cell-mediated immunity in children born to mothers with incident cervical intraepithelial neoplasia (CIN) and to those constantly HPV negative. *J Transl Med* (2015) 13:1–11. doi:10.1186/s12967-015-0733-4
321. Leachman SA et al. Ubiquitin-fused and/or multiple early genes from cottontail rabbit papillomavirus as DNA vaccines. *J Virol* (2002) 76:7616–7624. doi:10.1128/jvi.76.15.7616-7624.2002
322. Coleman N et al. Immunological events in regressing genital warts. *Am J Clin Pathol* (1994) 102:768–774. doi:10.1093/ajcp/102.6.768
323. Esposito I et al. MHC class II invariant chain-adjuvanted viral vectored vaccines enhances T cell responses in humans. *Sci Transl Med* (2020) 12: doi:10.1126/scitranslmed.aaz7715
324. Raab D et al. The GeneOptimizer Algorithm: using a sliding window approach to cope with the vast sequence space in multiparameter DNA sequence optimization. *Syst Synth Biol* (2010) 4:215–225. doi:10.1007/s11693-010-9062-3
325. Liu Z et al. Systematic comparison of 2A peptides for cloning multi-genes in a polycistronic vector. *Sci Rep* (2017) 7: doi:10.1038/s41598-017-02460-2
326. Asbach B et al. Priming with a Potent HIV-1 DNA Vaccine Frames the Quality of Immune Responses prior to a Poxvirus and Protein Boost. *J Virol* (2019) 93: doi:10.1128/JVI.01529-18
327. Sarwar UN et al. Safety and immunogenicity of DNA vaccines encoding Ebolavirus and Marburgvirus wild-type glycoproteins in a phase I clinical trial. *J Infect Dis* (2015) 211:549–557. doi:10.1093/infdis/jiu511
328. Joseph S et al. A Comparative Phase I Study of Combination, Homologous Subtype-C DNA, MVA, and Env gp140 Protein/Adjuvant HIV Vaccines in Two Immunization Regimes. *Front Immunol* (2017) 8:149. doi:10.3389/fimmu.2017.00149
329. Pantaleo G et al. Safety and immunogenicity of a multivalent HIV vaccine comprising envelope protein with either DNA or NYVAC vectors (HVTN 096): a phase 1b, double-blind, placebo-controlled trial. *Lancet HIV* (2019) 6:e737–e749. doi:10.1016/S2352-3018(19)30262-0
330. Boussif O et al. A versatile vector for gene and oligonucleotide transfer into cells in culture and in vivo: polyethylenimine. *Proc Natl Acad Sci* (1995) 92:7297 LP – 7301. doi:10.1073/pnas.92.16.7297

331. Nielsen KN et al. Priming of CD8 T cells by adenoviral vectors is critically dependent on B7 and dendritic cells but only partially dependent on CD28 ligation on CD8 T cells. *J Immunol* (2014) 193:1223–1232. doi:10.4049/jimmunol.1400197
332. Kim JH et al. High cleavage efficiency of a 2A peptide derived from porcine teschovirus-1 in human cell lines, zebrafish and mice. *PLoS One* (2011) 6:e18556. doi:10.1371/journal.pone.0018556
333. Liu Y et al. Multiple Functions of Human Papillomavirus Type 16 E6 Contribute to the Immortalization of Mammary Epithelial Cells. (1999) 73:7297–7307. doi:10.1128/JVI.73.9.7297-7307.1999
334. Wieking BG et al. A Non-oncogenic HPV 16 E6/E7 Vaccine Enhances Treatment of HPV Expressing Tumors. *Cancer Gene Ther* (2013) 19:667–674. doi:10.1038/cgt.2012.55.A
335. Edmonds C et al. A Point Mutational Analysis of Human Papillomavirus Type 16 E7 Protein. *J Virol* (1989) 63:2650–2656. doi:10.1128/jvi.63.6.2650-2656.1989
336. Barouch DH et al. A human T-cell leukemia virus type 1 regulatory element enhances the immunogenicity of human immunodeficiency virus type 1 DNA vaccines in mice and nonhuman primates. *J Virol* (2005) 79:8828–8834. doi:10.1128/JVI.79.14.8828-8834.2005
337. Ewaisha R et al. Serum Immune Profiling for Early Detection of Cervical Disease. *Theranostics* (2017) 7:3814–3823. doi:10.7150/thno.21098
338. Dersh D et al. A SIINFEKL-Based System to Measure MHC Class I Antigen Presentation Efficiency and Kinetics. *Methods Mol Biol* (2019) 1988:109–122. doi:10.1007/978-1-4939-9450-2_9
339. Grujic M et al. Fusion of a viral antigen to invariant chain leads to augmented T-cell immunity and improved protection in gene-gun DNA-vaccinated mice. *J Gen Virol* (2009) 90:414–422. doi:10.1099/vir.0.002105-0
340. Brulet J-M et al. DNA vaccine encoding endosome-targeted human papillomavirus type 16 E7 protein generates CD4+ T cell-dependent protection. *Eur J Immunol* (2007) 37:376–384. doi:10.1002/eji.200636233
341. Yalcin B et al. Commercially available outbred mice for genome-wide association studies. *PLoS Genet* (2010) 6:e1001085. doi:10.1371/journal.pgen.1001085
342. Genticel. Phase II Study of HPV Therapeutic Vaccine in HPV Infected Women With Normal Cytology or ASCUS/LSIL. (2013) Available at: https://clinicaltrials.gov/show/NCT01957878 [accessed July 15, 2021]
343. Gan L et al. Fusion of CTLA-4 with HPV16 E7 and E6 enhanced the potency of therapeutic HPV DNA vaccine. *PLoS One* (2014) 9:e108892. doi:10.1371/journal.pone.0108892
344. van de Wall S et al. Potent therapeutic efficacy of an alphavirus replicon DNA vaccine expressing human papilloma virus E6 and E7 antigens. *Oncoimmunology* (2018) 7: doi:10.1080/2162402X.2018.1487913
345. Choi YJ et al. A Phase II, Prospective, Randomized, Multicenter, Open-Label Study of GX-188E, an HPV DNA Vaccine, in Patients with Cervical Intraepithelial Neoplasia 3. *Clin Cancer Res* (2020) 26:1616 LP – 1623. doi:10.1158/1078-0432.CCR-19-1513
346. Turnstone Biologics C. This is a Trial of MG1-E6E7 With Ad-E6E7 and Atezolizumab in Patients With HPV Associated Cancers (Kingfisher). (2018) Available at: https://clinicaltrials.gov/ct2/show/NCT03618953 [accessed July 15, 2021]
347. Garza-Morales R et al. HPV-16 E7 Antigen Has Prophylactic and Therapeutic E ffi cacy in a Cervical Cancer Mouse Model. *Cancers (Basel)* (2019) 11:1–12.
348. Chaturvedi AK. Beyond cervical cancer: burden of other HPV-related cancers among men and women. *J Adolesc Health* (2010) 46:S20-6. doi:10.1016/j.jadohealth.2010.01.016
349. Kreimer AR et al. Screening for human papillomavirus-driven oropharyngeal cancer: Considerations for feasibility and strategies for research. *Cancer* (2018) 124:1859–1866. doi:10.1002/cncr.31256
350. Landoni F et al. Randomised study of radical surgery versus radiotherapy for stage Ib-IIa cervical cancer. *Lancet (London, England)* (1997) 350:535–40. doi:10.1016/S0140-6736(97)02250-2
351. Mehra R et al. Efficacy and safety of pembrolizumab in recurrent/metastatic head and neck squamous cell carcinoma: pooled analyses after long-term follow-up in KEYNOTE-012. *Br J Cancer* (2018) 119:153–159. doi:10.1038/s41416-018-0131-9
352. Bauml J et al. Pembrolizumab for Platinum- and Cetuximab-Refractory Head and Neck Cancer: Results From a Single-Arm, Phase II Study. *J Clin Oncol* (2017) 35:1542–1549. doi:10.1200/JCO.2016.70.1524
353. Tewari KS et al. Survival with Cemiplimab in Recurrent Cervical Cancer. *N Engl J Med* (2022) 386:544–555. doi:10.1056/NEJMoa2112187
354. Anderson KS et al. HPV16 antibodies as risk factors for oropharyngeal cancer and their association with tumor HPV and smoking status. *Oral Oncol* (2015) 51:662–667. doi:10.1016/j.oraloncology.2015.04.011
355. Study Details | Safety, Reactogenicity and Immunogenicity of Adenovirus Serotype 26 (Ad26)- and Modified Vaccinia Ankara (MVA)-Vectored Vaccine Components in Otherwise Healthy Women With HPV16 or HPV18 Infection of the Cervix | ClinicalTrials.gov. doi:NCT03610581
356. Neckermann P et al. Design and Immunological Validation of Macaca fascicularis Papillomavirus Type 3 Based Vaccine Candidates in Outbred Mice: Basis for Future Testing of a Therapeutic Papillomavirus Vaccine in NHPs. *Front Immunol* (2021) 12:4409. doi:10.3389/fimmu.2021.761214
357. Powell AA et al. Real-world data shows increased reactogenicity in adults after heterologous compared to homologous prime-boost COVID-19 vaccination, March-June 2021, England. *Euro Surveill* (2021) 26: doi:10.2807/1560-7917.ES.2021.26.28.2100634
358. Grunwitz C et al. HPV16 RNA-LPX vaccine mediates complete regression of aggressively growing HPV-positive mouse tumors and establishes protective T cell memory. *Oncoimmunology* (2019) doi:10.1080/2162402X.2019.1629259
359. Van Der Sluis TC et al. Vaccine-Induced tumor necrosis factor- Producing T cells synergize with cisplatin to promote

tumor cell death. *Clin Cancer Res* (2015) 21:781–794. doi:10.1158/1078-0432.CCR-14-2142
360. van der Sluis TC et al. Therapeutic Peptide Vaccine-Induced CD8 T Cells Strongly Modulate Intratumoral Macrophages Required for Tumor Regression. *Cancer Immunol Res* (2015) 3:1042–1051. doi:10.1158/2326-6066.CIR-15-0052
361. Nielsen M et al. Reliable prediction of T-cell epitopes using neural networks with novel sequence representations. *Protein Sci* (2003) 12:1007–1017. doi:10.1110/ps.0239403
362. Lundegaard C et al. NetMHC-3.0: accurate web accessible predictions of human, mouse and monkey MHC class I affinities for peptides of length 8-11. *Nucleic Acids Res* (2008) 36:W509-12. doi:10.1093/nar/gkn202
363. Andreatta M et al. Gapped sequence alignment using artificial neural networks: application to the MHC class I system. *Bioinformatics* (2016) 32:511–517. doi:10.1093/bioinformatics/btv639
364. Borowicz S et al. The Soft Agar Colony Formation Assay. *JoVE* (2014)e51998. doi:doi:10.3791/51998
365. Schindelin J et al. Fiji: an open-source platform for biological-image analysis. *Nat Methods* (2012) 9:676–682. doi:10.1038/nmeth.2019
366. Janik P et al. The effect of estrone-progesterone treatment on cell proliferation kinetics of hormone-dependent GR mouse mammary tumors. *Cancer Res* (1975) 35:3698–704.
367. Peng S et al. Development of a DNA vaccine targeting human papillomavirus type 16 oncoprotein E6. *J Virol* (2004) 78:8468–8476. doi:10.1128/JVI.78.16.8468-8476.2004
368. Shooshtari P et al. Correlation analysis of intracellular and secreted cytokines via the generalized integrated mean fluorescence intensity. *Cytometry A* (2010) 77:873–80. doi:10.1002/cyto.a.20943
369. Schmitt M et al. The HPV transcriptome in HPV16 positive cell lines. (2011) 25:108–113. doi:10.1016/j.mcp.2011.03.003
370. Zwaveling S et al. Established human papillomavirus type 16-expressing tumors are effectively eradicated following vaccination with long peptides. *J Immunol* (2002) 169:350–358. doi:10.4049/jimmunol.169.1.350
371. Someya M et al. Association between cancer immunity and treatment results in uterine cervical cancer patients treated with radiotherapy. *Jpn J Clin Oncol* (2020) 50:1290–1297. doi:10.1093/jjco/hyaa149
372. Chen H et al. Immunoscore system combining CD8 and PD-1/PD-L1: A novel approach that predicts the clinical outcomes for cervical cancer. *Int J Biol Markers* (2020) 35:65–73. doi:10.1177/1724600819888771
373. Porter SS et al. Host cell restriction factors that limit transcription and replication of human papillomavirus. *Virus Res* (2017) 231:10–20. doi:10.1016/j.virusres.2016.11.014
374. Baedyananda F et al. Elevated HPV16 E1 Expression Is Associated with Cervical Cancer Progression. *Intervirology* (2017) 60:171–180. doi:10.1159/000487048
375. van Poelgeest MIE et al. Vaccination against Oncoproteins of HPV16 for Noninvasive Vulvar/Vaginal Lesions: Lesion Clearance Is Related to the Strength of the T-Cell Response. *Clin Cancer Res* (2016) 22:2342–2350. doi:10.1158/1078-0432.CCR-15-2594
376. Steffensen MA et al. Pre-existing vector immunity does not prevent replication deficient adenovirus from inducing efficient cd8 t-cell memory and recall responses. *PLoS One* (2012) 7: doi:10.1371/journal.pone.0034884
377. ClinicalTrialsRegister.eu. A Phase 1b/2 Randomised, Placebo-controlled, Dose-ranging Study to Evaluate Safety, Tolerability and Immunogenicity of a Chimpanzee Adenovirus (ChAdOx1)-vectored Multigenotype High Risk Human Papillomavirus (hrHPV) Vaccine and Modified Vaccinia Ankara (MV. *EudraCT 2019-001890-98, HPV001*Cited 2021 Jan 19.
378. Stittelaar KJ et al. Safety of modified vaccinia virus Ankara (MVA) in immune-suppressed macaques. *Vaccine* (2001) 19:3700–3709. doi:10.1016/s0264-410x(01)00075-5
379. Imvanex | European Medicines Agency. Available at: https://www.ema.europa.eu/en/medicines/human/EPAR/imvanex [Accessed June 13, 2023]
380. JYNNEOS | FDA. Available at: https://www.fda.gov/vaccines-blood-biologics/jynneos [Accessed June 13, 2023]
381. Orlova OV et al. Development of Modified Vaccinia Virus Ankara-Based Vaccines: Advantages and Applications. *Vaccines* (2022) 10: doi:10.3390/vaccines10091516
382. Koch T et al. Safety and immunogenicity of a modified vaccinia virus Ankara vector vaccine candidate for Middle East respiratory syndrome: an open-label, phase 1 trial. *Lancet Infect Dis* (2020) 20:827–838. doi:10.1016/S1473-3099(20)30248-6
383. Stittelaar KJ et al. Protective immunity in macaques vaccinated with a modified vaccinia virus Ankara-based measles virus vaccine in the presence of passively acquired antibodies. *J Virol* (2000) 74:4236–4243. doi:10.1128/jvi.74.9.4236-4243.2000
384. Wyatt LS et al. Enhanced cell surface expression, immunogenicity and genetic stability resulting from a spontaneous truncation of HIV Env expressed by a recombinant MVA. *Virology* (2008) 372:260–272.
385. Boilesen DR et al. Efficacy and Synergy with Cisplatin of an Adenovirus Vectored Therapeutic E1E2E6E7 Vaccine against HPV Genome-Positive C3 Cancers in Mice. *Cancer Immunol Res* (2023) 11:261–275. doi:10.1158/2326-6066.CIR-22-0174
386. Yuen L et al. Oligonucleotide sequence signaling transcriptional termination of vaccinia virus early genes. *Proc Natl Acad Sci U S A* (1987) 84:6417–6421. doi:10.1073/pnas.84.18.6417
387. Chakrabarti S et al. Compact, synthetic, vaccinia virus early/late promoter for protein expression. England (1997). doi:10.2144/97236st07
388. Ramakrishnan MA. Determination of 50% endpoint titer using a simple formula. *World J Virol* (2016) 5:85–86. doi:10.5501/wjv.v5.i2.85

389. Pfaffl MW. A new mathematical model for relative quantification in real-time RT-PCR. *Nucleic Acids Res* (2001) 29:e45. doi:10.1093/nar/29.9.e45
390. Kremer M et al. "Easy and Efficient Protocols for Working with Recombinant Vaccinia Virus MVA BT - Vaccinia Virus and Poxvirology: Methods and Protocols," in, ed. S. N. Isaacs (Totowa, NJ: Humana Press), 59–92. doi:10.1007/978-1-61779-876-4_4
391. Holmes K et al. Detection of siRNA induced mRNA silencing by RT-qPCR: considerations for experimental design. *BMC Res Notes* (2010) 3:53. doi:10.1186/1756-0500-3-53
392. McCann N et al. Viral vector vaccines. *Curr Opin Immunol* (2022) 77:102210. doi:10.1016/j.coi.2022.102210
393. Wyatt LS et al. Development of a replication-deficient recombinant vaccinia virus vaccine effective against parainfluenza virus 3 infection in an animal model. *Vaccine* (1996) 14:1451–1458. doi:https://doi.org/10.1016/S0264-410X(96)00072-2
394. Faqih L et al. Genetic stability of SIV Gag/Tat gene inserted into Del-II in modified vaccinia virus ankara after serial passage of recombinant vector in pCEFs cells. *J Virol Methods* (2023) 312:114651. doi:10.1016/j.jviromet.2022.114651
395. Chiu W-L et al. Vaccinia virus J1R protein: a viral membrane protein that is essential for virion morphogenesis. *J Virol* (2002) 76:9575–9587. doi:10.1128/jvi.76.19.9575-9587.2002
396. Scheiflinger F et al. Evaluation of the thymidine kinase (tk) locus as an insertion site in the highly attenuated vaccinia MVA strain. *Arch Virol* (1996) 141:663–669. doi:10.1007/BF01718324
397. Manuel ER et al. Intergenic region 3 of modified vaccinia ankara is a functional site for insert gene expression and allows for potent antigen-specific immune responses. *Virology* (2010) 403:155–162. doi:10.1016/j.virol.2010.04.015
398. Chen H et al. A novel adenoviral vector carrying an all-in-one Tet-On system with an autoregulatory loop for tight, inducible transgene expression. *BMC Biotechnol* (2015) 15:4. doi:10.1186/s12896-015-0121-4
399. Cottingham MG et al. Preventing spontaneous genetic rearrangements in the transgene cassettes of adenovirus vectors. *Biotechnol Bioeng* (2012) 109:719–728. doi:10.1002/bit.24342
400. Wyatt LS et al. Correlation of immunogenicities and in vitro expression levels of recombinant modified vaccinia virus Ankara HIV vaccines. *Vaccine* (2008) 26:486–493. doi:10.1016/j.vaccine.2007.11.036
401. Malherbe DC et al. Modified vaccinia Ankara vaccine expressing Marburg virus-like particles protects guinea pigs from lethal Marburg virus infection. *NPJ vaccines* (2020) 5:78. doi:10.1038/s41541-020-00226-y
402. Qu J et al. The Roles of the Ubiquitin-Proteasome System in the Endoplasmic Reticulum Stress Pathway. *Int J Mol Sci* (2021) 22: doi:10.3390/ijms22041526
403. Ostankovitch M et al. Regulated folding of tyrosinase in the endoplasmic reticulum demonstrates that misfolded full-length proteins are efficient substrates for class I processing and presentation. *J Immunol* (2005) 174:2544–2551. doi:10.4049/jimmunol.174.5.2544
404. Dolan BP et al. Defective ribosomal products are the major source of antigenic peptides endogenously generated from influenza A virus neuraminidase. *J Immunol* (2010) 184:1419–1424. doi:10.4049/jimmunol.0901907
405. Yewdell JW et al. Defective ribosomal products (DRiPs): a major source of antigenic peptides for MHC class I molecules? *J Immunol* (1996) 157:1823–1826.
406. Bourdetsky D et al. The nature and extent of contributions by defective ribosome products to the HLA peptidome. *Proc Natl Acad Sci* (2014) 111:E1591–E1599. doi:10.1073/pnas.1321902111
407. Youn JW et al. Pembrolizumab plus GX-188E therapeutic DNA vaccine in patients with HPV-16-positive or HPV-18-positive advanced cervical cancer: interim results of a single-arm, phase 2 trial. *Lancet Oncol* (2020) 21:1653–1660. doi:10.1016/S1470-2045(20)30486-1
408. Hillemanns P et al. 881TiP A multi-centre, open-label phase II trial of the combination of VB10.16 and atezolizumab in patients with advanced or recurrent, non-resectable HPV16 positive cervical cancer. *Ann Oncol* (2020) 31:S645–S646. doi:https://doi.org/10.1016/j.annonc.2020.08.1020
409. Bhuyan PK et al. Durability of response to VGX-3100 treatment of HPV16/18 positive cervical HSIL. *Hum Vaccin Immunother* (2021) 17:1288–1293. doi:10.1080/21645515.2020.1823778
410. Swadling L et al. A human vaccine strategy based on chimpanzee adenoviral and MVA vectors that primes, boosts, and sustains functional HCV-specific T cell memory. *Sci Transl Med* (2014) 6:261ra153-261ra153.
411. Ewer KJ et al. Protective CD8+ T-cell immunity to human malaria induced by chimpanzee adenovirus-MVA immunisation. *Nat Commun* (2013) 4:2836.
412. Barouch DH et al. Vaccine protection against acquisition of neutralization-resistant SIV challenges in rhesus monkeys. *Nature* (2012) 482:89–93.
413. Stephen SL et al. Chromosomal integration of adenoviral vector DNA in vivo. *J Virol* (2010) 84:9987–9994. doi:10.1128/JVI.00751-10
414. Faurez F et al. Biosafety of DNA vaccines: New generation of DNA vectors and current knowledge on the fate of plasmids after injection. *Vaccine* (2010) 28:3888–3895. doi:10.1016/j.vaccine.2010.03.040
415. Nichols WW et al. Potential DNA vaccine integration into host cell genome. *Ann N Y Acad Sci* (1995) 772:30–39. doi:10.1111/j.1749-6632.1995.tb44729.x
416. Šmahel M et al. Systemic administration of CpG oligodeoxynucleotide and levamisole as adjuvants for gene-gun-delivered antitumor DNA vaccines. *Clin Dev Immunol* (2011) 2011:176759. doi:10.1155/2011/176759
417. Yan J et al. Induction of antitumor immunity in vivo following delivery of a novel HPV-16 DNA vaccine encoding an E6/E7 fusion antigen. *Vaccine* (2009) 27:431–440. doi:10.1016/j.vaccine.2008.10.078
418. Boursnell ME et al. Construction and characterisation of a recombinant vaccinia virus expressing human

papillomavirus proteins for immunotherapy of cervical cancer. *Vaccine* (1996) 14:1485–1494. doi:10.1016/s0264-410x(96)00117-x

419. Nguyen M et al. A Mutant of Human Papillomavirus Type 16 E6 Deficient in Binding ⌴ -Helix Partners Displays Reduced Oncogenic Potential In Vivo. (2002) 76:13039–13048. doi:10.1128/JVI.76.24.13039
420. Phelps WC et al. Structure-Function Analysis of the Human Papillomavirus Type 16 E7 Oncoprotein. (1992) 66:2418–2427.
421. Shi WEI et al. Human Papillomavirus Type 16 E7 DNA Vaccine : Mutation in the Open Reading Frame of E7 Enhances Specific Cytotoxic T-Lymphocyte Induction and Antitumor Activity. (1999) 73:7877–7881.
422. Trimble CL et al. Safety, efficacy, and immunogenicity of VGX-3100, a therapeutic synthetic DNA vaccine targeting human papillomavirus 16 and 18 E6 and E7 proteins for cervical intraepithelial neoplasia 2/3: a randomised, double-blind, placebo-controlled phase 2b trial. *Lancet (London, England)* (2015) 386:2078–2088. doi:10.1016/S0140-6736(15)00239-1
423. Hollenberg RK et al. Safety and immunogenicity of VGX-3100 formulations in a healthy young adult population. *Hum Vaccin Immunother* (2020) 16:1404–1412. doi:10.1080/21645515.2019.1695459
424. Kim TJ et al. Clearance of persistent HPV infection and cervical lesion by therapeutic DNA vaccine in CIN3 patients. *Nat Commun* (2014) 5:5317. doi:10.1038/ncomms6317
425. Trimble CL et al. A phase I trial of a human papillomavirus DNA vaccine for HPV16+ cervical intraepithelial neoplasia 2/3. *Clin cancer Res an Off J Am Assoc Cancer Res* (2009) 15:361–367. doi:10.1158/1078-0432.CCR-08-1725
426. Greinacher A et al. Thrombotic Thrombocytopenia after ChAdOx1 nCov-19 Vaccination. *N Engl J Med* (2021) 384:2092–2101. doi:10.1056/NEJMoa2104840
427. Mendonça SA et al. Adenoviral vector vaccine platforms in the SARS-CoV-2 pandemic. *npj Vaccines* (2021) 6:97. doi:10.1038/s41541-021-00356-x
428. Chavda VP et al. Replicating Viral Vector-Based Vaccines for COVID-19: Potential Avenue in Vaccination Arena. *Viruses* (2022) 14: doi:10.3390/v14040759
429. Greinacher A et al. Anti-platelet factor 4 antibodies causing VITT do not cross-react with SARS-CoV-2 spike protein. *Blood* (2021) 138:1269–1277. doi:10.1182/blood.2021012938
430. Krutzke L et al. Process- and product-related impurities in the ChAdOx1 nCov-19 vaccine. *Elife* (2022) 11: doi:10.7554/eLife.78513
431. Greinacher A et al. Insights in ChAdOx1 nCoV-19 vaccine-induced immune thrombotic thrombocytopenia. *Blood* (2021) 138:2256–2268. doi:10.1182/blood.2021013231
432. Kemper M et al. Successful Treatment of Vaccine-Induced Immune Thrombotic Thrombocytopenia in a 26-Year-Old Female Patient. *Acta Haematol* (2021) 145:210–213. doi:10.1159/000519451
433. Remy-Ziller C et al. Immunological characterization of a modified vaccinia virus Ankara vector expressing the human papillomavirus 16 E1 protein. *Clin Vaccine Immunol* (2014) 21:147–155. doi:10.1128/CVI.00678-13
434. Baldwin PJ et al. Vaccinia-expressed human papillomavirus 16 and 18 e6 and e7 as a therapeutic vaccination for vulval and vaginal intraepithelial neoplasia. *Clin cancer Res an Off J Am Assoc Cancer Res* (2003) 9:5205–5213.
435. Brun J-L et al. Regression of high-grade cervical intraepithelial neoplasia with TG4001 targeted immunotherapy. *Am J Obstet Gynecol* (2011) 204:169.e1-169.e8. doi:https://doi.org/10.1016/j.ajog.2010.09.020
436. Vellinga J et al. Challenges in Manufacturing Adenoviral Vectors for Global Vaccine Product Deployment. *Hum Gene Ther* (2014) 25:318–327. doi:10.1089/hum.2014.007
437. Coulibaly S et al. The nonreplicating smallpox candidate vaccines defective vaccinia Lister (dVV-L) and modified vaccinia Ankara (MVA) elicit robust long-term protection. *Virology* (2005) 341:91–101. doi:10.1016/j.virol.2005.06.043
438. Jordan I et al. Elements in the Development of a Production Process for Modified Vaccinia Virus Ankara. *Microorganisms* (2013) 1:100–121. doi:10.3390/microorganisms1010100
439. Hellner K et al. Conference Poster: Interim Analysis of APOLLO Trial: ChAdOx1 and MVA Heterologous Prime-boost (VTP-200) Immunotherapeutic in Low-grade HPV-related Cervical Lesions (NTC04607850). in *International Papilloma Virus Conference 2023*, 2023.
440. de Sanjosé S et al. HPV in genital cancers (at the exception of cervical cancer) and anal cancers. *Presse Med* (2014) 43:e423–e428. doi:https://doi.org/10.1016/j.lpm.2014.10.001
441. Kong L et al. Correction to: Analysis of the role of the human papillomavirus 16/18 E7 protein assay in screening for cervical intraepithelial neoplasia: a case control study. *BMC Cancer* (2020) 20:1027. doi:10.1186/s12885-020-07547-0
442. Ebrahimi N et al. Human papillomavirus vaccination in low- and middle-income countries: progression, barriers, and future prospective . *Front Immunol* (2023) 14: Available at: https://www.frontiersin.org/articles/10.3389/fimmu.2023.1150238
443. Duncan J et al. A Call for Low- and Middle-Income Countries to Commit to the Elimination of Cervical Cancer. *Lancet Reg Heal Am* (2021) 2:None. doi:10.1016/j.lana.2021.100036
444. Dare AJ et al. Ensuring Global Access to Cancer Medicines: A Generational Call to Action. *Cancer Discov* (2023) 13:269–274. doi:10.1158/2159-8290.CD-22-1372
445. Ferreira RG et al. Adenoviral Vector COVID-19 Vaccines: Process and Cost Analysis. *Processes* (2021) 9: doi:10.3390/pr9081430
446. Ang KK et al. Human Papillomavirus and Survival of Patients with Oropharyngeal Cancer. *N Engl J Med* (2010) 363:24–35. doi:10.1056/NEJMoa0912217

447. Strohl MP et al. De-intensification strategies in HPV-related oropharyngeal squamous cell carcinoma-a narrative review. *Ann Transl Med* (2020) 8:1601. doi:10.21037/atm-20-2984
448. Economopoulou P et al. De-Escalating Strategies in HPV-Associated Head and Neck Squamous Cell Carcinoma. *Viruses* (2021) 13: doi:10.3390/v13091787
449. Morand GB et al. Therapeutic Vaccines for HPV-Associated Oropharyngeal and Cervical Cancer: The Next De-Intensification Strategy? *Int J Mol Sci* (2022) 23: doi:10.3390/ijms23158395
450. Gillison ML et al. Prevalence of oral HPV infection in the United States, 2009-2010. *JAMA* (2012) 307:693–703. doi:10.1001/jama.2012.101
451. Wittekindt C et al. HPV - A different view on Head and Neck Cancer. *Laryngorhinootologie* (2018) 97:S48–S113. doi:10.1055/s-0043-121596
452. Roman BR et al. Epidemiology and incidence of HPV-related cancers of the head and neck. *J Surg Oncol* (2021) 124:920–922. doi:10.1002/jso.26687
453. Milano G et al. Human Papillomavirus Epidemiology and Prevention: Is There Still a Gender Gap? *Vaccines* (2023) 11: doi:10.3390/vaccines11061060
454. Akhatova A et al. Prophylactic Human Papillomavirus Vaccination: From the Origin to the Current State. *Vaccines* (2022) 10: doi:10.3390/vaccines10111912
455. Lenzi A et al. Rome Consensus Conference - statement; human papilloma virus diseases in males. *BMC Public Health* (2013) 13:117. doi:10.1186/1471-2458-13-117
456. Zhou P et al. A pneumonia outbreak associated with a new coronavirus of probable bat origin. *Nature* (2020) 579:270–273. doi:10.1038/s41586-020-2012-7
457. WHO WHO. WHO Coronavirus (COVID-19) Dashboard | WHO Coronavirus (COVID-19) Dashboard With Vaccination Data. Available at: https://covid19.who.int/ [Accessed November 6, 2023]
458. Su S et al. Epidemiology, Genetic Recombination, and Pathogenesis of Coronaviruses. *Trends Microbiol* (2016) 24:490–502. doi:10.1016/j.tim.2016.03.003
459. Bönisch S et al. Effects of Coronavirus Disease (COVID-19) Related Contact Restrictions in Germany, March to May 2020, on the Mobility and Relation to Infection Patterns . *Front Public Heal* (2020) 8: Available at: https://www.frontiersin.org/articles/10.3389/fpubh.2020.568287
460. Liu CY et al. Rapid Review of Social Contact Patterns During the COVID-19 Pandemic. *Epidemiology* (2021) 32:781–791. doi:10.1097/EDE.0000000000001412
461. Wrapp D et al. Cryo-EM structure of the 2019-nCoV spike in the prefusion conformation. *Science* (2020) 367:1260–1263. doi:10.1126/science.abb2507
462. Walls AC et al. Structure, Function, and Antigenicity of the SARS-CoV-2 Spike Glycoprotein. *Cell* (2020) 181:281-292.e6. doi:10.1016/j.cell.2020.02.058
463. Yan R et al. Structural basis for the recognition of SARS-CoV-2 by full-length human ACE2. *Science* (2020) 367:1444–1448. doi:10.1126/science.abb2762
464. Wang Q et al. Structural and Functional Basis of SARS-CoV-2 Entry by Using Human ACE2. *Cell* (2020) 181:894-904.e9. doi:10.1016/j.cell.2020.03.045
465. Hoffmann M et al. SARS-CoV-2 Cell Entry Depends on ACE2 and TMPRSS2 and Is Blocked by a Clinically Proven Protease Inhibitor. *Cell* (2020) 181:271-280.e8. doi:10.1016/j.cell.2020.02.052
466. Polack FP et al. Safety and Efficacy of the BNT162b2 mRNA Covid-19 Vaccine. *N Engl J Med* (2020) 383:2603–2615. doi:10.1056/NEJMoa2034577
467. Baden LR et al. Efficacy and Safety of the mRNA-1273 SARS-CoV-2 Vaccine. *N Engl J Med* (2020) 384:403–416. doi:10.1056/NEJMoa2035389
468. Keech C et al. Phase 1-2 Trial of a SARS-CoV-2 Recombinant Spike Protein Nanoparticle Vaccine. *N Engl J Med* (2020) 383:2320–2332. doi:10.1056/NEJMoa2026920
469. Zhang Y et al. Safety, tolerability, and immunogenicity of an inactivated SARS-CoV-2 vaccine in healthy adults aged 18-59 years: a randomised, double-blind, placebo-controlled, phase 1/2 clinical trial. *Lancet Infect Dis* (2021) 21:181–192. doi:10.1016/S1473-3099(20)30843-4
470. Widyasari K et al. A Review of the Currently Available Antibody Therapy for the Treatment of Coronavirus Disease 2019 (COVID-19). *Antibodies (Basel, Switzerland)* (2023) 12: doi:10.3390/antib12010005
471. Markov P V et al. The evolution of SARS-CoV-2. *Nat Rev Microbiol* (2023) 21:361–379. doi:10.1038/s41579-023-00878-2
472. Tregoning JS et al. Progress of the COVID-19 vaccine effort: viruses, vaccines and variants versus efficacy, effectiveness and escape. *Nat Rev Immunol* (2021) 21:626–636. doi:10.1038/s41577-021-00592-1
473. Lazarevic I et al. Immune Evasion of SARS-CoV-2 Emerging Variants: What Have We Learnt So Far? *Viruses* (2021) 13: doi:10.3390/v13071192
474. Chaguza C et al. Rapid emergence of SARS-CoV-2 Omicron variant is associated with an infection advantage over Delta in vaccinated persons. *Med (New York, NY)* (2022) 3:325-334.e4. doi:10.1016/j.medj.2022.03.010
475. Choi JY et al. SARS-CoV-2 Variants of Concern. *Yonsei Med J* (2021) 62:961–968. doi:10.3349/ymj.2021.62.11.961
476. Hoffmann M et al. SARS-CoV-2 variants B.1.351 and P.1 escape from neutralizing antibodies. *Cell* (2021) 184:2384-2393.e12. doi:10.1016/j.cell.2021.03.036
477. Mlcochova P et al. SARS-CoV-2 B.1.617.2 Delta variant replication and immune evasion. *Nature* (2021) 599:114–119. doi:10.1038/s41586-021-03944-y
478. Mannar D et al. SARS-CoV-2 Omicron variant: Antibody evasion and cryo-EM structure of spike protein-ACE2

complex. *Science* (2022) 375:760–764. doi:10.1126/science.abn7760
479. Schubert M et al. Human serum from SARS-CoV-2-vaccinated and COVID-19 patients shows reduced binding to the RBD of SARS-CoV-2 Omicron variant. *BMC Med* (2022) 20:102. doi:10.1186/s12916-022-02312-5
480. Wagner R et al. Estimates and Determinants of SARS-Cov-2 Seroprevalence and Infection Fatality Ratio Using Latent Class Analysis: The Population-Based Tirschenreuth Study in the Hardest-Hit German County in Spring 2020. *Viruses* (2021) 13: doi:10.3390/v13061118
481. Peterhoff D et al. Population-based study of the durability of humoral immunity after SARS-CoV-2 infection . *Front Immunol* (2023) 14: Available at: https://www.frontiersin.org/articles/10.3389/fimmu.2023.1242536
482. Einhauser S et al. Time Trend in SARS-CoV-2 Seropositivity, Surveillance Detection- and Infection Fatality Ratio until Spring 2021 in the Tirschenreuth County-Results from a Population-Based Longitudinal Study in Germany. *Viruses* (2022) 14: doi:10.3390/v14061168
483. Carnell GW et al. SARS-CoV-2 Spike Protein Stabilized in the Closed State Induces Potent Neutralizing Responses. *J Virol* (2021) 95:e0020321. doi:10.1128/JVI.00203-21
484. Peterhoff D et al. Comparative Immunogenicity of COVID-19 Vaccines in a Population-Based Cohort Study with SARS-CoV-2-Infected and Uninfected Participants. *Vaccines* (2022) 10: doi:10.3390/vaccines10020324
485. Einhauser S et al. Spectrum Bias and Individual Strengths of SARS-CoV-2 Serological Tests—A Population-Based Evaluation. *Diagnostics* (2021) 11: doi:10.3390/diagnostics11101843
486. Muruato AE et al. A high-throughput neutralizing antibody assay for COVID-19 diagnosis and vaccine evaluation. *Nat Commun* (2020) 11:4059. doi:10.1038/s41467-020-17892-0
487. Nie J et al. Establishment and validation of a pseudovirus neutralization assay for SARS-CoV-2. *Emerg Microbes Infect* (2020) 9:680–686. doi:10.1080/22221751.2020.1743767
488. Riepler L et al. Comparison of Four SARS-CoV-2 Neutralization Assays. *Vaccines* (2020) 9: doi:10.3390/vaccines9010013
489. Barnes CO et al. SARS-CoV-2 neutralizing antibody structures inform therapeutic strategies. *Nature* (2020) 588:682–687. doi:10.1038/s41586-020-2852-1
490. Peterhoff D et al. A highly specific and sensitive serological assay detects SARS-CoV-2 antibody levels in COVID-19 patients that correlate with neutralization. *Infection* (2021) 49:75–82. doi:10.1007/s15010-020-01503-7
491. Yang J et al. A vaccine targeting the RBD of the S protein of SARS-CoV-2 induces protective immunity. *Nature* (2020) 586:572–577. doi:10.1038/s41586-020-2599-8
492. Riester E et al. Performance evaluation of the Roche Elecsys Anti-SARS-CoV-2 S immunoassay. *J Virol Methods* (2021) 297:114271. doi:10.1016/j.jviromet.2021.114271
493. Liu W et al. Evaluation of Nucleocapsid and Spike Protein-Based Enzyme-Linked Immunosorbent Assays for Detecting Antibodies against SARS-CoV-2. *J Clin Microbiol* (2020) 58: doi:10.1128/JCM.00461-20
494. Tan CW et al. A SARS-CoV-2 surrogate virus neutralization test based on antibody-mediated blockage of ACE2–spike protein–protein interaction. *Nat Biotechnol* (2020) 38:1073–1078. doi:10.1038/s41587-020-0631-z

9.4 Danksagung

Das Schreiben einer Doktorarbeit ist nicht nur die Leistung einer einzelnen Person. So wurde auch ich von zahlreichen Menschen sehr unterstützt, weshalb ich mich hier gerne schriftlich dafür bedanken möchte. Zu aller erst bedanke ich mich herzlich bei meinem Doktorvater Prof. Dr. Ralf Wagner für die Möglichkeit, meine Doktorarbeit in seiner Arbeitsgruppe machen zu können. Vielen Dank, dass du mich so gefördert hast, dass du immer ein offenes Ohr hattest und auch auf meine Vorschläge und Kritiken eingegangen bist. Noch dazu hast du mir kreative Möglichkeiten offengehalten, mich experimentell frei zu entfalten.

Ein herzliches Dankeschön gebührt auch Dr. Benedikt Asbach, denn ich konnte immer bei Fragen und Problemen bei dir Rat finden. Ich schätze die wissenschaftlichen Diskussionen mit dir sehr. Deine akribische Genauigkeit hat mir schon bei so manchen Fragenstellungen einen Ausweg gezeigt, den ich zuvor leicht übersehen hatte. Vielen Dank, dass du meine Arbeit so oft bereichert hast.

Ein sehr großes Dankeschön gilt an alle Kollegen aus dem THERIN Projekt: Silke Schrödel, Cordula Pertl, Torsten Willert und Christian Thirion von Sirion Biotech GmbH (jetzt Reevity), Alexander Karlas, Ingo Jordan und Volker Sandig von ProBioGen AG und Ditte Boilesen sowie Peter Holst von der Universität Kopenhagen bzw. InProTher ApS. Ohne euch wären die ganzen Ergebnisse nicht zu Stande gekommen. Ganz besonderer Dank gilt dabei Ditte, ohne dich wären die Tierexperimente nicht möglich gewesen. Danke dass wir uns auf dem gemeinsamen Weg durch die Doktorarbeit so ergänzt haben.

Vielen Dank an meine Masterstudenten Sebastian (Basti) Einhauser und Madlen Mohr für eure tatkräftige Unterstützung in dem einen oder anderen Projekt dieser Arbeit. Danke auch an die ganzen, hier nicht namentlich erwähnten Studenten, die ich im Laufe meiner Doktorandenzeit betreut und dadurch auch mal neue Sichtweisen entdeckt habe.

Ich möchte mich ganz herzlich bei den aktuellen und ehemaligen Mitarbeitern der AG Wagner bedanken, im Speziellen sind dies: Basti, Martina, Benny, Richi, Mirko, Anja, Meli, Dave, David und Franz. Vielen Dank für die gemeinsame Zeit, sowohl im Labor als auch privat. Ganz besonders hervorheben möchte ich hier meine Laborkollegin Dr. Martina Billmeier, mit der ich mir fast seit Beginn der Doktorarbeit das 64er Labor teile. Danke für all die guten Gespräche, deine Expertise bei der MVA-Arbeit und dafür, dass du immer hilfsbereit warst, sowohl im Labor, als auch privat. Auch wenn ich dich oben schon genannt hab, Basti, möchte ich mich an dieser Stelle nochmal bedanken, da du nicht nur als mein Student, sondern noch viel mehr, als guter Kumpel da warst, um über ernste als auch über witzige Themen zu philosophieren. Ihr beiden (Basti und Martina) wart die Stimmungskanonen, wenn ich mal wieder bis zum Hals in Arbeit war.

Vielen Dank an die ganzen Kollegen im IMHR, welche immer wieder als Ansprechstationen zur Verfügung standen und bei denen ich mir Tipps für meine Experimente einholen konnte: Gertrud, Martin, Josef, Jürgen, Hans-Helmut, Tamara, Markus und Valentin.

Mit unter den größten Dank gilt meinen Eltern. Ohne euch, wäre meine lange Ausbildung nie möglich gewesen. Vielen Dank, dass ihr mich bedingungslos unterstützt und mir den Rücken freigehalten habt.

Die letzten Zeilen sind für dich, liebe Manuela. Danke für alles, dafür, dass du immer für mich da bist und dass du mich so sehr motiviert hast. Danke, dass immer gerne deine Zeit mit mir verbringst.